CYCLIC USE OF HALF-CALCINED DOLOMITE AND MAGNESIUM OXIDE FOR THE REMOVAL OF SULFUR COMPOUNDS FROM GASES AT ELEVATED PRESSURES

by

GEORGE LAN-YUH KAN

A dissertation submitted to the Graduate Faculty in Engineering in partial fulfillment for the degree of Doctor of Philosophy, The City University of New York.

This manuscript has been read and accepted for the Graduate Faculty in Engineering in satisfaction of the dissertation requirement for the degree of Doctor of Philosophy.

1/21/77 — Date

Arthur M. Squires — Chairman of Examining Committee

1/21/77 — Date

Jacques E. Benveniste — Executive Officer

Prof. Arthur M. Squires (Chairman)
Prof. Robert A. Graff
Prof. Amos Turk
Prof. Leslie L. Isaacs
Dr. Melvyn Pell

The City University of New York

To my parents, from whom I learned love.

Abstract

Cyclic Use of Half-Calcined Dolomite and Magnesium Oxide for the Removal of Sulfur Compounds from Gases at Elevated Pressures

by

George L. Kan

Adviser: Professor Arthur M. Squires

The duPont Thermogravimetric Analyzer, as previously modified by Dobner, has been perfected for rapidly changing gas atmosphere and for conducting a large number of reaction cycles with different gas atmospheres within one day's operation.

We have examined two reaction cycles for removing sulfur species from a gas mixture at high pressure:

1. Half-calcined dolomite for removal of hydrogen sulfide:

$$[CaCO_3+MgO] + H_2S = [CaS+MgO] + H_2O + CO_2 \qquad (D)$$

$$[CaS+MgO] + H_2O + CO_2 = [CaCO_3+MgO] + H_2S. \qquad (B)$$

The major result for this cycle has been to show that higher temperatures for the absorption, reaction (D), and lower temperatures for the regeneration, reaction (B), tend to reduce the steady, "final" absorptive capacity of the solid for hydrogen sulfide after a number of cycles have been made (in general, about seven). Expressions of the Arrhenius type (see Section 6.05) were found to correlate final absorption capacity with temperature of each of the two reactions of the cycle.

A lead was obtained late in the research suggesting further study varying the composition of steam/CO_2 mixtures used for reaction (B). Such study may reveal a special composition that affords significantly higher final absorption capacities than we

have yet been able to achieve.

2. Magnesium oxide for removal of sulfur dioxide:

$$MgO + SO_2 + 1/2\ O_2 = MgSO_4 \qquad (F)$$

$$MgSO_4 + H_2\ (\text{or } CO) = MgO + SO_2 + H_2O\ (\text{or } CO_2) \qquad (G)$$

Our research has given the first data we know of for this cycle, and has given strong signs that it can be conducted repeatedly, indefinitely, with no permanent damage to the solid that would lead to loss of absorptive capability of the MgO.

Our data point to a temperature between about 750°C and 900°C for the absorption step, reaction (F), whose rate appears to be determined by diffusion through a product layer of $MgSO_4$. The effective diffusivity of reacting gases through this layer is so low -- less than about 0.2% of the diffusivity in open space -- that the practical use of the cycle is probably limited to relatively small particles, for example, of about 50 micrometers.

Our data show that the regeneration step, reaction (G), should be conducted at 900°C or above. The rate of this step is strongly influenced by temperature, higher temperatures giving higher rates.

We have found that the absorption, reaction (F), is strongly catalyzed by platinum and palladium, and this finding is a lead for further work to identify cheaper catalysts, iron oxide being a good candidate for study.

Acknowledgments

I thank Professors Arthur M. Squires and Robert A. Graff for their guidance and interest. Dr. Melvyn Pell of Conoco Coal Development Company, Dr. Lawrence A. Ruth of Exxon Research & Development Corporation, and Dr. Samuel Dobner of Coalcon, Inc. gave valuable suggestions.

Dr. Richard D. Harvey and his colleagues of the Illinois State Geological Survey provided substantial help in the research. They furnished starting solid materials for some of the experiments.

Help from shop personnel of the Chemical Engineering Department, working under Mr. John Bodnaruk's supervision, is also deeply appreciated.

Research Project EP4-3 of the Empire State Electric Energy Research Corporation supported a major part of this work.

Special thanks goes to my wife, Nancy, for her patience and encouragement.

Presentations and Publications

Some of the results reported herein have been presented as follows:

Arthur M. Squires, "The City College Clean Fuels Institute: Programs for (I) Gasification of Coal in High-Velocity Fluidized Beds and (II) Hot Gas Cleaning," presentation at Symposium Clean Fuels from Coal, Institute of Gas Technology, June 23-27, 1975, Chicago, Illinois. Published in the volume of papers from the Symposium, pp. 681-731.

Arthur M. Squires, "Studies of Hot Gas Cleaning," presentation at University Contractors Conference, University of Utah, held at Park City, Utah, October 22-23, 1975.

Samuel Dobner, George L. Kan, Robert A. Graff, Arthur M. Squires, "Modification of a Thermobalance for High Pressure Process Studies," paper 68d presented at the 68th Annual AIChE Meeting, Los Angeles, California, November 16-20, 1975.

Robert A. Graff, George L. Kan, and Arthur M. Squires, "Cyclic Studies of Magnesium Oxide as a Sulfur Acceptor at Elevated Pressure," the Proceedings of the Fourth International Conference on Fluidized Bed Combustion, Dec. 9-11, 1975, McLean, Virginia, pp. 45-53, the MITRE Corp. (1976).

Samuel Dobner, George L. Kan, Robert A. Graff, Arthur M. Squires, "A Thermobalance for High Pressure Process Studies," Thermochimica Acta, 16, 251-265 (1976).

George L. Kan, Arthur M. Squires, Robert A. Graff, "High Pressure TGA Studies on the Cyclic Use of Half-Calcined Dolomite to Remove Hydrogen Sulfide," Preprints Division of Fuel Chemistry, 172nd Meeting ACS, San Francisco, California, August 29-September 3, 1976.

Richard D. Harvey, George L. Kan, Robert A. Graff, Arthur M. Squires, "Behavior of Dolomite in Absorption of H_2S from Fuel Gas," World Mining and Metals Technology, 1, 163-188, Amer. Inst. of Mining, Metallurgical and Petrochemical Engineers, New York, N.Y. (1976).

TABLE OF CONTENTS

Table of Contents (cont.) Page

Table of Contents (cont.) Page

Table of Contents (cont.)

List of Tables

List of Figures

List of Figures (cont.) Page

List of Figures (cont.) Page

List of Figures (cont.) Page

List of Figures (cont.) Page

List of Figures (cont.) Page

List of Figures (cont.) Page

List of Figures (cont.) Page

1.0 General Introduction

1.01 The Problem of Sulfur in Fossil Fuels

Presence of sulfur in fossil fuels creates problems in their combustion for generating electricity, both from corrosion of power-plant equipment and from pollution of the atmosphere. For several decades, the electricity industry has studied and implemented measures for dealing with these problems, for example:

(1) Combustion of oil with lowered excess air to reduce formation of sulfur trioxide that corrodes cold-end boiler equipment when stack temperature falls below the sulfuric acid dewpoint.

(2) Development of electrostatic precipitators of efficiency beyond 99% in order to remove the fine particulate matter on which sulfur trioxide and sulfuric acid tend to concentrate. The late John J. Grob of Consolidated Edison Company of New York played an important role in pioneering precipitators of higher efficiency in the 1950's.

(3) Devising and testing, often with disappointing results, a rich variety of approaches to the scrubbing of sulfur dioxide from stack gas.

(4) Mechanical cleaning of coal to reduce pyritic sulfur.

(5) Hydrogenation of fuel oils to reduce sulfur.

(6) Solvent refining of coal and other approaches to reducing organic sulfur in coal through action of hydrogen gas.

In recent years, two-stage combustion has received increasing attention as another approach to the sulfur problem. The fuel gases from the first stage of two-stage combustion contain sulfur primarily in form of hydrogen sulfide. This can be removed from the fuel gases by a variety of chemistries, which at least some engineers regard in general to be "easier" to implement than the chemistries under consideration for removing sulfur dioxide.

Two-stage combustion in power generation is, of course, an old idea. Before electricity-generating installations reached a scale appropriate for use of a steam turbine, the combination of a gas producer and gas engine competed, both in cost and thermal efficiency, with the combination of a steam boiler and reciprocating steam engine. What is today called "low-Btu gas" was then called power gas. A few French installations provided iron oxide boxes to remove hydrogen sulfide before the power gas was supplied to the engine, but the prevailing opinion was that presence of hydrogen sulfide could not harm an Otto engine (1). The early French experiment, however, demonstrated in principle an approach to the suppression of sulfur emissions from power generation that has recently attracted strong advocates.

Two-stage combustion under pressure is an approach to the firing of a gas turbine with coal or heavy residual oil.

Another potential solution to the sulfur problem is seen in newly appreciated techniques for burning fuels in fluidized beds. Combustion in fluidized beds is old art for the petroleum, metallurgical, and chemical process industries, and is finding increasing favor as an approach to elimination of many wastes.

A number of approaches to fluidized bed combustion of coal and residual fuel oil are under examination, and each deserves the attention of the electricity industry:

(1) The "classic" fluidized bed boiler is a bubbling bed of either inert solid or of an active solid, such as limestone, for capture of sulfur dioxide. This has been investigated by Pope, Evans and Robbins of Alexandria, Virginia, the British National Coal Board, Raymond Hoy and his team at BCURA Industrial Laboratories at Leatherhead, England, Exxon Research and Engineering, Argonne National Laboratories, and others. Heat-exchange tubes are placed in the bed, generally for raising steam, to control the temperature of the bed.

(2) The "fast fluidized bed" (2) is under study at The City College Clean Fuels Institute, Battelle Memorial Institute, and elsewhere. The advantage of the fast bed is that the coefficient for transfer of heat from the bed to steaming tubes placed in the bed can be varied independently of the fluidizing-gas velocity, and this gives the operator another handle on bed temperature, permitting him to turn down the equipment without large changes of solid inventory. Another advantage of the fast bed is that a finely divided solid can be used to accept sulfur dioxide, and this is in general conducive to better acceptor utilization.

(3) Shallow fluidized bed combustion devices were invented and studied by the late Professor Douglas Elliott of

the University of Aston in Birmingham, England. Early payoffs for these devices are probably to be found in small-scale applications. Nevertheless, easy turndown of heat removal suggests that they may find application in large-scale equipment as heat-removal zones in heat communication with more conventional fluidized bed combustion zones.

Squires (3) has reviewed these various types of fluidized beds and their application to combustion.

Fluidized bed combustion under pressure is a second approach to the firing of a gas turbine with coal or heavy residual oil.

1.02 Motivation of the Research Reported Here

The approaches to the problem of sulfur as well as the needs of the electricity industry are so many and various that only a foolish person would insist today upon one single solution, or even upon a small family of solutions. A number of the techniques now under consideration may survive, in some form, in various commercial embodiments for various of the industry's needs.

The research reported here was motivated by the broad idea that the electricity industry needs ways to burn coal in a gas turbine.

Evidence of the value of gas turbines to the industry is to be seen, quite simply, in the record of its purchases of these machines. Uncertain supplies of clean gaseous and liquid fuels is a threat to the industry's future reliance upon gas turbines.

As noted earlier, one approach to use of coal in a gas turbine is two-stage combustion under pressure. Hydrogen sulfide

and particulate matter would be removed from fuel gas between a gasification step and a combustion step, both conducted at elevated pressure.

Although technologies exist for removing contaminants from fuel gas at near atmospheric temperature, the interest of The City College Clean Fuels Institute has been to examine possibilities for new technologies whereby hydrogen sulfide and dust would be removed at elevated temperature, thereby achieving a significant improvement in thermal efficiency of a combined-cycle power system (4).

In accord with this interest, one aspect of the present research has been to study use of half-calcined dolomite to remove hydrogen sulfide from a fuel gas at elevated pressure and elevated temperature. Work with half-calcined dolomite occupied the major part of the time devoted to this research.

The second approach to firing coal for a gas turbine, noted earlier, depends heavily upon finding a suitable solid acceptor for the sulfur dioxide generated within the fluidized-bed combustion under pressure. A minor part of the time available for the research was spent exploring use of magnesium oxide to remove sulfur dioxide from combustion gases.

In both studies, the solid acceptors were used cyclically in repeated absorptions of either hydrogen sulfide or sulfur dioxide, each absorption step being followed by a regeneration step to restore the original solid. The regeneration step is devised to provide sulfur in form of hydrogen sulfide, which can readily be converted to elemental sulfur by the well-known Claus process.

To sum up: The research reported here is intended to be a contribution toward solutions of the specific problem of burning coal under pressure with use of a regenerable solid acceptor to capture sulfur species at elevated temperature and thereby to limit their release to the environment, either as sulfur dioxide or as a solid waste.

1.03 Organization of This Thesis

Part I deals with half-calcined dolomite as an acceptor for hydrogen sulfide, and Part II treats magnesium oxide and its reaction with sulfur dioxide. The two Parts can be read independently, according to the reader's interest in gasification or combustion respectively.

For convenient reference, the sections of the thesis are numbered consecutively throughout both Parts.

Part I: CYCLIC USE OF HALF-CALCINED DOLOMITE FOR REMOVAL OF HYDROGEN SULFIDE FROM FUEL GASES AT ELEVATED PRESSURE

2.0 Introduction to Part I

2.01 Clean Power Systems Using Dolomite as Sulfur Acceptor

Dolomite is a true chemical species, $CaCO_3 \cdot MgCO_3$.

We express half- and fully-calcined dolomite by the formulas $[CaCO_3+MgO]$ and $[CaO+MgO]$ respectively, to indicate that each solid comprises an intimate intermingling of microscopic crystallites of MgO and the respective calcium compound.

There is no volume change, nor indeed any change of particle shape, when dolomite is calcined gently to produce $[CaCO_3+MgO]$.

The same may be said if dolomite is calcined to produce [CaO+MgO] at a temperature below about 1000°C. The molecular volume of $CaCO_3 \cdot MgCO_3$ is about 64.2 cm^3/g-mole. It is sufficient to consider the following molecular volumes,

MgO: 11.05 cm^3/g-mole,

CaO: 16.9 cm^3/g-mole,

$CaCO_3$: 36.9 cm^3/g-mole,

to understand that both half- and fully-calcined dolomite are porous and display appreciable internal surface.

The molecular volume of CaS is 25.8 cm^3/g-mole. Squires (5) proposed in 1966 that half- or fully-calcined dolomite might be advantageously used in clean power systems as an acceptor for hydrogen sulfide from the first, gasification stage of a two-stage combustion. His 1966 paper gave data showing that fully calcined dolomite can be converted in good yield to [CaS+MgO] and regenerated by action of steam and carbon dioxide at elevated pressure followed by a calcination. The reaction sequence is:

$$[CaO+MgO] + H_2S = [CaS+MgO] + H_2O \quad (A)$$

$$[CaS+MgO] + H_2O + CO_2 = [CaCO_3+MgO] + H_2S \quad (B)$$

$$[CaCO_3+MgO] = [CaO+MgO] + CO_2 \quad (C)$$

He obtained dry effluent gas from reaction (B) containing 20 to 24% hydrogen sulfide, levels satisfactory for a conventional Claus system to convert this species to sulfur.

Although Squires (5) contemplated use of half-calcined dolomite as an acceptor for hydrogen sulfide, it remained for Ruth et al. (6) in 1970 to demonstrate the reaction

$$[CaCO_3+MgO] + H_2S = [CaS+MgO] + H_2O + CO_2 \quad (D)$$

This can be followed by reaction (B), which of course is the reverse of reaction (D), to restore the starting solid material.

Graff et al. (7) in 1970 elaborated a number of clean power systems employing the two cyclic chemistries:

1. The fully-calcined dolomite cycle:
   Reactions (A), (B), and (C).
2. The half-calcined dolomite cycle:
   Reactions (D) and (B).

Figure 1 is from their paper, and schematically illustrates use of the half-calcined dolomite cycle together with a panel bed filter (8, 9) for simultaneous removal of dust and sulfur species from a fuel gas ahead of a combustion to supply hot gases to a gas turbine.

Conoco Coal Development Company has worked for several years on a process employing the half-calcined dolomite cycle (10). The half-calcined dolomite is fluidized in a reactor by fuel gas which is produced by gasification of coal fluidized by air and steam within another reactor. The hydrogen sulfide generated by coal gasification reactions is captured by the half-calcined dolomite fluidized bed. The bed is at elevated pressure and is intended to supply fuel gas for combustion ahead of a gas turbine.

Westinghouse Electric Corporation has also worked on a system employing the half-calcined dolomite cycle (11). The half-calcined dolomite acceptor is present in a fluidized bed of coal undergoing carbonization. Since this bed is fluidized by fuel gases from a gasification bed that receives char from the carbonization bed, hydrogen sulfide evolved both from carbonization and from the upstream gasification stage are removed by the acceptor. Like the Conoco System, the process would work at elevated pressure to supply fuel gas to a gas turbine.

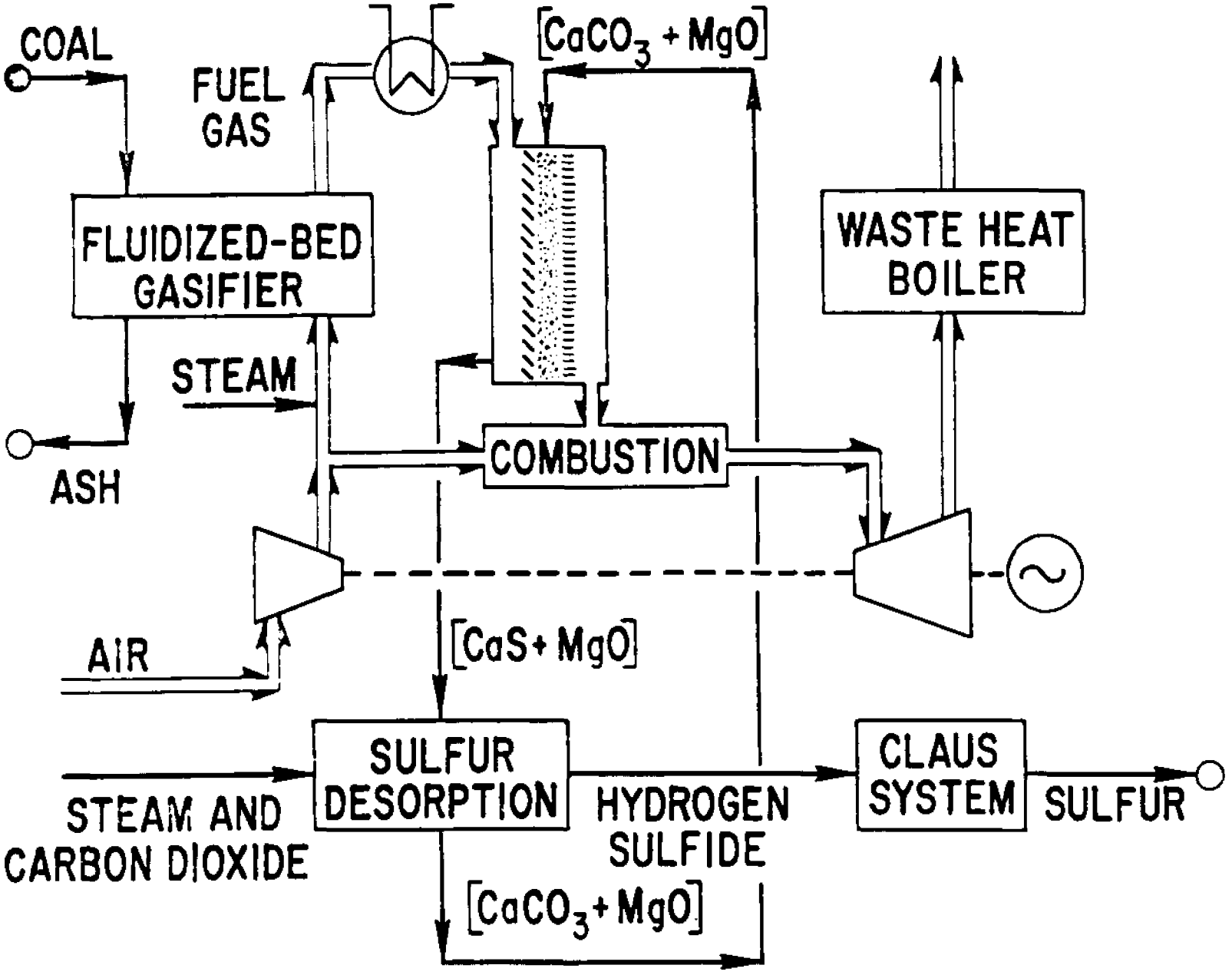

Figure 1. Concept for power generation by combined-cycle system incorporating a fluidized-bed gasifier for coal and a panel-bed filter for simultaneous removal of dust and sulfur.

Air Products, U.S. Steel, Heurtey of France, and others have also worked in recent years on fuel generation schemes employing one or the other of The City College dolomite acceptor cycles.

2.02 Status of Work on Dolomite Cycles

Research efforts at The City College Clean Fuels Institute have provided differential reaction kinetic information on reactions (A) and (D) at atmospheric pressure (6, 12-15), and to a limited extent on reaction (B) (14) and reaction (C) (16).

Workers at Westinghouse (17, 18) have provided a limited amount of differential reaction kinetic data for the half-calcined dolomite cycle, reactions (D) and (B), working at 10 atmospheres. However, the regeneration reaction (B) was conducted at partial pressures of steam and carbon dioxide of only 1 atmosphere each. This limit on the partial pressures of the regenerating gases put a limit on the equilibrium content of hydrogen sulfide that might be realized from reaction (B). The Westinghouse data confirmed The City College results indicating that sulfur absorption reaction (D) is a lively reaction. The data were characterized by a decline in conversion of calcium sulfide to calcium carbonate with number of absorption-regeneration cycles. In one example, the conversion dropped from 68% for the first regeneration by reaction (B) to about 12% after 21 cycles.

Conoco's effort (10) has provided practical integral reaction kinetic information for the half-calcined dolomite cycle with both reactions being conducted in fluidized beds at 15 atmospheres. Conoco also experienced sharp decline in the acceptor's capacity to absorb hydrogen sulfide after a number of cycles.

Westinghouse (11) has reported that reaction (B) is lively for a wide variety of dolomitic stone, and practical tests at ERDA's research center at Morgantown, West Virginia, have confirmed the liveliness of the reaction in removing hydrogen sulfide from producer gas (19).

The disappointing decline in acceptor capacity in Conoco's tests parallels Conoco Coal Development Company's earlier experience with declining capacity when calcined dolomite is used cyclically to accept carbon dioxide in this company's Carbon Dioxide Acceptor Gasification Process*. This process uses the cycle:

$$[CaCO_3+MgO] = [CaO+MgO] + CO_2 \qquad (C)$$

$$[CaO+MgO] + CO_2 = [CaCO_3+MgO] \qquad (E)$$

We had thought the decline in capacity that Conoco had experienced was brought about by the high temperatures, generally beyond 1,040°C, that are used in Conoco's gasification process for the calcination reaction (C). In 1971, L. Sterns, a Senior in Chemical Engineering at The City College, conducted work at atmospheric pressure on the simple calcination and recarbonation cycle, reactions (C) and (E), but limiting the calcination temperature to about 925° to 975°C. Sterns experienced a decline in capacity even at these lower temperatures for the calcination, and Dobner (16) extended Sterns' data to higher pressures, with similar results.

---

*Conoco Coal Development Company was formerly called Consolidation Coal Company.

2.03 Aims of this Research

The principle aims of the research were:

(1) To obtain the first differential reaction kinetic data for the half-calcined dolomite cycle when it is conducted repeatedly at elevated pressure, up to about 20 atmospheres, with steam and carbon dioxide present in regeneration reaction (B) at partial pressures also appreciably beyond atmospheric pressure.

(2) To explore the decline in capacity of the regenerated half-calcined dolomite to absorb hydrogen sulfide after a number of cycles as a function of temperature and pressure level and composition of the gas mixtures used.

Of these aims, we regarded (2) as the most important. Our hope at the outset of the research was to identify the most favorable combination of temperatures, pressure level, and composition of gas mixtures from standpoint of preserving a high capacity of the acceptor to absorb hydrogen sulfide.

2.04 Experimental Approach

The reactions to be studied produce weight changes of the solids. Capacity and reactivity data can be readily obtained by continuously recording the weight of the solid during its reaction.

A mixture of the desired reaction gases was premixed and then passed over the solid at a sufficient rate to prevent any substantial change in the composition of the mixture. The composition of the gas mixture was in accordance with thermodynamic data such that only a single reaction could occur. Fine powders were used in most of the experiments to minimize interference from diffusion effects.

A modified duPont 950 Thermogravimetric Analyzer (TGA) was used, capable of operating at high pressure with high partial pressures of steam and with corrosive gases also present. The TGA can continuously record the weight of the solid versus time for an isothermal run, or weight versus temperature in nonisothermal operation. A digital temperature indication was provided.

2.05 Reporting of Results

The report here emphasizes the capacity history of the solid reactant after many cycles. Rate information is also given.

Effects of pressure, temperature, and gas composition are discussed.

3.0 Supporting Data

3.01 Previous Related Work

Ruth (6, 15) conducted experiments on absorption of hydrogen sulfide by half-calcined dolomite at atmospheric pressure. He investigated temperatures from 550° to 800°C for partial pressures of hydrogen sulfide from 0.005 to 0.2 atmospheres. Carbon dioxide was present in sufficient amount to prevent dissociation of calcium carbonate, and hydrogen was present in an amount to prevent dissociation of hydrogen sulfide.

Ruth found the reaction of hydrogen sulfide with half-calcined dolomite to be extremely fast, indeed, faster than the reaction of hydrogen sulfide with fully-calcined dolomite. For example, at 800°C and 0.05 atmosphere hydrogen sulfide, half-calcined dolomite achieves 50% conversion to [CaS+MgO] in only 14 seconds, while the fully-calcined dolomite requires 280 seconds. As a further example of the comparison of the reactivity of half- and fully-calcined dolomite, Figure 2 illustrates the course of the reaction of half- and fully-calcined dolomite at atmospheric pressure with a gas containing 5% hydrogen sulfide.

Working at The City College in 1972, J. Singh conducted six half-calcined dolomite cycles at atmospheric pressure. Figure 3 shows Singh's data. The most striking feature of the data is the decline in capacity of the solid to absorb hydrogen sulfide. After six cycles, it could absorb only about 35% as much sulfur as its stoichiometric content of calcium would suggest. On the other hand, the initial rates of both reaction (D)

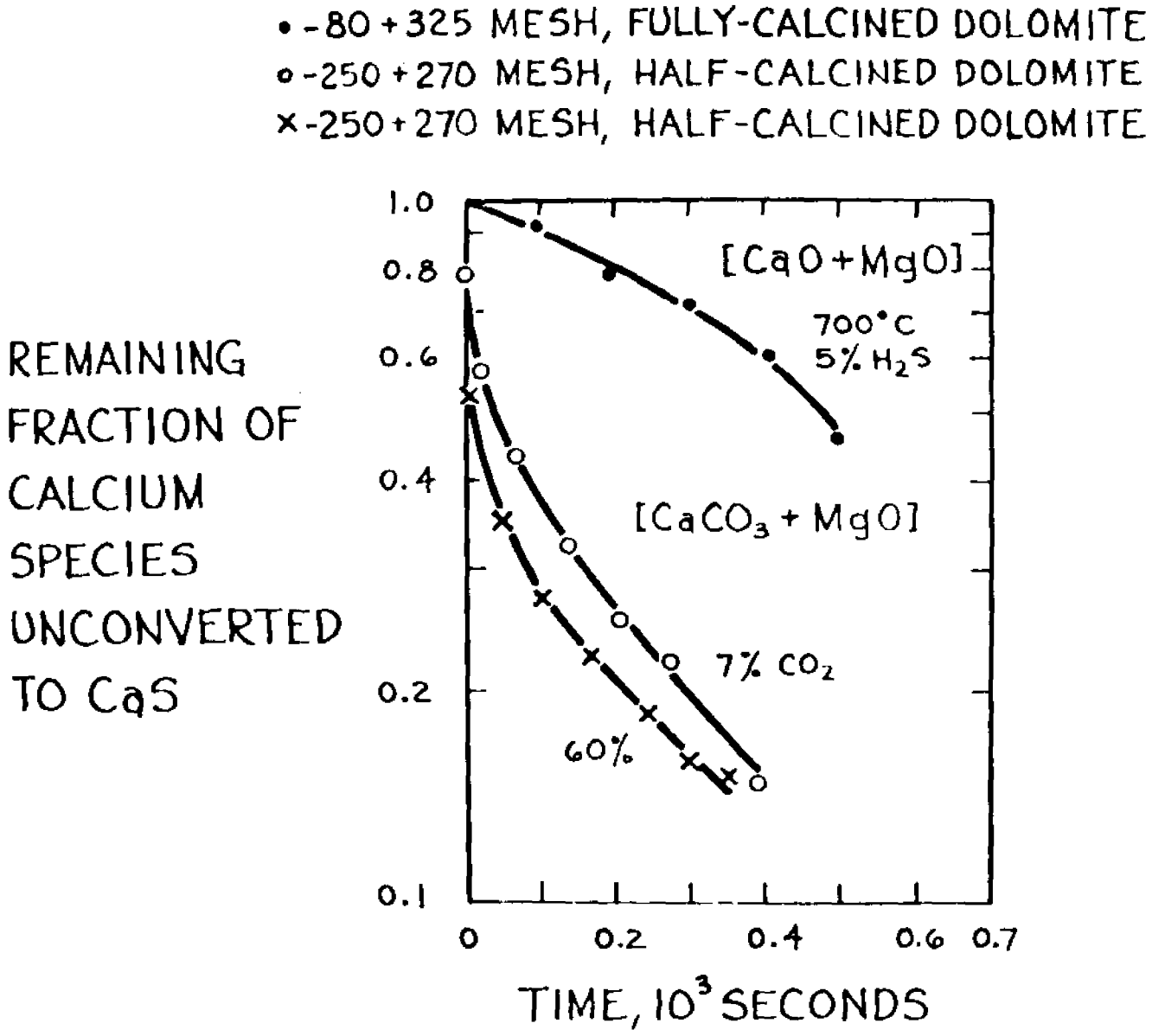

Figure 2. Comparison of reactivities of half- and fully-calcined dolomite at atmospheric pressure and 700°C. Gas contained 5% hydrogen sulfide.

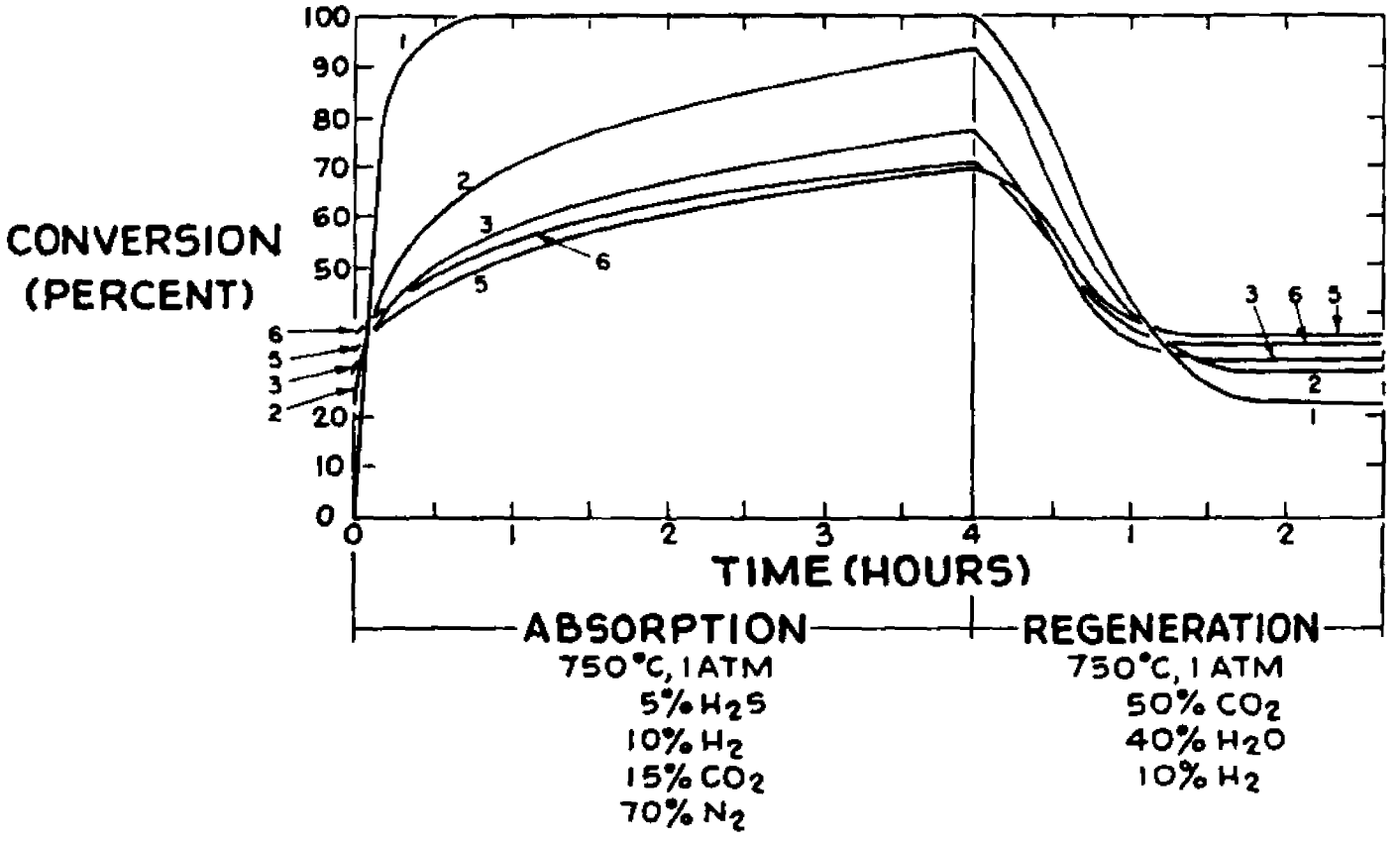

Figure 3. The City College data for the half-calcined dolomite cycle at atmospheric pressure. The numbers alongside the curves indicate the order of the six reaction cycles.

seen at the left in Figure 3, and reaction (B), seen at the right, do not change much with cycling.

As mentioned earlier, Westinghouse (17, 18) reported limited differential reaction kinetic data for the half-calcined dolomite cycle at 10 atmospheres, but with partial pressures of steam and carbon dioxide of only 1 atmosphere each in the regeneration reaction (B). Absorptions were typically at about 870°C, and regenerations were typically at about 700°C. The rate of the regeneration reaction (B) was about the same as in The City College data shown in Figure 3. Initial absorptions reached 50% conversion of the solid in about 5 minutes.

Figure 4 gives data obtained by Conoco Coal Development Company (20) in pilot-scale experiments on the half-calcined dolomite cycle conducted in fluidized beds. Plotted in Figure 4 are the calcium sulfide levels in the solid at the beginning and conclusion of each absorption step. The difference between the two curves plotted in Figure 4 is the capacity of the solid for absorbing hydrogen sulfide in the respective cycle. It will be seen that the capacity falls quickly to a low value, on the order of 10% of the stoichiometric capability of the stone, after the first cycle. The solid displays only 6% of its theoretical capacity at the end of the 12th cycle.

Pell (14) studied the fully-calcined dolomite cycle at 1 atmosphere using a sphere that was 0.65 cm in diameter. It is now surprising, in light of the foregoing data for the half-calcined dolomite cycle, to remark that the absorption capacity of Pell's stone remained steady at substantially 100% conversion to calcium sulfide even after 5 cycles carried out at 5 different

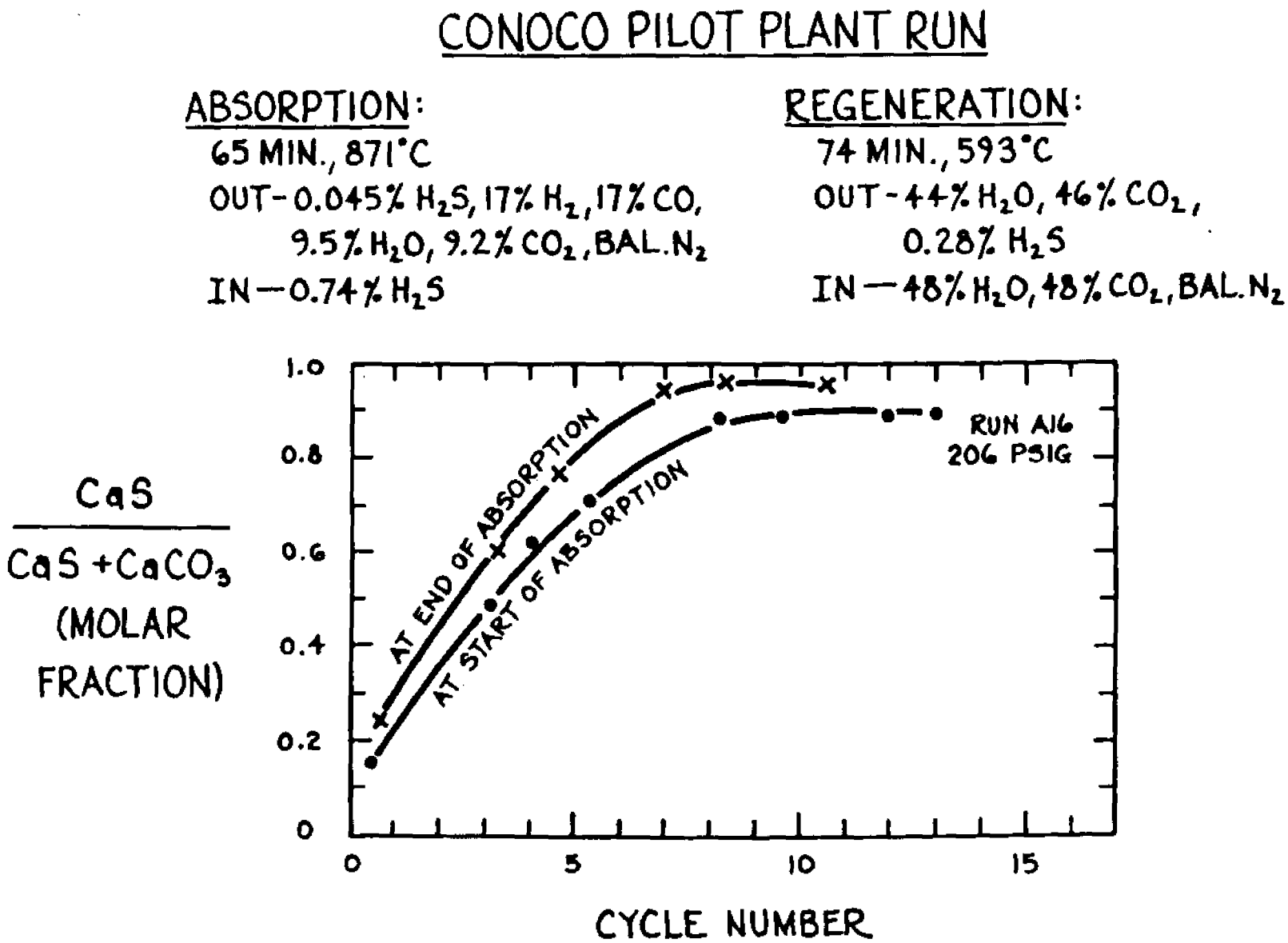

Figure 4. Data by Conoco Coal Development Company (21) for half-calcined dolomite cycle at 15 atmospheres.

temperatures. An Arrhenius plot of the apparent rate constants for the cycles would not suggest any drastic decline in reactivity between second and fifth cycles. There was an increase in reactivity as reflected in the reaction rate between the first and second cycles.

Sterns, as mentioned earlier, studied the cycle of full calcination and recarbonation of dolomite at atmospheric pressure. Figure 5 shows the course of five selected recarbonation steps from a run by Sterns at 700°C with 50/50 steam and carbon dioxide. As Figure 5 indicates, the capacity of the stone to absorb carbon dioxide fell to roughly 55% to 60% of the stoichiometric capability after 30 cycles, although the initial reaction rate for absorption of carbon dioxide by the solid remained substantially unchanged.

Dobner (16) conducted dolomite calcination-recarbonation cycles at elevated pressure, and showed that both his and Sterns' data for capacity to absorb carbon dioxide plot as straight lines versus the number of cycles, both variables being plotted on a logarithmic scale. Figures 6 and 7 give examples of Sterns' and Dobner's data plotted in this way. Figure 8 is Dobner's plot of earlier data from Conoco Coal Development Company (21, 22) for cyclic recarbonation of calcined dolomite in a continuous bench-scale process unit where the steps were conducted in fluidized beds, and it is seen that Conoco's data also give straight lines in the log-log plot. Dobner discussed alternative models that might explain the deactivation of the solid for the absorption reaction that Figures 6, 7 and 8 display.

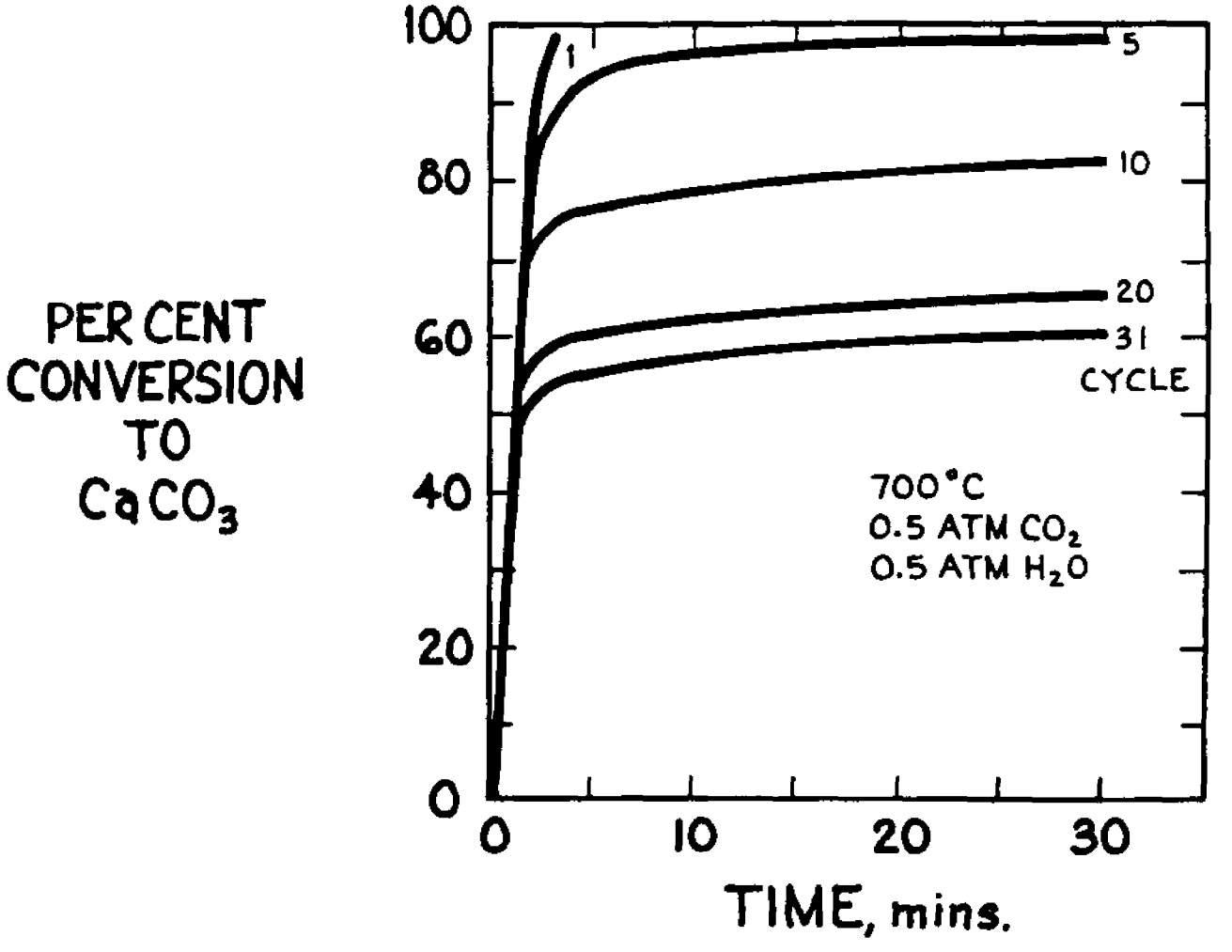

Figure 5. The City College data (L. Sterns) for recarbonation of fully-calcined dolomite at 700°C and 1 atmosphere with a 50/50 mixture of steam and carbon dioxide. After each recarbonation, the solid was calcined noniso-thermally at a heating rate of 10° to 15°C per minute, carried to 925°C in 1 atmosphere of carbon dioxide, the sample being finally held at 925°C in nitrogen for an additional 15 to 30 minutes before being cooled to 700°C for the next recarbonation.

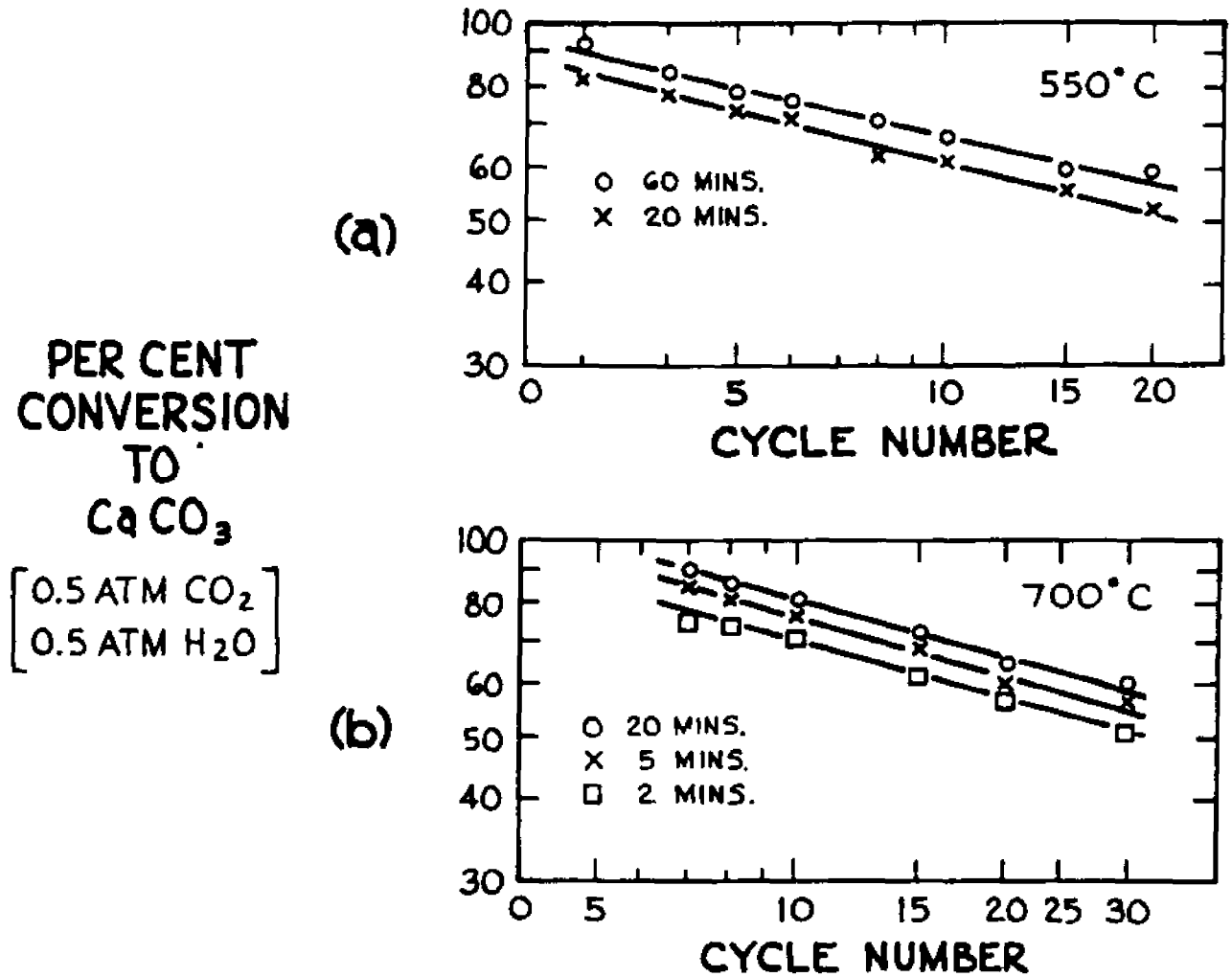

Figure 6. The City College data (L. Sterns) for cyclic recarbonation of calcined dolomite at atmospheric pressure in 50/50 mixture of steam and carbon dioxide at (a) 550°C and (b) 700°C.

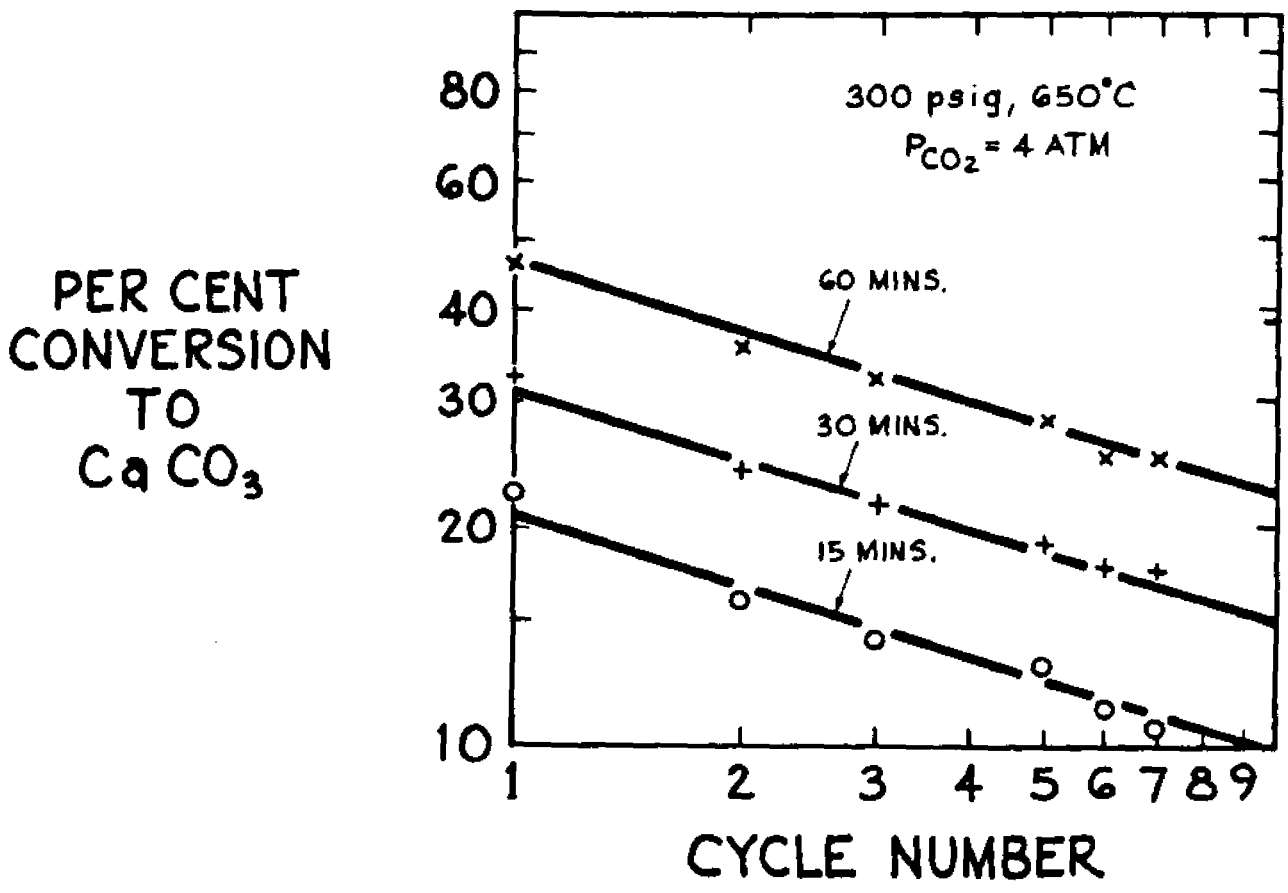

Figure 7. The City College data (16) for cyclic recarbonation of calcined dolomite at 21 atmospheres, 650°C, with 4 atmospheres partial pressure of carbon dioxide.

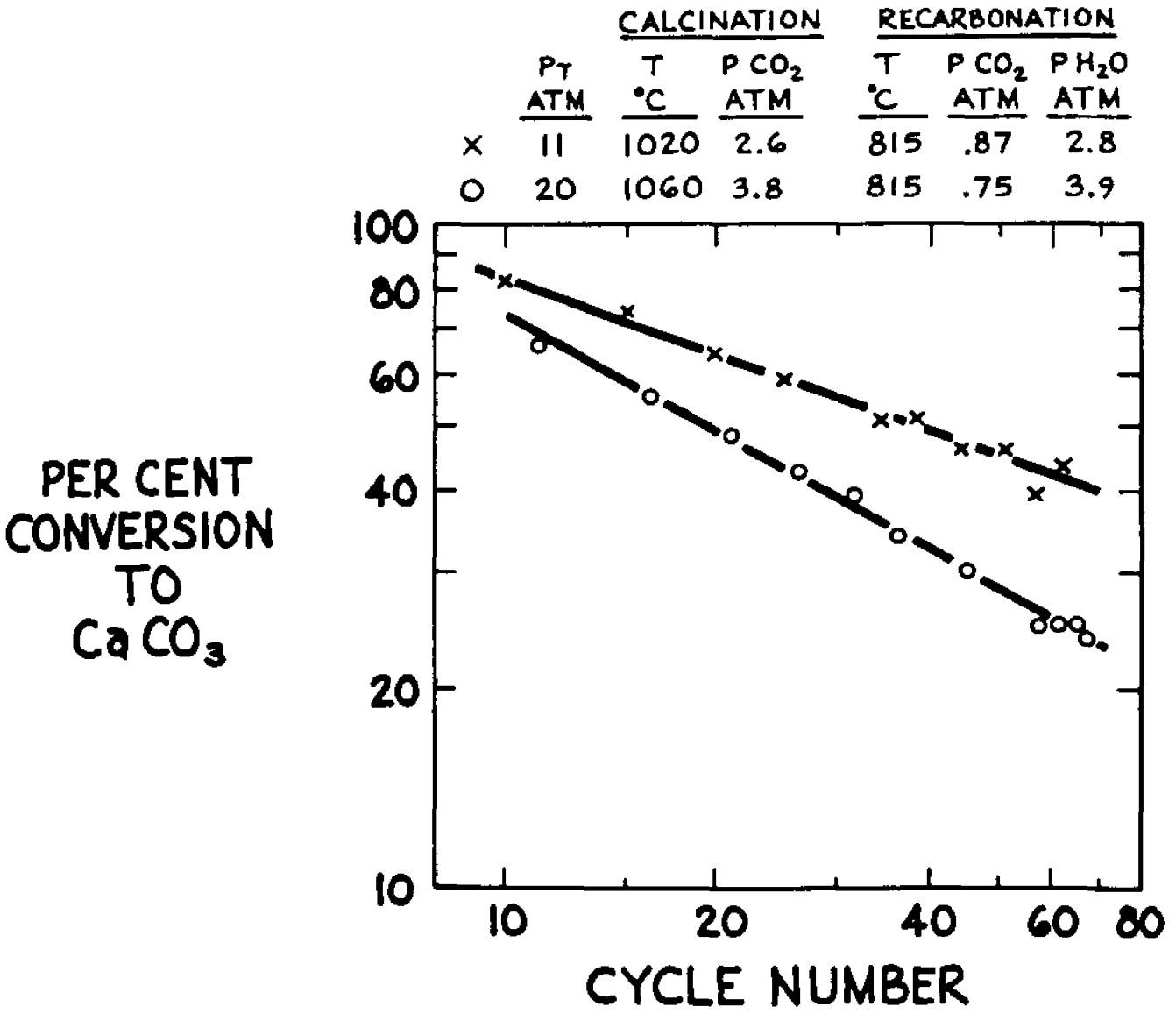

Figure 8. Conoco Coal Development Company's data (21, 22) for cyclic recarbonation of calcined dolomite under the conditions noted in a continuous bench-scale process unit where the steps were conducted in fluidized beds.

3.02 Review of Dolomite Chemistry

Squires (5) reviewed the literature before about 1966 on dolomite chemistry relating to the present research. Dolomite is a true chemical species, $CaCO_3 \cdot MgCO_3$. It is a member of a class of rhombohedral carbonates, which includes calcite ($CaCO_3$) and magnesite ($MgCO_3$). These carbonates are built of alternating layers of carbonate ions and cations. In dolomite, ideally, cation planes populated entirely by Mg^{++} alternate with planes populated entirely by Ca . Natural dolomite often diverges from the ideal of one atom of magnesium for each atom of calcium, the latter being present in excess. True dolomites richer in magnesium are seldom, if indeed ever, encountered.

Dolomite is a common rock of wide distribution throughout the world, and often occurs in a state of high purity. In the United States and Canada, important dolomitic deposits exist in Ohio, California, Wisconsin, Pennsylvania, Nevada, Utah, Illinois, Connecticut, Massachusetts, Ontario, and Quebec.

Dolomite decomposes in two steps when heated gently under moderate carbon dioxide pressures. The first stage of dolomite decomposition, which is believed to be a diffusion controlled process, produces an intermingling of microscopic crystallites of $CaCO_3$ and MgO. At a higher temperature, which corresponds to the equilibrium decomposition temperature of calcium carbonate at the prevailing partial pressure of carbon dioxide, the second stage of decomposition occurs.

The decomposition of calcium carbonate to calcium oxide and carbon dioxide is readily reversible, but the decomposition of magnesium carbonate is not. Magnesium carbonate shows no tendency to react with carbon dioxide at the experimental conditions used in this research. It should be pointed out, however, that magnesium oxide takes up carbon dioxide readily at room temperature in the presence of water vapor.

There is no volume change, nor indeed any change of particle shape, when dolomite is calcined gently to produce [$CaCO_3$+MgO]. The same may be said if dolomite is calcined to produce [CaO+MgO] at a temperature below about 1000°C.

Except at low carbon dioxide partial pressures, the application of heat decomposes dolomite in two stages. At the rather high temperatures and moderate carbon dioxide pressures typical of a calcination process, the calcite produced at the first stage is essentially pure calcium carbonate. On the other hand, if dolomite is decomposed at extremely high carbon dioxide pressures, the product consists of a mixture of crystallites of magnesium oxide and crystallites of a magnesian calcite, i.e., a calcite containing magnesium carbonate in solid solution.

If the first stage of calcination is conducted at around 600°C and 100 mm Hg of carbon dioxide, predominantly single-crystal x-ray patterns for calcite are to be seen, as if the calcite were present as crystallites oriented exactly in the same way as in the original lattice. At 800°C and 650 mm Hg of carbon dioxide, powder calcite x-ray patterns are seen, as if recrystallization and randomization of the calcite crystallites have occurred.

Haul (23) gave surface area and porosity data for half- and fully-calcined dolomite derived from a "dolomite" of unspecified analysis. The table below gives a comparison of Haul's porosity data at 800°C with "ideal" porosities calculated from molar volumes of the relevant chemical species (see page 7).

The comparison suggests that at least some of the pores in the materials prepared at 800°C may not be accessible.

	"Ideal" Porosity	Haul's Value
[CaO-MgO]	36.2 cm^3/g-"mole"	23.2 cm^3/g-"mole"
[$CaCO_3$+MgO]	16.2	10.8

Haul reported surfaces areas of half- and fully-calcined dolomite prepared at 800°C to be 6.7 and 56.2 m^2/gram respectively. The fully-calcined material showed a decline in surface area from 800°C to 1000°C, the value at the latter temperature being about 5 m^2/gram. Borgwardt and Harvey (24) gave a value of 4 m^2/gram for a solid prepared by fully calcining dolomite at 980°C for two hours.

Scanning electron microscope pictures of calcines show clearly the spongy, porous nature of the material. Fully-calcined dolomite has a granular structure in which small, roughly spherical calcium oxide grains appear to be distributed around larger grains of periclase (magnesium oxide). The calcium oxide grains occur in clusters which retain much of the granular character of the original stone, and many of the grains appear to be partly fused to the underlying grains of periclase. The grains have diameters of about 0.1 to 0.5 microns, while the clusters are generally 1 to 15 microns (25, 26).

3.03 Equilibrium Data and Reaction Conditions

Squires et al. (12) reviewed the thermodynamic data available relating to reactions (A) through (E) and gave expressions for the relevant equilibrium.

The equilibrium for reaction (A) is favorable for absorption of sulfur over a wide range of temperature:

$$\log_{10} [H_2O]/[H_2S] = 3,519.2/T - 0.268 \qquad (1)$$

where the brackets signify mole fraction and temperature T is in degrees Kelvin.

Equilibrium for reaction (D) is favorable for absorption of sulfur only at relatively high temperatures, above about 800°C.

$$\log_{10}[H_2O][CO_2]P/[H_2S] = 7.253 - 5,280.5/T \qquad (2)$$

where pressure P is in atmospheres.

The decomposition pressure of calcium carbonate, an expression of equilibrium for reaction (C), is given by

$$\log_{10} P_{CO_2} = -8,799.7/T + 7.521 \qquad (3)$$

Equilibria for reactions (B) and (E) are of course the negatives of expressions (2) and (3) respectively.

When reaction (B) is used to regenerate half-calcined dolomite, it must be carried out at elevated pressure to obtain a useful result, i.e., a sufficiently high concentration of hydrogen sulfide in the product gas, and is preferably conducted at as low a temperature as possible. In general, the practical efficacy of the half-calcined dolomite cycle is enhanced if

reactions (D) and (B) are conducted at as widely separated temperatures as possible. This means that reaction (D) should ideally be conducted at a temperature just below the temperature at which calcium carbonate would decompose, according to reaction (3), at the prevailing pressure of carbon dioxide in the fuel gas to be desulfurized. Reaction (B) should be conducted at as low a temperature as practicable kinetic limitations will allow. One object of the present research has been to shed light upon what this lowest practicable temperature for reaction (B) might be.

It should be noted that equilibrium for conversion of magnesium oxide to magnesium sulfide is unfavorable at all reaction conditions of practicable interest, since the presence of even a relatively small content of water vapor in the fuel gas to be desulfurized will prevent this conversion. As Ruth (15) discovered, however, the conversion can occur in a laboratory kinetic experiment if a simulated fuel gas is used in the experiment that is too dry. The experimentalist, therefore, needs to keep his eye on the equilibrium for this conversion, given in Table 1 (15), and maintain a steam level to prevent formation of magnesium sulfide in his experiment. Ruth calculated the values in Table 1 from the JANAF Tables.

Hydrogen sulfide can dissociate to a significant extent at typical reaction temperatures for the experiments. The JANAF Tables give equilibrium constants for formation of hydrogen sulfide from hydrogen and S_2 vapor, and these constants were used to calculate concentrations of hydrogen needed to limit the dissociation of hydrogen sulfide.

Table 1

Equilibrium Constant for the Reaction

$$MgO_{(s)} + H_2S_{(g)} = H_2O_{(g)} + MgS_{(s)}$$

$T^{\circ}K$	K_p
700	0.0047
800	0.0092
900	0.0154
1000	0.0230
1100	0.0317
1200	0.0412
1300	0.0511

4.0 Theoretical Background

4.01 Noncatalytic Reaction of Gas and Solid

Reactions (B) and (D), the reactions of concern for this research, are of the general type

$$P(solid)+Q(gas) = R(solid)+S(gas)$$

In the general case for a bed of fine powder sample, reaction occurs in nine steps each capable of contributing to a concentration gradient. They are:

(1) Diffusion or gaseous reactant from the bulk of gas stream through a surrounding film to the surface of the bed of powder.

(2) Diffusion of gaseous reactants through bed to the individual particles.

(3) Diffusion of gaseous reactants through the micropores of the particle to the individual crystallites.

(4) Diffusion of gaseous reactant through the solid product layer of individual crystallites to the solid reactant.

(5) Chemical reaction of gaseous reactant with the solid reactant.

(6) Diffusion of gaseous products through the solid product layer to the surface of individual crystallites.

(7) Diffusion of gaseous products through the micropores back to the surface of individual particles.

(8) Diffusion of gaseous products through the bed back to the surface of the bed.

(9) Diffusion of gaseous products through the gas film back to the bulk of the gas.

Any one of the above steps may be rate limiting. However, no single step must necessarily be rate limiting throughout the complete extent of the reaction. Nor is the rate limiting step necessarily the same under different experimental conditions and different history of the solid (27).

A usual goal of kinetic research is to find a mathematical expression for reaction rate as a function of reaction variables such as time, temperature, pressure, gaseous concentration, solid conversion, etc. This goal, however, must be approached with extreme caution for a heterogeneous gas-solid reaction. It is not in general possible to make unequivocal interpretations of the reaction mechanism if a mathematical rate expression were to be given. First order gas-solid reactions, for example, may occur in a nucleation limited reaction of microcrystalline powders (28), or may result from an exponential particle size distribution together with a reaction that occurs in a shrinking core manner (29, 30).

It must be appreciated that the study of the noncatalytic reaction of a solid and a gas is generally much more difficult than study of catalytic systems, where a solid merely provides a surface on which a reaction can occur. In the former instance, the solid steadily loses active surface as the reaction proceeds, whereas a catalyst in general has a constant surface area. In noncatalytic systems of the type studied in this research, the overwhelming majority of reaction surface lies within the pores of each particle of solid. This is also a situation often faced in study of catalytic systems, but in our case, the internal pore structure of the solid does not remain constant, but changes with

time. For example, as a solit product forms, pores may be plugged, thereby sealing off reaction surface and stopping or greatly slowing the reaction.

The overall rate of noncatalytic solid-gas reactions in general, therefore, depends upon physical as well as upon chemical rate processes, and some of the physical rate processes are intimately related to the solit microstructure encountered during the course of the reaction. Even if, by judicious choice of experimental conditions, some of the diffusional steps enumerated above are eliminated or controlled so that their effect may be calculated, nevertheless, still other physical effects can remain to complicate the "true" chemical kinetics. This is what makes the study of noncatalytic solid-gas reactions so difficult.

In our research, the situation is further complicated by the fact that the physical condition of the solid reactant can be expected to change in some secular fashion with repeated use of the solid in the half-calcined dolomite cycle. Although the "true" chemical kinetic situation may remain a given, the changing physical structure of the solid may render the task of finding out these "true" kinetics doubly difficult.

In light of these considerations, the strategy selected for the present research has been to concentrate most effort upon the secular changes in the absorption solid, as reflected primarily by its capacity to absorb hydrogen sulfide in successive cycles and also, secondarily, by the initial rate of uptake of hydrogen sulfide or the initial rate of the regeneration reaction (B). Not only would the information obtained from this strategy have

the most practical value, from standpoint of development of a process for desulfurizing fuel gas, but also it could easily turn out that the information is a necessary prelude to any subsequent effort to discover "true" kinetics.

4.02 Ruth's Kinetic Curiosities for Reaction (D)

Although the temperature of technical interest for use of reaction (D) is around 800°C or higher, Ruth (6, 15) also studied the reaction at temperatures as low as 450°C in the hope that the results would shet light upon subsequent research planned for study of reaction (B).

The work at lower temperatures revealed kinetic curiosities that highlight the remarks of the preceding Section 4.01. A strong influence of carbon dioxide upon the course of reaction (D) was discovered. An example of this influence is shown in Figure 9. The reaction of a fresh sample of half-calcined dolomite with a gas containing 5% hydrogen sulfide "dropped dead" at a conversion of about 20 to 25% of the solid to calcium sulfide when the carbon dioxide pressure in the gas was 3% or 13%. At 30% carbon dioxide, the reaction proceeded a bit further, but at 60% carbon dioxide, the reaction proceeded rapidly to essentially full conversion.

Reference to Figure 2 illustrates that carbon dioxide also has an effect upon the course of reaction (D) at 700°C, although the effect is much less than at 600°C. The level of carbon dioxide partial pressure has essentially no effect upon the rate at 800°C.

Ruth (15) succeeded in correlating the initial rate of uptake of hydrogen sulfide by fresh half-calcined dolomite at temperatures

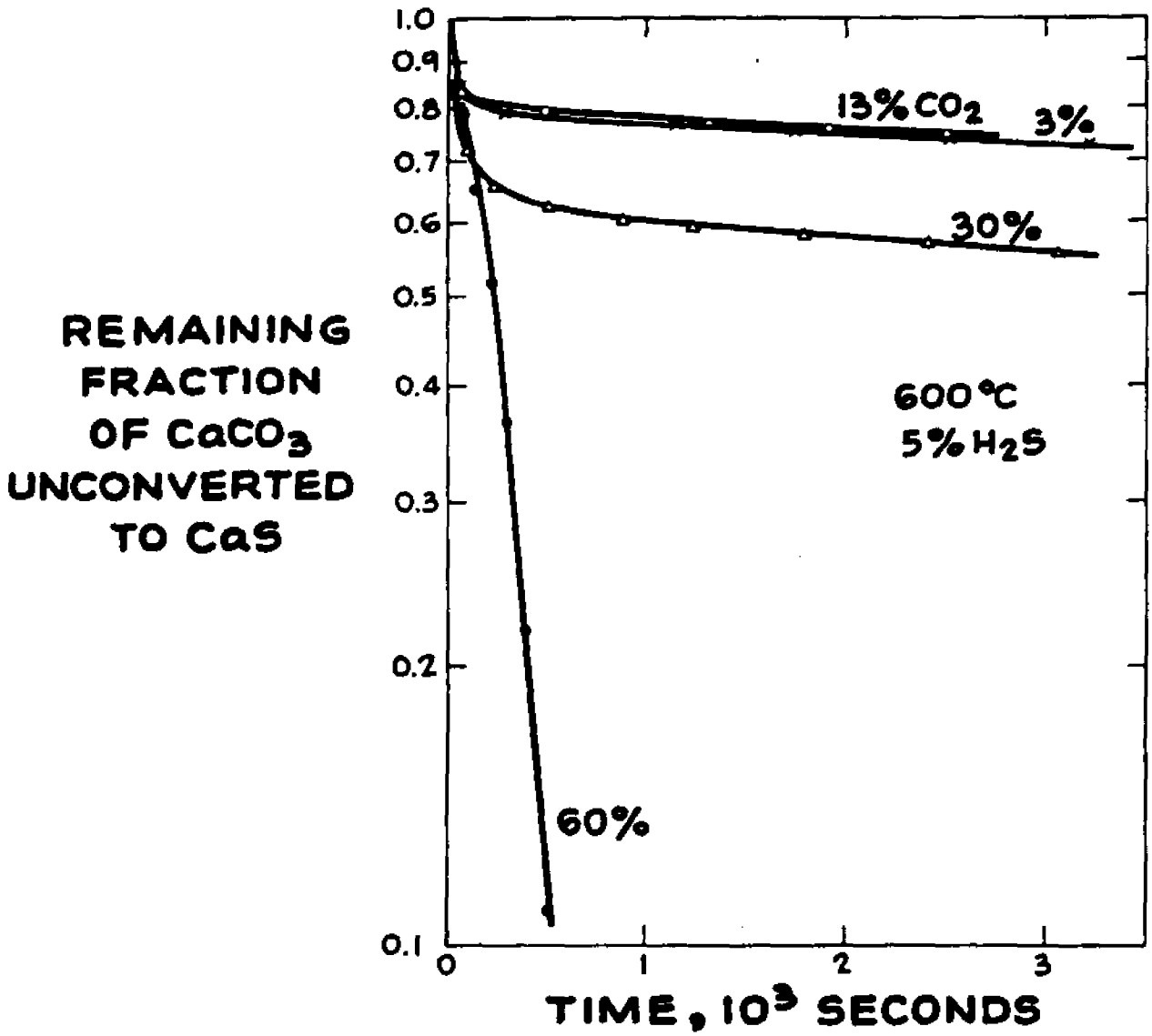

Figure 9. The City College data (6, 15) for reaction of fresh samples of half-calcined dolomite with gas containing 5% hydrogen sulfide and various levels of carbon dioxide at 600°C and atmospheric pressure.

below about upp°C. He found two distinct kinetic regimes at high and low partial pressures of carbon dioxide. The data for low carbon dioxide displayed half-order kinetics and an activation energy of 20.5 kilocalories/g-mole. The data for high carbon dioxide level displayed first-order kinetics and an activation energy of 37.7 kilocalories/g-mole.

Ruth remarked that the initial rate of uptake of hydrogen sulfide is greater at low carbon dioxide levels than at high levels if the temperature is around 600°C or below. The tendency for the absorption reaction at low carbon dioxide level to "drop dead" at a small conversion of calcium carbonate to calcium sulfide is greater the lower the temperature, and so is the degree to which the initial rate of absorption at low carbon dioxide is greater than the initial rate at high carbon dioxide.

From these facts, Ruth hypothesized that the explanation of the flagging of the absorption reaction at low temperatures and low carbon dioxide levels may be due to a blockage of the interior of a calcium carbonate crystallite by an impermeable layer of calcium sulfide product. Such a blockage might arise, for example, if the rate of progress of a reaction interface int the interior of a crystallite should outstrip a rate of "annealing" of the product layer, where such annealing is needed to produce porosity in this layer.

Ruth's hypothesis is of course an invitation to make physical inspections of solid products of reactions (B) and (D). A preliminary effort to inspect products of reaction (D), reported in the Appendix of Ruth's theis (15), suggested that high levels of carbon

dioxide at 600°C may promote formation of large numbers of fine crystallites of calcium sulfide that do not protect the underlying calcium carbonate from further reaction. It was suggested that carbon dioxide perhaps enhances nucleation of calcium sulfide crystals. On the other hand, the inspections made it appear that at low levels of carbon dioxide a smaller number of large calcium sulfide crystals form and grow together to close off the surface.

Examples are to be found in the literature for instances where the physical form of crystallites produced by a chemical reaction can depend upon the reaction environment. On example, of interest for the present research, was given by Bachmann and Cremer (31), whose electron microscopic examination of crystallites of magnesium oxide formed by decomposition of microcrystalline magnesium carbonate are different in character at high and low partial pressures of carbon dioxide. The microcrystalline magnesium carbonate decomposes to form a conglomerate of small, well-shaped crystallites of magnesium oxide that conform to the external morphology of the original solid reactant. The crystals are larger when the carbon dioxide pressure is higher, indicating that under conditions where the deconposition rate is depressed the growth of product crystals is favored over the nucleation of new crystallites. Also, as temperature of decomposition is raised, the frequency of nucleation increases, and the crystallite size of the resulting magnesium oxide is reduced (29, 32).

4.03 Reducing Influence of Some Diffusional Steps

It is desirable in an experimental situation to reduce the influence of diffusional steps (1), (2), (8), and (9) noted in Section 4.01 above, because these steps greatly complicate interpretation of kinetic results.

The effects of steps (1) and (9) can be determined by gradually increasing the reaction gas flow rate while holding the bed depth constant and by observing any change in reaction rate. When there is no further change in reaction rate with increase in gas flow rate, kineticists generally assume that film diffusion steps are no longer influencing the rate.

Effects of steps (2) and (8) can be examined by making runs that use different amounts of sample, i.e., that vary the depth of bed. Ruth (15) found that a small sample needed to be used at his highest temperatures in order to exclude influence of these steps, because his rates for reaction (D) on fresh half-calcined samples were so fast.

The effects of internal diffusion within particles can be reduced or eliminated by decreasing the size of particles of the powder studied. Weisz et al. (33) elucidated the effect of particle size by giving Arrhenius plots of the rate of burnoff of carbon from cracking catalyst beads and powders. The plots for powders were straight, but those for beads "drooped" at higher temperatures (lower values of 1/T), indicating diffusional resistance within the beads.

Ruth (15) demonstrated an effectiveness factor of 0.97 for fresh .alf-calcined dolomite particles undergoing reaction (D)

at 800°C and 1 atmospher with gas containing 1% hydrogen sulfide, the particles being -250+270 mesh in size.

Denbigh and Beveridge (34) studied oxidation of spheres of zinc sulfide between 500° and 1,440°C. They found the reaction rate to be chemically controlled in the lower part of the temperature range, but found diffusion to be controlling at higher temperatures. Furthermore, when little zinc oxide had been formed at the beginning of a run at higher temperatures, they attributed mass transfer resistance to the aerodynamic boundary layer surrounding the sphere. At later times in the reaction, when more zinc oxide was present, they attributed diffusional resistance to the oxide layer.

5.0 Experimental Techniques

Since the reactions (B) and (D) under study each produce a weight change, the thermogravimetric method can provide differential kinetics for reaction of a sample of solid spread as a fine powder in a thin layer on a balance pan, the gaseous reactants flowing past the solid at a rate sufficient to preclude any substantial change in a known gas composition.

The City College Clean Fuels Institute has three thermogravimetric analytical set-ups:

(1) One is for working at atmospheric pressure and can handle samples up to about 5 grams. It is built around an Ainsworth recording balance (12, 14). It has been used in this research for preparing samples of reacted solids for inspection.

(2) Another, also for atmospheric pressure, uses the duPont 900 Thermal Analyzer and 950 Thermogravimetric Analyzer, the latter having been modified to accept gases containing steam and corrosive agents such as hydrogen sulfide and sulfur dioxide (6, 15). It has not been used in this research.

(3) A third set-up, developed by Dobner (16), is built around an extensively modified duPont 950 Thermogravimetric Analyzer. It is capable of working at pressures up to about 30 atmospheres and at high partial pressures of steam in presence of corrosive agents.

Dobner's instrument has been the workhorse of the present research. His description (16) will be abstracted below in

the interest of the completeness of this report. We will note, however, certain modifications of Dobner's instrument that became necessary during the course of the present work.

5.01 duPont Thermogravimetric Analyzer

The instrument used in the work consists of two separate units: the duPont 900 Thermal Analyzer, which includes a temperature programmer-controller and X-Y recorder, and the duPont 950 Thermogravimetric Analyzer, which contains an electrobalance and furnace.

The balance capacity is effectively 150 mg, and the weight sensitivity is variable from 0.20 mg/inch to 20 mg/inch in seven steps. This means that at the maximum sensitivity attainable, a weight change of 0.02 mg should be easily seen. For a typical sample size of 40 mg, weight changes corresponding to as little as 0.3% conversion of [$CaCO_3$+MgO] to [CaS+MgO] can be recorded.

The instrument can be used in an isothermal mode to 1,000°C, in which case the recorded produces a graph of sample weight versus time. Alternatively, the instrument can be used in a nonisothermal mode, with the temperature raised at a uniform rate to as high as 1,200°C and at rates up to 30°C/minute. In the latter mode, a graph of sample weight versus sample temperature is produced.

5.02 Modification of duPont Thermogravimetric Analyzer for High Pressure Studies

Dobner (16) achieved pressurization of the Thermogravimetric Analyzer (TGA) by enclosing the balance and furnace module inside

a pressure vessel, as shown in Figure 10. Designed for 450 psig by Autoclave Engineers, the pressure vessel is approximately 3 feet long and 10 inches in inside diameter. The unit consists of a horizontal pressure shell mounted on rails to permit easy access to the TGA. There is a fixed bulkhead through which all instrument and flow connections are made. Heat generated by the TGA is removed by a cooling water jacket surrounding the pressure shell. Safety precautions include a one-half-inch rupture disc located in the bulkhead and a five-eighths-inch plywood pressure shield to protect operating personnel. The pressure shield facing the bulkhead end of the vessel is thicker, i.e., one-and-one-quarter-inch plywood.

Figure 11 illustrates Dobner's modifications of the working space of the duPont TGA. He reduced the open space for the sample pan to a length along the balance tube of only about one-half inch, in order to limit the space available for development of a convection cell. Until this open space was reduced just as much as possible, Dobner observed large temperature differences between thermocouple and temperature standards placed upon the balance pan. The cause of the temperature differences was traced to development of vigorous convection cells at higher pressures. Convection is of course not a serious problem for operation of the duPont TGA at atmospheric pressure.

As Figure 11 illustrates, reaction gas flowing toward a sample on the balance pan passes first through a packing of Vycor cyclinders that were prepared by breaking Vycor rod of one-eighth-inch diameter into lengths of about one-eighth inch.

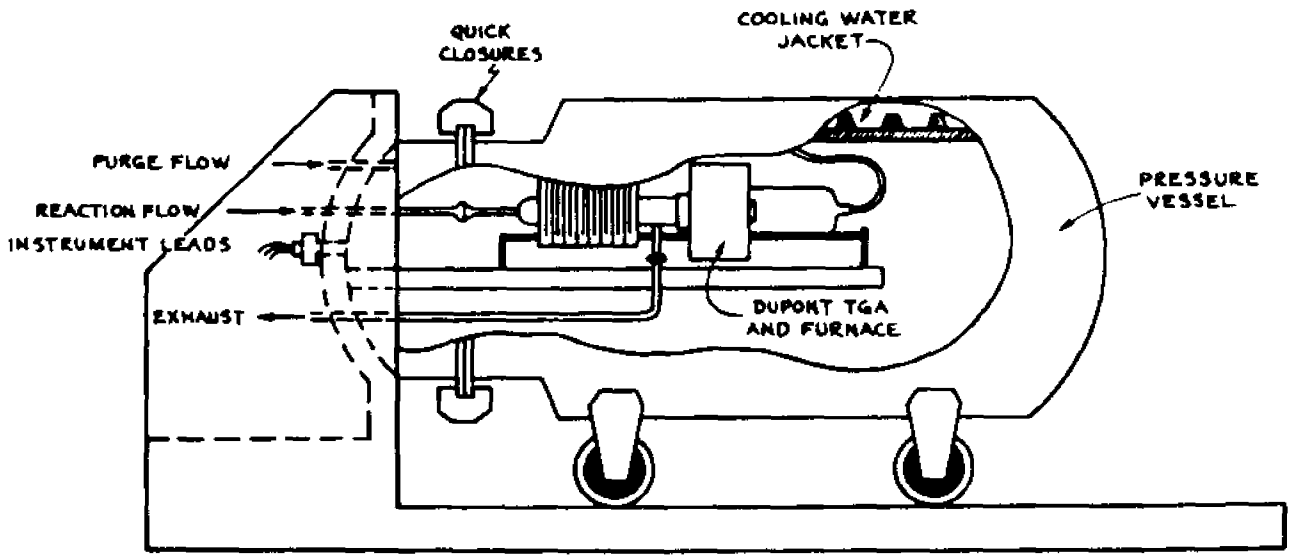

Figure 10. duPont 950 Thermogravimetric Analyzer in pressure cartridge developed by Dobner (16).

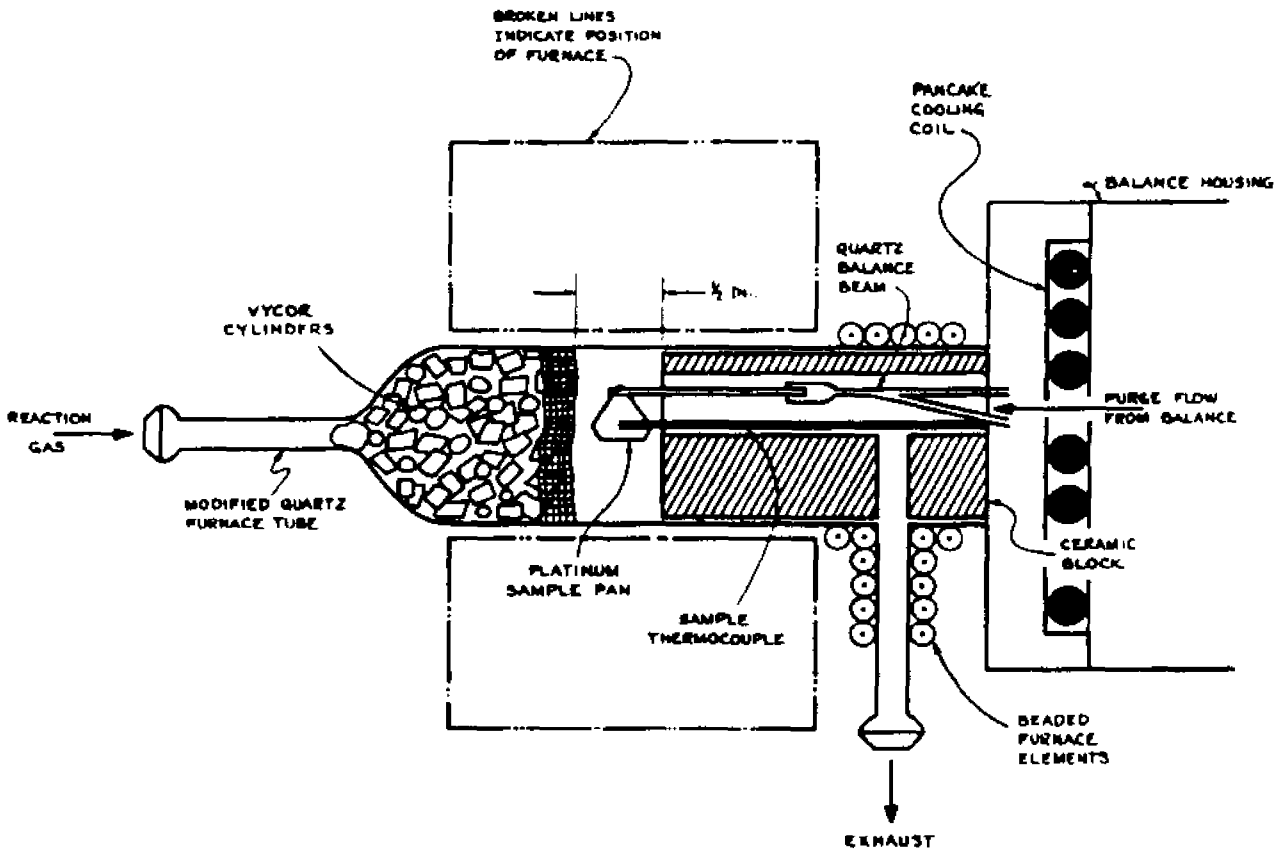

Figure 11. Working space of duPont 950 Thermogravimetric Analyzer, as modified by Dobner (16) for work at high pressure with gases containing steam and corrosive agents. Also shown is the pancake cooling coil added to Dobner's set-up during the present research.

Reaction gas leaving the sample flows through a passage in a ceramic block that substantially fills the space between sample and balance housing. The passage also affords space for a quartz balance beam that carries the sample pan. A separate passage in the ceramic block houses the sample thermocouple in a tight fit; this passage is not seen in the view shown by Figure 11. A purge flow of nitrogen leaves the balance housing, seen at the right in Figure 11, through an opening provided for the quartz balance, and the nitrogen purge flow then enters the passage in the ceramic block. A transverse passage in the block, situated about one-and-one-half inches from the balance housing, carried the combined flow of reaction gas and purge nitrogen to a sidearm of the quartz furnace tube, from which the gases exhaust from the tube.

A platinum balance pan was used throughout studies of the half-calcined dolomite cycle for removing hydrogen sulfide from a gas mixture.

Experience with the arrangement of Figure 11 has confirmed Dobner's expectation that it can be operated over a wide range of experimental situations, at high partial pressures of steam and in presence of corrosive agents, with freedom from condensation of moisture on the quartz balance beam, penetration of steam into the balance housing, or damage to delicate balance parts from corrosion.

Early in this research, several failures of the balance movement occurred, and at first, these were thought to be a result of intermittent penetration of hydrogen sulfide into the balance housing. Metallurgical examinations, however, suggested that overheating of balance parts was a more likely explanation of the

failures. It appeared that the sluminum metal block housing the balance did not afford sufficient capability for removing heat from the beaded furnace elements placed along the quartz furnace tube and sidearm for exhaust of reaction gases. A one-eighth inch pancake cooling coil was installed on the face of the aluminum balance housing, as illustrated in Figure 11, and thereafter no breakdowns of the balance were experienced.

Another minor modification of Dobner's set-up arose from a need for the connections between quartz furnace tube and stainless steel ball joints to be adjustable in order to tolerate small differences in dimensions among the several quartz balance tubes used in the research. Flexible hoses of 304 stainless steel proved unsatisfactory, since they could not withstand corrosion by wet hydrogen sulfide at high temperature. The problem was solved by using one-eighth inch tubing of 316 stainless steel with a little U-bend together with ball joints of stainless steel at each connection to the furnace tube, i.e., for both inlet and exhaust of reaction gas.

5.03 Flow System for the Pressure Thermobalance

The principle difficulty in designing a high pressure dynamic flow system for the thermobalance with corrosive gas atmospheres was the absolute necessity for maintaining stable flow of gases while providing continuous balanceing of pressure inside the thermobalance with its surrounding atmosphere. Unsteady flows to the pressure thermobalance could result in inadvertent introduction of corrosive gases into the balance housing.

Figure 12 is a schematic diagram of the flow system for the

pressurized thermobalance. Inlet pressures of the various gases are controlled using standard cylinder regulators. Lo-flow regulated rotameters are used for flow measurement and for control of individual gases. System pressure is maintained by a lo-flow back pressure regulator, of the hand-loading, piston type, through which all gases are vented. The regulator is from Circle Seal (BPR-7).

Pressure is equalized between inside of thermobalance tube and a far larger space within the pressure vessel by a pressure balance line between a point just upstream of the back-pressure regulator and the pressure vessel. There is a vent in the pressure balance line. Depressurization of the unit is achieved via the opening of this vent. Pressurization of the unit is achieved by allowing purge nitrogen to flow through the purge line and a bypass line at the same time.

Because of the large range of concentrations of the various gases to be used in the research, it was necessary to prepare our own gas mixtures. Schutte and Koerting Lo-Flo rotameters are used in the set-up. They have a 10-to-1 range for a tube-float combination, and can withstand pressures up to 400 psig. Their tested calibrated accuracy is about 2 percent of full scale. The minimum measurable flow with the stated accuracy is about 2 cm^3 (actual)/min. At a presssure of 300 psig and a total reaction gas flow of 100 cm^3 (actual)/min this translates to a minimum measurable gas composition of 2 percent. Below this minimum, purchased gas mixtures must be used.

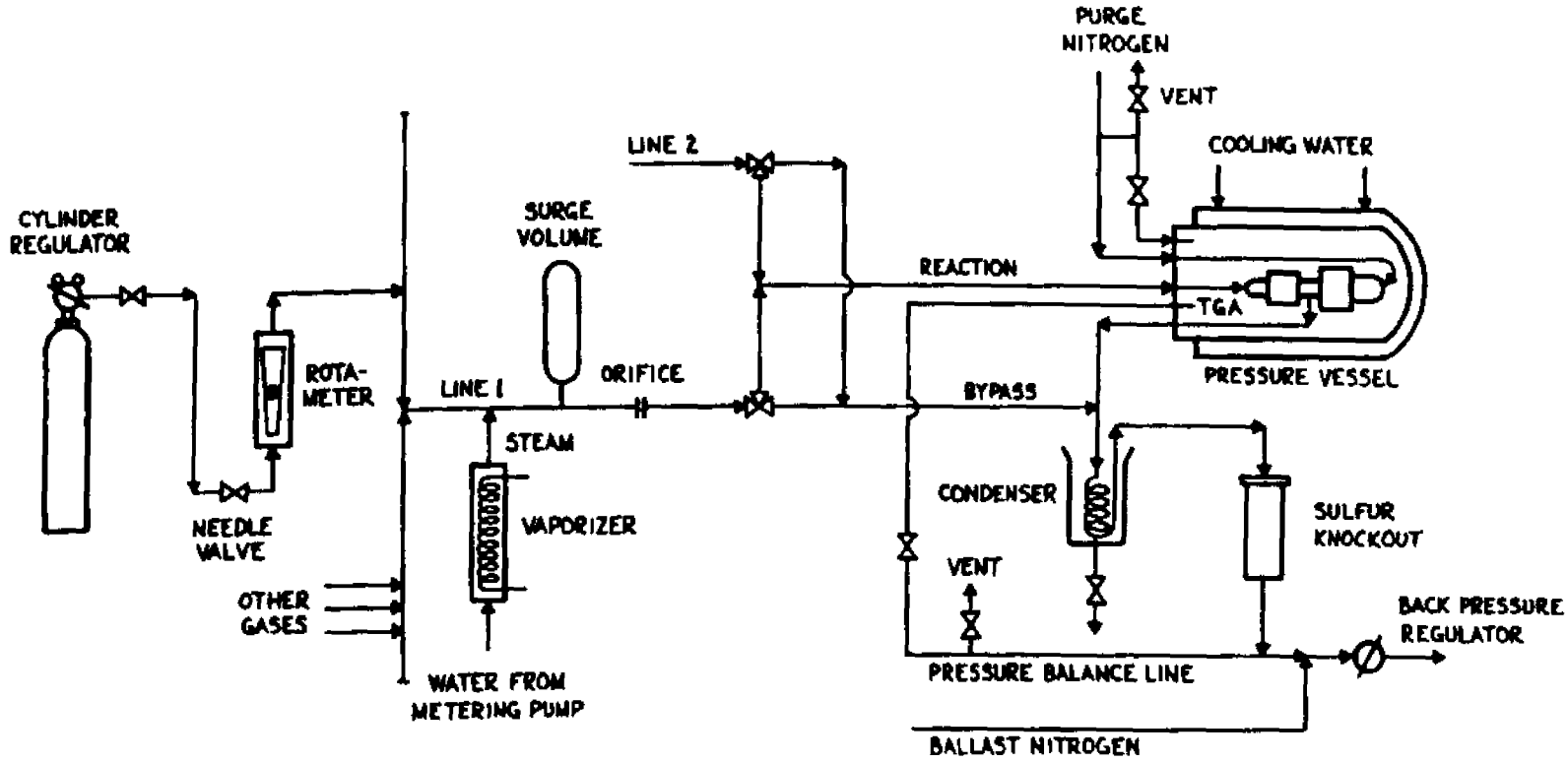

Figure 12. Flow system for pressurized thermobalance (16). The location of the pressure balance line was changed in the present research to the position shown.

Calibration of the flowmeters was made using either a Brooks Calibrator, a wet test meter, or a bubble meter. For hydrogen sulfide, only the latter method proved feasible.

Corrosive gases (hydrogen sulfide and sulfur dioxide) have their own feed line (not seen in Figure 12) to the pressurized thermobalance. A three-way solenoid must be activated in order to direct these gases to the thermobalance, thus providing additional protection for the balance. Mixing of the corrosive gas with the remaining reaction gases takes place close to the pressure vessel in order to minimize need for corrosion-resistant fittings and valves in the flow system.

All valves and fittings are manufactured by Hoke, and have performed reliably. The three-way ball valves fo leak occasionally as a result of deformation and creep of a teflon seat at pressure, and the valves must therefore be checked regularly.

All lines leading to and from the thermobalance are heated to beyond 300°C to prevent condensation of steam.

In order to prevent damage to the back pressure regulator as well as to prevent deposition of sulfur in the regulator if it were to handle a gas containing hydrogen sulfide, gases from the thermobalance or bypass are first dried in a condenser at 0°C and then desulfurized in a zinc oxide bed.

The location of the pressure balance line was changed in the course of the present research from the location provided by Dobner. He had placed this line between the supply of nitrogen and the balance housing. However, as he noted in his thesis (16), the back-pressure valve available would cycle roughly $\pm$ 5 psig during

an operation at pressures near 300 psig and at typical flows of 400 cm^3 (actual)/min. The cycling of the valve produced "breathing" inside the thermobalance.

During some early runs, the volume inside the pressure vessel but outside of the thermobalance was isolated. Because of heat rejected by the furnace and heating tapes, the pressure of gas inside the vessel could increase to about 25 psi higher than the pressure inside the thermobalance. This usually caused leaks to appear between the two volumes, or it caused the quartz furnace tube to crack. The pressure balance line solved this problem by providing passage for immediate relief of slight pressure build-up inside the vessel. It should be noted that if the pressure in the vessel should fall below the setting of back pressure regulator, reaction gas mixture would flow into the vessel through balance line. This back flowing gas mixture is virtually free of hydrogen sulfide on account of the presence of the zinc sulfide sulfur knockout.

Even after the pressure balancing line was placed in the present position, cyclic fluctuations in pressure in the thermobalance caused cyclic drift in the observed weight of a sample. Sometimes the system pressure would cycle in the vicinity of $\pm$ 10 psig of the pre-set pressure, a range of cycling larger than that reported by Dobner. The problem was solved by adding a ballast flow of nitrogen just before the back pressure regulator. A high rate of flow of the ballast nitrogen makes the back pressure regulator relatively immune to fluctuations of the total flow coming from the balance, and therefore the regulator was able to hold the back pressure steady. This high rate of ballast nitrogen also

blows off any zinc oxide powder entrained by exiting gas mixture thereby preventing its deposition inside the back pressure regulator.

The reaction gas flow system is designed with duplicate sets of feed lines. This permits one reaction gas mixture to flow into the thermobalance while another gas mixture is either being prepared or awaiting the next step in a reaction cycle. A system of three-way solenoid valves (Laurence Catalog No. 330817S) is situated close to the pressure vessel, and this system can instantaneously switch one reaction gas stream to the thermobalance while diverting the other reaction gas stream, thus bypassing the thermobalance.

Steam is available to only one of the gas feed lines, so that only one reaction gas mixture in a reaction cycle can contain steam.

Steam is generated by supplying water to a vaporizer from a metering pump. As Dobner recongnized (16), the Harvard Apparatus 975 syringe injection pump that he worked with had many difficulties, and it was replaced for this research by an ISCO LC pump capable of pumping up to 3 ml/min of liquid to 2000 psig. It is a single stroke pump working from a reservoir containing up to 375 ml of liquid, and has given satisfaction.

Dobner's vaporizer is illustrated in Figure 13. A water-cooled hypodermic needle (22 gauge stainless steel) feeds water vertically into a packed bed (five- sixteenths inch outside diameter) of oxidized copper beads (20 mesh). The bed is heated externally to 600°C by beaded furnace wire. The other reaction gases are heated to above saturation temperature in a packed bed preheater before being mixed with the steam. The preheater has beads of borosilicate glass (1.5 mm) packed in two feet of one-quarter

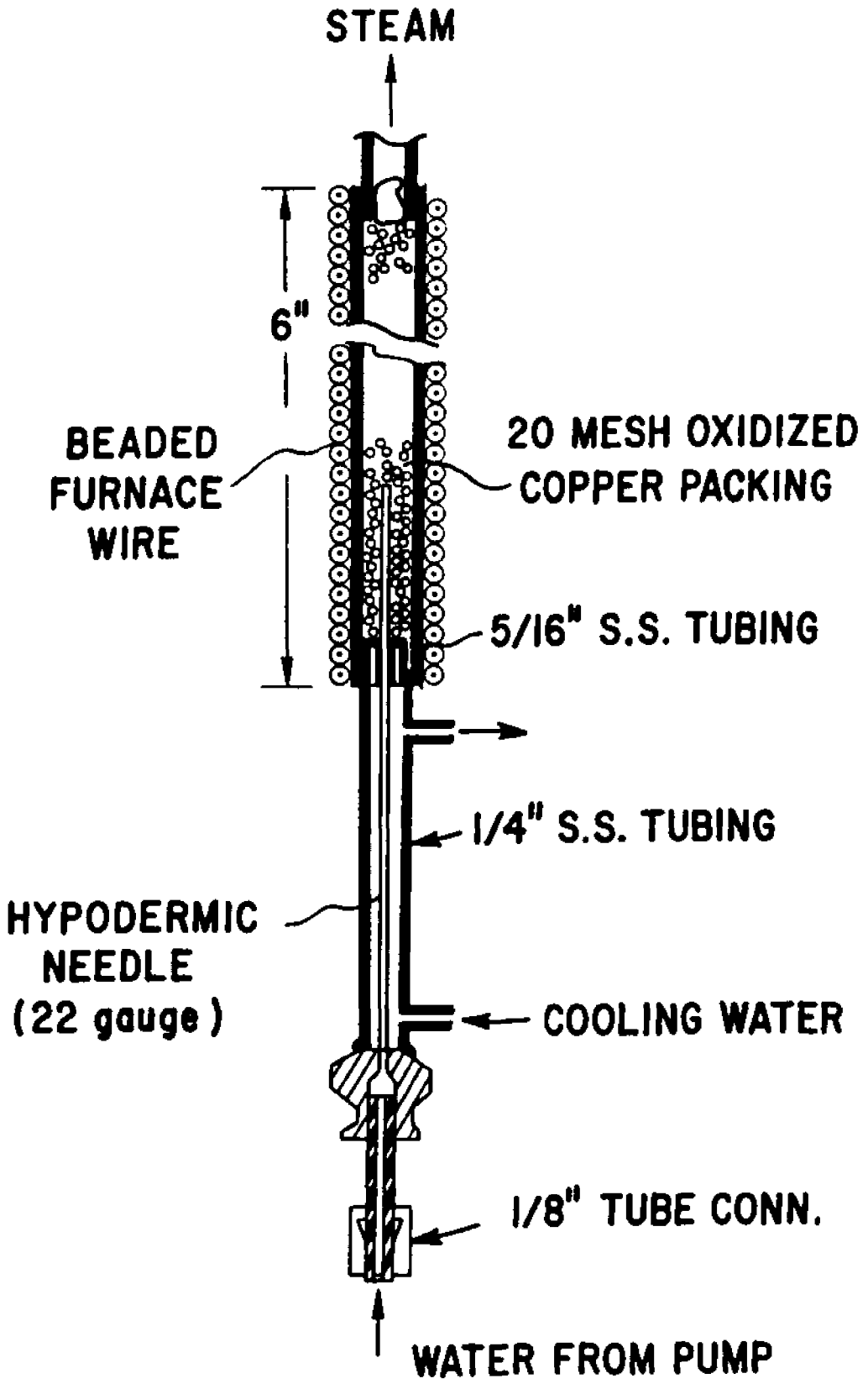

Figure 13. Dobner's vaporizer (16) for generating steam for high pressure thermobalance.

inch tubing.

Vaporization of water in the vaporizer of Figure 13 is not a steady state process, but takes place explosively as each droplet is converted to vapor. The dynamics of the flow system for the high pressure thermobalance are such that any pulses generated during vaporization could be propagated, if not suppressed, as far as the balance housing. Indeed, one of the most time-consuming problems that Dobner faced in development of the pressure thermobalance was overcoming the penetration of steam into the cooler parts of the balance that arose from pressure pulses originating in the vaporizer. He finally achieved pulseless flow of steam by placing a surge volume of 2 liters and an orifice (C_v = 0.002) in the steam line from the vaporizer.

5.04 Calibration of Sample Thermocouple

A routine procedure, based upon Perkin-Elmer magnetic standards (35), has been adopted for calibrating temperature of the sample thermocouple. The procedure is executed each time a different set of gas compositions or pressure is planned or a new sample pan or thermocouple is used. In general, the indicated temperature is accurate to within about 15°C, except for temperatures beyond 800°C, where indicated temperatures begin to lag. While the accuracy of the indicated temperature leaves something to be desired, the sample temperature with calibration for a specific run condition can be reproducibly determined to within about 5°C.

5.05 Performance of High Pressure Thermobalance

The noise level on the weight scale that is caused by combined flows of purge gas and reaction gas has been measured. At 0 psig and 600°C and a total gas flow of 1100 cm^3 (0 psig, 77°F)/min of nitrogen, the noise level is less than $\pm$ 0.002 mg. At 300 psig and 600°C and a total gas flow of 300 cm^3 (300 psig, 77°F)/min, the noise level is $\pm$ 0.02 mg.

Nine runs were made to determine the effect on sample weight of temperature, pressure, total volumetric gas flow, ratio of reaction gas flow to purge nitrogen flow (where the "reaction gas" was nitrogen), and geometry and size of sample. Calibration curves were obtained. Sample weight generally increases withe each of these variables, with the exception of pressure. The sample weight decreases with increasing pressure because of buoyancy forces.

Penetration of purge gas into the reaction gas zone was determined. The experiment was accomplished using oxygen as the "purge gas" and nitrogen as the "reaction gas", and with finely powdered copper at 600°C as the sample. Penetration can be detected and measured by comparing a rate of weight gain in the experiment with the rate if a known mixture of oxygen and nitrogen is used as a reaction gas. The results of the experiment showed that penetration is negligible for 800 cm^3 (300 psig, 77°F)/min of purge oxygen and 100 cm^3 (300 psig, 77°F)/min of reaction nitrogen.

Buoyancy force was determined by observing the weight change at a constant temperature as pressure was varied in absence of a flow of gas. For example, the indicated weight declines by 0.53 mg for an empty sample pan in going from atmospheric pressure to 300

psig in nitrogen. From this measurement, the volume to the left of the fulcrum of the balancing level is calculated to be 0.0215 cm^3 greater than the volume to the right. Using this volume relationship, calculations can be made to reckon weight corrections for other situations encountered in this research (for example, when a quartz sample pan replaces the platinum pan or when samples of various materials are present on the pan) by considering gas and material densities, and the calculated weight corrections ought to be within about 10 percent of true values.

5.06 Experimental Solids and Half-Calcination Procedure

All runs were made with dolomite from the Greenfield formation in Ohio supplied by Davon Incorporated from their Plum Run quarry. Chemical analysis of the dolomite was performed by Lucius Pitkin, Inc. of New York City, with the following results:

Component	Weight Percent
Mg as MgO	20.14
Ca as CaO	29.40
Fe as Fe_2O_3	0.76
SiO_2	1.70
Al as Al_2O_3	0.54

This analysis gives a molar ration of Ca/Mg = 1.049.

Powder was prepared by grinding small chunks of rock with a mortar and pestle and sieving to prepare a -250+270 mesh cut. The small chunks were taken from a number of rocks, rather than from just a few, in order to get a sample more representative of Greenfield stone.

In order to determine the fractional conversion of [$CaCO_3$+MgO] to [CaS+MgO] from the change in weight, it is necessary to know the capacity of the sample of half-calcined dolomite to absorb hydrogen sulfide. The analysis given above predicts a weight loss of 0.147 mg per mg of dolomite sample for complete reaction from the half-calcined form to the sulfided form. This is in good agreement with an average value of 0.155 obtained from seven runs that were carried to completion at atmospheric pressure and at temperatures beyond 800°C. Individual values for the several runs are given below:

Run Number	Fractional Weight Loss at End of Run
T-15	0.144
T-16	0.153
T-17	0.162
T-21	0.163
T-22	0.162
T-23	0.158
T-46	0.146

The value 0.155 has been used in calculating conversions reported here.

Half-calcination was done at run pressure in the TGA with a programmed rise in temperature of 20°C per minute. Initially the gas was 50/50 nitrogen/carbon dioxide. Half of the nitrogen was replaced by an equal amount of steam when the temperature reached 300°C, and the heating was contained until the temperature reached about 800°C.

5.07 Tests for Possible Catalytic Role of Platinum

As Section 11.01 will discuss, in our work with absorption of sulfur dioxide from oxygen-containing gases by magnesium oxide we discovered a catalytic role toward the reaction of the platinum gauze and platinum balance pan of our TGA.

Accordingly, we felt it necessary to check for the possibility that platinum might play a catalytic role in the absorption of hydrogen sulfide by half-calcined dolomite. There was no *a priori* reason to suspect such a catalytic effect.

A run (T-190) was made with a quartz balance pan and with no platinum gauze present in an effort to duplicate results of an earlier run (T-114) made with a platinum pan six months earlier. The final capacity for T-190 was 18%, only 0.9 of the final capacity of 22% for T-114. Although this might be an acceptable check for some of our experiments, it was taken as a serious difference because excellent reproducibility had been obtained earlier for runs at the conditions of T-114 using a platinum pan (e.g., runs T-100 and T-114 were two months apart and each gas a final capacity of 22%).

A calibration run (T-193) was then made to calibrate the temperature using a platinum pan. Applying results obtained from T-193, we made run T-194 with a platinum pan under identical conditions as T-114, to obtain again the same final capacity of 22%.

Another calibration run (T-196) was made to calibrate the temperature using a quartz pan. Applying the results of this run, we made run T-197 with a quartz pan under otherwise identical conditions as runs T-114 and T-194. The average of the capacities shown by the last three cycles of run T-197 was 22%.

We concluded that the discrepancy between runs T-190 and T-114 had been caused by erroneous temperatures in the former, and was not caused by a catalytic effect fo the platinum pan.

6.0 Results

The heart of the present research has been a series of cyclic runs devoted primarily to investigating effects of temperature of the absorption reaction,

$$[CaCO_3+MgO] + H_2S = [CaS+MgO] + H_2O + CO_2. \quad (D)$$

and of temperature of the regeneration reaction,

$$[CaS+MgO] + H_2O + CO_2 = [CaCO_3+MgO], \quad (B)$$

upon the capacity of the regenerated half-calcined dolomite, $[CaCO_3+MgO]$, to absorb hydrogen sulfide.

Unless otherwise noted, all runs were made with a single batch of ground powder, -250+270 mesh. All runs at elevated pressure were made at 300 psig (21.4 atmospheres).

Reaction temperature was varied from 500° to 1,000°C. In most runs, the time of absorption and the time of regeneration were maintained constant throughout the run. Most high-pressure runs were made with 0.5% hydrogen sulfide present in the absorption step, and a few runs used 0.7%.

As is evident, the research did not focus upon fiding rate expressions for the two reactions as functions of gas composition, like much academic kinetic research. It was felt that exploration of effects of reaction temperature upon absorption capacity of the solid was much more important. However, some qualitative information did emerge connecting rates with gas compositions, and this limited information is also given here.

Because variability in behavior of dolomite samples had been seen in earlier research in our laboratory (14, 15), we ran two runs on our sample at atmospheric pressure for comparison with a run by Ruth. Figure 14 gives the comparison. The variability seen in Figure 14 is not unusual, if compared with the earlier research, and we concluded that our sample was essentially similar to Ruth's.

Figure 15 illustrates a convention used in subsequent figures for reporting absorption and regeneration conditions, cycle numbers, and other pertinent information directly upon the figure giving the reaction data.

6.01 Data for Runs with Absorption and Regeneration at Same Temperature

Figures 15 and 16 illustrate two ways we have used to report data from a run consisting of a number of cycles of reactions (D) and (B).

Figure 15 is a "zigzag chart." The upward, solid line shows the increase in the molar fraction of calcium sulfide in the solid during an absorption step, and the sloping, dashed line shows the decrease in calcium sulfide molar fraction as this substance is converted to calcium carbonate in the subsequent regeneration step. The conditions for the absorption and regeneration are noted at the top of the figure. Both reactions were conducted at 731°C in the run reported in Figure 15. About 10 seconds is needed to shift from the absorption gas mixture, shown on the left at the top of Figure 15, to the regeneration gas shown on the right, and vice versa.

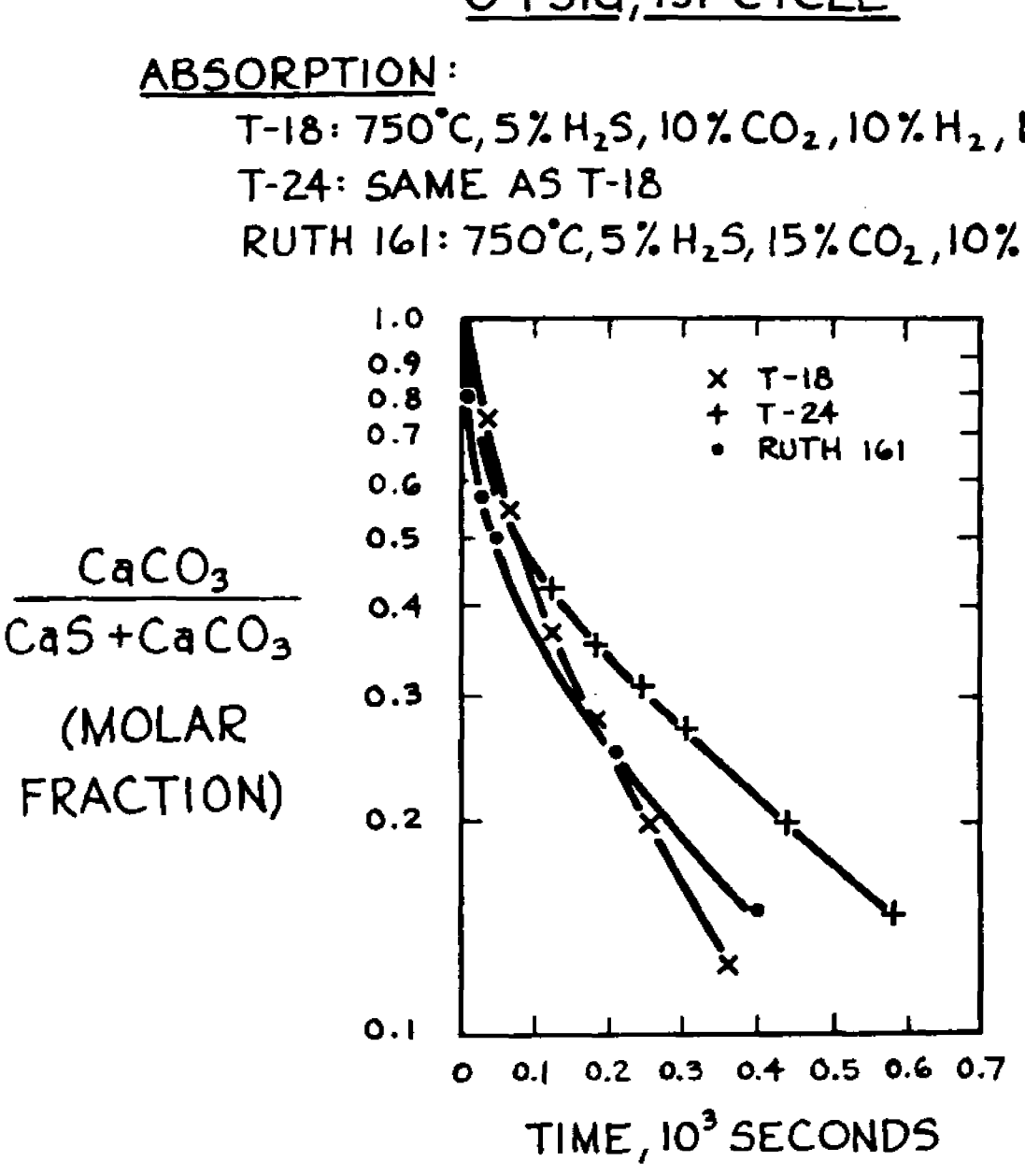

Figure 14. Duplicate runs at atmospheric pressure compared with a run at similar conditions by Ruth (15).

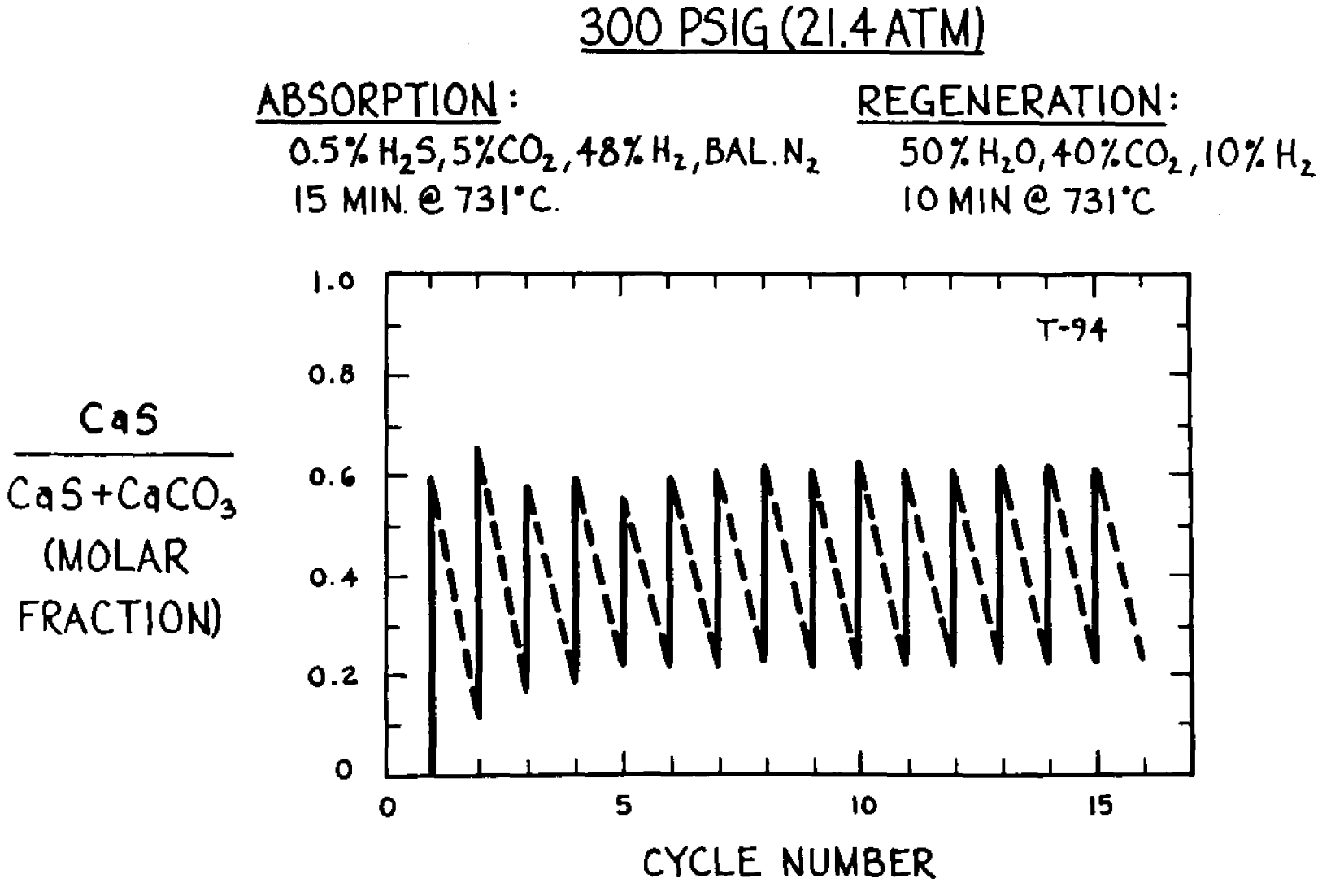

Figure 15. Zig-Zag Chart for Run T-94.

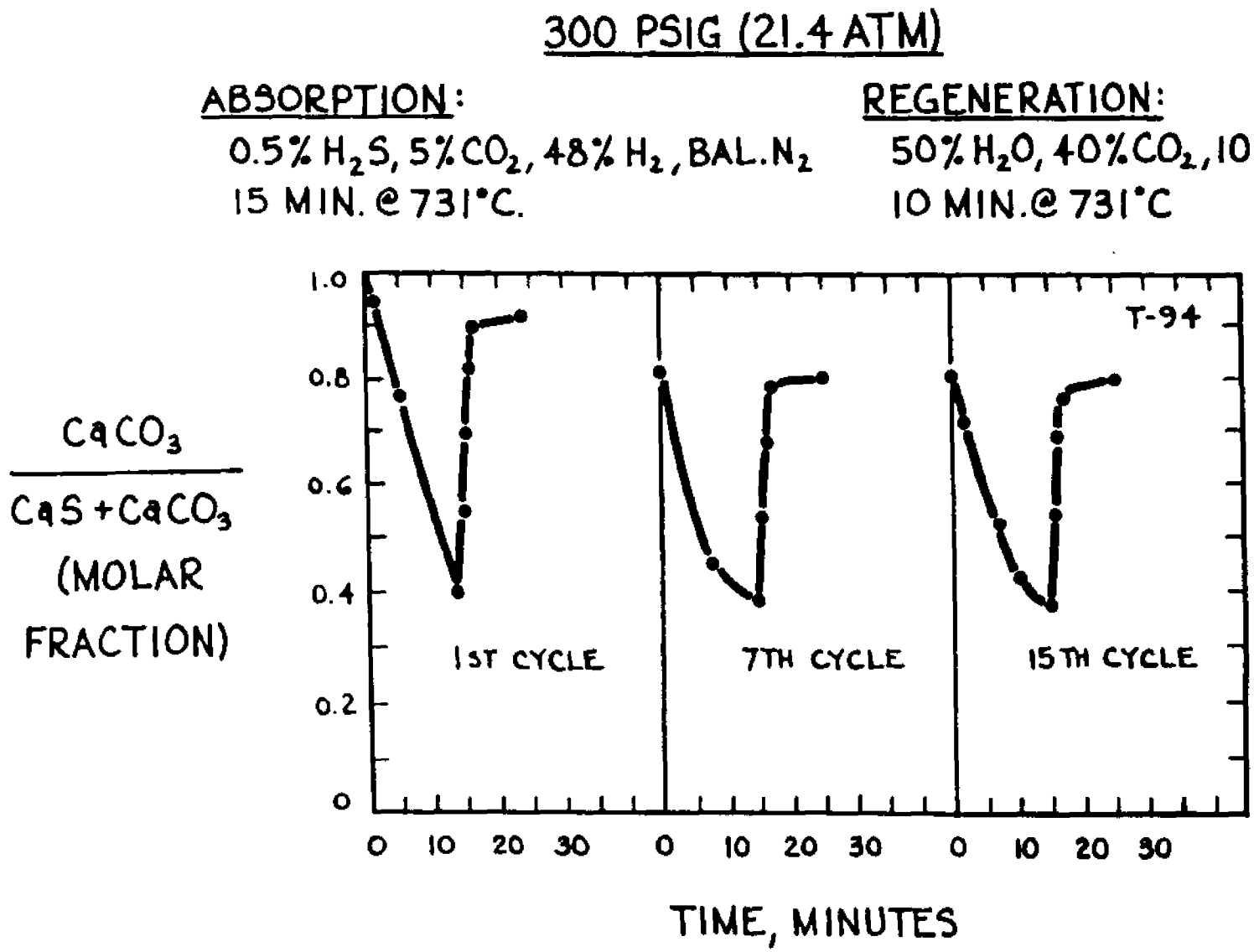

Figure 16. Rate data for three selected cycles of Run T-94.

Figure 16 gives molar fraction of calcium carbonate in the solid as a function of time during the first, seventh, and fifteenth cycle of the run reported in Figure 15. The calcium carbonate content of the solid declines during the absorption reaction (D), and increases during regeneration reaction (B).

A striking feature of the data in Figure 16 is that the regeneration reaction is extremely rapid at 21.4 atmospheres and 731°C, in contrast to the slow reaction exhibited by the data at atmospheric pressure and 750°C, seen in Figure 3. There does not seem to be much change in the rate of this reaction with cycling, nor indeed, in the absorption rate either.

Figure 17 provides a comparison of regeneration rate at 300 psig and 0 psig obtained in this research, for runs in which both absorptions and regenerations were conducted at 750°C. The striking effect of pressure upon regeneration rate is again illustrated.

It does not follow inevitably, however, that the effect illustrated in Figure 17 is simply a kinetic effect brought about by an influence of pressure upon the "true" rate of reaction of steam and carbon dioxide with calcium sulfide surface. The calcium sulfide made at elevated pressure, for example, might have a different physical form, or other physical effects brought about by the change in pressure may dominate the "true" kinetics.

Figure 18 is a zigzag chart for a run in which both absorption and regeneration were conducted at 676°C, and Figure 19 is a plot giving rate information. Again, the striking speed of the

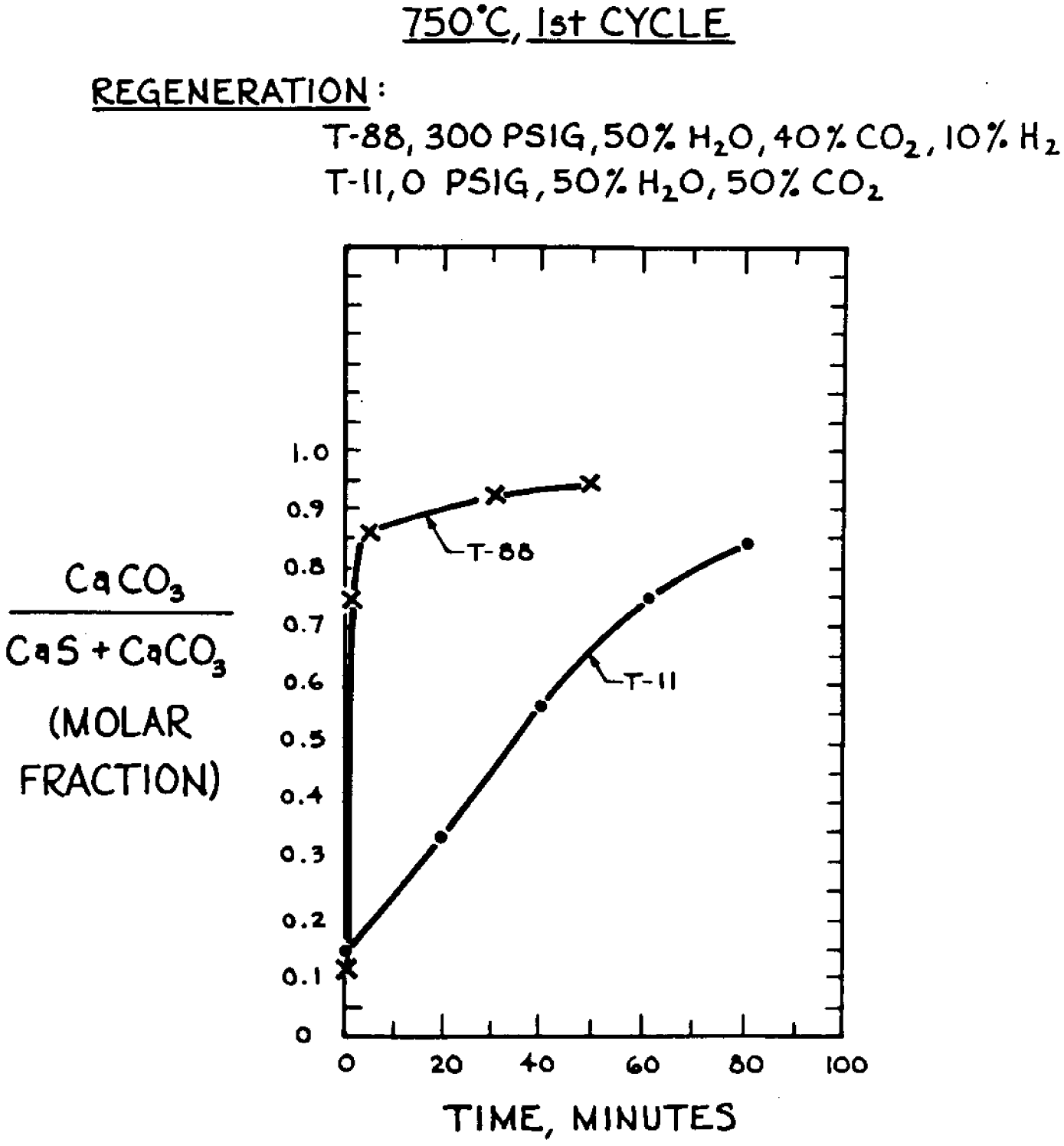

Figure 17. Illustrative comparison of rate of regeneration at atmospheric pressure and 21.4 atmospheres.

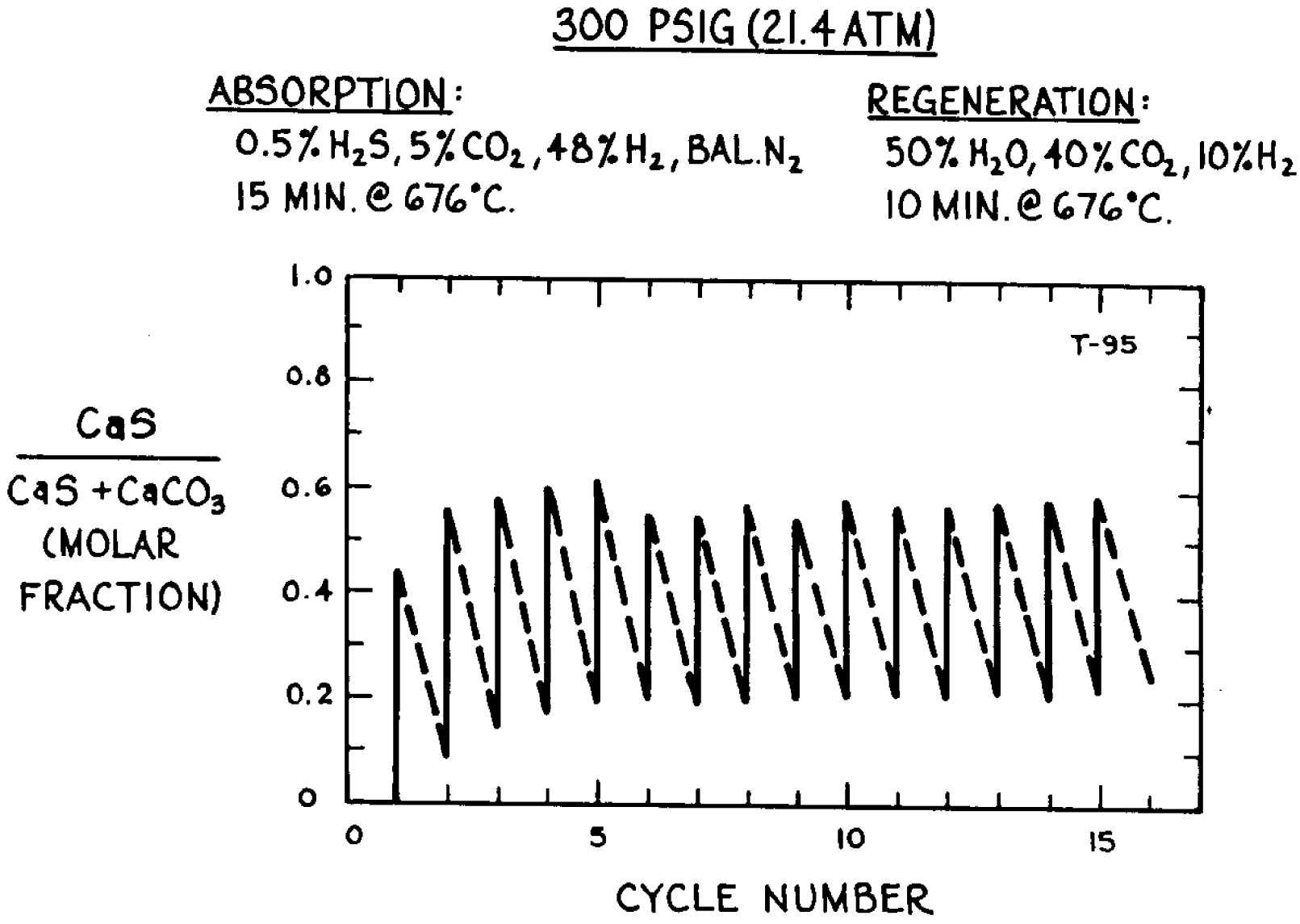

Figure 18. Zig-Zag chart for Run T-95.

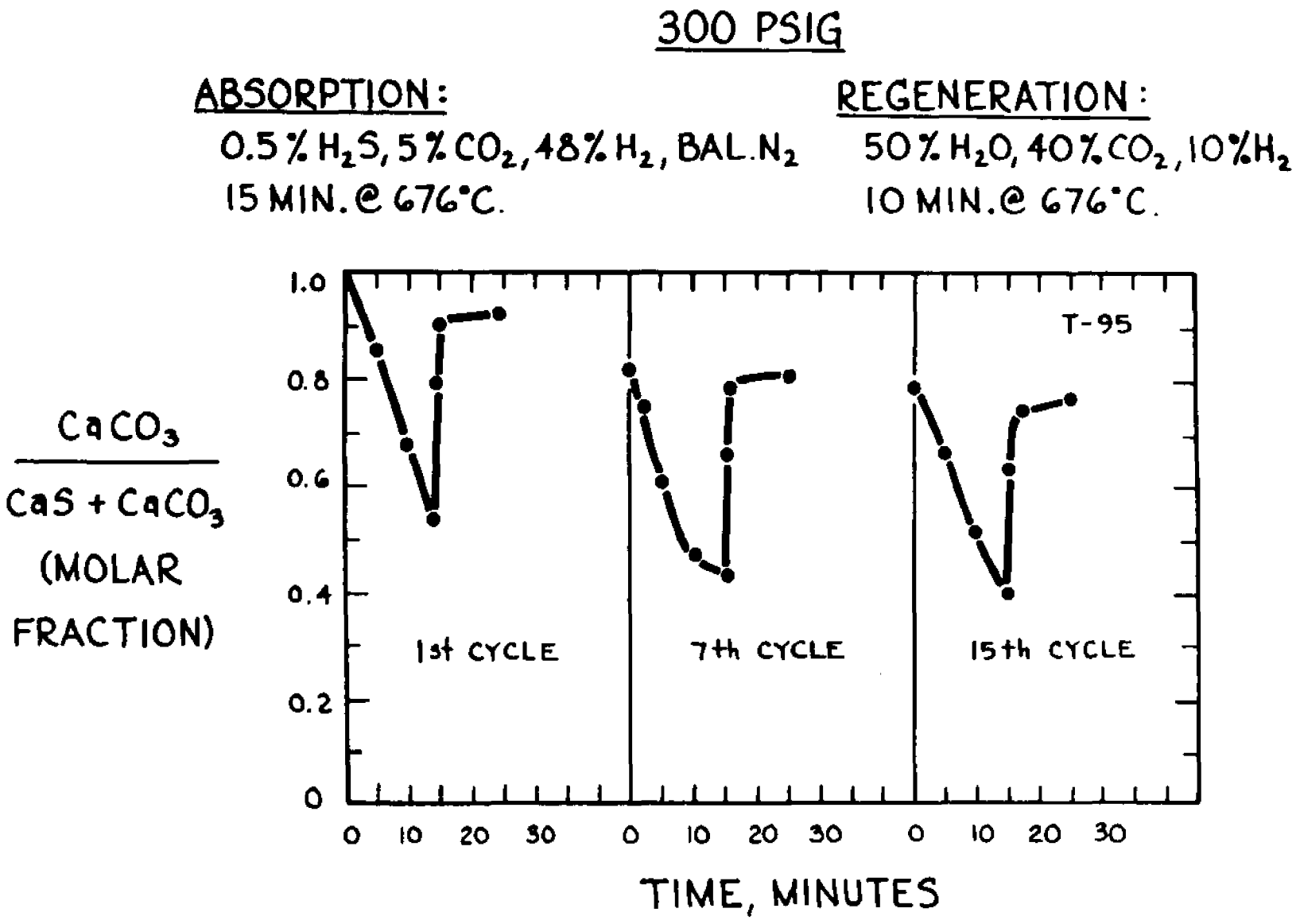

Figure 19. Rate data for Run T-95.

regeneration reaction is evident, and Figures 20 and 21 are a corresponding pair of figures for another run with both reactions at 676°C, but with a longer period of time for absorption and a shorter period for regeneration. It is evident from a comparison of Figures 18 and 20 that the final absorptive capacity of the solid is increased by the transfer of time from the regeneration step to the absorption step. The reason for this is apparent from a comparison of Figures 19 and 21. Substantially, all of the regeneration that the indicated reaction conditions can afford is accomplished in about one minute, and any subsequent time devoted to regeneration is wasted. On the other hand, increasing the time for absorption from 15 to 22.5 minutes caused some additional absorption to occur.

6.02 Data Showing Effect of Regeneration Temperature on Absorptive Capacity

Figures 22 and 23 are for a run with absorption at 731°C and regeneration at 618°C. The total cycle took 25 minutes. Of this time, 1.5 minutes were spent in heating the sample, and 4.5 minutes in cooling. Both heating and cooling were carried out with absorption gas flowing over the sample. Regeneration was carried out in 4 minutes, since the results discussed in Section 6.01 indicated that longer regeneration times did not increase the ultimate absorptive capacity of the solid sample.

Figures 24 and 25 are for absorption at 731°C and regeneration at 560°C, with regeneration carried out in 2 minutes. Figures 26 and 27 are for a run similar in every respect, except in that of

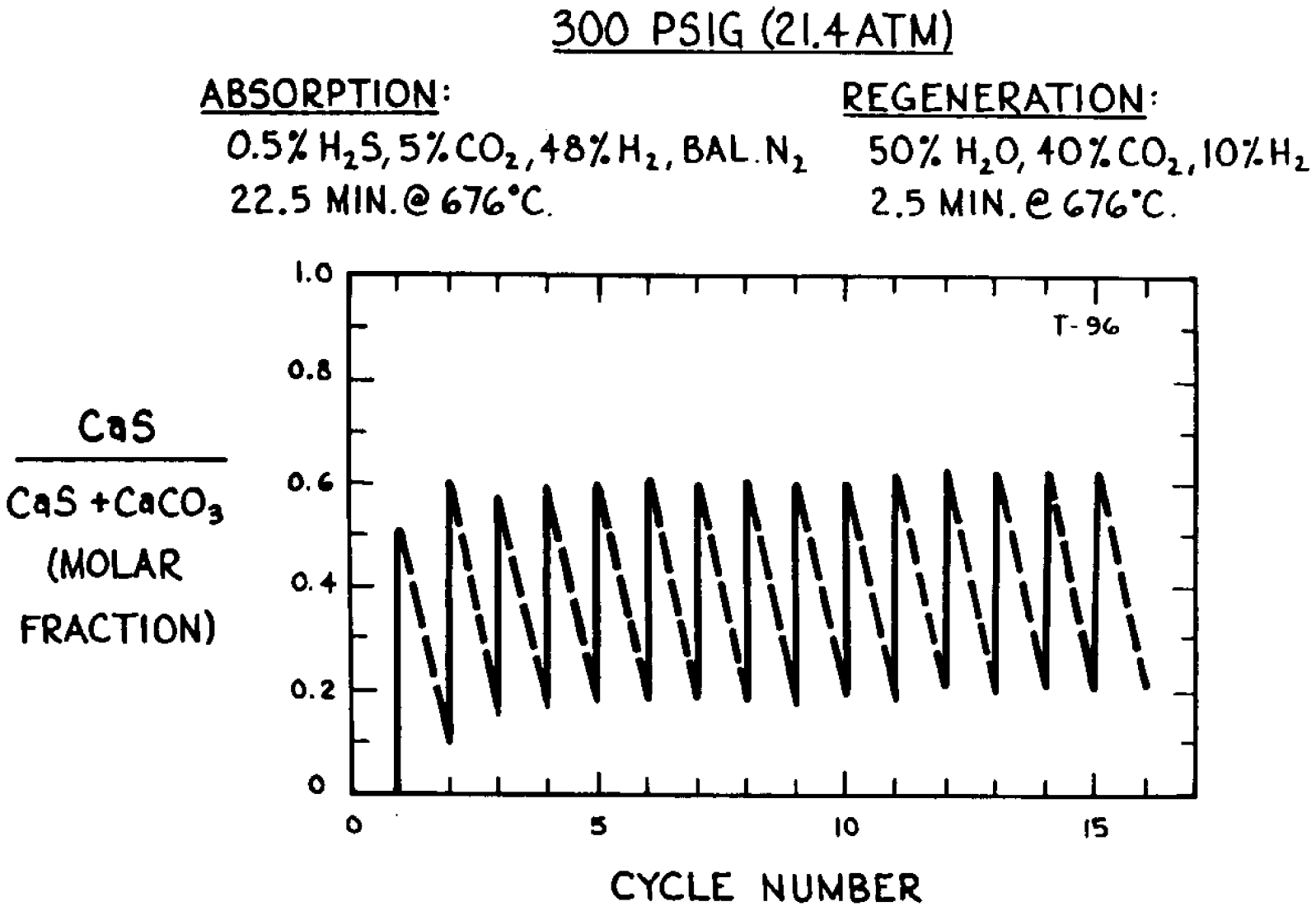

Figure 20. Zig-Zag chart for Run T-96.

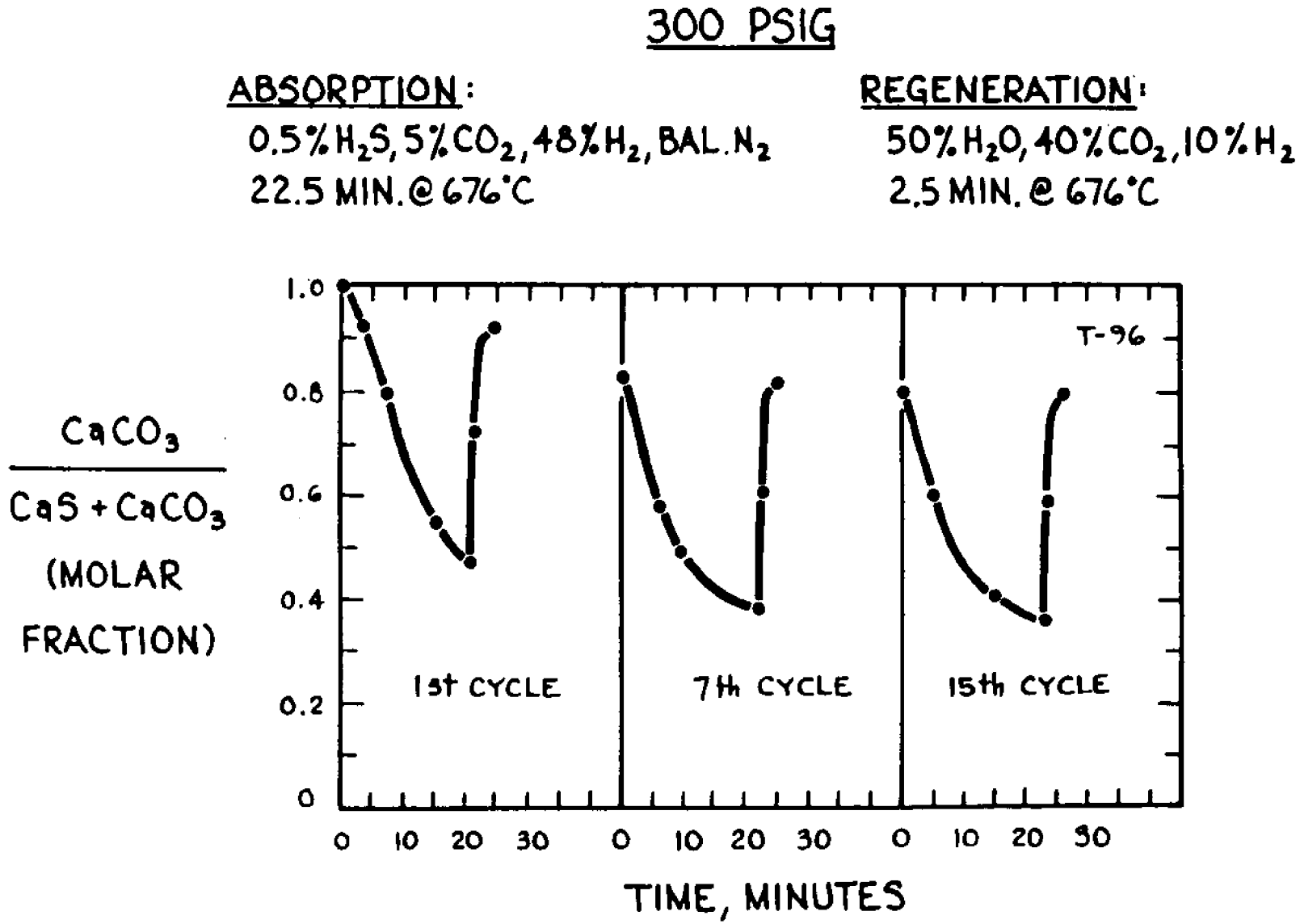

Figure 21. Rate data for Run T-96.

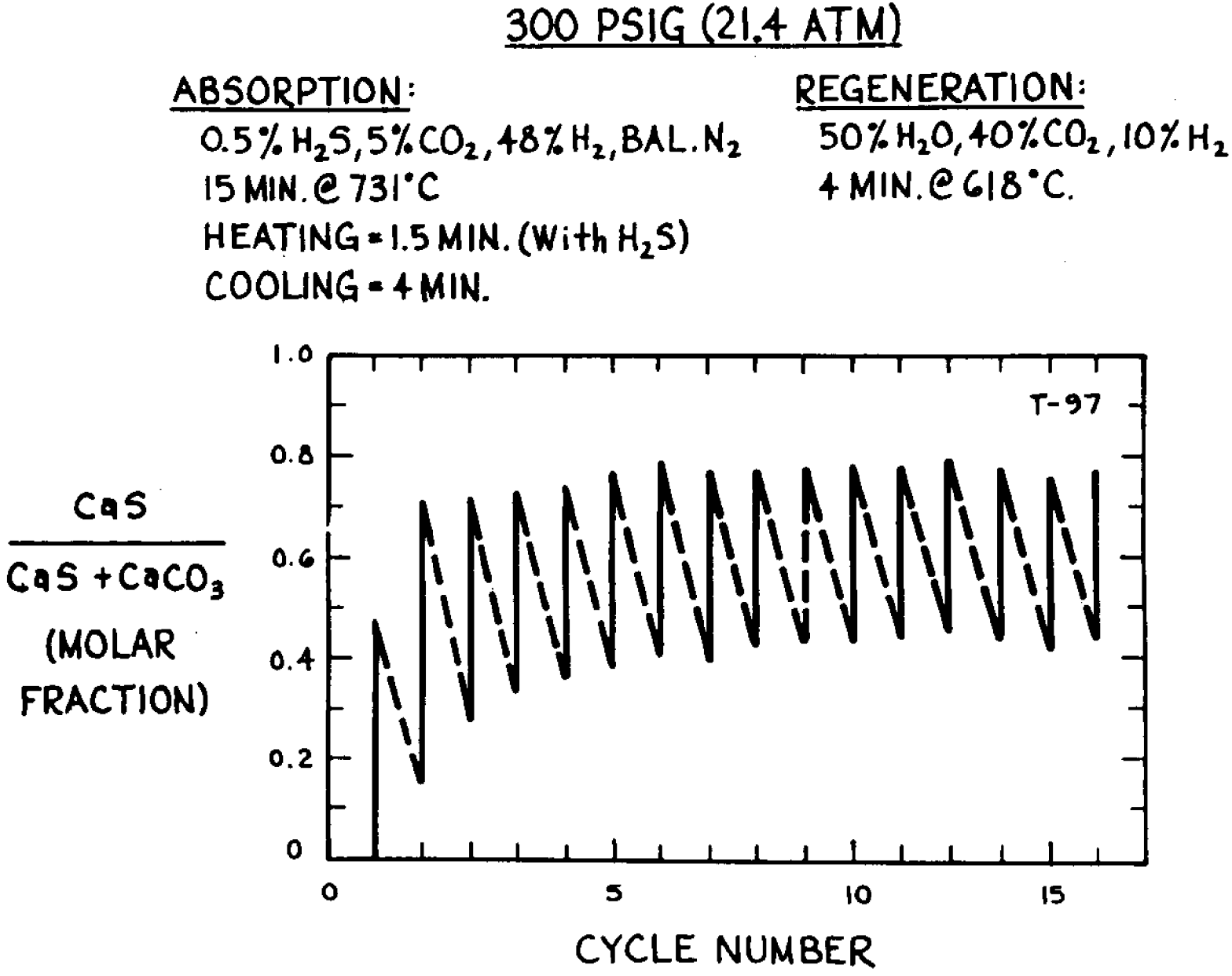

Figure 22. Zig-Zag chart for Run T-97.

300 PSIG

ABSORPTION:

0.5% H_2S, 5% CO_2, 48% H_2, BAL. N_2
15 MIN. @ 731°C.
1.5 MIN. HEATING (With H_2S)
4.5 MIN. COOLING

REGENERATION

50% H_2O, 40% CO_2, 10% H_2
4 MIN. @ 618°C

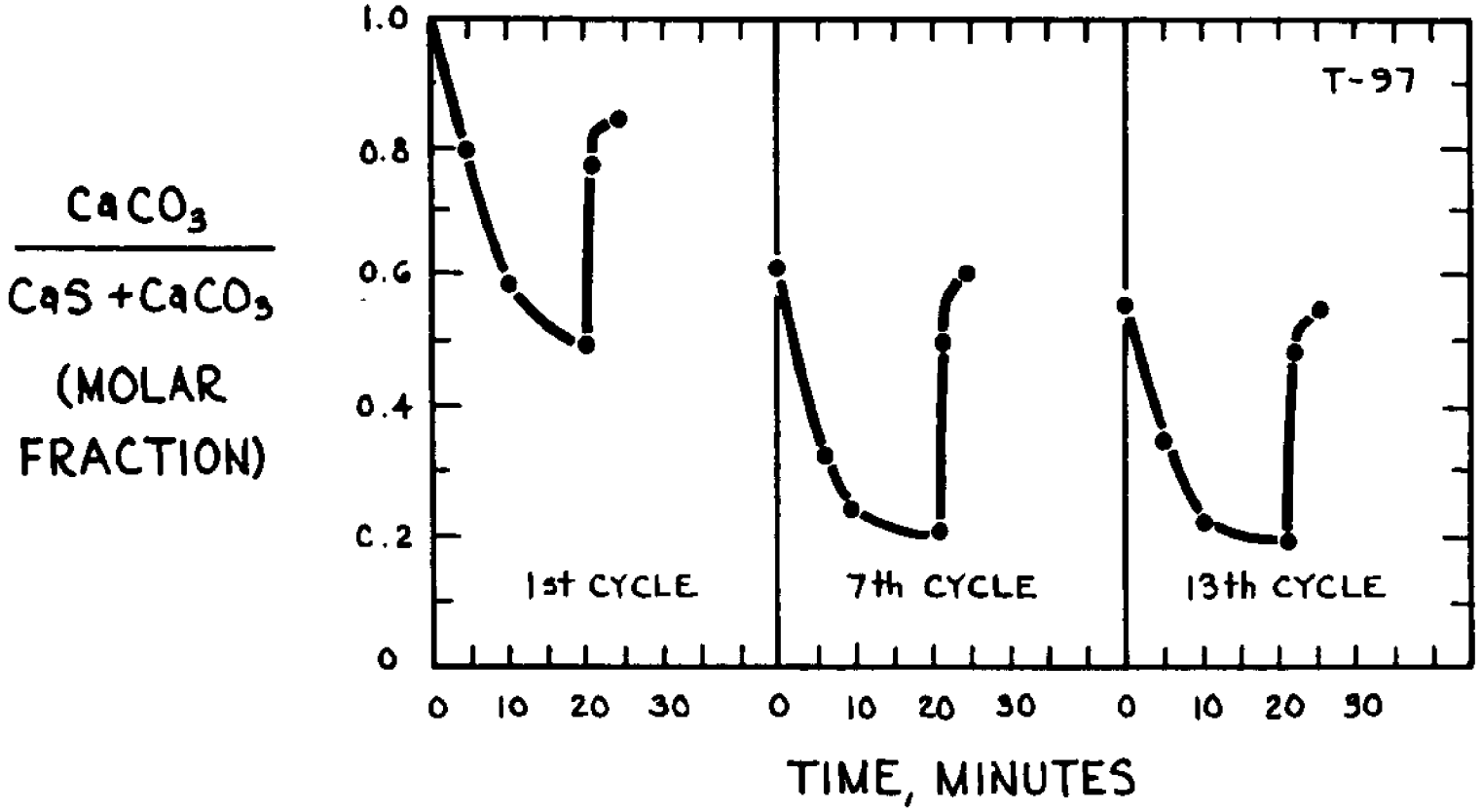

Figure 23. Rate data for Run T-97.

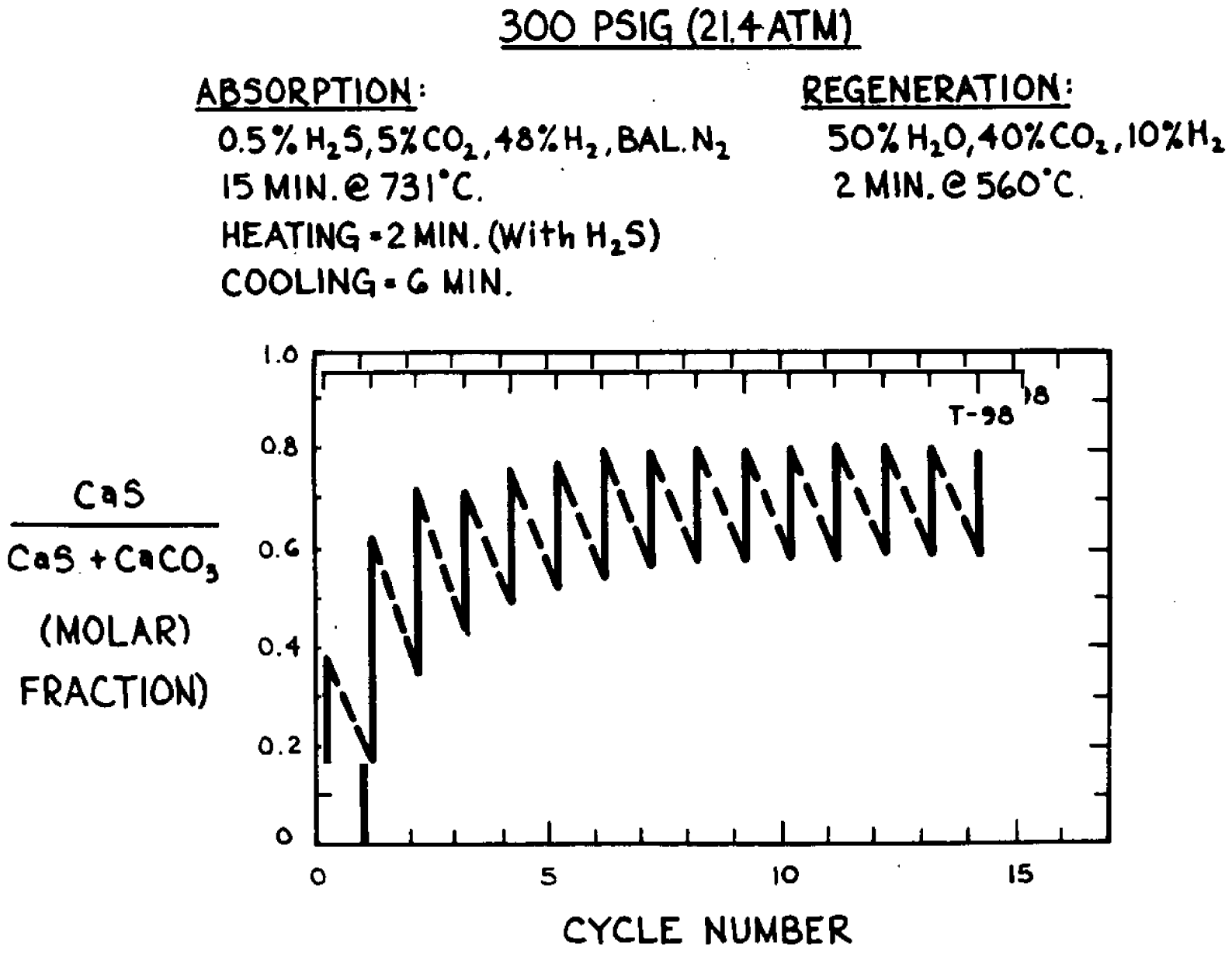

Figure 24. Zig-Zag chart for Run T-98.

300 PSIG

ABSORPTION:

0.5% H_2S, 5% CO_2, 48% H_2, BAL. N_2

15 MIN. @ 731°C.

2 MIN. HEATING (With H_2S)

6 MIN. COOLING

REGENERATION:

50% H_2O, 40% CO_2, 10% H_2

2 MIN. @ 560°C.

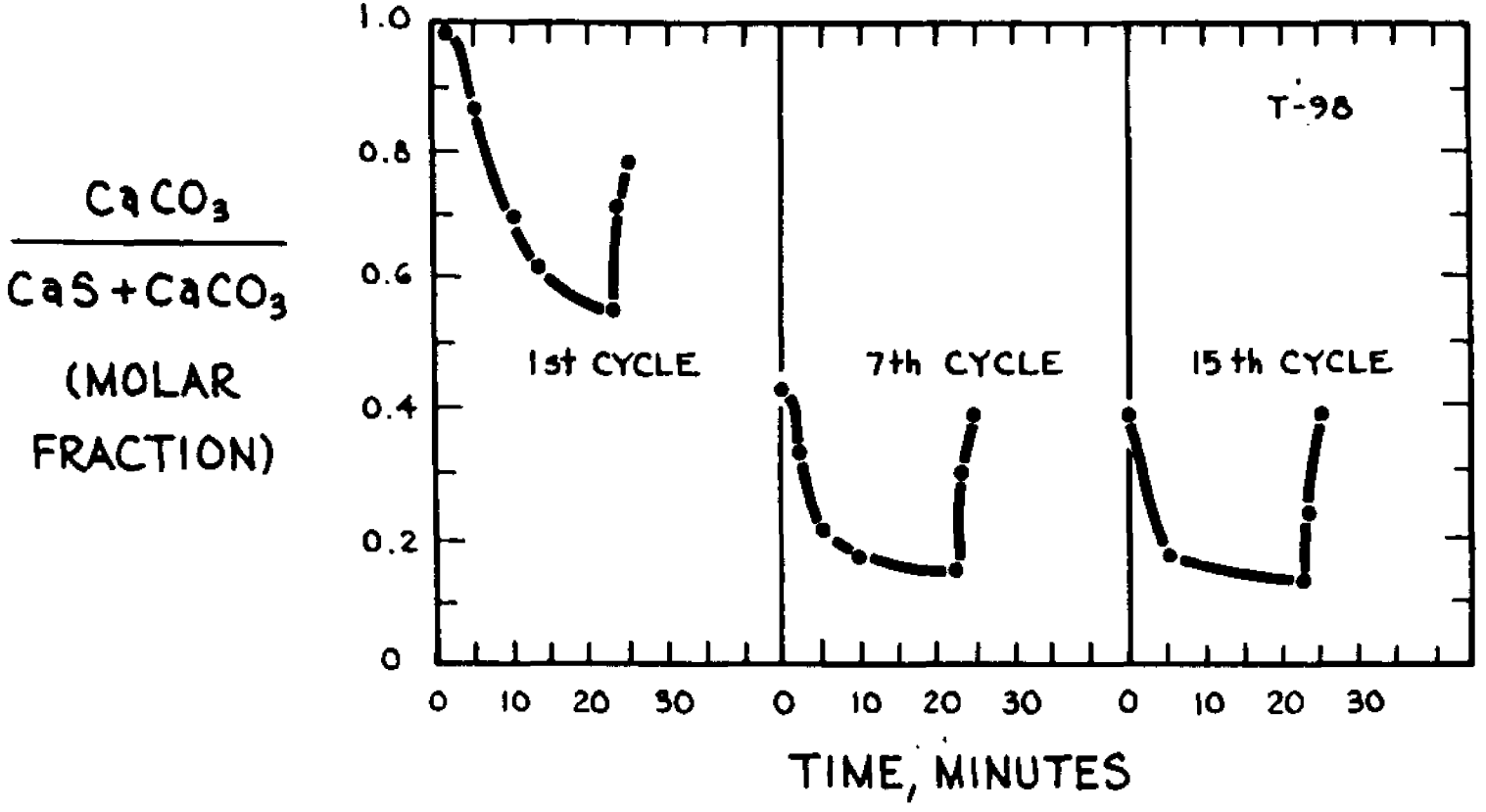

Figure 25. Rate data for Run T-98.

300 PSIG (21.4 ATM)

ABSORPTION:

0.5% H_2S, 5% CO_2, 48% H_2, BAL. N_2

13 MIN. @ 731°C.

HEATING = 2 MIN. (ex H_2S)

COOLING = 6 MIN.

REGENERATION:

50% H_2O, 40% CO_2, 10% H_2

4 MIN. @ 560°C.

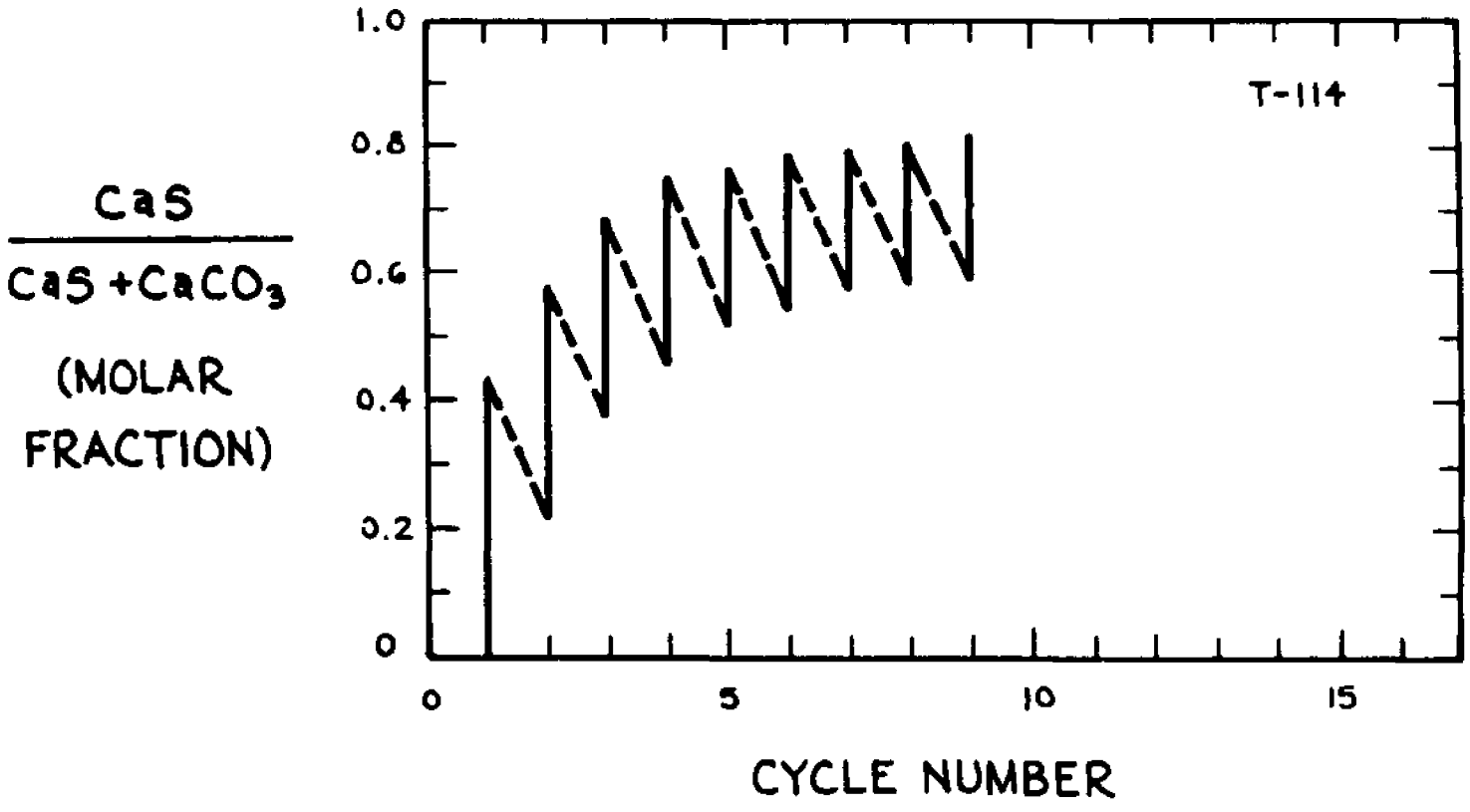

Figure 26. Zig-Zag chart for Run T-114.

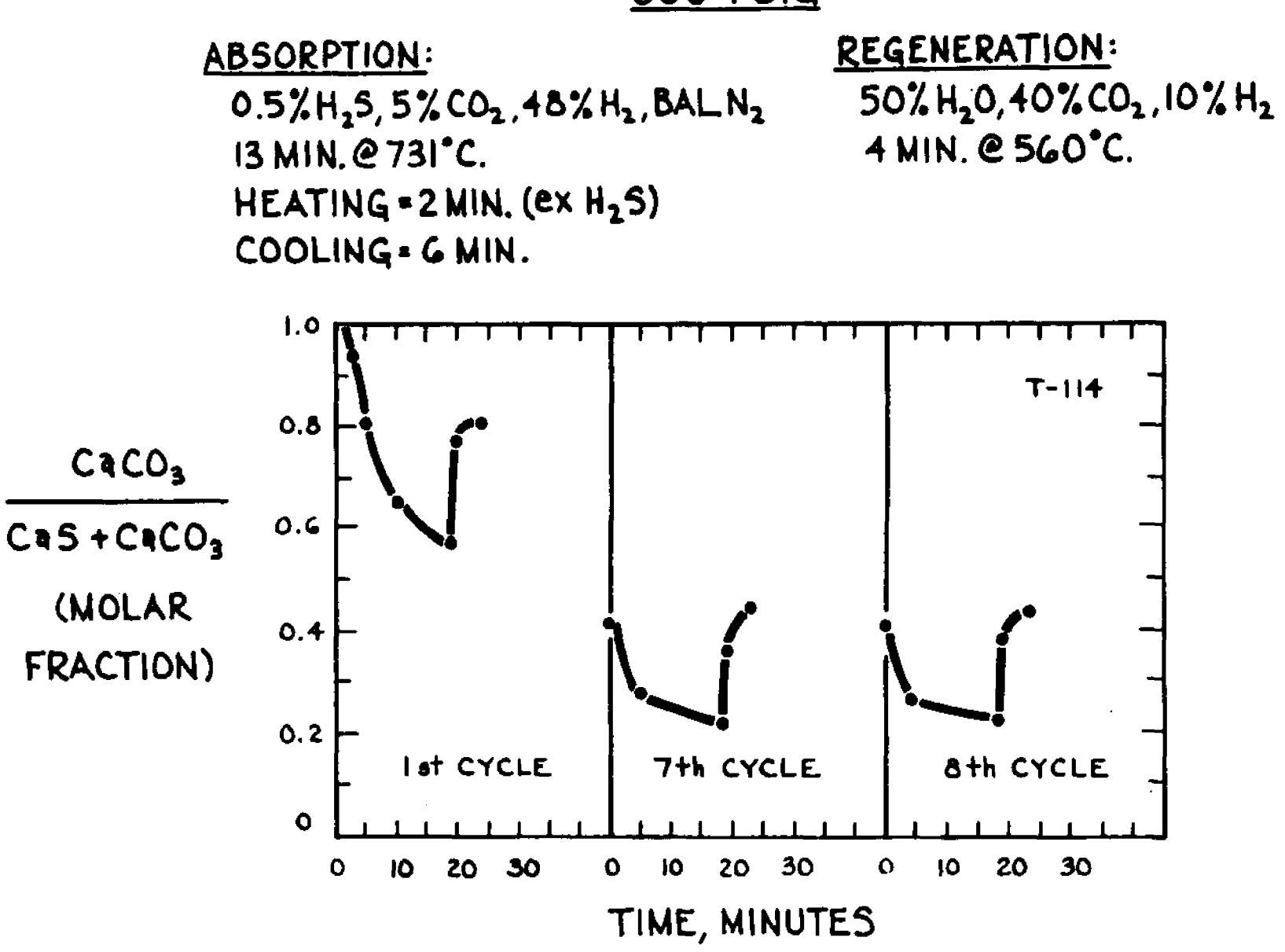

Figure 27. Rate data for Run T-114.

the total 25 minute cycle, 4 minutes were devoted to regeneration, and hydrogen sulfide was absent from absorption gas mixture during the two minutes heating from 560°C to 731°C. The longer regeneration time did not seem to have much effect, and the run of Figures 26 and 27 was terminated early.

Figures 28 and 29 are for absorption at 731°C and regeneration at 504°C.

300 PSIG (21.4 ATM)

ABSORPTION:

0.5% H_2S, 5% CO_2, 48% H_2, BAL. N_2
11 MIN. @ 731°C.
HEATING = 2 MIN. (With H_2S)
COOLING = 8 MIN.

REGENERATION:

50% H_2O, 40% CO_2, 10% H_2
4 MIN. @ 504°C.

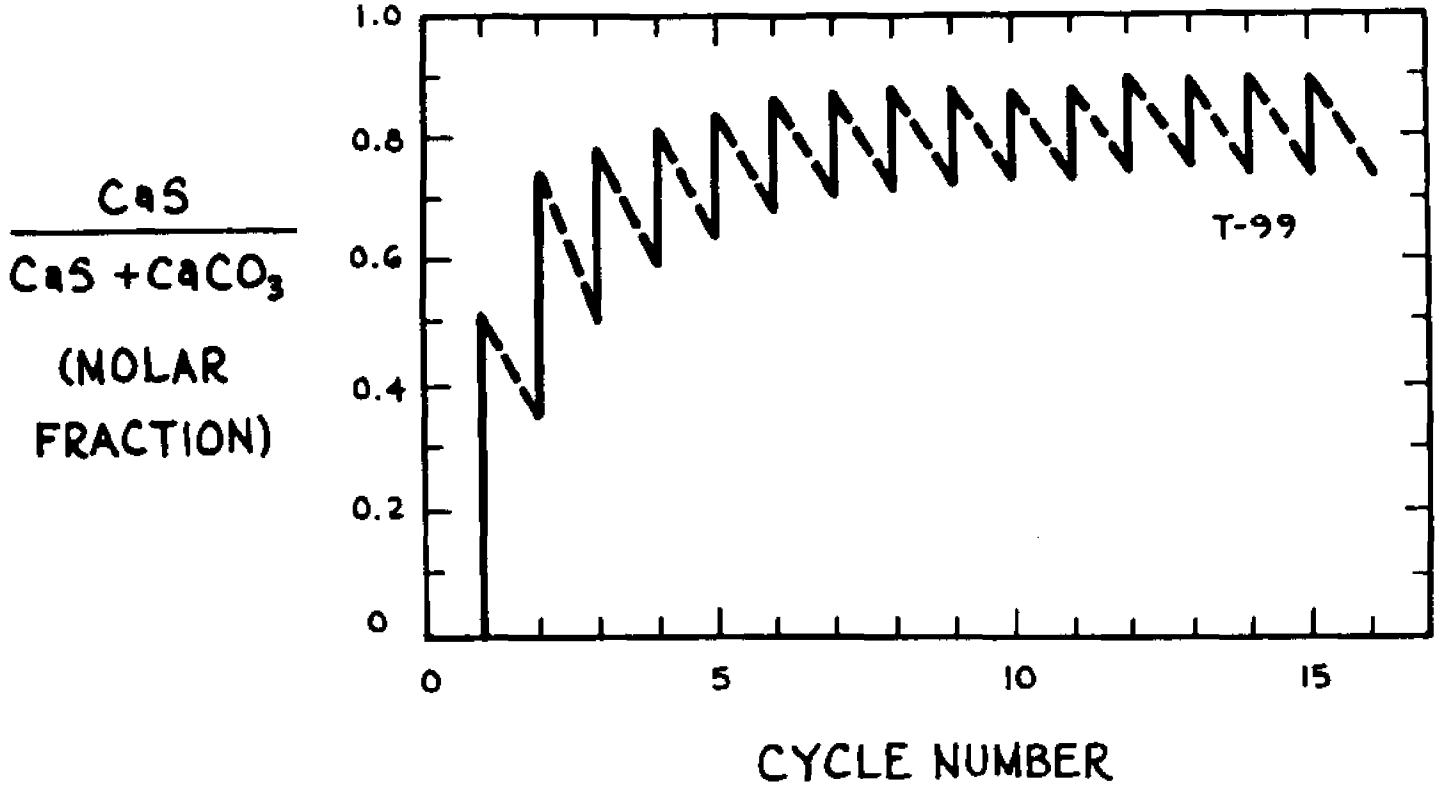

Figure 28. Zig-Zag chart for Run T-99.

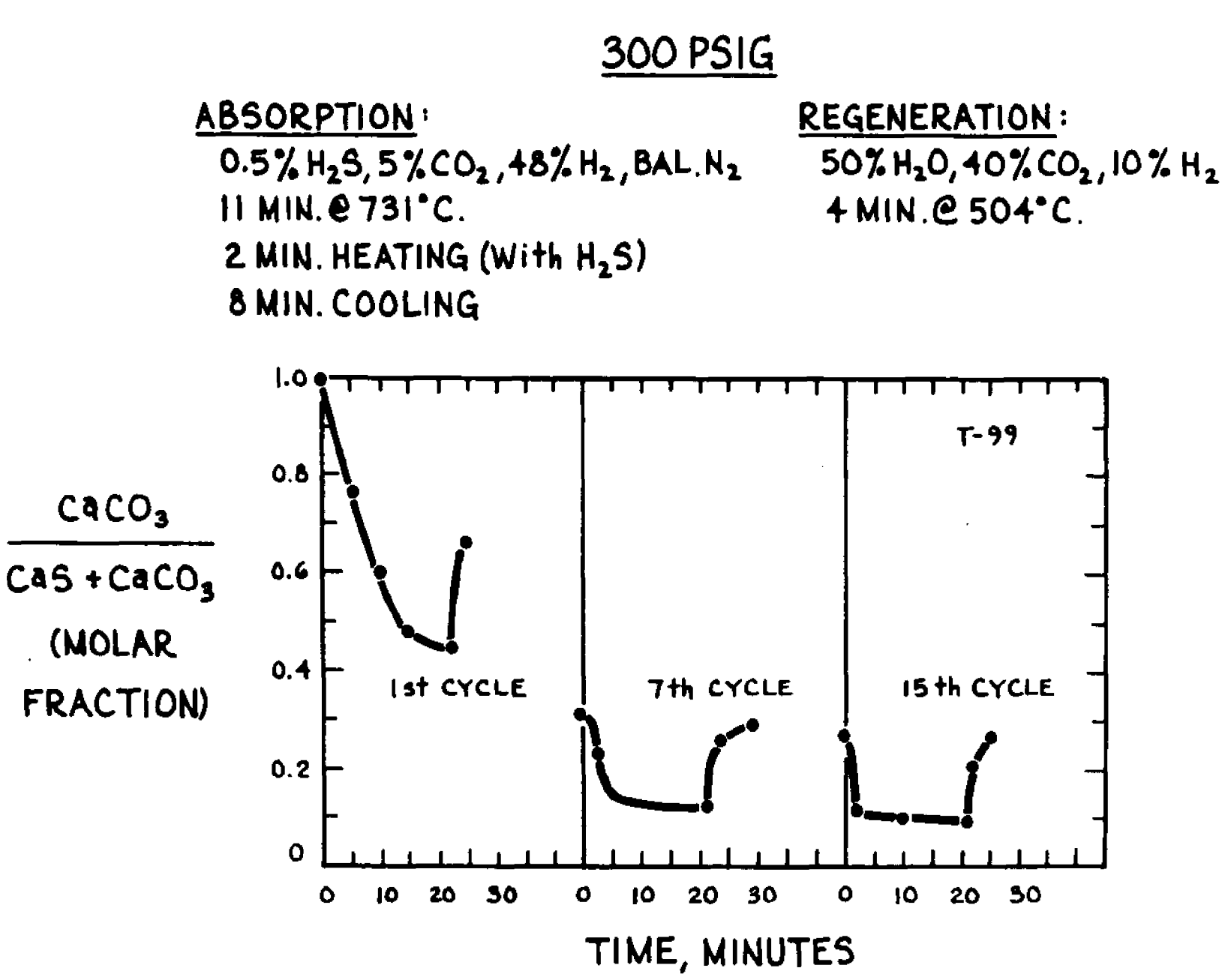

Figure 29. Rate data for Run T-99.

6.03 Run Testing Effect of Hydrogen in Regeneration Gas at 560°C

Figures 30 and 31 are plots for a run similar in every respect to the one plotted in Figures 26 and 27 above, except in that 10% nitrogen was substituted for 10% hydrogen in the steam and carbon dioxide mixture used in the regeneration step. The substitution of nitrogen seemed to have little effect at the 560°C temperature of the regeneration, and subsequent runs, reported in the Section 6.04 to follow, were conducted with a 50/50 mixture of steam and carbon dioxide.

Figure 32 gives rate data for the final cycle (the 15th) of the run illustrated in Figures 30 and 31 alongside data for the final cycle (the 8th) of the run illustrated in Figures 26 and 27. Figure 32 would suggest that presence of 10% hydrogen does not have a large effect upon the initial rate of the regeneration reaction at 560°C.

300 PSIG (21.4 ATM)

ABSORPTION:

0.5% H_2S, 5% CO_2, 48% H_2, BAL. N_2

13 MIN. @ 731°C.

HEATING = 2 MIN. (With H_2S)

COOLING = 6 MIN.

REGENERATION:

50% H_2O, 40% CO_2, 10% N_2

4 MIN. @ 560°C.

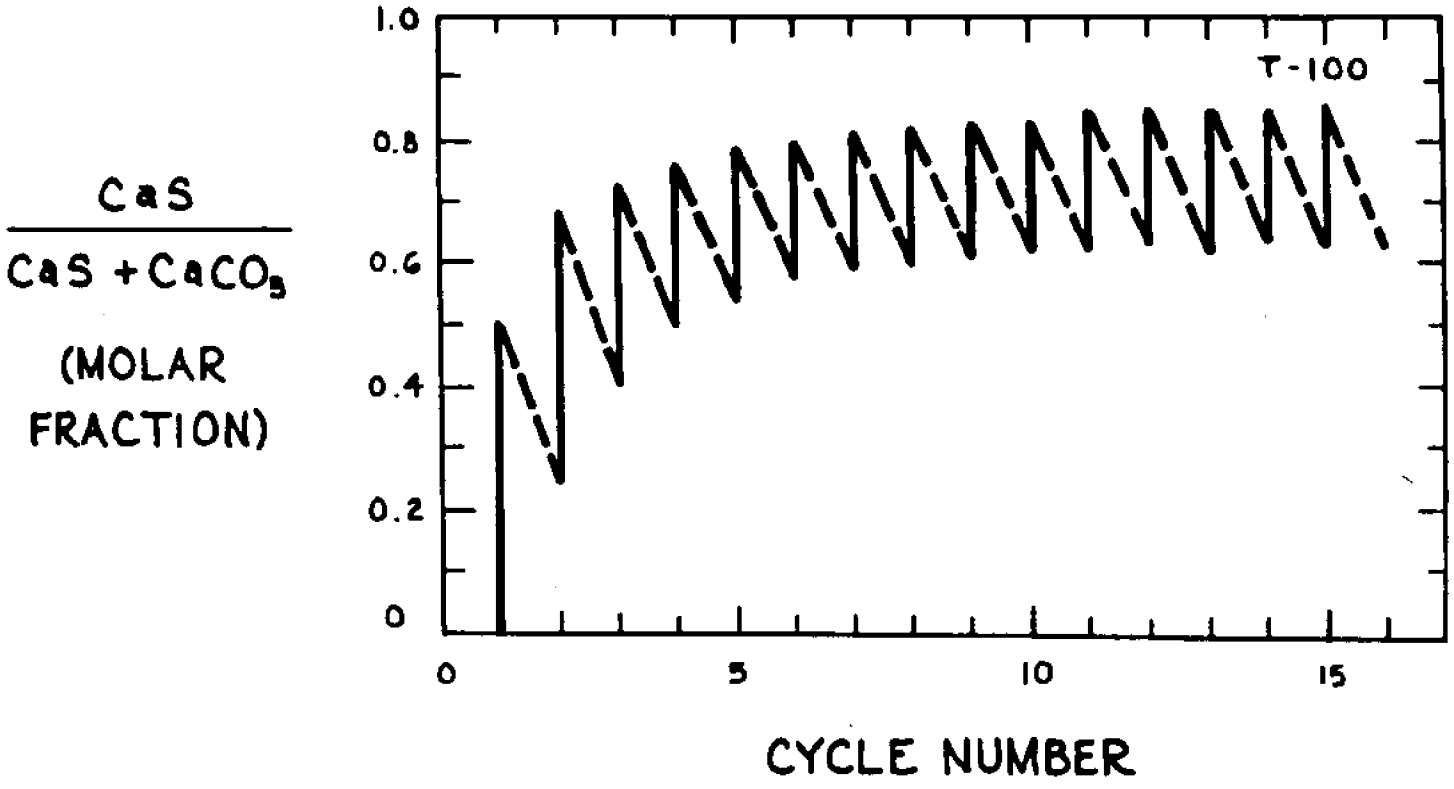

Figure 30. Zig-Zag chart for Run T-100.

300 PSIG

ABSORPTION:

0.5% H_2S, 5% CO_2, 48% H_2, BAL. N_2
13 MIN. @ 731°C.
2 MIN. HEATING (With H_2S)
6 MIN. COOLING

REGENERATION:

50% H_2O, 40% CO_2, 10% N_2
4 MIN. @ 560°C.

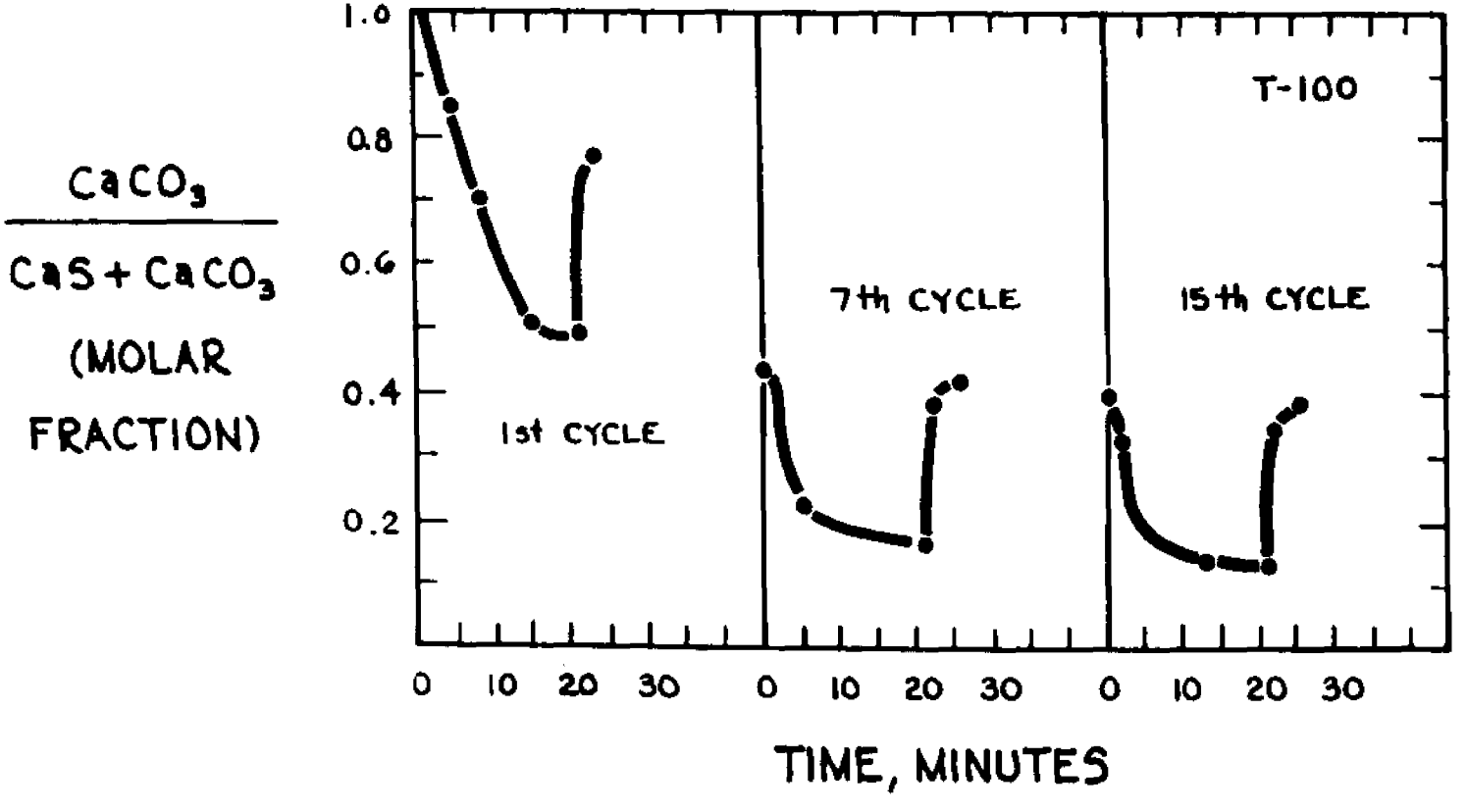

Figure 31. Rate data for Run T-100.

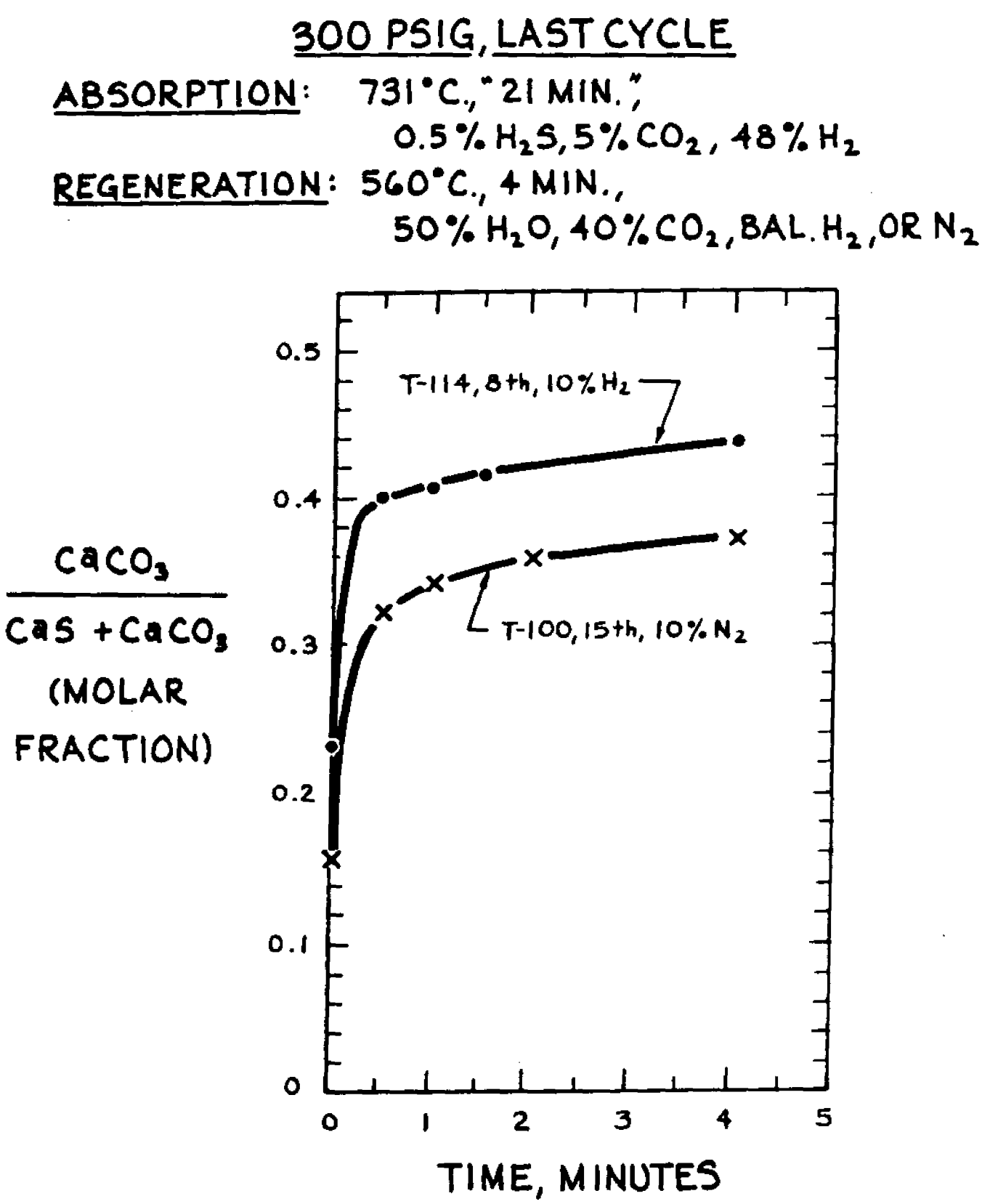

Figure 32. Rate data for final regeneration in runs with hydrogen and nitrogen present in regeneration gas at 760°C.

6.04 Data Showing Effect of Absorption Temperature on Absorptive Capacity

Figures 33 through 40 give data for a series of runs in which the regeneration temperature was held at 550°C and the absorption temperature was 700°C (Figures 33 through 36), 800°C (Figures 37 and 38), and 900°C (Figures 39 and 40).

The regeneration time was 4 minutes in the run summarized in Figures 33 and 34, and was 21 minutes in Figures 35 and 36. There was no marked improvement in final capacity at the longer regeneration time.

300 PSIG (21.4 ATM.)

ABSORPTION:
0.5% H_2S, 48% H_2, 5% CO_2, BAL. N_2
13 MIN. @ 700°C
HEATING = 2 MIN. (ex H_2S)
COOLING = 6 MIN.

REGENERATION:
50% H_2O, 50% CO_2
4 MIN. @ 550°C

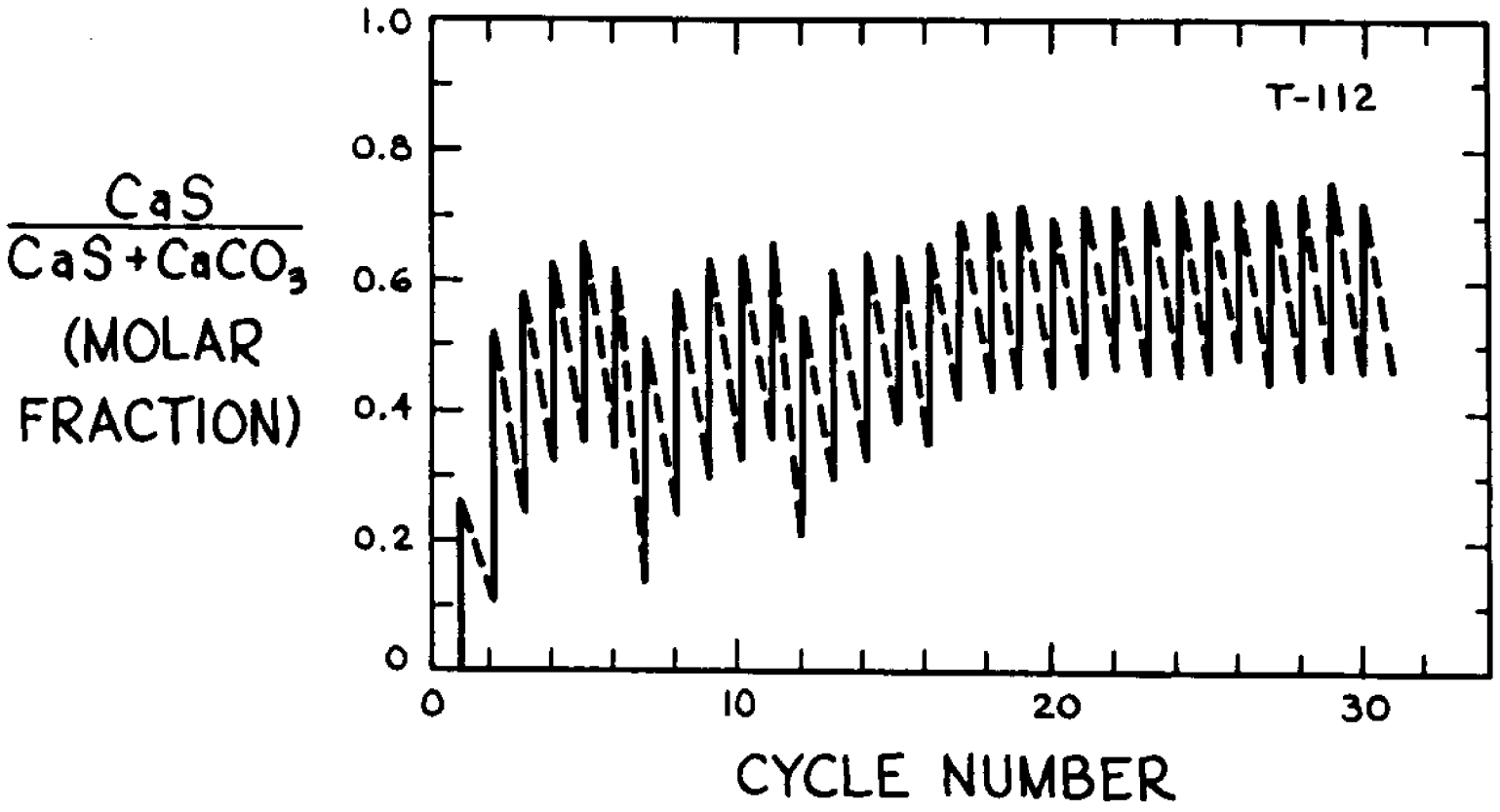

Figure 33. Zig-Zag chart for Run T-112.

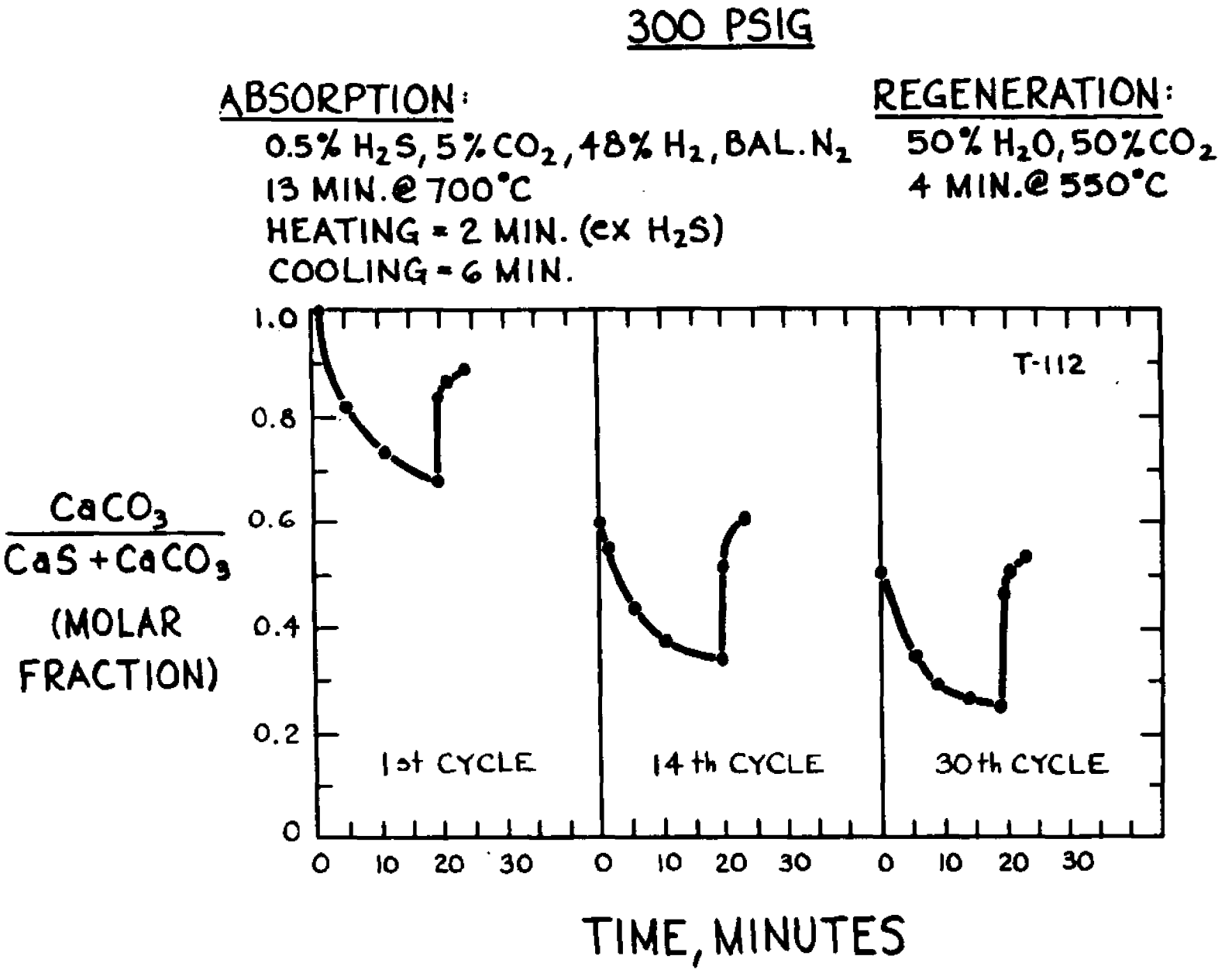

Figure 34. Rate data for Run T-112.

300 PSIG (21.4 ATM)

ABSORPTION:

0.5% H_2S, 5% CO_2, 48% H_2, BAL. N_2
13 MIN. @ 700°C.
HEATING = 2.5 MIN. (ex H_2S)
COOLING = 6 MIN.

REGENERATION:

50% H_2O, 50% CO_2
21 MIN. @ 550°C.

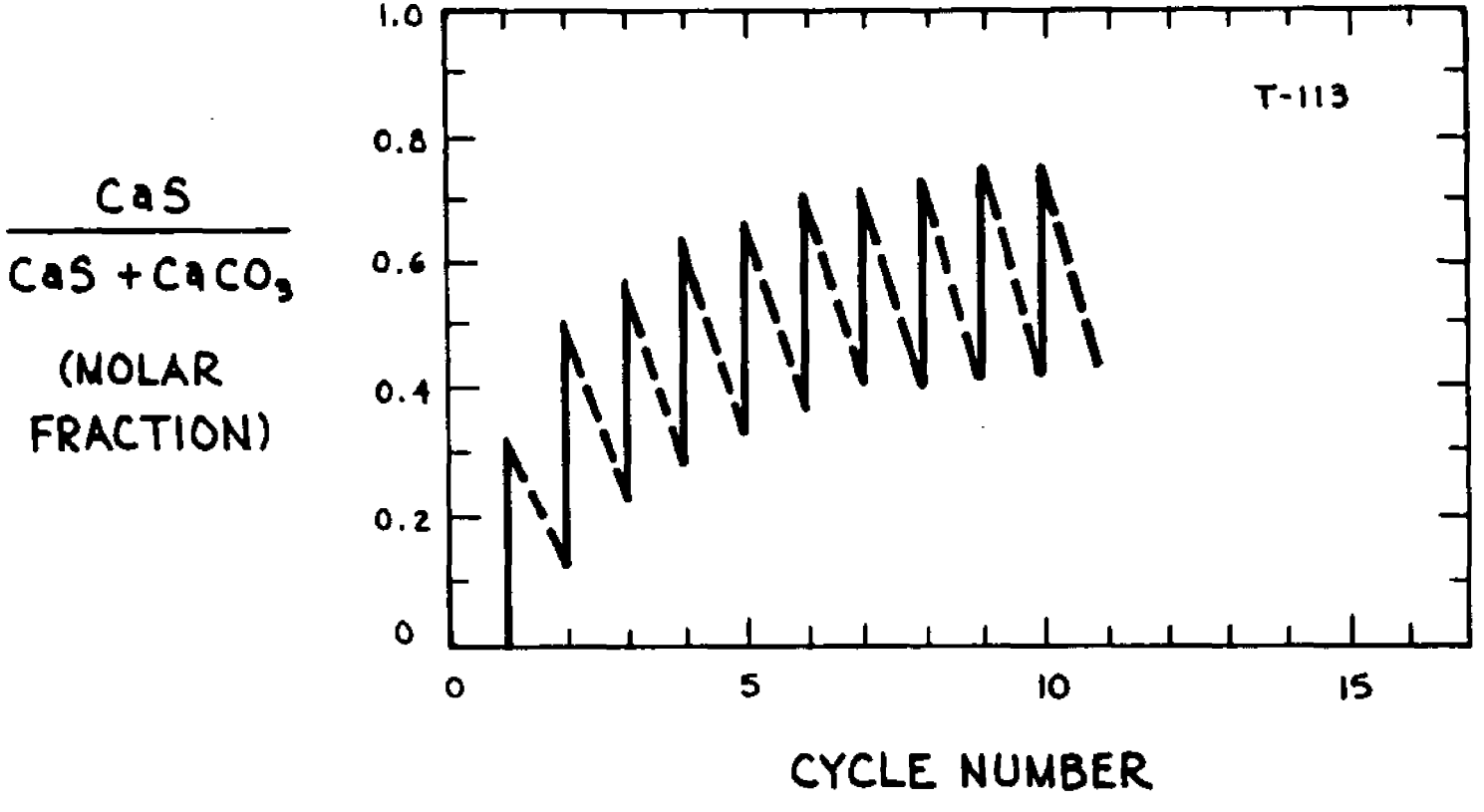

Figure 35. Zig-Zag chart for Run T-113.

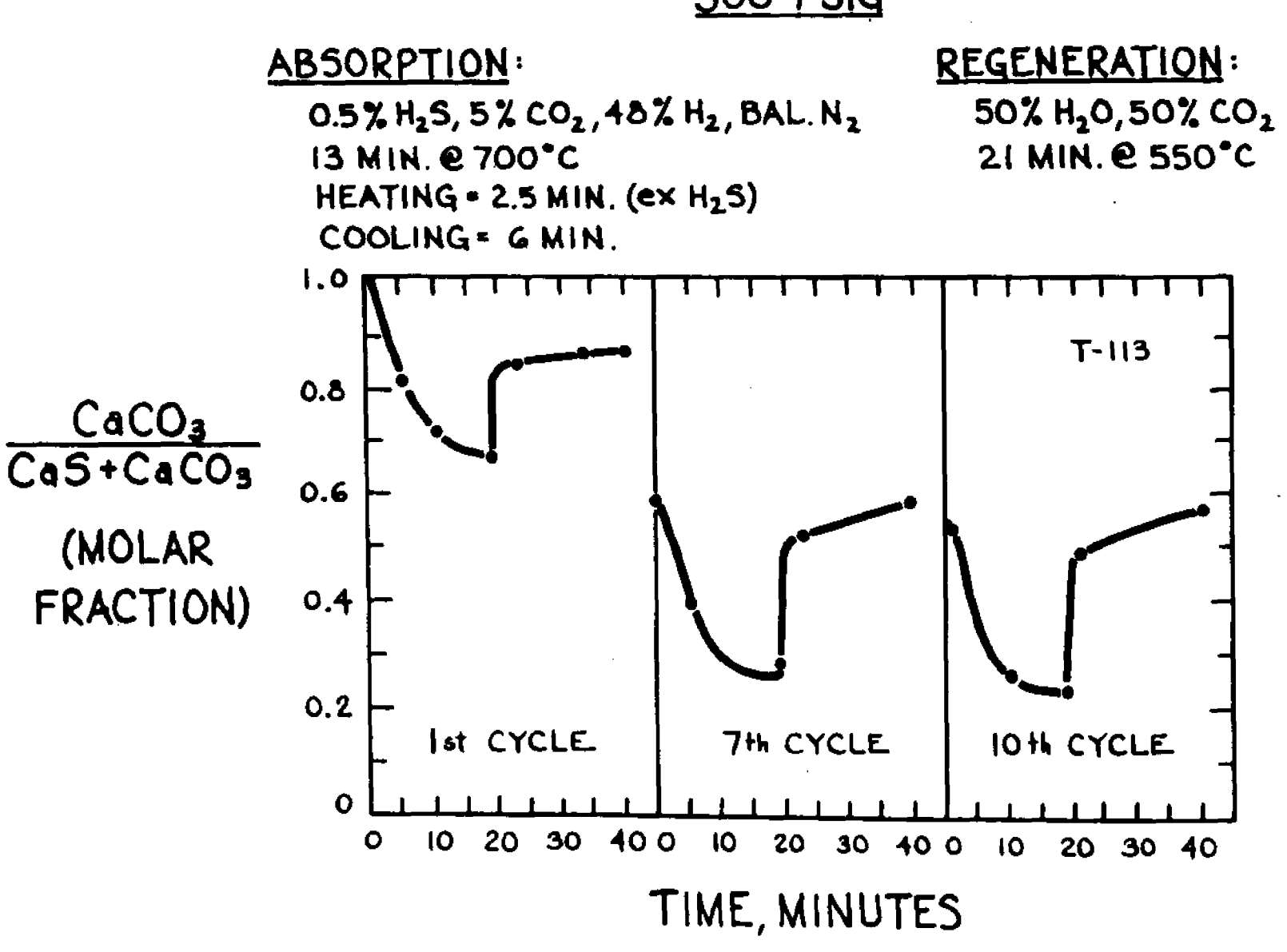

Figure.36. Rate data for Run T-113.

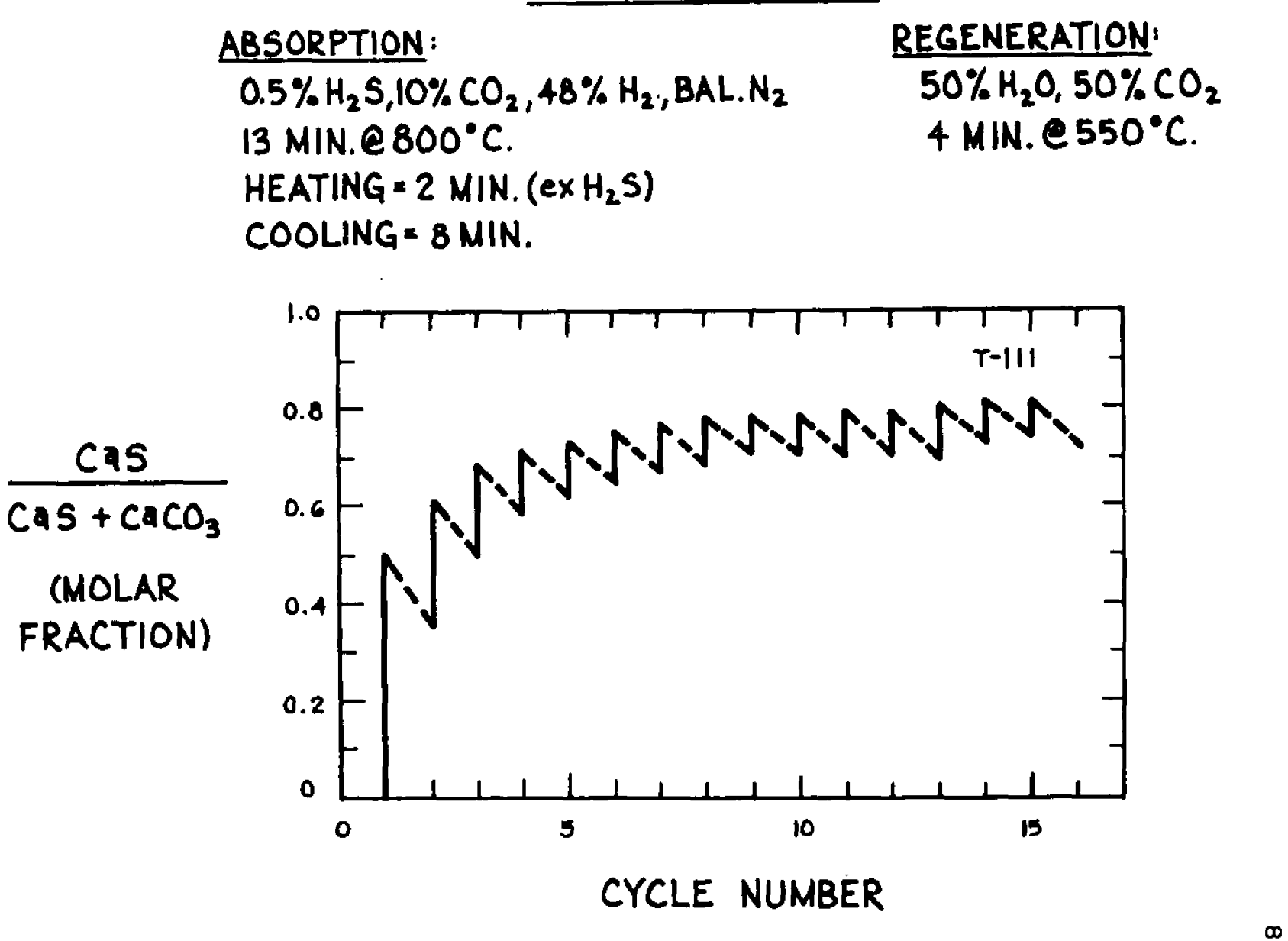

Figure 37. Zig-Zag chart for Run T-111.

300 PSIG

ABSORPTION:
0.5% H_2S, 10% CO_2, 48% H_2, BAL. N_2
13 MIN. @ 800°C.
HEATING = 2 MIN. (ex H_2S)
COOLING = 8 MIN.

REGENERATION:
50% H_2O, 50% CO_2
4 MIN. @ 550°C.

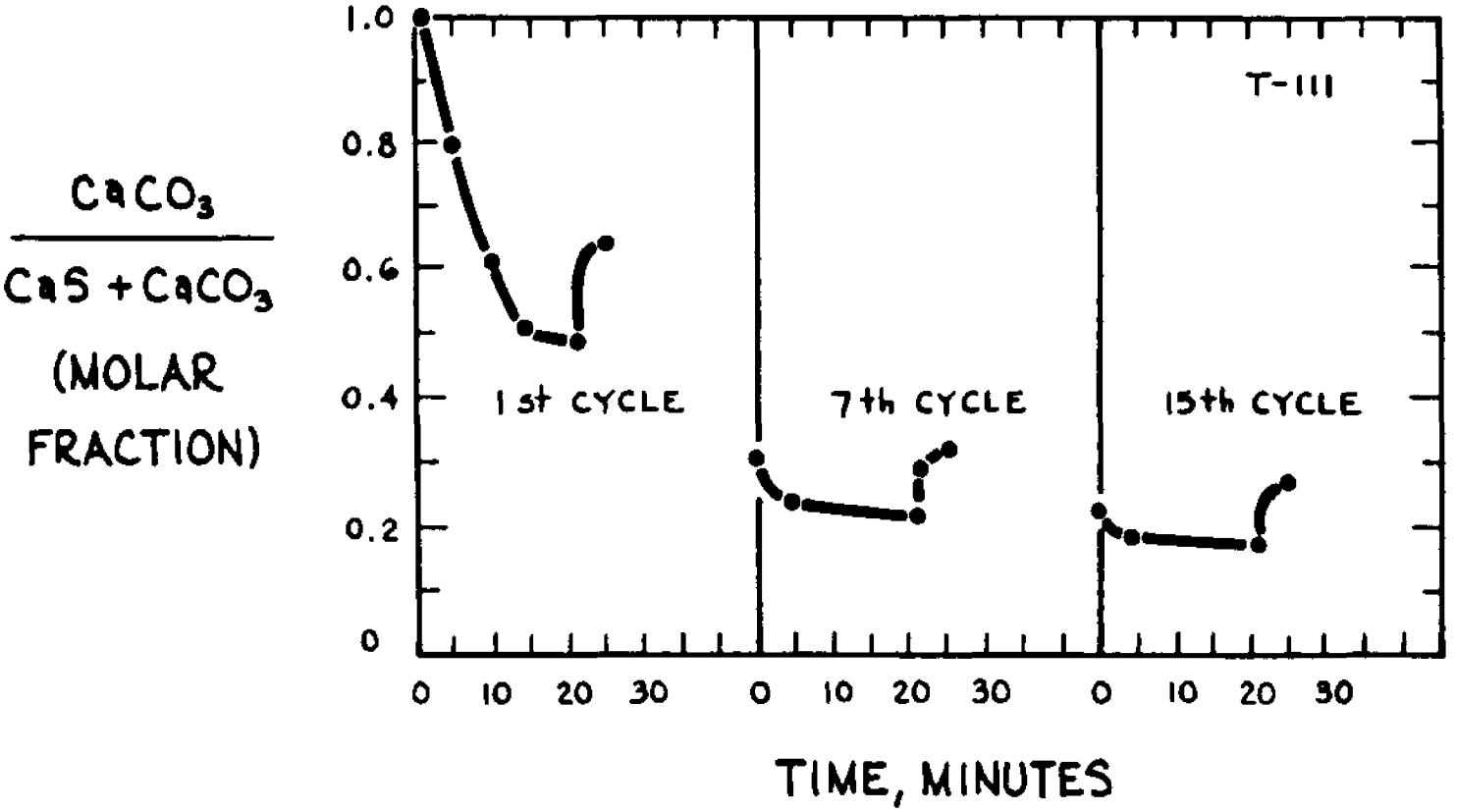

Figure 38. Rate data for Run T-111.

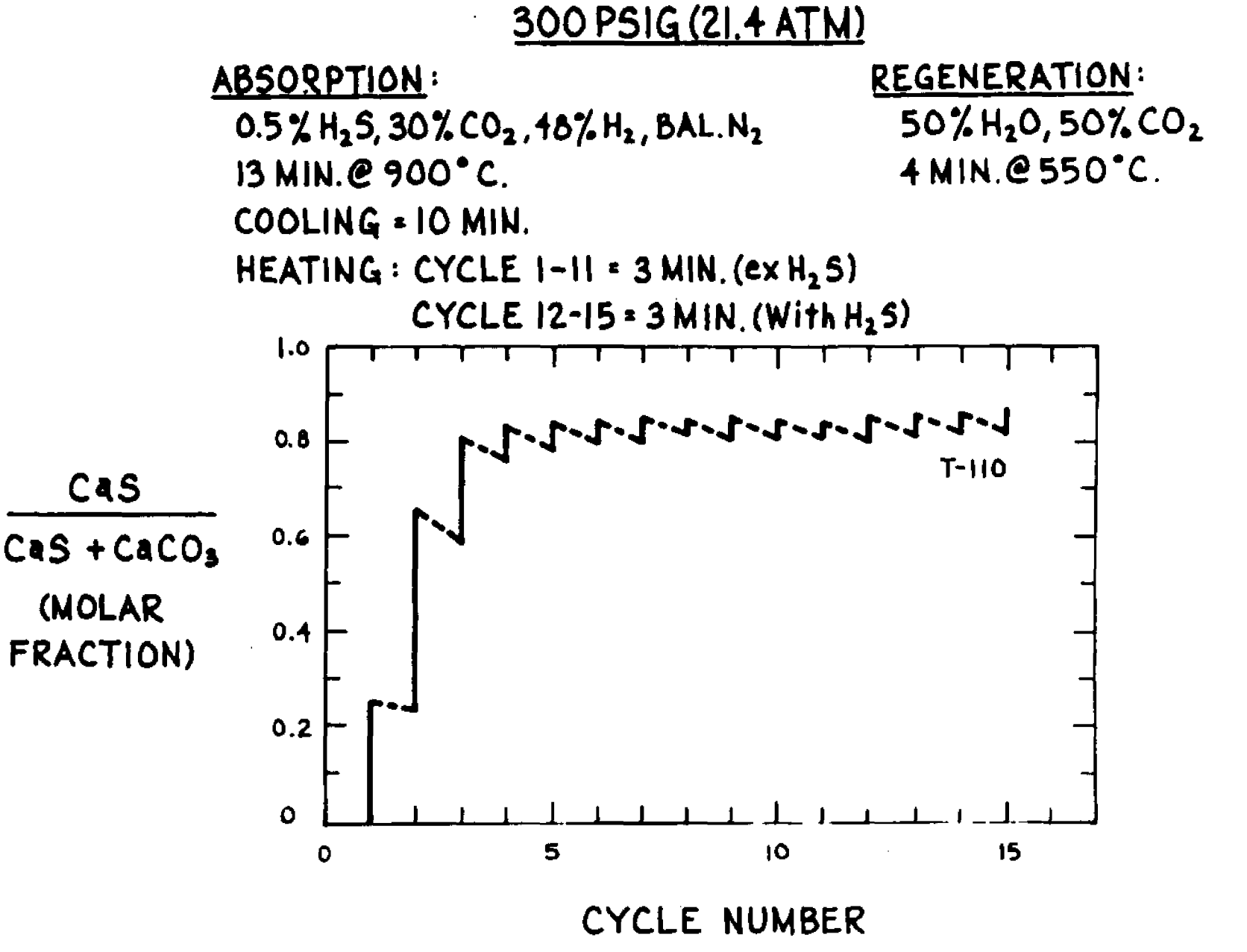

Figure 39. Zig-Zag chart for Run T-110.

300 PSIG

ABSORPTION:
0.5% H_2S, 30% CO_2, 48% H_2, BAL. N_2
13 MIN. @ 900°C.
COOLING = 10 MIN.
HEATING: CYCLE 1–11 = 3 MIN. (ex H_2S)
CYCLE 12–15 = 3 MIN. (With H_2S)

REGENERATION:
50% H_2O, 50% CO_2
4 MIN. @ 550°C.

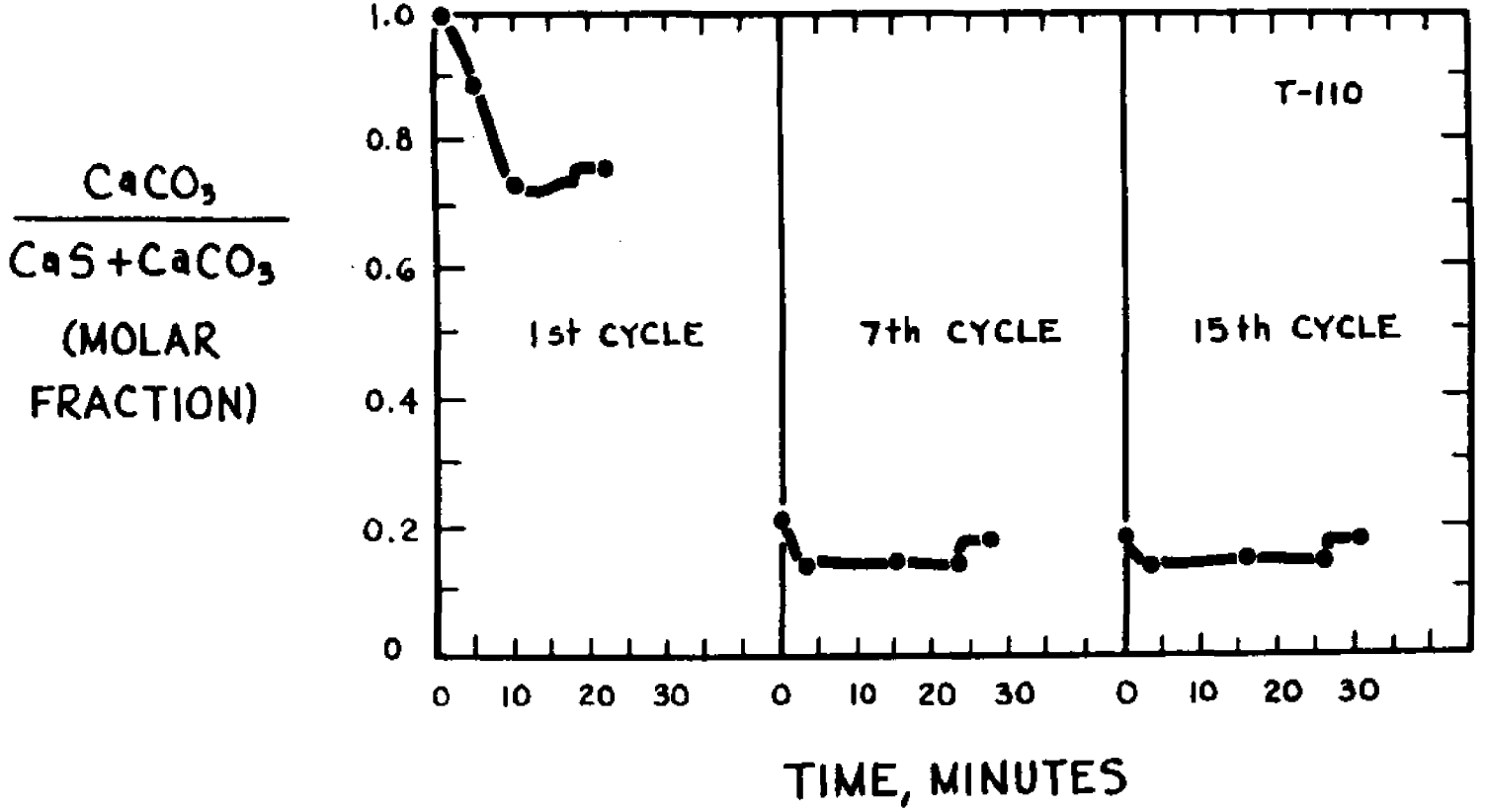

Figure 40. Rate data for Run T-110.

6.05 Discussion of Data Showing Effects of Regeneration and Absorption Temperatures upon Absorptive Capacity

Table 2 lists the runs from which the effect of regeneration temperature upon capacity may be judged.

Figure 41 gives plots of absorptive capacity versus cycle number for three runs with absorption at 731°C and with regeneration at three temperature levels noted in the figure. It is seen that the absorptive capacity tends to approach a constant "final" value after about the seventh cycle.

Figure 42 shows rate data for the last cycle of absorption and regeneration for each of the three runs of Figure 41.

A striking feature of Figure 42 is that the initial rate of the regeneration reaction does not appear to vary with temperature; only the capacity varies. It would appear that the regeneration reaction at the indicated partial pressures of carbon dioxide and steam is extremely rapid. The rate was probably diffusion controlled in our experiments.

We have discovered that the logarithms of the "final" capacities at a given absorption temperature give a straight-line plot versus the reciprocal of the absolute temperature at which the regeneration reaction is carried out. Figure 43 illustrates this plot. Although only three points have been used to plot Figure 43, inspection of values from other runs in Table 2 show that they support the position and trend of the line plotted.

The line in Figure 43 is given by

$$\log_{10} C = 3.7127 - 1,974/T_R \qquad (4)$$

where C = "final" absorptive capacity in percent, and T_R = regeneration temperature in °K.

Table 2

Cyclic Runs with Different Regeneration Temperatures (All data at 300 psig)[1,6]

	Absorption			Regeneration	
Run #	Temp. °C	Time, Min.	Final Capacity, %	Temp. °C	Time, Min.
T-94	731	15	40 (15)[5]	731	10
T-95	676	15	36 (15)	676	10
T-96	676	22.5	42 (15)	676	2.5
T-97[3]	731	21 (1.5-15-4.5)[2]	32 (15)	618	4
T-99[4]	731	21 (2-11-8)	15 (15)	504	4
T-100	731	21 (2-13-6)	22 (15)	560	4
T-114	731	21 (2-13-6)[7]	22 (9)	560	4

1. All half-calcinations were made at 25% H_2O, 50% CO_2, 25% N_2 up to 787°C, except T-94 up to 731°C.
2. Numbers in parentheses indicate heating time, time at temperature, and cooling time respectively.
3. After half-calcination, T-97 sample was cooled to room temperature in 50%CO_2 and 50% N_2. First absorption started next day after heating up in 50% CO_2, 50% N_2 to 731°C.
4. After half-calcination, T-99 sample was cooled to room temperature in 50%CO_2 and 50% N_2. First absorption started next day after heating up in 25% H_2O, 50% CO_2, 25% N_2 to 731°C.
5. Numbers in parentheses indicate last cycle number.
6. 0.5% H_2S, 5% CO_2, 48% H_2, balance N_2 for absorption; 50% H_2O, 40% CO_2, 10% H_2 for regeneration except 10% N_2 instead of 10% H_2 for T-100.
7. H_2S not present during heating.

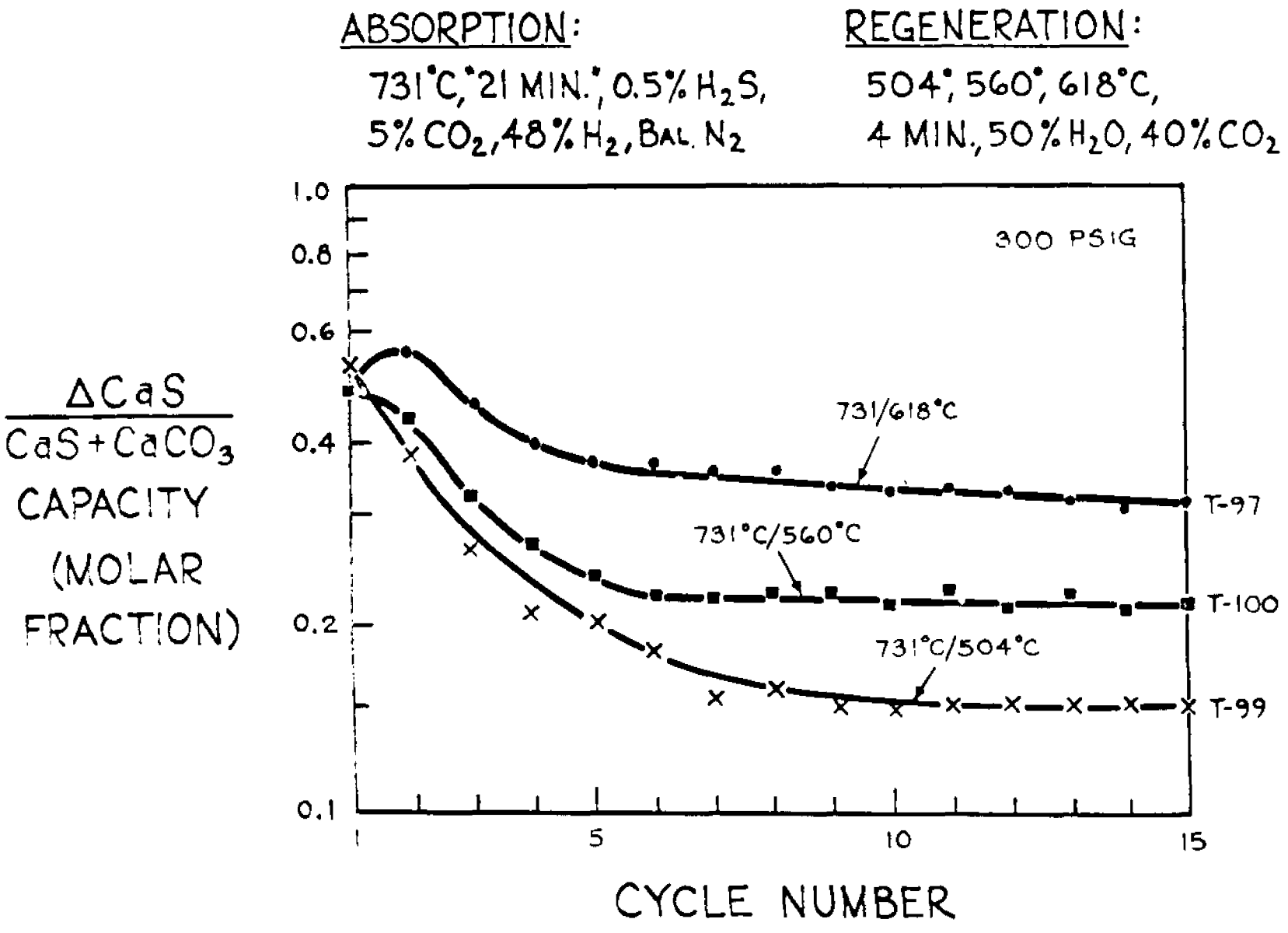

Figure 41. Capacity versus cycle number for three runs with absorptions at 731°C (the first temperature designated alongside each curve) and regenerations at 618°C, and 504°C, and 560°C, (the second temperature).

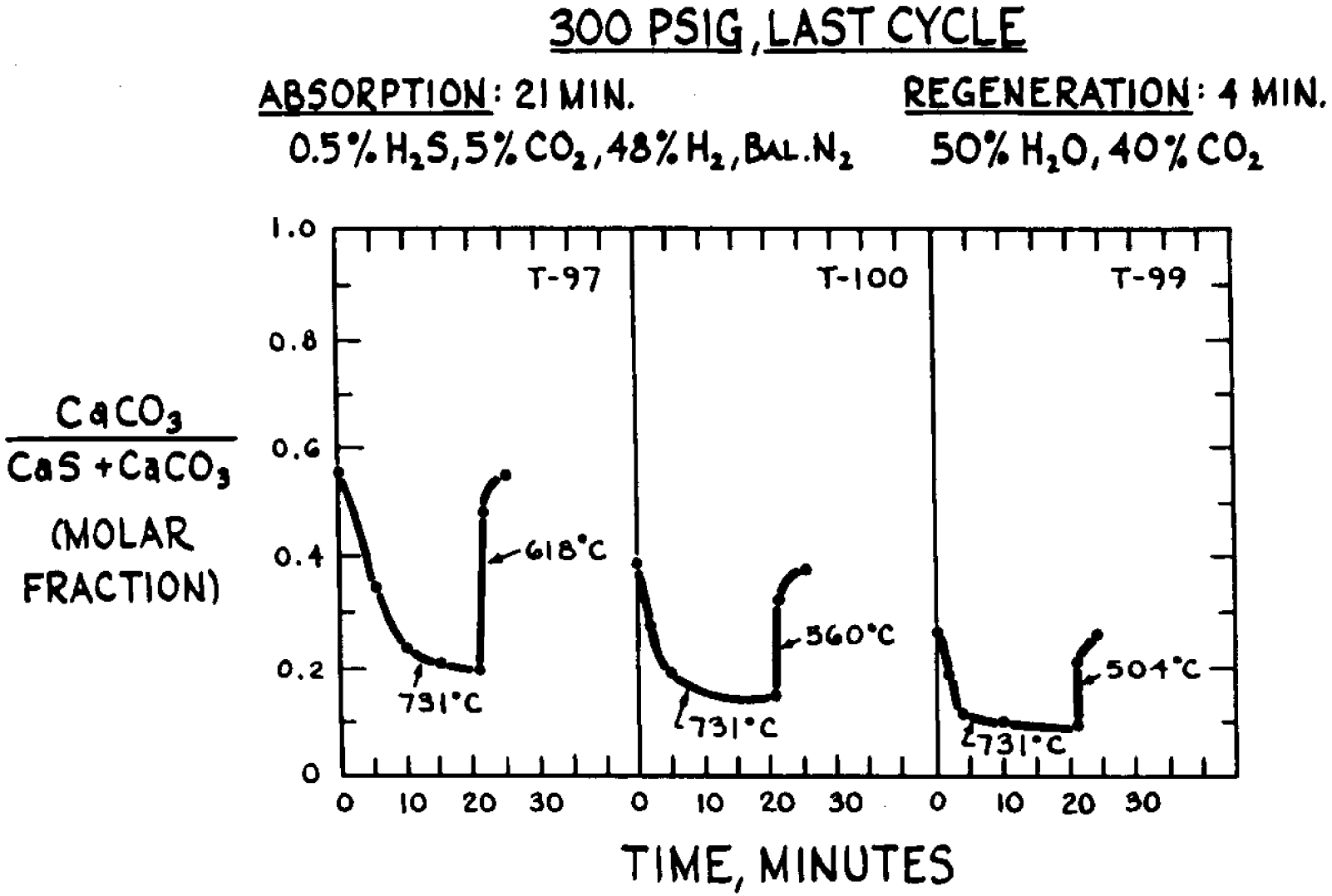

Figure 42. Rate data for last cycle of absorption and regeneration in three runs showing effect of regeneration temperature upon capacity.

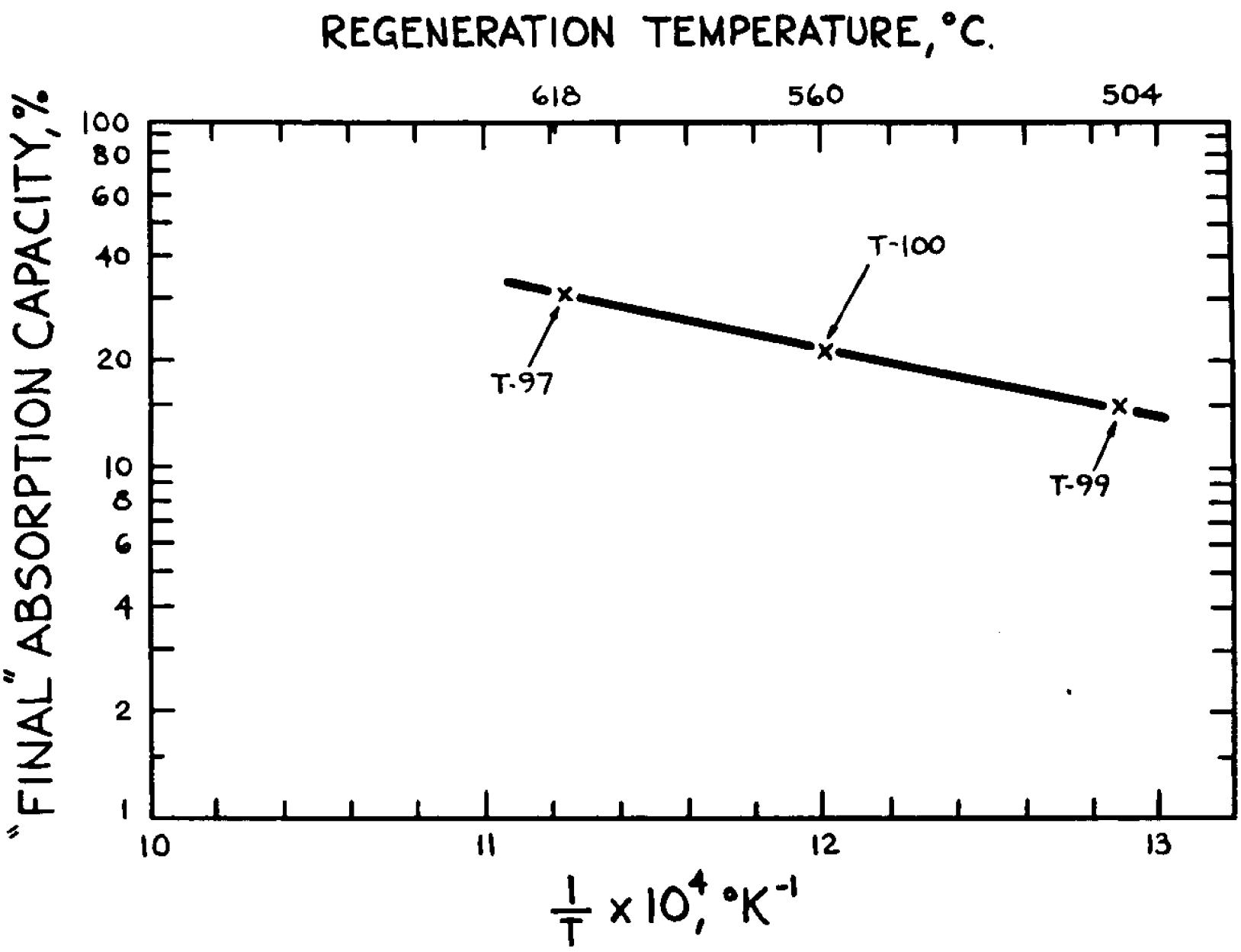

Figure 43. Logarithm of "final" capacity versus reciprocal absolute temperature of regeneration, for absorptions at 731°C.

Table 3 lists the runs from which the effect of absorption temperature upon capacity may be judged.

Figure 44 gives plots of absorptive capacity versus cycle number for four runs with regeneration at 550°C or 560°C and with absorption at four temperature levels noted in the figure. As in Figure 41, capacity is seen to level off to a "final" value at about the eighth cycle.

Figure 45 shows rate data for the last cycle of absorption and regeneration for each of the four runs of Figure 44.

It is striking that the initial rate of absorption after a number or cycles does not appear to vary much with temperature.

We have discovered that the logarithms of "final" capacities at a given regeneration temperature give a straight-line plot versus the reciprocal of the absolute temperature at which the absorption is conducted. Figure 46 illustrates this plot.

The line in Figure 46 is given by

$$\log_{10} C = 4{,}789/T_A - 3.4805 \qquad (5)$$

where C = "final" absorptive capacity in percent, and T_A = absorption temperature in °K.

The information given in Figures 43 and 46 is perhaps the most significant obtained in the present research. It is impossible not to remark that the trends in these figures are disappointing. From a process point of view, it is better to conduct absorption at the highest temperature consistent with the partial pressure of carbon dioxide in the gas to be desulfurized and the desire not to convert the solid into fully-calcined material. It

Table 3

Cyclic Runs with Different Absorption Temperatures

(All data at 300 psig)[1]

Run #	Absorption Temp. °C	Absorption Time min.	Absorption Capacity at Last Cycle, %	Absorption Gases, Bal N_2 $H_2S/CO_2/H_2$	Desorption Temp. °C	Desorption Time min.	Desorption Gases, Bal N_2 $H_2O/CO_2/H_2$
T-110	900	23 (3-13-10)[2,5]	4 (15)[4]	0.5/30/48	550	4	50/50/0
		26 (3-13-10)[3]					
T-111	800	21 (2-13-8)[5]	9 (15)	0.5/10/48	550	4	50/50/0
T-112	700	19 (2-13-6)[5]	29 (30)	0.5/ 5/48	550	4	50/50/0
T-113	700	19 (2.5-13-6)[5]	33 (10)	0.5/ 5/48	550	21	50/50/0
T-114	731	19 (2-13-6)[5]	22 (9)	0.5 5/48	560	4	50/40/10

1. All half-calcinations were made at 25% H_2O, 50% CO_2, 25% N_2 up to 787°C.
2. Numbers in parentheses indicate heating, at, cooling times in the same order.
3. H_2S gas present during heating from twelfth cycle to fifteenth cycle.
4. Numbers in parentheses indicate last cycle number.
5. H_2S absent during heating.

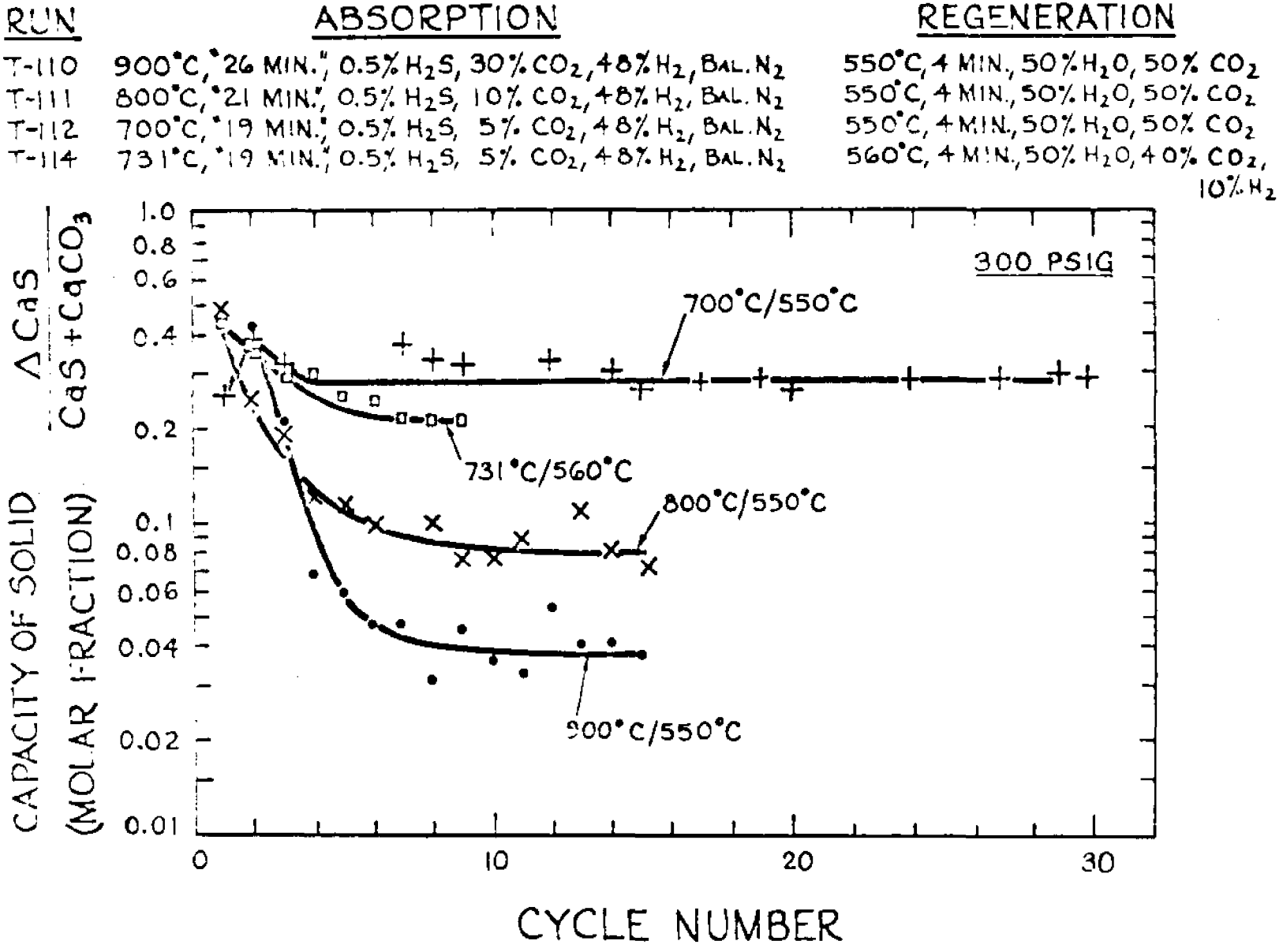

Figure 44. Capacity versus cycle number for four runs with regenerations at 550° or 560°C (the second temperature designated alongside each curve) and absorptions at 700°C, 731°C, 800°C, and 900°C (the first temperature).

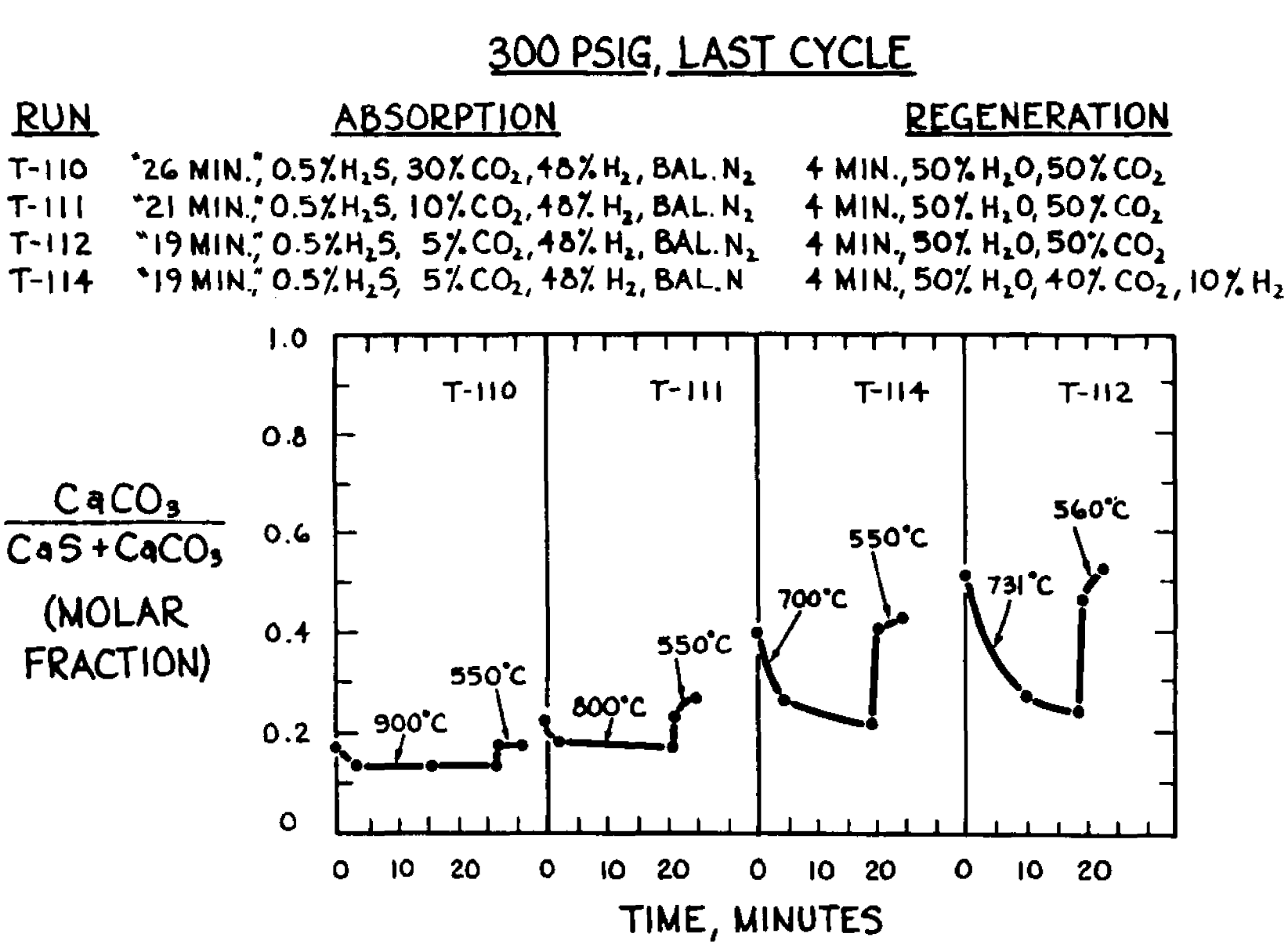

Figure 45. Rate data for last cycle of absorption and regeneration in four runs showing effect of absorption temperature upon capacity.

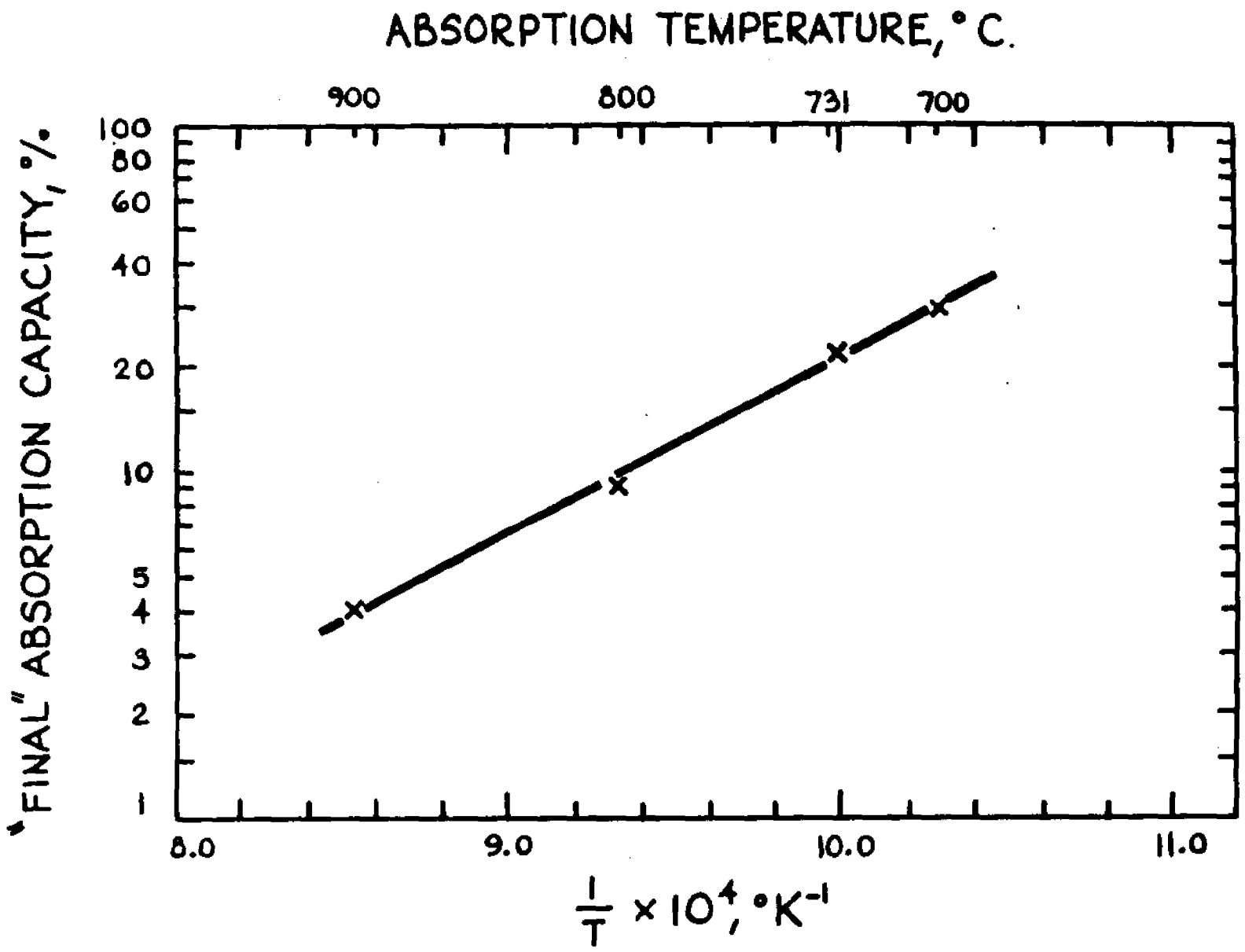

Figure 46. Logarithm of "final" capacity versus reciprocal absolute temperature of absorption, for regenerations at 550° and 560°C.

is better to conduct the regeneration at the lowest possible temperature that kinetic limitations will allow. [For a discussion of the favorable process temperatures, see Section 3.03 above.] It is unfortunate that the more favorable operating temperatures, from a pocess point of view, are less favorable from standpoint of solid absorptive capacity.

It is not likely that an explanation of the trends in Figures 43 and 46 will be simple.

6.06 Data Showing Effect of Varying Steam and Carbon Dioxide Levels during Regeneration

After the trends displayed in Figures 43 and 46 had been established, much of the remaining effort in this research was devoted to attempts to find conditions that might give better "final" absorptive capacity at a temperature around 550°C to 560°C.

Table 4 lists runs in which the levels of steam and carbon dioxide in regeneration gases were varied over wide ranges. As will be seen from the "final" capacities noted in the table, changing these variables had little effect upon the final capacity, except in that reducing the level of steam to 25%, in Run T-101, appeared to reduce the "final" capacity significantly.

Figures 47 and 48 give zigzag charts and rate data for the run at 25/75 steam/carbon dioxide. Figures 49 and 50 give information for 75/25 steam/carbon dioxide. Figures 51 and 52 give information for 90/10 steam/carbon dioxide. Figures 53 and 54 give information for 35/25/40 steam/carbon dioxide/hydrogen.

Table 4

Cyclic Runs with Various Regeneration Gases

(All data at 300 psig)[1]

	Absorption[2,3]				
Run No.	Temp. °C	Capacity at last cycle	Temp. °C	Capacity %	Gases, Bal N_2 $H_2O/CO_2/H_2$
T-100	731	22 (15)[4]	560	22	50/40/0
T-101	731	16 (15)	560	16	25/75/0
T-102	731	25 (15)	560	25	75/25/0
T-103	731	25 (15)	560	24	90/10/0
T-106	731	24 (11)	560	23	35/25/40

1. All runs were half-calcined with 25% H_2O, 50% CO_2, 25% N_2 up to 787°C.
2. All absorption times are "21" minutes which include heating and cooling time, all regeneration times are 4 minutes.
3. Absorption gases are the same for all the runs; i.e., 0.5% H_2S, 5% CO_2, 48% H_2.
4. Number of cycles made are shown in parentheses.

300 PSIG (21.4 ATM)

ABSORPTION:

0.5% H_2S, 5% CO_2, 48% H_2, BAL. N_2

13 MIN. @ 731°C.

HEATING = 2 MIN. (With H_2S)

COOLING = 6 MIN.

REGENERATION:

25% H_2O, 75% CO_2

4 MIN. @ 560°C.

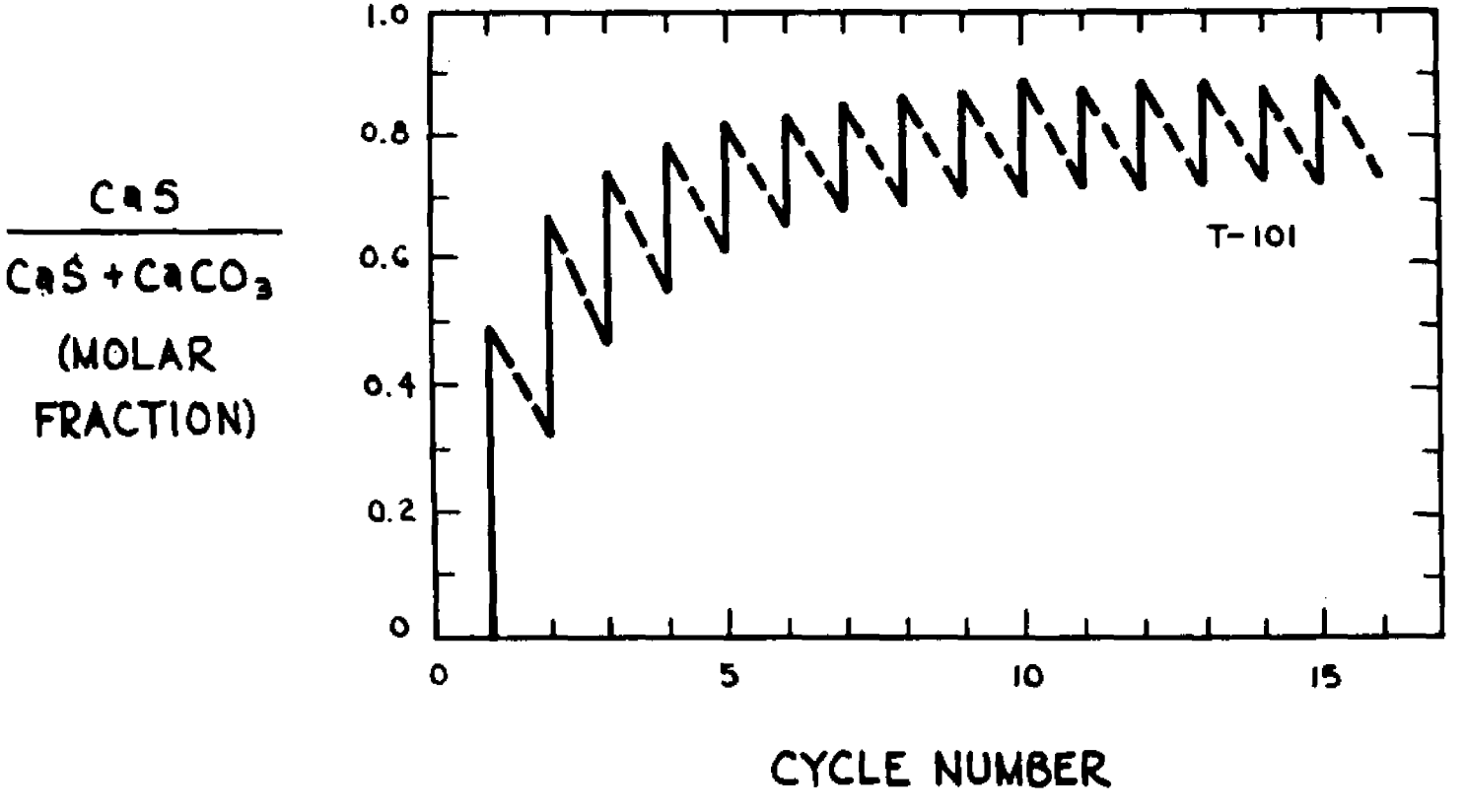

Figure 47. Zig-Zag chart for Run T-101.

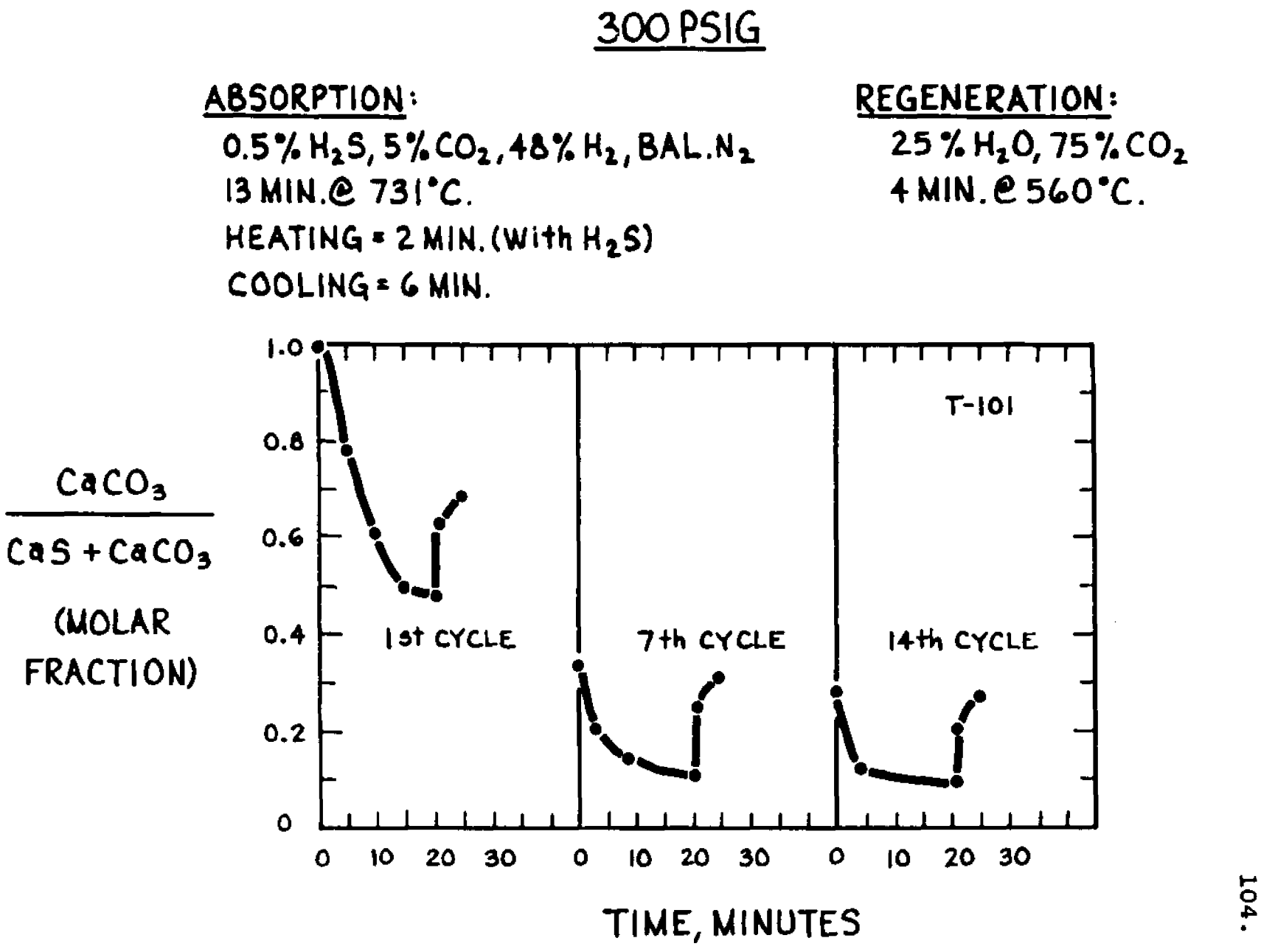

Figure 48. Rate data for Run T-101.

300 PSIG (21.4 ATM)

ABSORPTION:

0.5% H_2S, 5% CO_2, 48% H_2, BAL. N_2

13 MIN. @ 731°C.

HEATING = 2 MIN. (With H_2S)

COOLING = 6 MIN.

REGENERATION:

75% H_2O, 25% CO_2

4 MIN. @ 560°C.

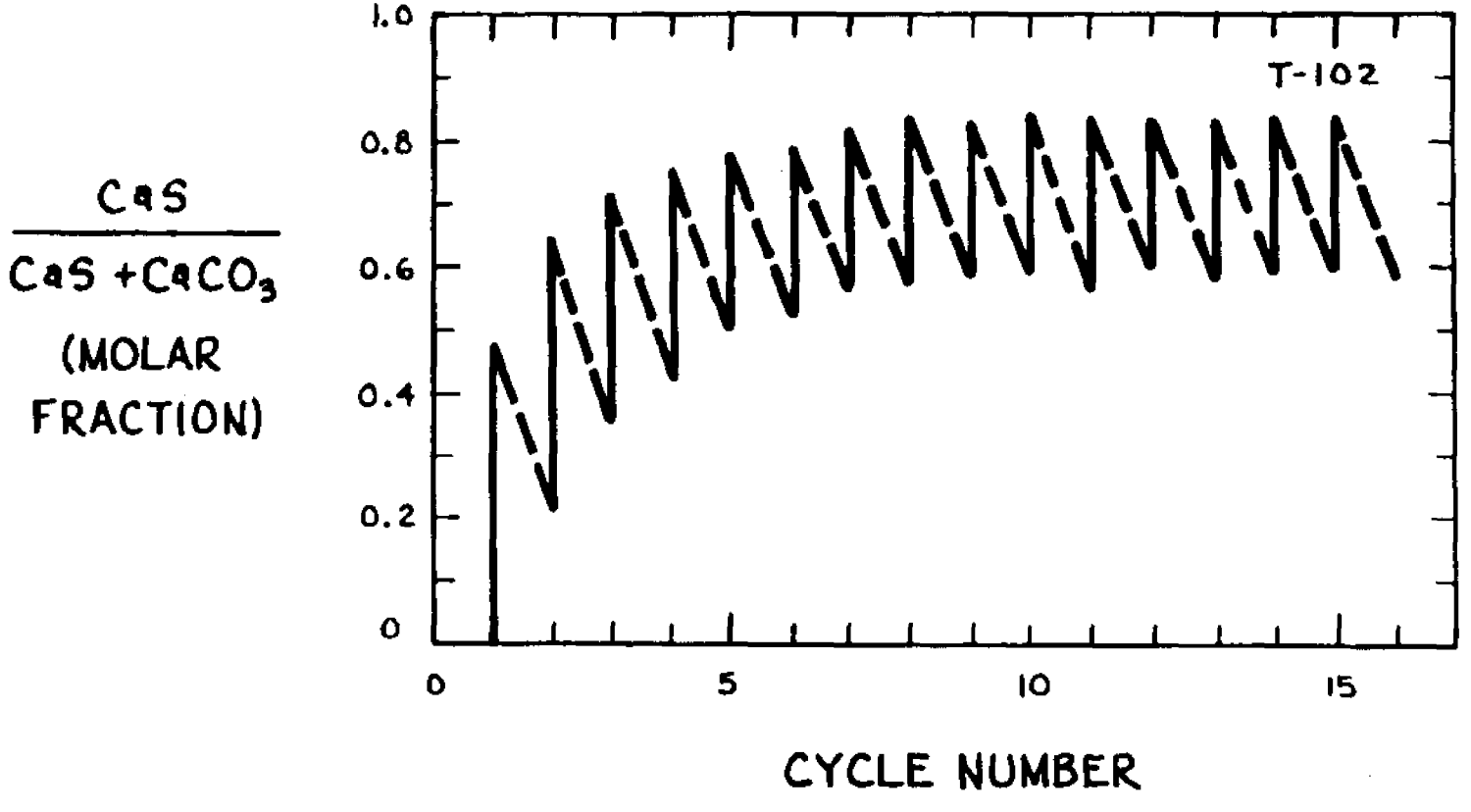

Figure 49. Zig-Zag chart for Run T-102.

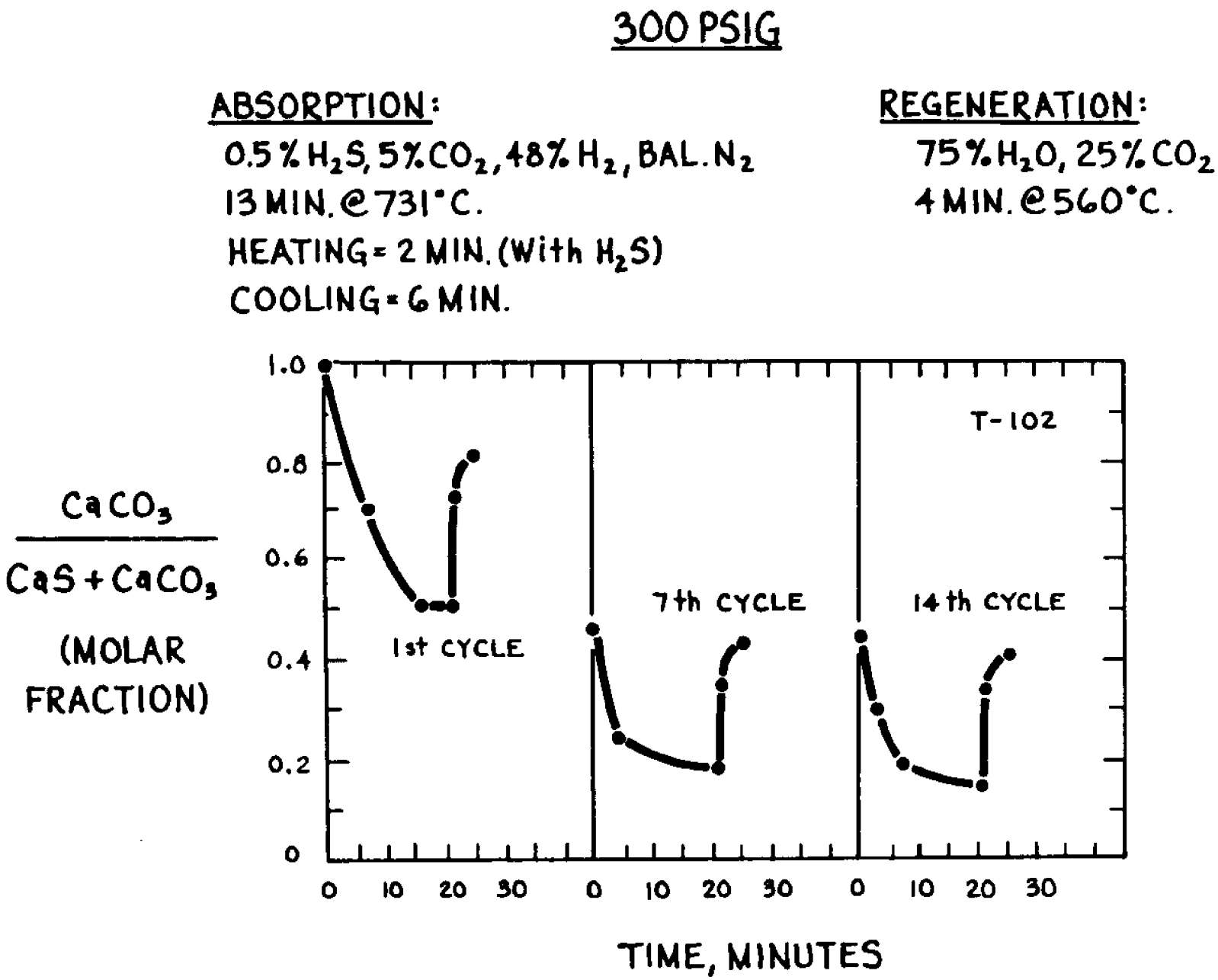

Figure 50. Rate data for Run T-102.

300 PSIG (21.4 ATM)

ABSORPTION:

0.5 % H_2S, 5 % CO_2, 48 % H_2, BAL. N_2
13 MIN. @ 731 °C.
HEATING = 2 MIN. (With H_2S)
COOLING = 6 MIN.

REGENERATION:

90 % H_2O, 10 % CO_2
4 MIN. @ 560 °C.

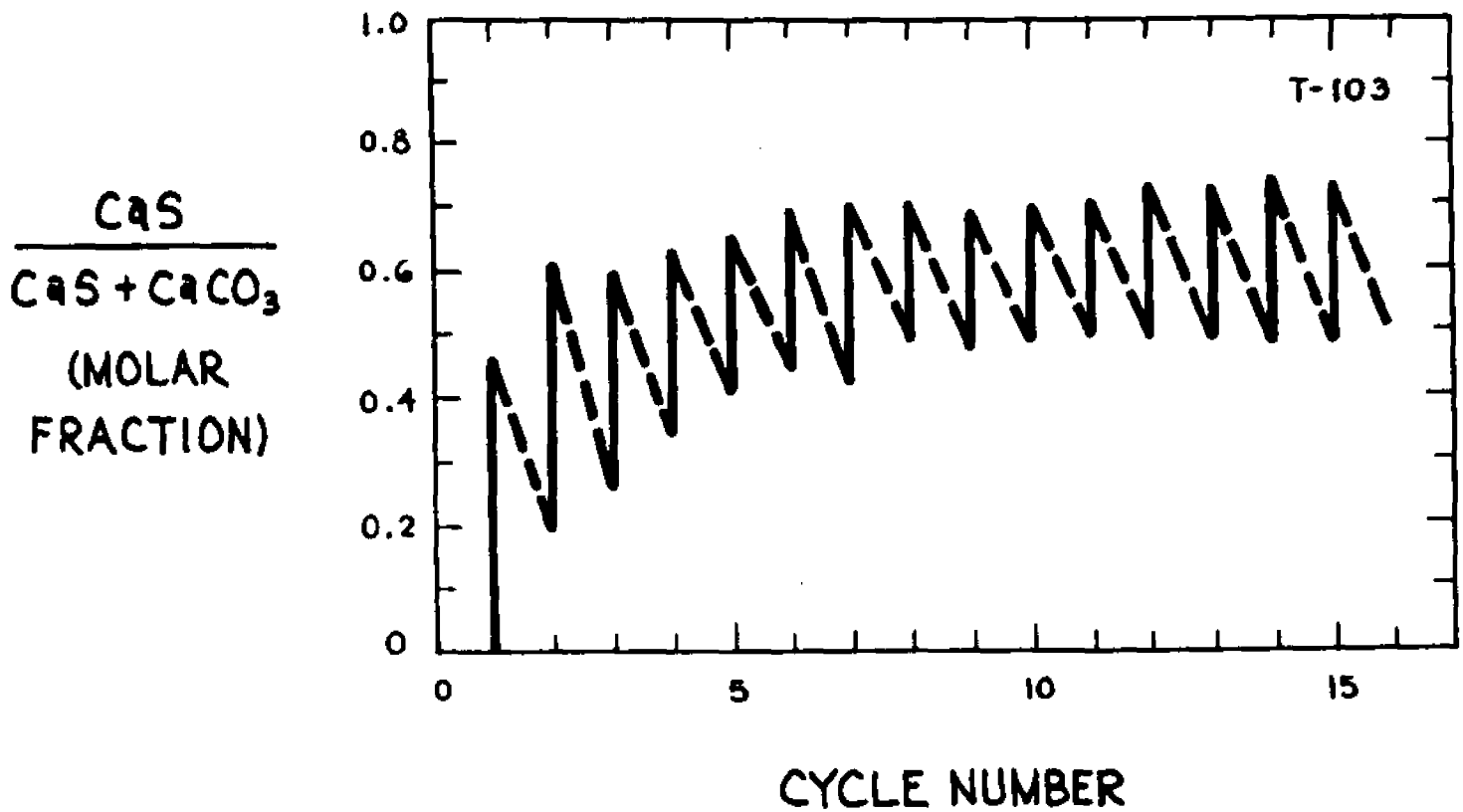

Figure 51. Zig-Zag chart for Run T-103.

300 PSIG

ABSORPTION:

0.5% H_2S, 5% CO_2, 48% H_2, BAL. N_2

13 MIN. @ 731°C.

HEATING = 2 MIN. (With H_2S)

COOLING = 6 MIN.

REGENERATION:

90% H_2O, 10% CO_2

4 MIN. @ 560°C.

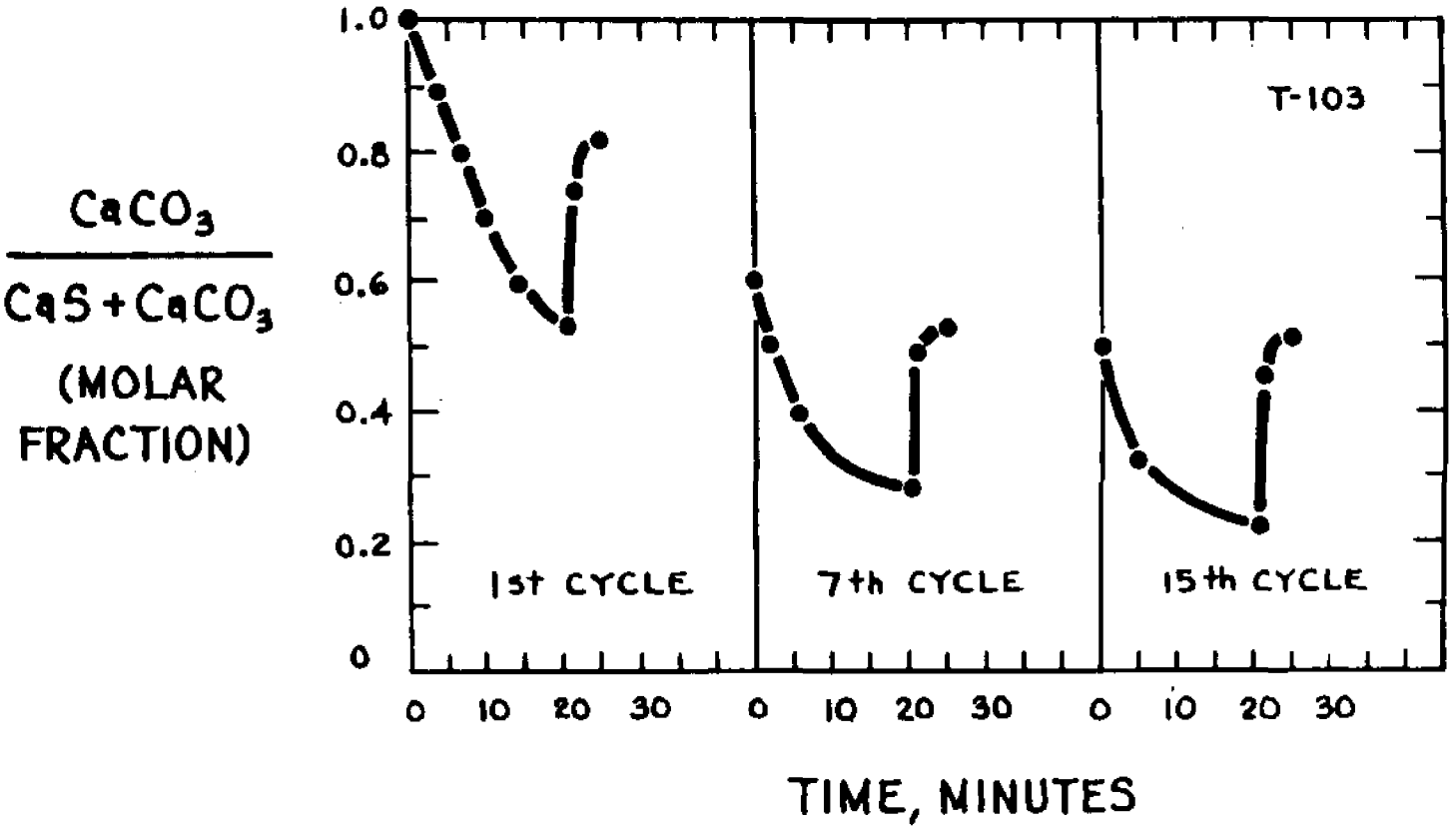

Figure 52. Rate data for Run T-103.

300 PSIG (21.4 ATM)

ABSORPTION:

0.5% H_2S, 5% CO_2, 48% H_2, BAL. N_2
13 MIN. @ 731°C°
HEATING = 2 MIN. (With H_2S)
COOLING = 6 MIN.

REGENERATION:

35% H_2O, 25% CO_2, 40% H_2
4 MIN. @ 560°C.

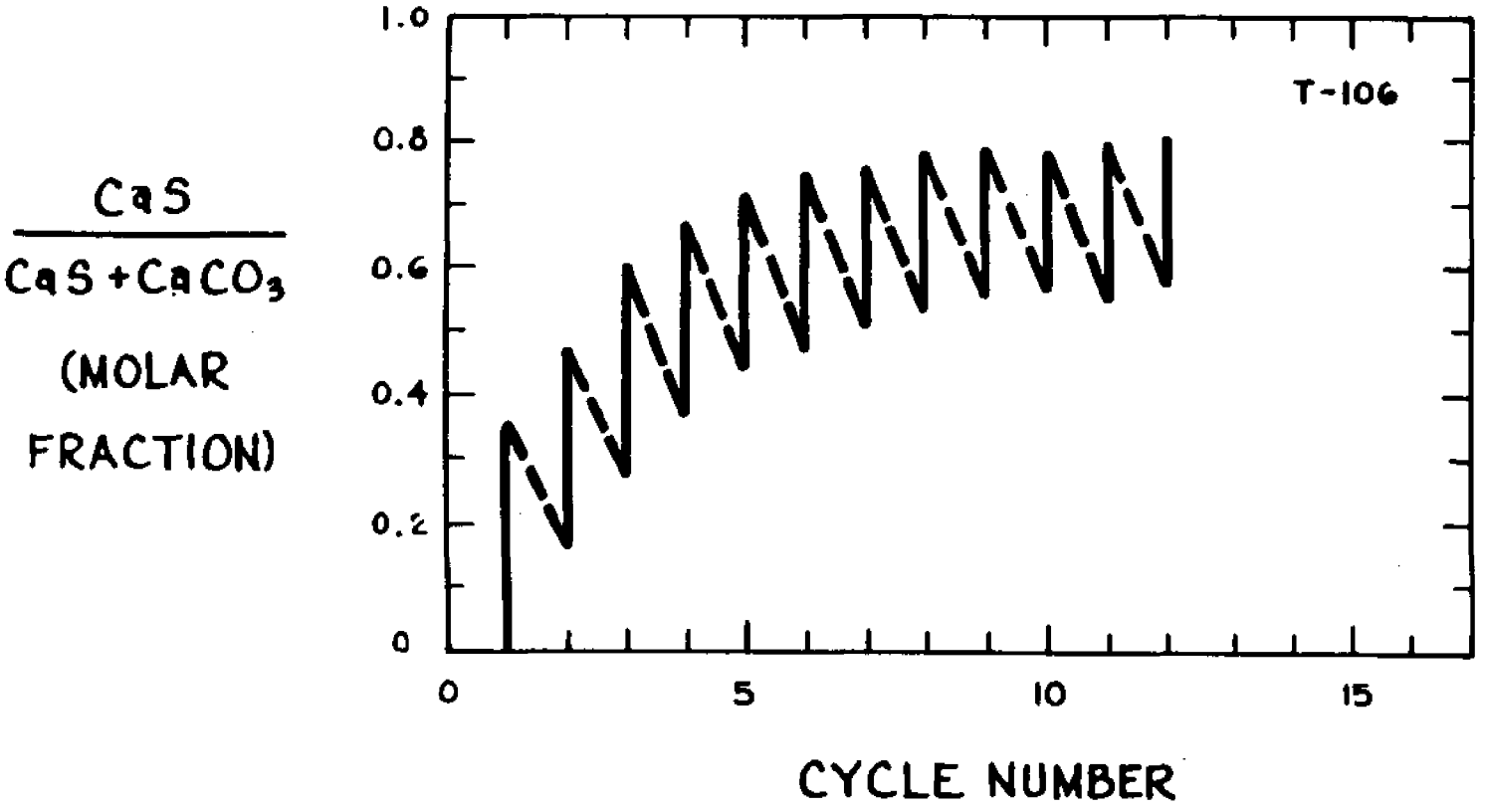

Figure 53. Zig-Zag chart for Run T-106.

300 PSIG

ABSORPTION:

0.5% H_2S, 5% CO_2, 48% H_2, BAL. N_2

13 MIN. @ 731°C.

HEATING = 2 MIN. (With H_2S)

COOLING = 6 MIN.

REGENERATION:

35% H_2O, 25% CO_2, 40% H_2

4 MIN. @ 560°C.

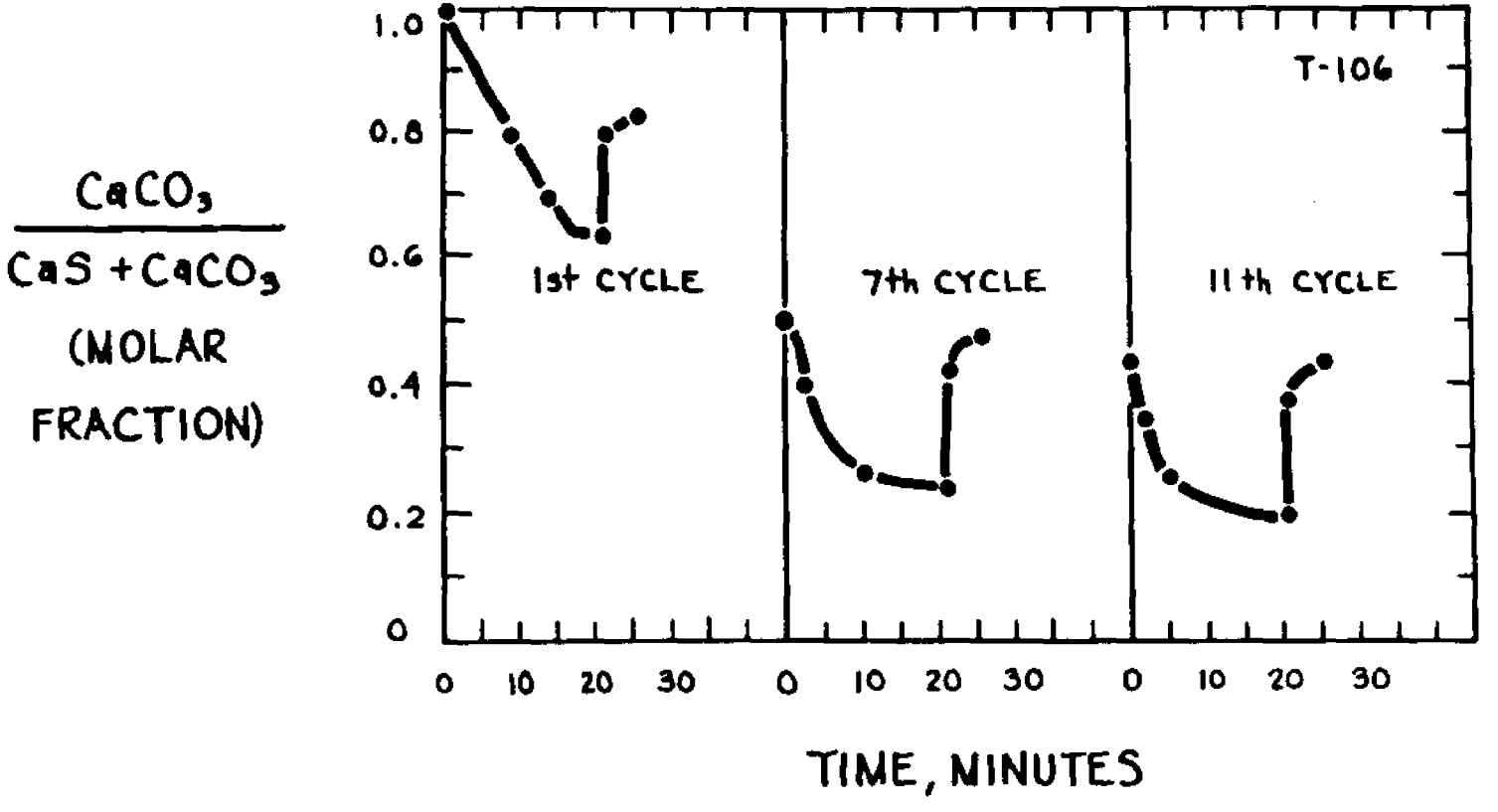

Figure 54. Rate data for Run T-106.

It should be noted that regenerations during the run summarized in Figures 51 and 52 were conducted at steam partial pressures of 19.3 atmospheres. For the pressure thermobalance, this run provided a severe test. Would it be free from troubles caused by condensation of steam on the cold quartz balance beam near the balance housing, or even within the housing itself? The thermobalance passed this test well.

Figures 55 and 56 give rate data for the regeneration step in the first and last cycles respectively of the runs in which the contents of steam and carbon dioxide were varied in the regeneration gas. In the final cycle data of Figure 56, there appears to be some trend in the initial rate of regeneration toward lower rates at lower steam partial pressure.

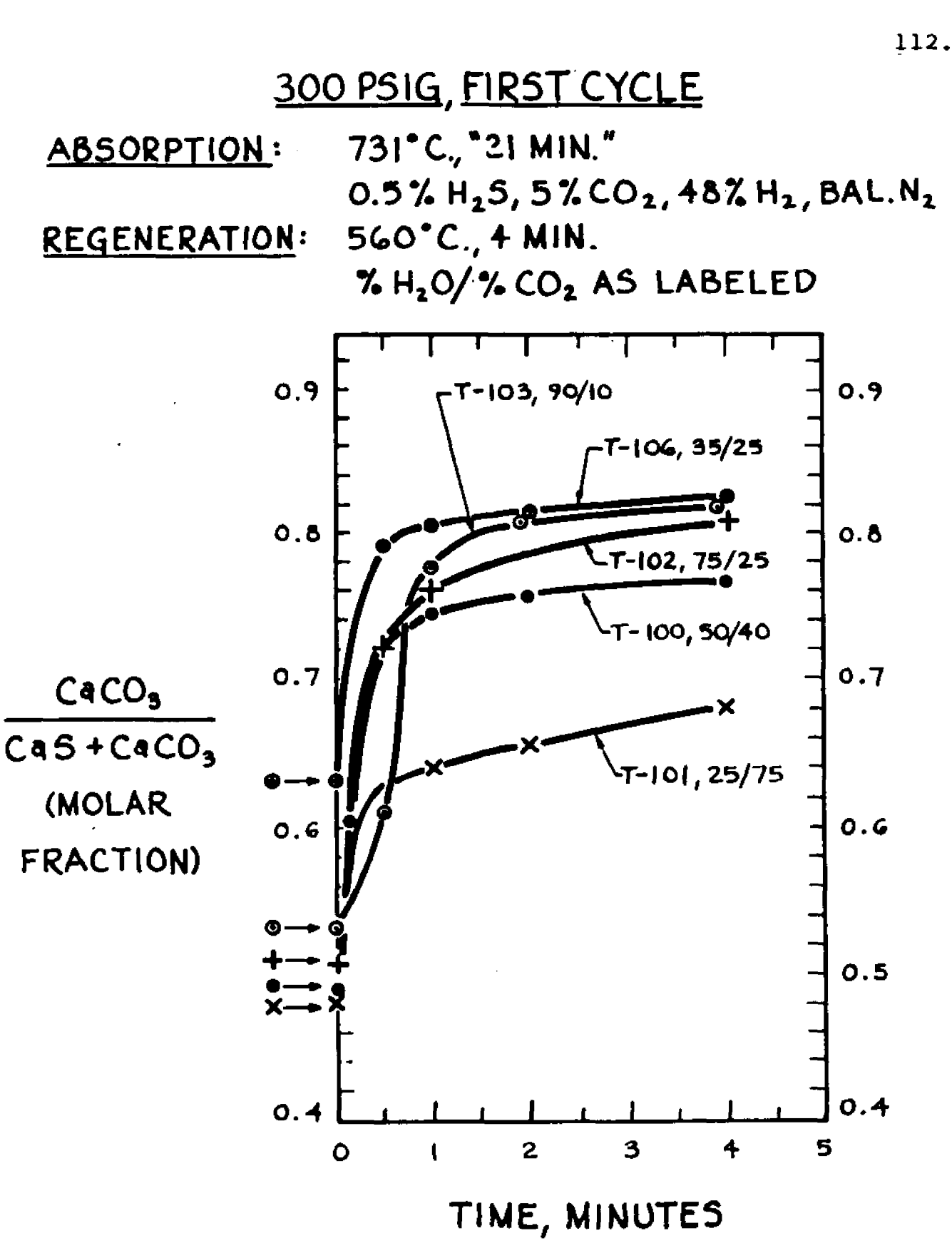

Figure 55. Rate data in first cycles of runs with varying contents of steam and carbon dioxide in regeneration gas.

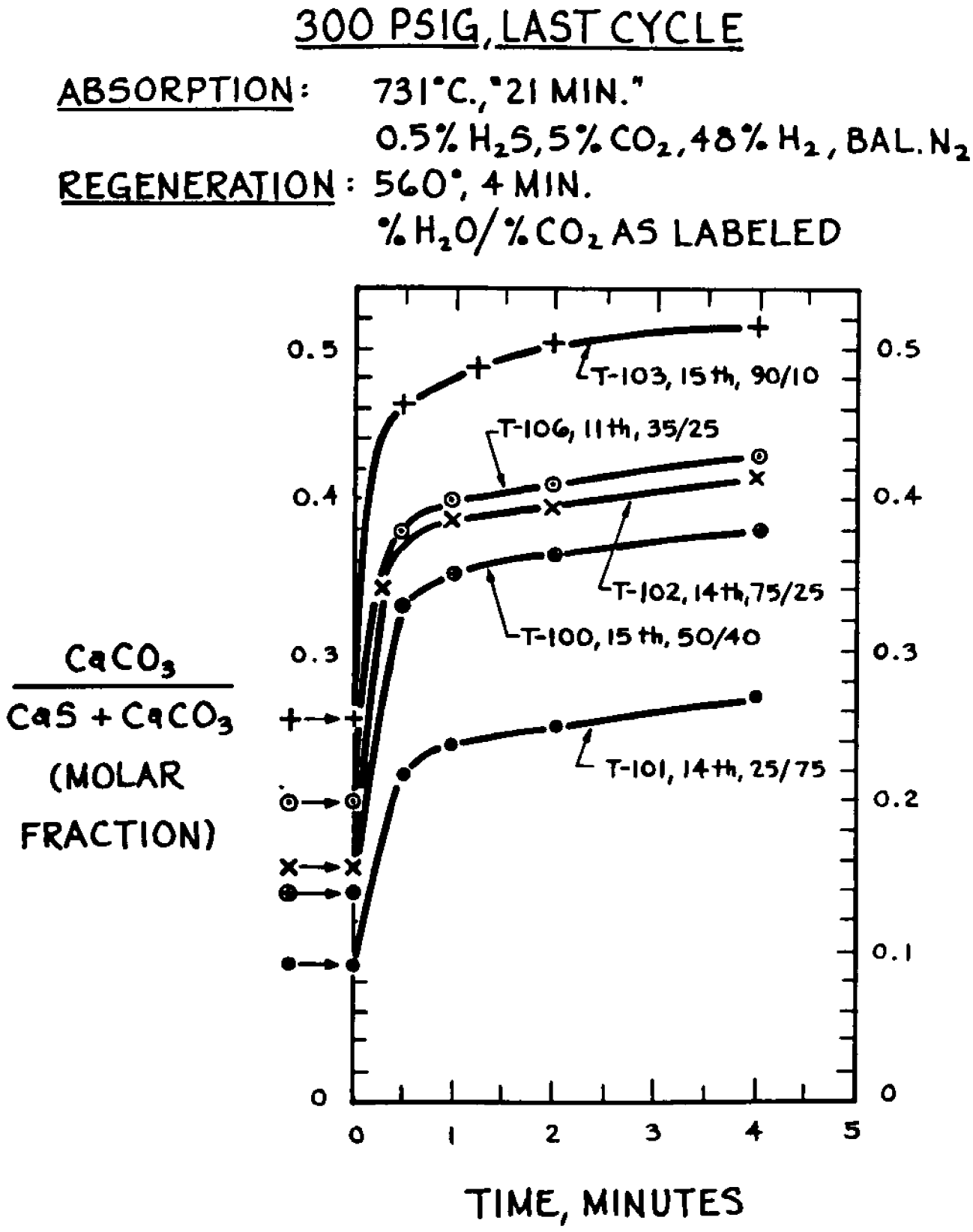

Figure 56. Rate data in last cycles of runs with varying contents of steam and carbon dioxide in regeneration gas.

6.07 Data Showing Striking Variations in Capacity with Changes in Composition of Regeneration Gas within a Single Run of 27 Cycles

Late in the research effort, it occurred to us that there might be a parallel between the way in which the regeneration reaction (B) tends to "drop dead" at 300 psig after only a part of the calcium sulfide present has been converted to calcium carbonate and the way in which the absorption reaction (D) was observed by Ruth (15) to "drop dead" at low temperatures. [See Section 4.02 above.] In the case of both reactions, the conversion at which the reaction flags is less at lower temperatures.

Ruth had hypothesized that the tendency for the reaction to flag at partial conversions was related to a surface blockage, and further, that this blockage was related to a reaction rate that was "too fast", i.e., that some rate process conducive to formation of a porous product layer was overwhelmed by too fast rate of formation of this layer.

It was therefore reasonable to suppose that the regeneration reaction of interest here might extend to larger conversions of sulfide to carbonate if a regeneration gas mixture could be found at which its initial rate is slower.

Ruth (15) had found that the initial rate of the absorption reaction (D) at low temperatures was slowed by presence of a product gas, carbon dioxide, and the reaction proceeded to complete conversion. It was logical, therefore, to hope that the regeneration reaction (B) might respond favorably to presence of the product gas, hydrogen sulfide.

A run was undertaken with the plan to explore the influence of hydrogen sulfide upon the regeneration reaction (B) at 550°C.

Table 5 lists the conditions for the regeneration step in the 27 cycles of the run which resulted from this plan. The first six cycles were conducted with our usual regeneration gas mixture in order to "stabilize" the sample. The absorption temperature was 700°C.

Addition of hydrogen sulfide to the regeneration gas in the 7th, 9th, and 13th cycles of Table 5 did not seem to improve absorptive capacity significantly.

However, reduction of carbon dioxide to 4% of the gas mixture did have a pronounced effect, increasing the absorption capacity for a succeeding absorption step significantly, i.e., from around 30% in earlier runs to between about 45% and 50%.

Other variations in the absorption atmosphere seemed to have relatively small effect toward improving capacity. In particular, reduction of the steam content to 4% of the gas mixture, in cycles 21 through 25, seemed if anything to reduce the absorption capacity.

The final regeneration, in the 27th cycle, confirmed the effect of reducing carbon dioxide level upon increasing capacity.

Table 5

Details of Regeneration Conditions and Capacities of Run T-198

(All regenerations conducted at 300 psig and 550°C. The absorption temperature was 700°C, and absorption gas was 0.5% H_2S, 5% CC_2, 48% H_2, balance N_2).

Cycle No.	Time, min.	Gaseous Concentration % $H_2O/CO_2/H_2S/H_2$, Balance N_2	Absorption Capacity after Regeneration %
1	4	50 /40 /0 /10	27.4
2	4	50 /40 /0 /10	29.4
3	4	50 /40 /0 /10	37.9
4	4	50 /40 /0 /10	32.3
5	4	50 /40 /0 /10	33.8
6	4	50 /40 /0 /10	33.9
7	7.5	50 /40 /1 / 6.1	34.8
8	6	50 /40 /0 /10	33.4
9	6.5	50 /40 /2.01 / 2.22	34.5
10	8	50 / 4 /0 /10	47.0
11	10	50 / 4 /1 /10	45.9
12	20.5	50 / 4 /2.01 /10	53.5
13	8	40 /36 /4.82 / 5.33	37.3
14	6.7	25 /40 /0 /10	33.9
15	2	26.3 /42.1 /0 / 9.37	27.6[1]
16	7	25 /40 /1 /10	30.2
17	5.5	25 /40 /2.01 /10	30.5
18	9.5	25 / 4 /0 /10	37.1
19	25	25 / 4 /1 /10	43.0
20	4	25 / 4 /2.01 /10	1.7
21	8.5	4 /25 /0 /10	29.0
22	3	4 /25 /1 /10	0.1
23	18	4 /50 /0 /10	27.6
24	8	4 /50 /1 /10	24.1
25	12.5	4 /50 /2.01 /10	24.6
26	12.5	25 /25 /10 /11.1	0.0
27	34	40.8 /3.27 /1.64 / 8.18	45.1

1. Not completed.

Figures 57 through 63 give rate data for certain regenerations in the run summarized in Table 5. These rate data provide a tentative indication of effects of varying the composition of regeneration gas upon the rate of the regeneration reaction (B).

Figure 57 illustrates the effect of varying steam level in a number of regenerations in which the carbon dioxide level was relatively high, viz., 40% and 50%. The two righthand plots in Figure 57 show little effect upon rate of changing the steam concentration from 25% to 50%, but the lefthand plot indicates an appreciable decrease in rate at a steam concentration of 4%.

Figure 57 also illustrates absence of an effect of varying hydrogen sulfide concentration between 0% and 2% at the higher steam levels. The figure suggests a small effect of hydrogen sulfide upon rate at the low steam concentration of 4%.

Figure 58 is a plot of the rate data shown in Figure 57 for 1% hydrogen sulfide level, and Figure 59 is a plot for 2% hydrogen sulfide.

Figure 60 compares rate data for a steam level of 4% with data for higher steam levels, the carbon dioxide level being 25%. The data, like that in Figures 57 through 59, suggest a falling off in rate at low steam level.

Figure 61 compares rate data for 4% and 40% carbon dioxide at two steam levels, 25% and 50%. At both steam levels, the lower carbon dioxide level appears to produce a decrease in rate of the regeneration reaction.

Figure 62 gives rate data showing an effect of steam level upon rate at 1% hydrogen sulfide when the carbon dioxide level is low. [Notice that the solid curves in Figure 62 refer to the

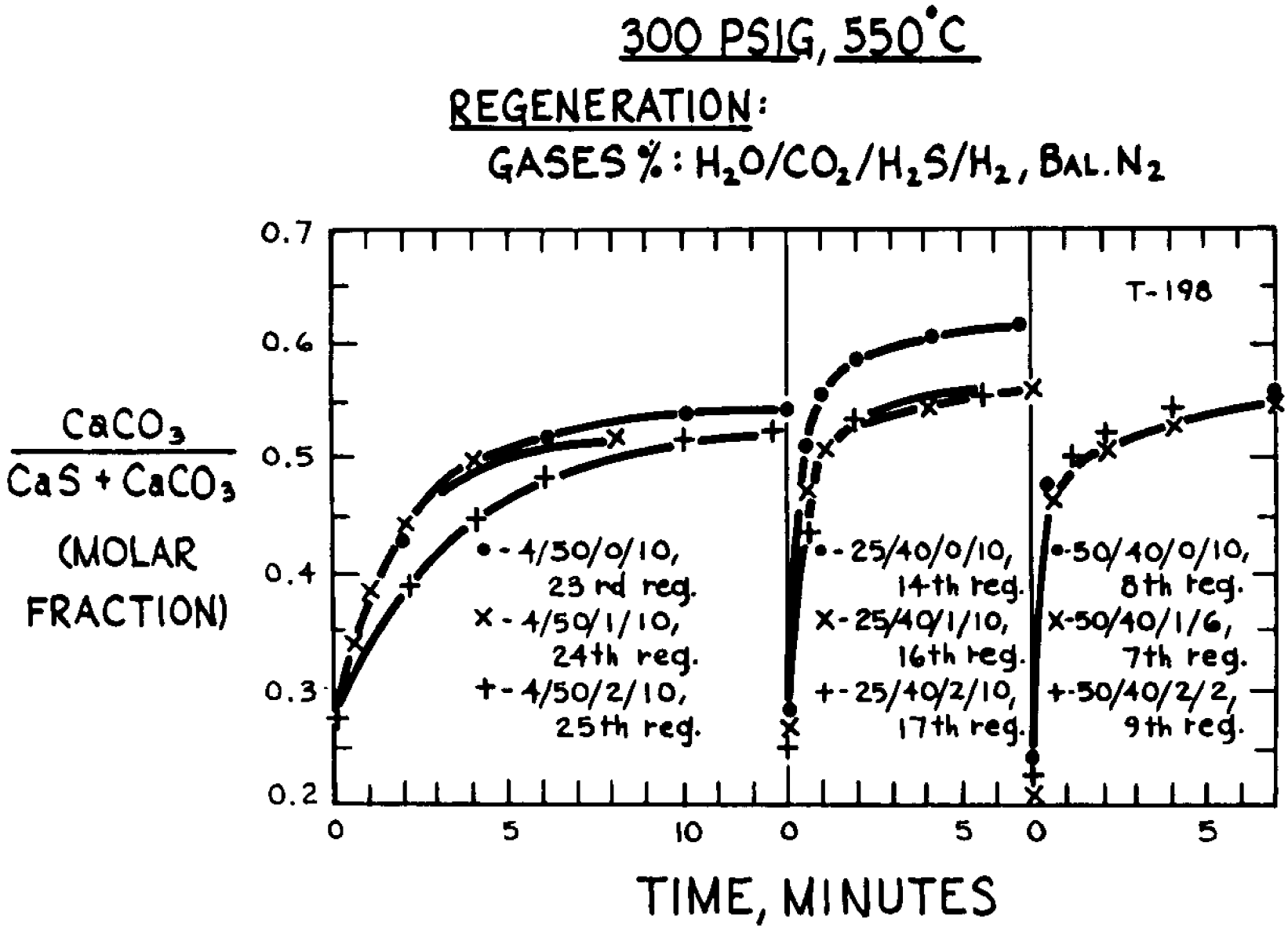

Figure 57. Rate data for certain regenerations in Run T-198, with varying gas mixtures.

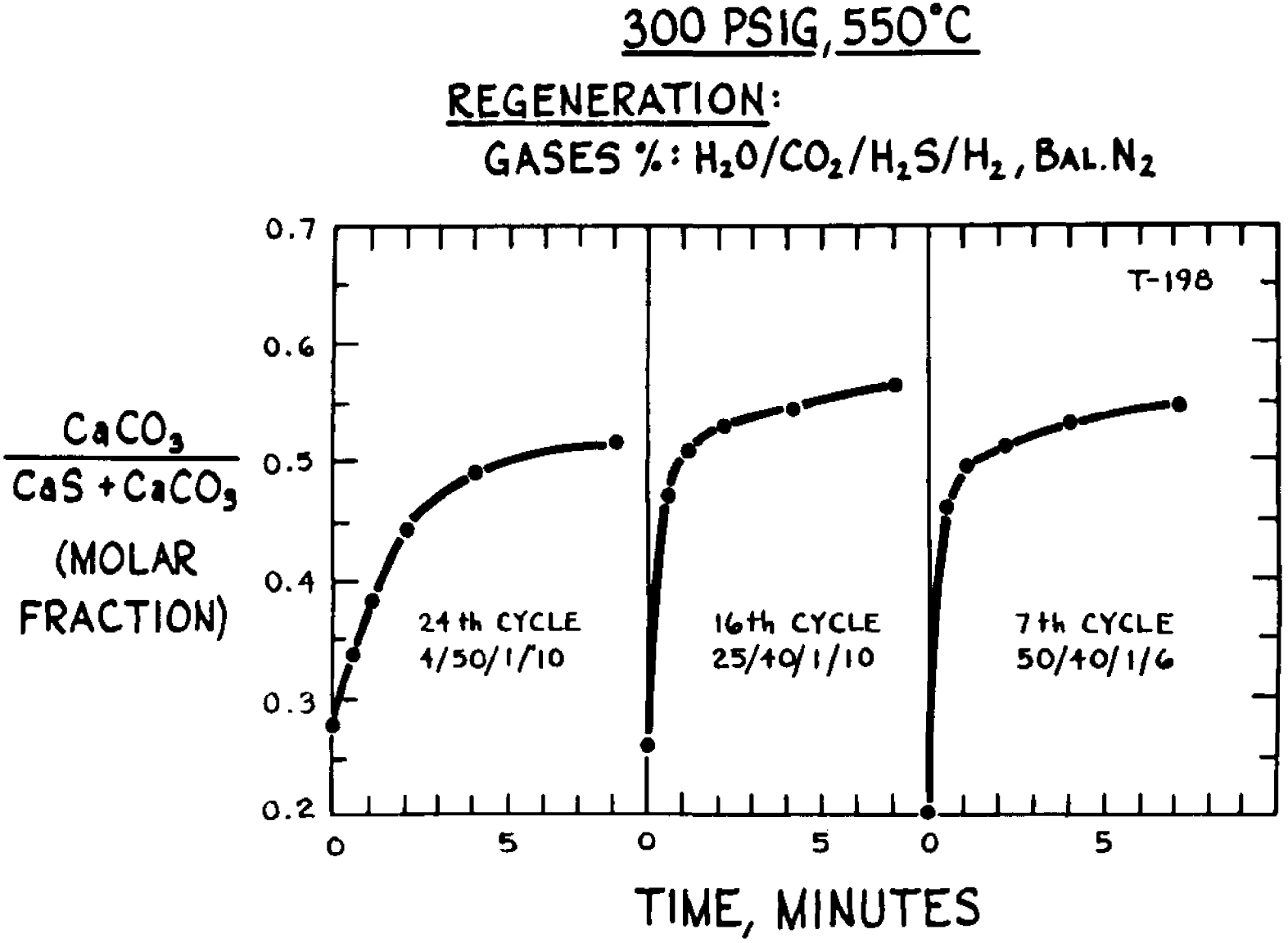

Figure 58. Rate data for certain regenerations in Run T-198, with varying gas mixtures.

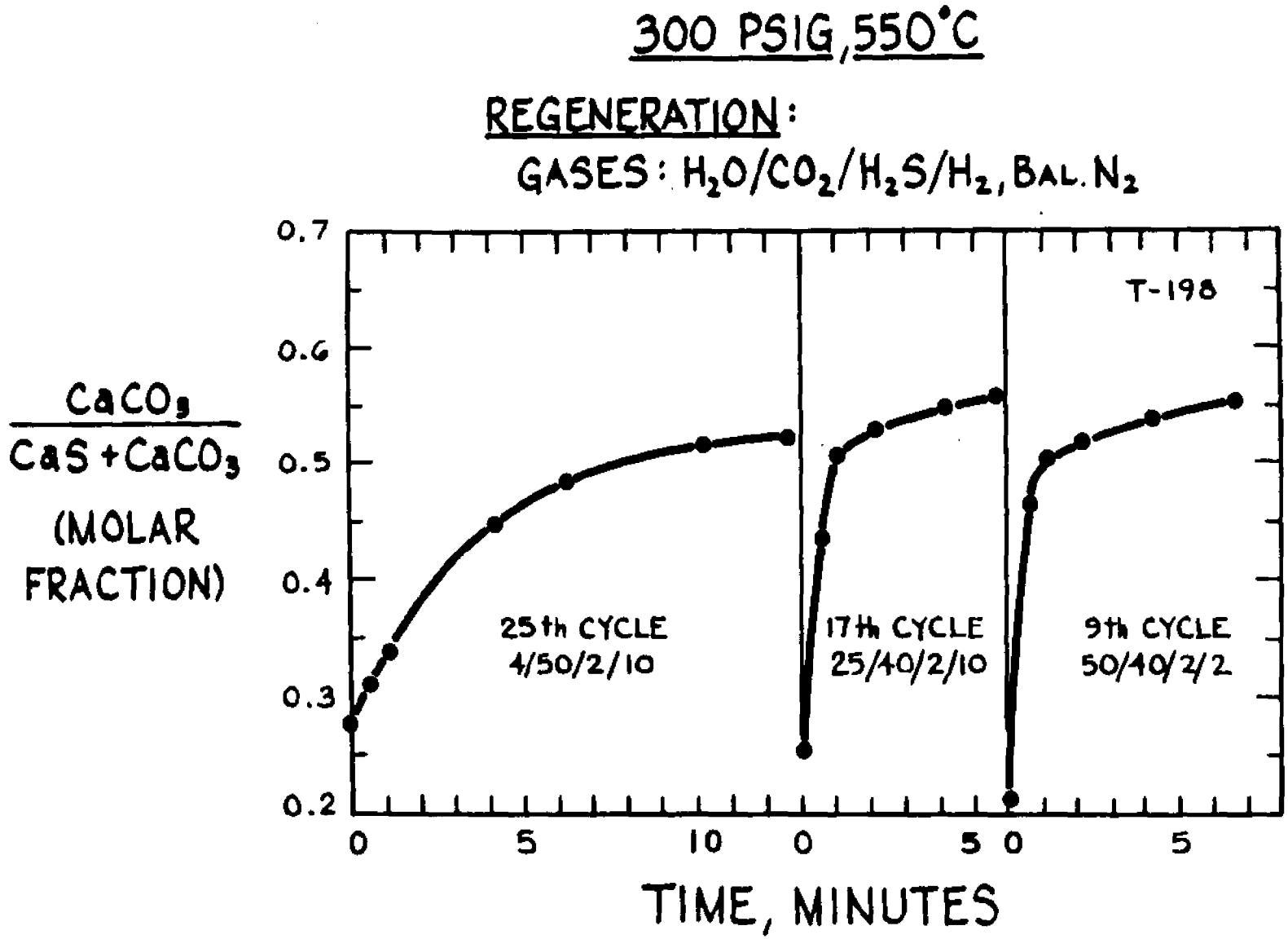

Figure 59. Rate data for certain regenerations in Run T-198, with varying gas mixtures.

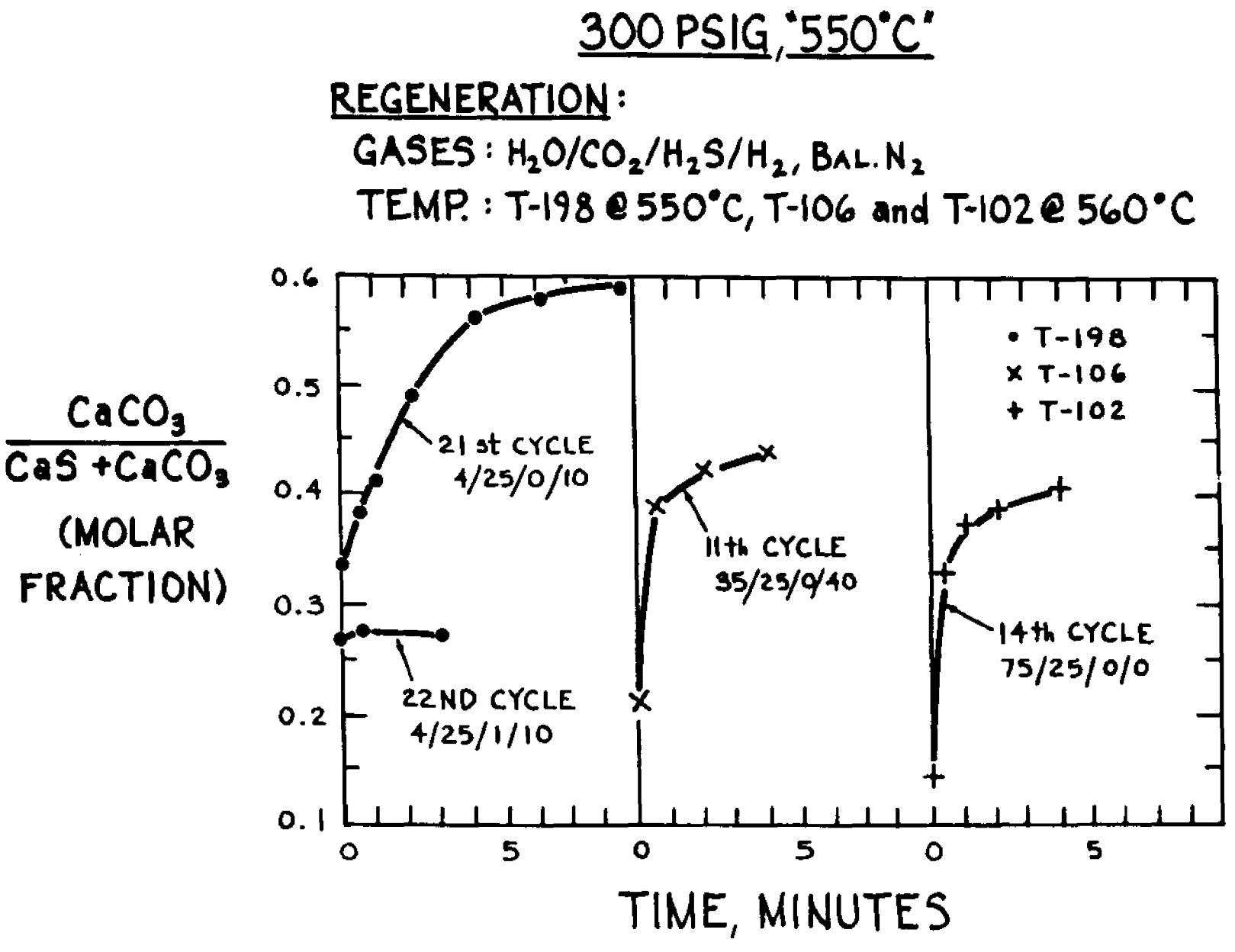

Figure 60. Rate data for certain regenerations in Run T-198, with varying gas mixtures, compared with rate data in Runs T-102 and T-106.

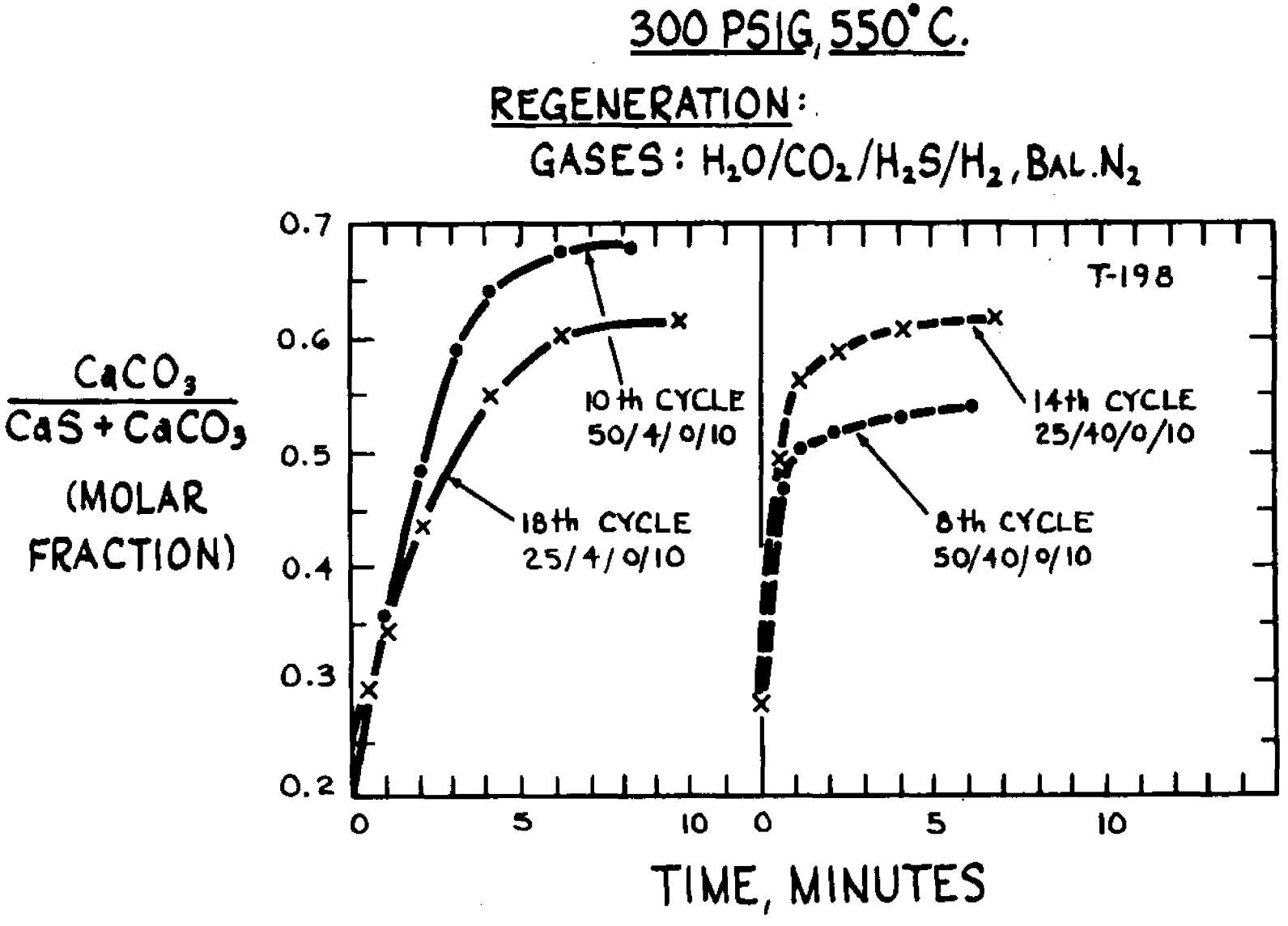

Figure 61. Rate data for certain regenerations in Run T-198, with varying gas mixtures.

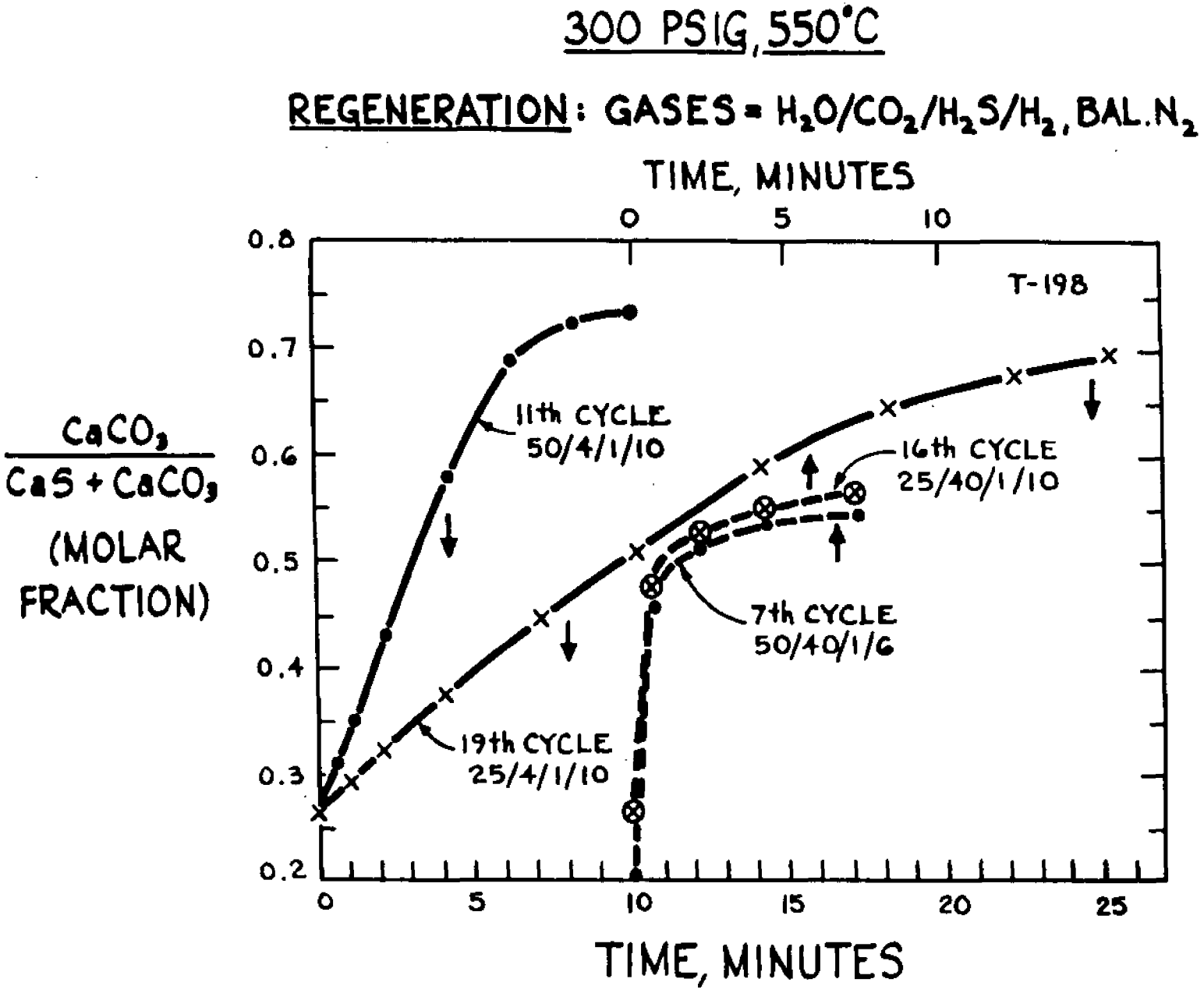

Figure 62. Rate data for certain regenerations in Run T-198, with varying gas mixtures.

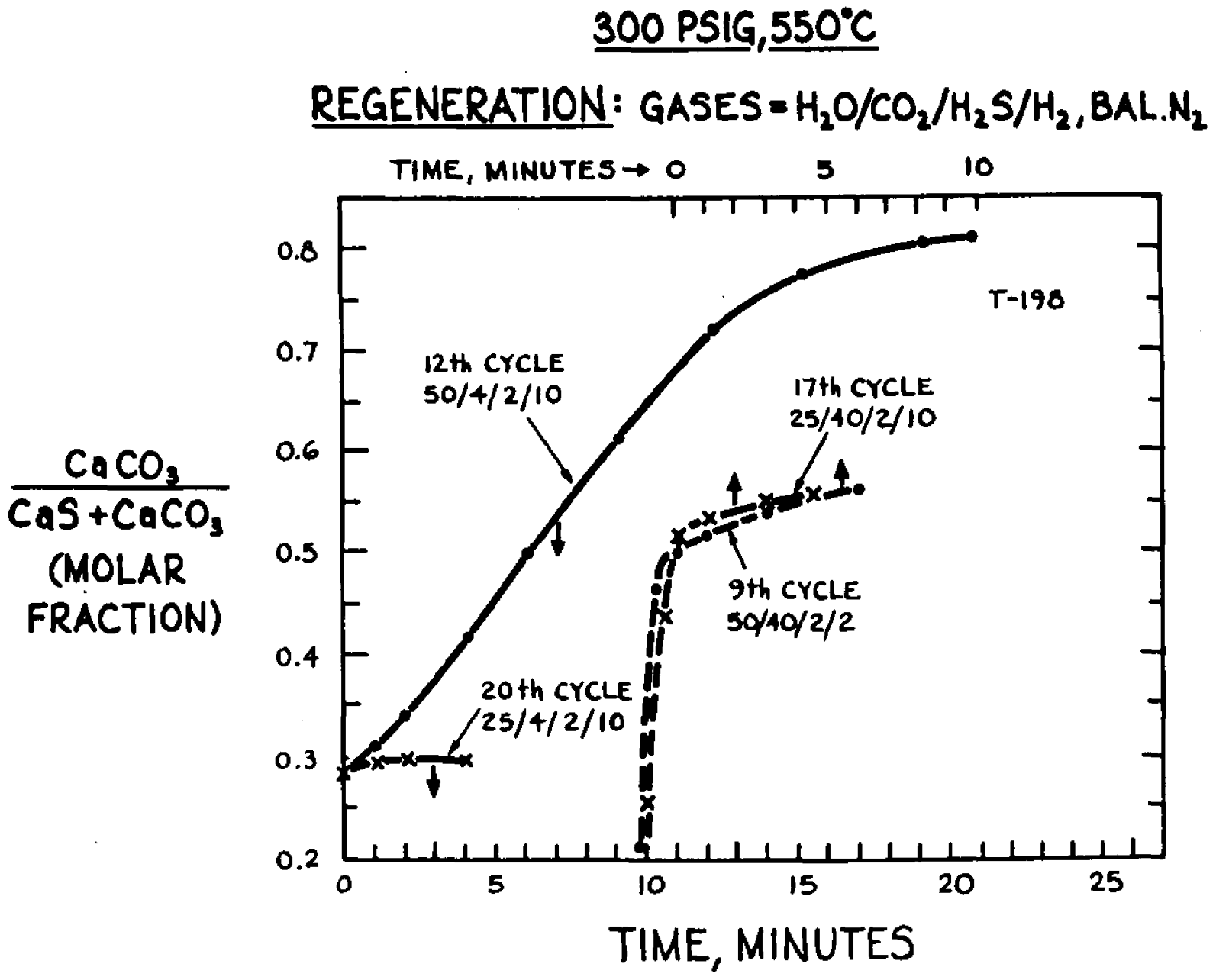

Figure 63. Rate data for certain regenerations in Run T-198, with varying gas mixtures.

time scale at the bottom of the figure, while the dashed curves refer to the scale at the top.] The regeneration gas in the 19th cycle contained hydrogen sulfide at about 46% of the equilibrium concentration for 550°C, the temperature of the regeneration. It does not appear that this is sufficiently close to equilibrium to account altogether for the markedly lower rate in the 19th cycle in comparison with the rate in the 11th cycle. It would appear from the data in Figures 61 and 62 that the dependence of rate upon steam, carbon dioxide, and hydrogen sulfide concentrations is a complex one.

Figure 63 is like Figure 62, save in that hydrogen sulfide concentration in Figure 63 is 2% instead of 1%. A similar response to steam level is seen, but more pronounced. At 2% hydrogen sulfide, steam level has no effect upon rate at 40% carbon dioxide, but a strong effect of steam upon rate is to be seen at 4% carbon dioxide. It should be noted that hydrogen sulfide in regeneration gas in the 20th cycle was about 71% of equilibrium for reaction (B), with the assumption that the gas comes to shift equilibrium as it reacts.

6.08 Discussion of Data Showing Variations in Capacity with Changes in Composition of Regeneration Gas

The effects seen in Figures 57 through 63 are reminiscent of Ruth's kinetic curiosities (15) [see Section 4.02.] Like Ruth's curiosities, the new effects may reflect differences in the way in which crystallites of calcium carbonate or calcium sulfide grow within the solid microstructure.

The new effects provide a strong lead for further research. Briefly, it would appear worthwhile to obtain data on the regeneration reaction at 21.4 atmospheres using freshly made, fully converted samples of [CaS+MgO], and using a wide variation in regeneration gas atmosphere. The data should be obtained in something like the same detail, insofar as gas composition is varied, as the data provided by Ruth (15) for the absorption reaction at atmospheric pressure.

The kinetic study should be paralleled by inspections of solids produced by the regeneration reaction.

It would seem worthwhile to conduct the recommended kinetic study without cycling until the first-cycle kinetics of the regeneration reaction are thoroughly elucidated. Cycling runs would then be advantageously carried out at selected compositions of the regeneration gas.

From the practical point of view, the hope of the further research would be to find a particular regeneration gas composition that affords significantly greater absorption capacity after a number of cycles than the capacities experienced in the present research and summarized in Figures 43 and 46.

6.09 Data Indicating an Effect of Carbon Dioxide Level on Absorption Rate

By accident, a run was made with 25% carbon dioxide in the absorption gas mixture, instead of the 10% intended. It was surprising to discover that the absorption reaction was very slow with 25% carbon dioxide, but was as fast as usual when the carbon

dioxide content was corrected to the 10% level. After two short cycles of absorption at the 10% level, a cycle was made with carbon dioxide again at the 25% level of the first cycle. Absorption at 25% carbon dioxide was faster than before, although not as fast as with 10% carbon dioxide.

This suggested the experiment for which rate data are shown in Figure 64. A large effect of carbon dioxide upon rate of absorption is seen. Ruth (15) saw little effect of carbon dioxide upon absorption rate at 750°C. He saw a similar effect to that shown in Figure 64 at lower temperatures, although, as we have noted earlier [Section 4.02], the lower rate of absorption at higher carbon dioxide levels appeared to be related to a greater conversion of calcium carbonate to calcium sulfide observed in runs at 600° and below.

The lead provided in Figure 64 was not pursued in this research, which concentrated upon finding absorptive capacity with cycling. Most absorptions in this research were conducted with 5% carbon dioxide in the absorption gas.

Further elucidation of the kinetics of the absorption reaction (D) as a function of composition of absorption gas is recommended, extending Ruth's findings to high pressure.

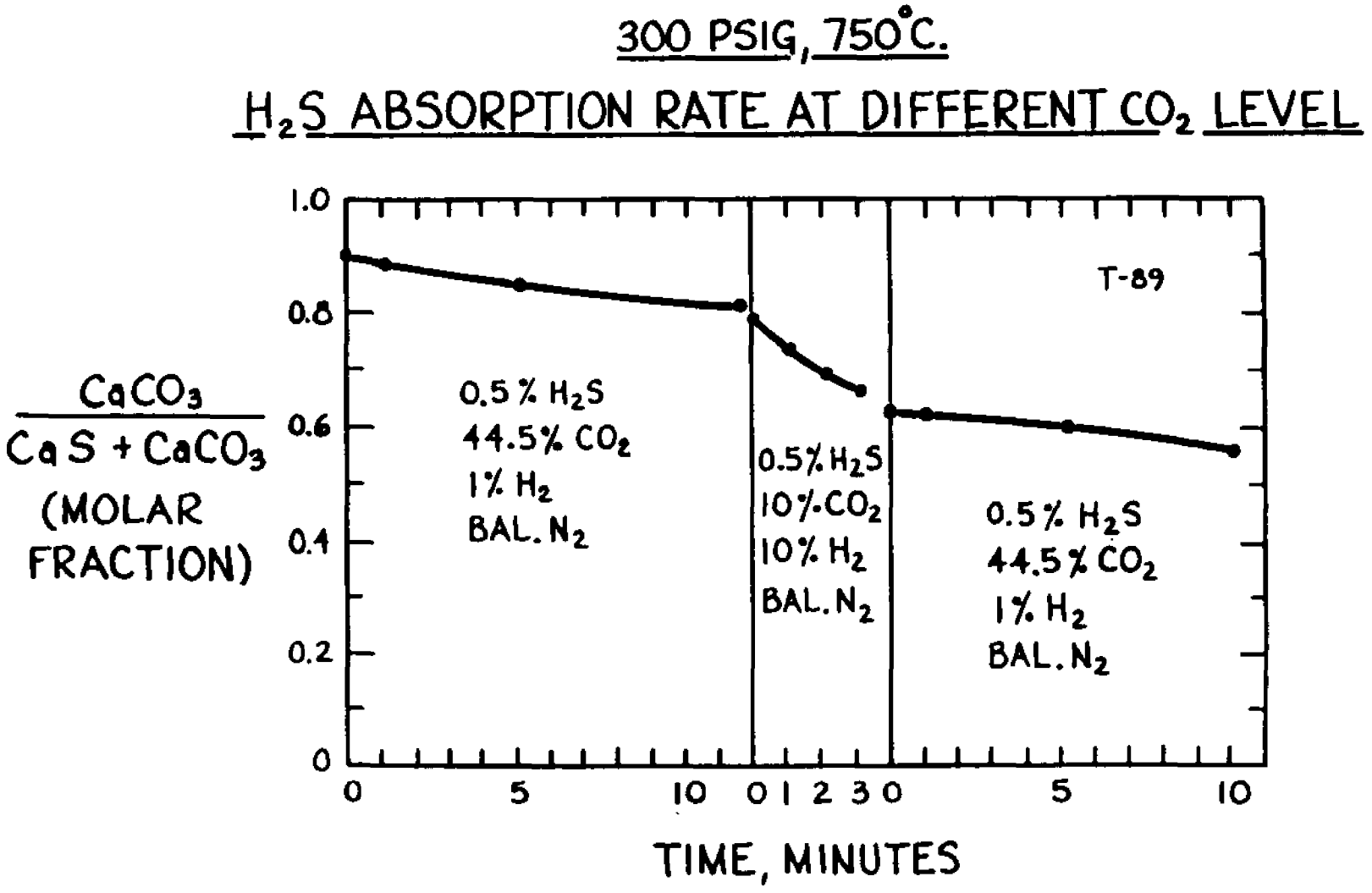

Figure 64. Absorption rate data for a run in which carbon dioxide level was varied.

6.10 Particular Cycles Conducted at Other Than Indicated Nominal Conditions

For the record, Table 6 lists certain cycles that were made at conditions different from the nominal conditions noted upon the figures above. These maverick cycles revealed no new behavior requiring a reconsideration of our overall conclusions concerning the half-calcined dolomite reaction cycle.

Table 6

Cycles at Conditions Different from Nominal Conditions

Run	Cycle	Condition
T-96	8th regeneration	6 minutes
T-97	14th absorption	10 minutes
T-97	14th regeneration	9 minutes
T-97	15th absorption	same as 14th absorption
T-97	15th regeneration	same as 14th regeneration
T-97	16th absorption	same as 14th absorption
T-100	12th regeneration	initial regeneration temperature was 595°C
T-110	1st absorption	8 minutes at 900°C
T-111	12th, 13th, 14th, 15th regeneration	use 50% H_2O, 40% CO_2, 10% H_2
T-112	6th absorption	8.5 minutes at 700°C
T-112	6th regeneration	4 minutes at 700°C
T-112	11th absorption	16 minutes at 550°C, 1 minute at 700°C
T-112	15th regeneration	4 minutes with 50% H_2O, 50% CO_2 at 550°C, overnight in N_2 at R.T. and 280 psia, 24 minutes with 25% H_2O, 50% CO_2 at 550°C

7.0 Summary of Findings

7.01 Development of High-Pressure Thermogravimetric Analyzer

We have completed the development of a thermogravimetric analyzer for use at high pressure and capable of rapid changes in temperature and gas atmosphere. The TGA is capable of conducting a large number of reaction cycles in a single day where the cycles consist of steps measured in minutes. The TGA can function at high partial pressures of steam. Our TGA has proved itself in this research to be rugged and reliable.

7.02 Dependence of Absorptive Capacity upon Process Temperatures

We have found that the absorptive capacity of half-calcined dolomite for hydrogen sulfide tends to approach a constant "final" value after about the seventh absorption-desorption cycle. This value is a strong function of both absorption temperature and regeneration temperature. Unfortunately, the trends with both temperatures are contrary to what a process designer might wish for. He would wish to operate the absorption at the highest possible temperature, short of that temperature at which calcium carbonate would decompose in the gas to be desulfurized. We would wish to operate the regeneration at the lowest possible temperature. The trends of capacity are toward lower capacities at both higher absorption and lower regeneration temperatures.

7.03 Effects of Gas Composition upon Regeneration

Exploratory work has shown striking effects of variation in gas composition upon the rate and extent of the regeneration

reaction. There is some tentative evidence indicating that certain gas compositions in which the regeneration gas already contains hydrogen sulfide at an appreciable fraction of equilibrium may slow down the regeneration reaction but at the same time allow the reaction to proceed to greater completion. This is a strong lead for further research.

7.04 Effects of Gas Composition upon Absorption

An accidental discovery that absorption proceeds more slowly with 25% carbon dioxide present instead of our usual 10% also provides a lead for further research that may lead to better understanding of reaction mechanism.

8.0 Recommendations for Further Research

(1) An understanding of the kinetic curiosities of Ruth may provide a strong lead toward future work to improve the absorptive capacity of half-calcined dolomite in the cycle for absorption of hydrogen sulfide. Work has been undertaken at McCrone Associates in Chicago as a step toward achieving such understanding, and their results will be reported in The City College Clean Fuels Institute's final report to Empire State Electric Energy Research Corporation.

(2) Our run T-198 (see Sections 6.07 and 6.08) provides a strong lead for further research to identify a composition of regeneration gas that might promote significantly higher final absorptive capacities after repeated cycles than this research has achieved.

(3) Further work should be accompanied by solid inspections that attempt to identify reasons for the curious effects of temperatures of absorption and regeneration upon final absorptive capacities revealed in this research, as well as variations of capacity with regeneration gas composition.

Part II: CYCLIC USE OF MAGNESIUM OXIDE FOR REMOVAL OF SULFUR DIOXIDE FROM COMBUSTION GASES AT ELEVATED PRESSURE

9.0 Introduction to Part II

Workers at The City College conducted exploratory experiments a number of years ago on the absorption of sulfur dioxide from combustion gases by half-calcined dolomite. The work was undertaken to explore the possibility of using half-calcined dolomite in cyclic fashion, with regeneration of the absorbent from the sulfate form by reduction and treatment with steam and carbon dioxide (36, 37).

Results reported subsequently by Argonne National Laboratories were unfavorable for the proposed regeneration cycle, since capacity of the absorbent for sulfur dioxide fell drastically after a very few cycles (38).

Other data appeared, however, indicating that half-calcined dolomite is an unusually effective absorbent for sulfur dioxide produced during fluidized-bed combustion of coal at elevated pressure (39). That is to say, the calcium values in the solid reacted almost quantitatively at elevated pressure, whereas calcium values in either calcined dolomite or limestone react appreciably less than stoichiometric conversion to calcium sulfate in fluidized-bed combustion at atmospheric pressure (3).

With these facts as background, our original plan in the present research was to conduct exploratory experiments hoping to elucidate the improvement in performance of half-calcined dolomite when pressure is increased.

We also hoped to obtain data bearing upon the operability of the cycle for regenerating half-calcined dolomite from sulfated product.

Tests of the absorption of sulfur dioxide by half-calcined dolomite at elevated pressure confirmed what we had already suspected from Narayanan's results (37), viz., that magnesium oxide as well as calcium carbonate in half-calcined dolomite reacts with sulfur dioxide in presence of oxygen. Moreover, our data for the half-calcined dolomite cycle strongly suggested that the reactivity of magnesium oxide toward sulfur dioxide was greatly enhanced at elevated pressure. This suggestion is consistent with the view that the better absorptivity of the half-calcined dolomite in fluidized-bed combustion at elevated pressure (39, 3) is a consequence of an improved absorptivity of the magnesium oxide portion of the solid.

Our tests of the half-calcined dolomite cycle at elevated pressure also tended to confirm Argonne's report (38) of a drastic decline in capacity of the absorbent following only a few cycles of regeneration.

These developments made it appear that a better research plan might be to explore the absorption powers of magnesium oxide toward sulfur dioxide at elevated pressure. In any event, these powers would need to be understood before much headway could be made in understanding the half-calcined dolomite cycle.

More important, however, was the consideration that a cycle based upon magnesia would be simpler from a process standpoint. It was also possible to hope that a magnesia cycle might not display a drastic loss in absorptivity upon repeated cycling of the absorbent.

As will appear in the Section 10.0 to follow, a cycle based upon magnesia would involve the following sequence of reactions:

$$MgO + SO_2 + 1/2\ O_2 = MgSO_4 \qquad (F)$$

$$MgSO_4 + H_2 = MgO + H_2O + SO_2 \qquad (G)$$

It should be emphasized that limited time was available for exploratory research on the magnesia cycle. Data reported here are best regarded as leads to further study rather than as bases for drawing a final, definite picture.

10.0 Supporting Data

The equilibrium decomposition pressure of magnesite, $MgCO_3$, is one atmosphere at about 410°C, but the rate of decomposition at this temperature is slow. Practicably, the solid must be heated to a higher temperature for decomposition to magnesium oxide. It is also to be noted that the recarbonation of magnesium oxide, perhaps because of its remarkably small molecular size and high specific gravity, is difficult (5). Even at 100 atmospheres, recarbonation at 500°C is extremely slow.

It would appear that the reaction of magnesium oxide with sulfur dioxide at elevated temperature is also intrinsically very slow. Wickert (40) stated that MgO will react with SO_2 only if oxygen and from 1% to 2% of iron oxide are present, i.e., according to reaction (F) on the preceding page. Wickert (41) obtained a patent for desulfurization of flue gases at 850°C by a mixture of 100 parts of MgO and 1 part of Fe_2O_3 in form of dust. He described the reaction mechanism as involving catalytic conversion of sulfur dioxide to sulfur trioxide, followed by fixation of the latter by MgO to form $MgSO_4$.

Pechkovskii (42) reported that the reaction of MgO, SO_2, and O_2 is small by comparison with reaction of $CaCO_3$ with the gaseous species. He studied the reaction of MgO and CaO with sulfur dioxide at temperatures from 500° to 800°C and with catalysts on the solids. The level of sulfur dioxide was varied from 2.5% to 20%, and this had a pronounced effect upon

conversions obtained. In all circumstances, far less MgO reacted than CaO. At 2.5% sulfur dioxide and 500°C, conversions of MgO even in runs where iron oxide catalyst was present did not exceed 22%, and uncatalyzed conversions were far smaller.

In a British patent, Moss (43) reported use of fluidized limestone and magnesia to remove sulfur dioxide from flue gases. The effects of variation in temperature, oxygen, sulfur dioxide level, and residence time are reported. Results indicated reactivity of MgO to be more sensitive to temperature than the reactivity of CaO. Maximum reactivities for MgO and CaO occur at 760°C and 875°C respectively. Desulfurization efficiency was reported for different levels of sulfur dioxide and oxygen, as well as a function of percentage of bed reacted. The reactivity of CaO was superior to that of MgO.

Marier and Dibbs (44) studied capture of sulfur dioxide by MgO and CaO in situations with and without iron oxide catalyst. They confirmed Wickert's view of the reaction mechanism, whereby SO_2 is converted to SO_3 before its absorption by the solid. Iron oxide catalyzed the conversion to SO_3.

Borgwardt and Harvey (24) found that sorption of sulfur dioxide by pre-calcined magnesite between 540° and 980°C could be attributed to its calcium oxide impurities. Magnesite calcined in situ, however, could absorb some sulfur dioxide. In 100 seconds, 30 milligrams of MgO powder (0.0096 centimeters in size) can absorb 1, 6.5, 2.6, and 1 milligram of sulfur dioxide at 540°, 650°, 760°, and 980°C respectively. As reported by other authors, they found calcined magnesite to be less reactive than other calcined species that they studied.

Hartman (45) used a differential reactor similar to Borgwardt's to study sulfate of magnesite by flue gases. He found sulfate contents determined by titration to agree with those calculated from a gain in weight of the solid sample.

To our best understanding, no one has studied reaction (F), the absorption of sulfur dioxide, under pressure. No data are available for reaction (G), and so no data exist that would provide a lead as to the fate of absorptive capacity of magnesium oxide toward sulfur dioxide after a number of cycles in which reactions (F) and (G) are conducted repeatedly in turn.

11.0 Experimental Techniques

Overall experimental arrangements for study of absorption of sulfur dioxide from oxygen-containing gases by magnesium oxide and for regenerating the resulting sulfated solid were generally similar to the arrangements already described in Section 5.0.

Runs were made with magnesium oxides produced from pure chemicals, as noted in sections on results, and also from a single sample of magnesite (see Section 11.03 below). In most of the runs starting with magnesite, the solid was used in form of a powder of -250+270 mesh and about 8 mg each run. One run each was made with a disc and a sphere fabricated from chunks of the same stone.

Gas compositions were varied as noted in sections on results. Some runs were made with nitrogen dioxide present to see if this had an effect. Runs were made with catalytic admixtures to the oxide.

11.01 Catalytic Role of Platinum

Unfortunately, a number of runs were made before the question was raised, is platinum in our TGA catalytic toward the sulfur dioxide absorption? Platinum appeared in our TGA set-up in two places: in a gauze to retain Vycor chips upstream of the sample pan and in the sample pan itself.

Once the question was raised, tests with and without platinum quickly demonstrated that platinum had exercised catalytic effect upon our earlier data. Figure 65 illustrates the effect. The three runs for which absorption rates during

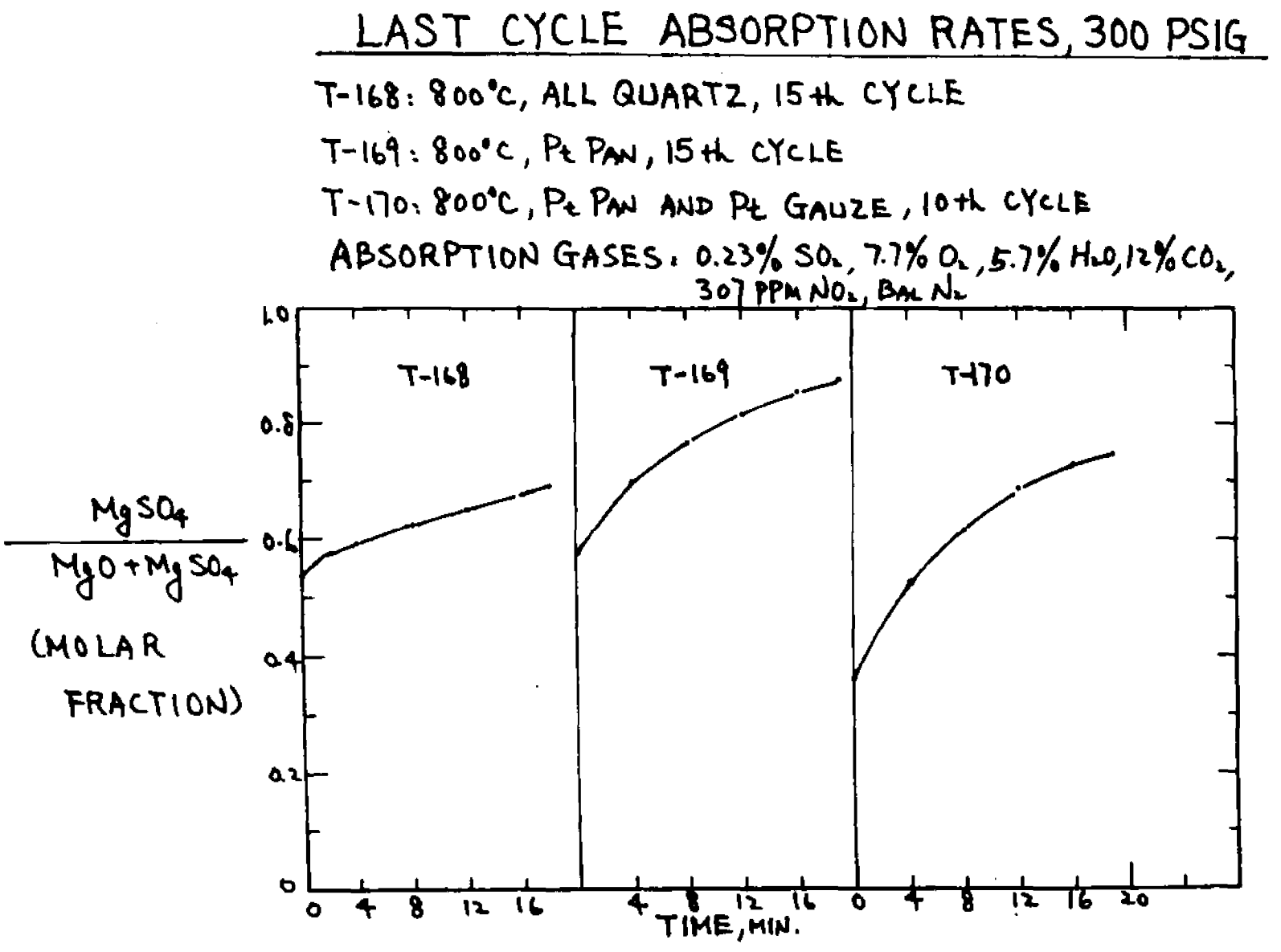

Figure 65. Runs showing effect of platinum upon rate of absorption of sulfur dioxide by magnesium oxide of -250+270 mesh.

each run's last cycle are plotted were made at 300 psig under identical conditions, except run T-168 used a quartz balance pan, run T-169 used a platinum pan, and both platinum pan and gauze appeared in run T-170. Reaction conditions are summarized in Table 7.

Figures 66, 67, and 68 are "zig-zag" plots for runs T-168, T-169, and T-170 respectively.

The catalytic effect of platinum is easily understood. Historically, it was used as a catalyst for the contact process for sulfuric acid production, i.e., as a catalyst for conversion of sulfur dioxide to the trioxide. The trioxide, as might be expected, is far more reactive than the dioxide (46, 47), and so higher capacities are achieved in runs with platinum present.

11.02 Level of Sulfur Trioxide in Exhaust from TGA

We became curious as to the level of sulfur trioxide in exhaust from the TGA. Accordingly, we used Flint's method (47, 48) to determine this level. We found it difficult to collect the misty steam droplets that appeared in the TGA effluent during our SO_2 studies, and we adopted an arrangement with a large primary condenser and a small secondary condenser having a scrubbing action. We were able with the arrangement to increase the efficiency of steam collection from about 70% to over 90%. From a titration of the condensate, we could measure the level of sulfur trioxide seen by the sample in the TGA. For five runs with a quartz pan, the trioxide levels were 48, 61, 42, 43, and 46 parts per million.

We obtained tentative data indicating that the trioxide level was higher than 111 parts per million in work with the platinum pan.

Table 7

Runs Made to Probe Catalytic Effect of Platinum Upon Calcined Magnesite as SO_2 Acceptor at 300 Psig

	Absorption				Regeneration			
Run #	Temp. °C	Time Min.	Last-Cycle Capacity %	Gases (Bal N_2)	Temp. °C	Time Min.	Capacity %	Gases (Bal N_2)
T-168	800	19	16	0.23% SO_2 7.7 % O_2 5.7 % H_2O 12 % CO_2 307 ppm NO_2	800	3	13	40 % H_2 5.7% H_2O
T-169	800	19	31	same as T-168	800	3	30	same as T-168
T-170	800	19	38	same as T-168	800	3	36	same as T-168

Notes:

1. Calcinations were done with 25% H_2O, 50% CO_2, 25% N_2 up to 800°C.
2. T-168 and T-169 had 15 cycles; T-170 had 10 cycles.

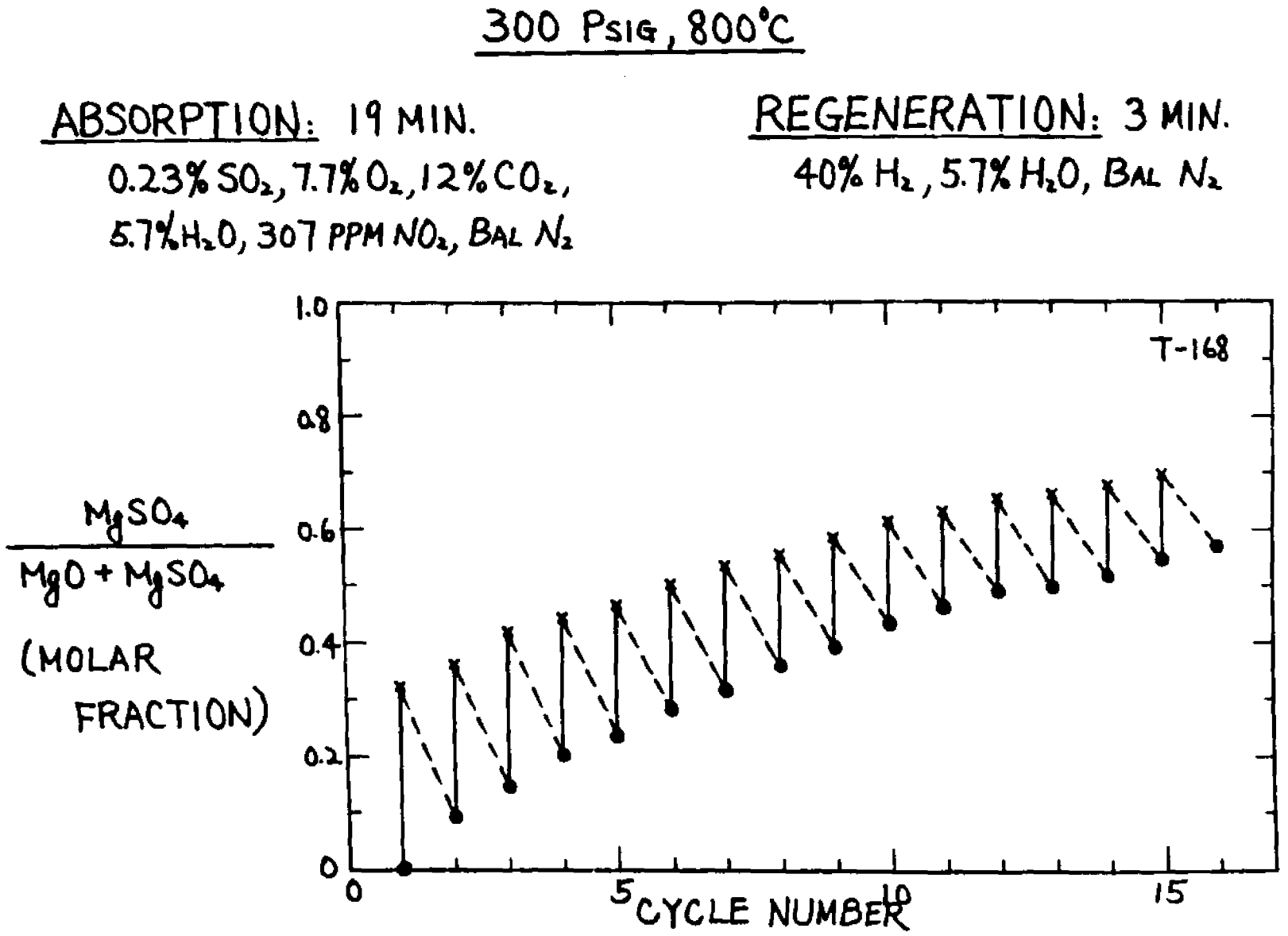

Figure 66. Zig-Zag figure of T-168.

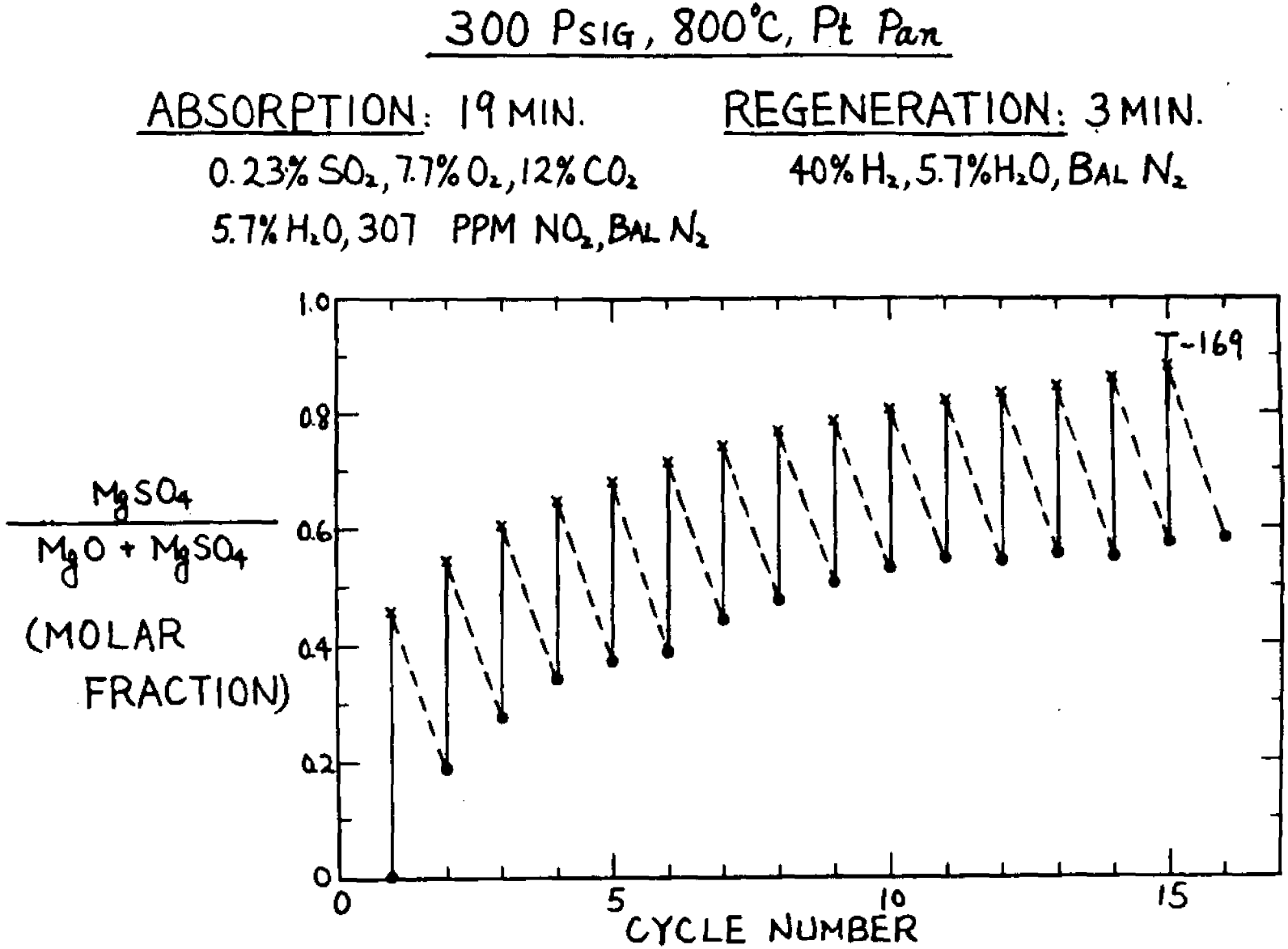

Figure 67. Zig-Zag figure of T-169.

300 PSIG, 800°C, Pt Pan and Gauze

ABSORPTION: 19 MIN.
0.23% SO_2, 7.7% O_2, 12% CO_2
5.7% H_2O, 307 PPM NO_2, BAL N_2

REGENERATION: 3 MIN.
40% H_2, 5.7% H_2O, BAL N_2

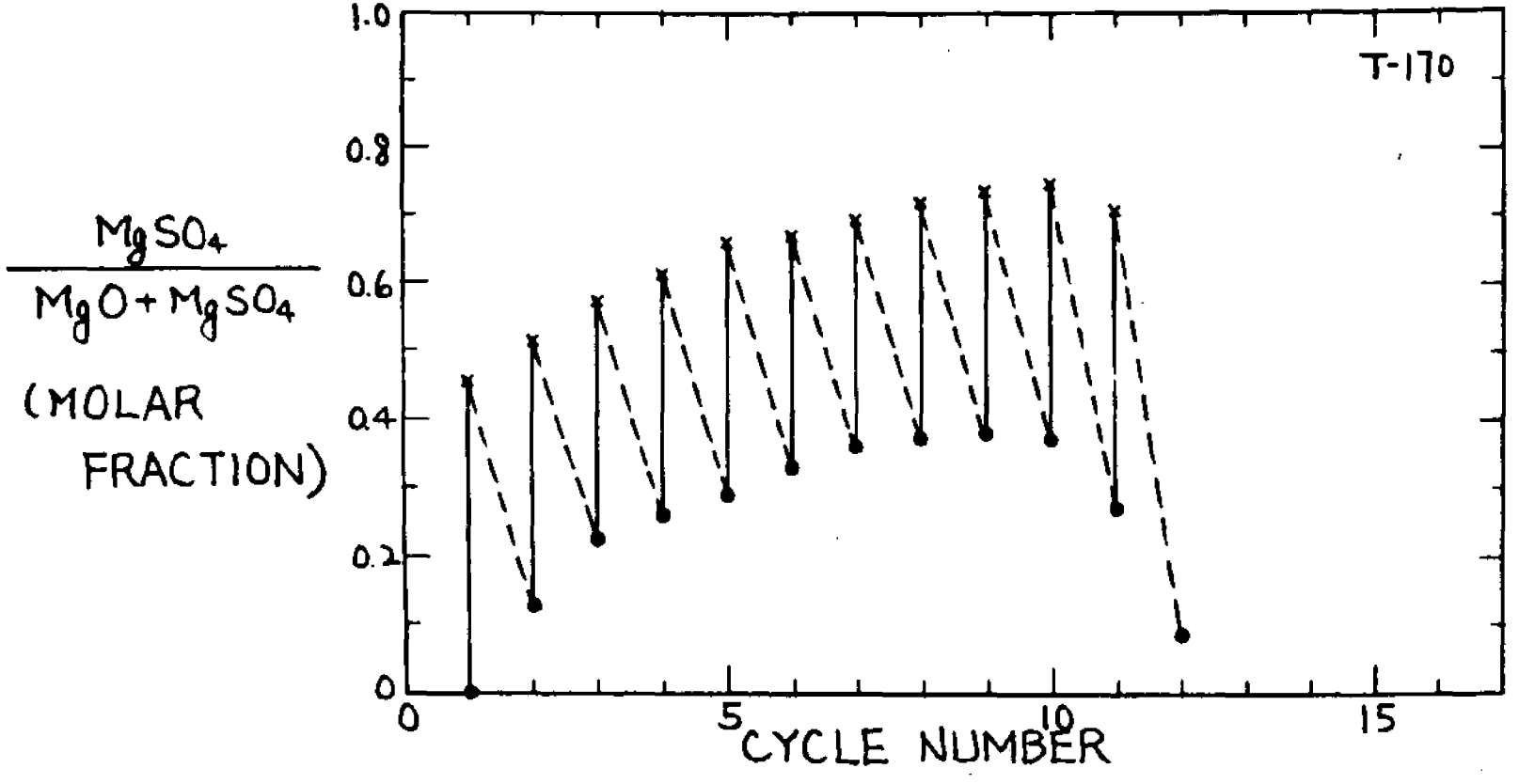

Figure 68. Zig-Zag figure of T-170.

We further investigated to test the possibility that a catalytic effect of the stainless steel tubing upstream of the TGA might create an abnormally high level of sulfur trioxide. We conducted run T-174 at 800°C with a quartz pan, and after stabilizing the solid with six cycles, the seventh cycle was made with no steam in the absorption gases. The capacity of the solid and rate of absorption were not affected by omission of steam. An eighth cycle was conducted without steam and with no heat supplied to the stainless steel tubing (which is normally kept at a temperature well above the dew-point of steam). Again, there was no sign of a change in rate between seventh and eighth absorption, and so it may be concluded that hot stainless steel has not provided an appreciable catalyzing effect during our other experiments.

11.03 Experimental Solids

Richard Harvey of the Illinois State Geological Survey supplied our sample of magnesite, and reported its composition as follows (49):

Oxides	Weight Percent
MgO	44.2
CaO	2.93
CO_2	50.96
SiO_2	0.47
Al_2O_3	0.08
FeO	0.07
K_2O	0.03
Na_2O	0.026
SO_3	0.01
SrO	0.01
P_2O_3	approx. 0.005
Fe_2O_3	less than 0.01
MnO	less than 0.01
TiO_2	less than 0.01
Cl	less than 0.02

The sample is from the Red Mountain District of Santa Clara County in California.

The capacity of the magnesium oxide for absorption of sulfur dioxide was calculated for each run from the weight loss observed during a calcination step. Calcinations were usually conducted in a 25/50/25 mixture of steam/CO_2/nitrogen with heating at about 20°C per minute to 800°C. From the weight loss, the percentage of $MgCO_3$ in a given sample of magnesite can easily be calculated. Typically, the value is 93% $\pm$ 2%. The percentage $MgCO_3$ calculated from the analysis given above is 92.5%, which is close to values obtained from weight loss.

12.0 Results

As we mentioned in Section 11.0, many runs were performed with platinum present in the TGA before we learned that platinum aided the absorption reaction by converting sulfur dioxide to the trioxide. Some of the early results are nevertheless worth reporting for qualitative indications which they provide. In what follows, we will repeat as necessary the information concerning presence or absence of platinum.

12.01 Effect of Pressure

Early runs, summarized in Figure 69, with platinum present revealed a striking effect of pressure upon the absorption of sulfur dioxide by reagent grade magnesia powder, and the course of a subsequent regeneration. Also shown is an absorption step for a powder obtained by calcining the Red Mountain magnesite of Section 11.03. The effect of pressure, not only upon reaction rate, but also upon the final degree of reaction, is striking. These data taught us that understanding the absorption of sulfur dioxide by half-calcined dolomite at elevated pressure would be a complicated business, and were a factor in our decision to study absorption by magnesia alone.

12.02 Reproducibility

Figures 70 and 71 show that the reproducibility of both absorption and regeneration steps -- i.e., reactions F and G respectively -- is good. Figure 70 is for two runs with platinum present, and Figure 71 is without platinum. Figure 72 is a zig-zag plot for one of the runs of Figure 70.

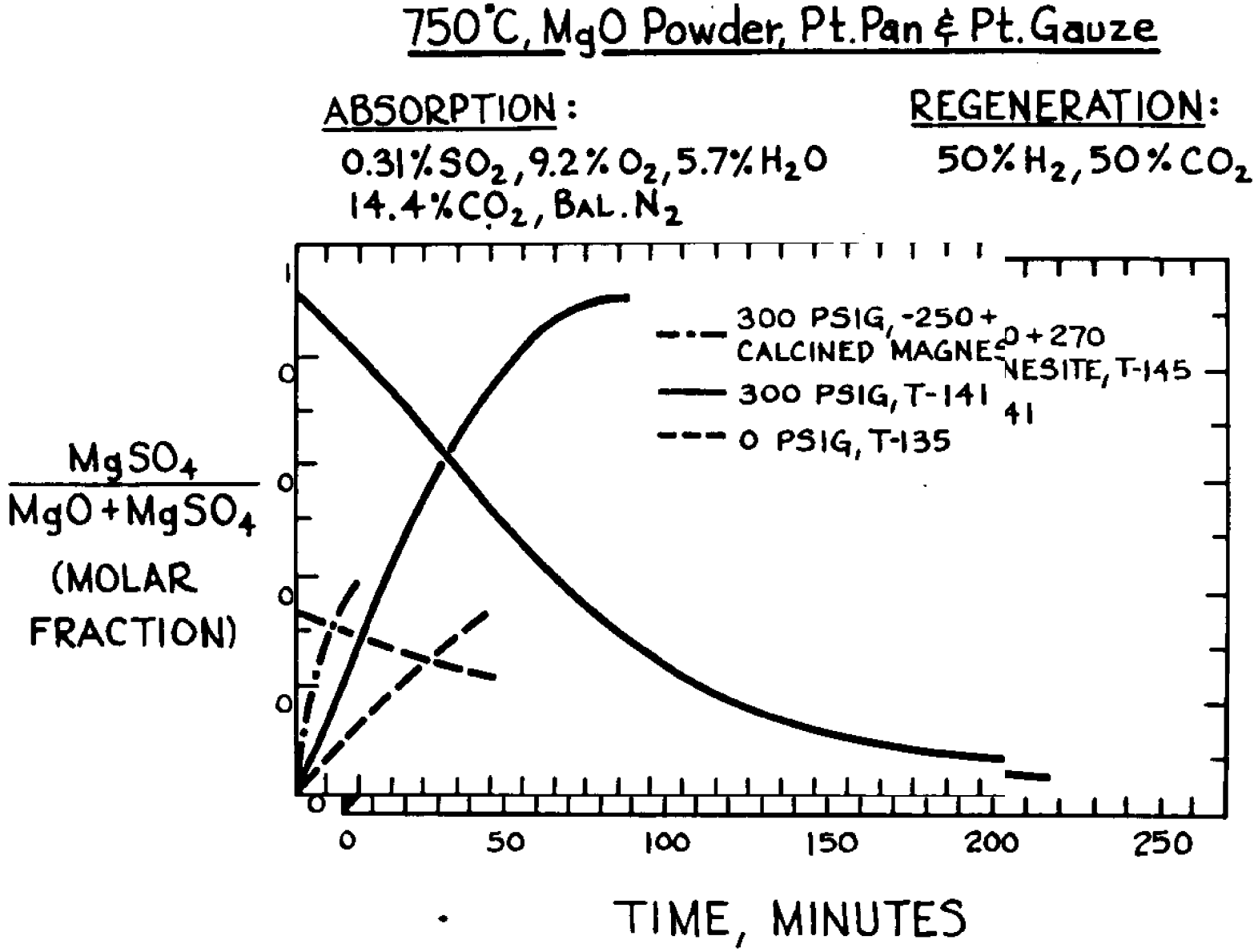

Figure 69. Cyclic rates for MgO powder as SO_2 acceptor at 0 and 300 psig.

300 PSIG, 800°C, Pt PAN and Pt GAUZE

ABSORPTION:
0.23% SO_2, 9.2% O_2, 5.7% H_2O, 13.1% CO_2
BAL N_2

REGENERATION:
40% H_2, 5.7% H_2O, BAL N_2

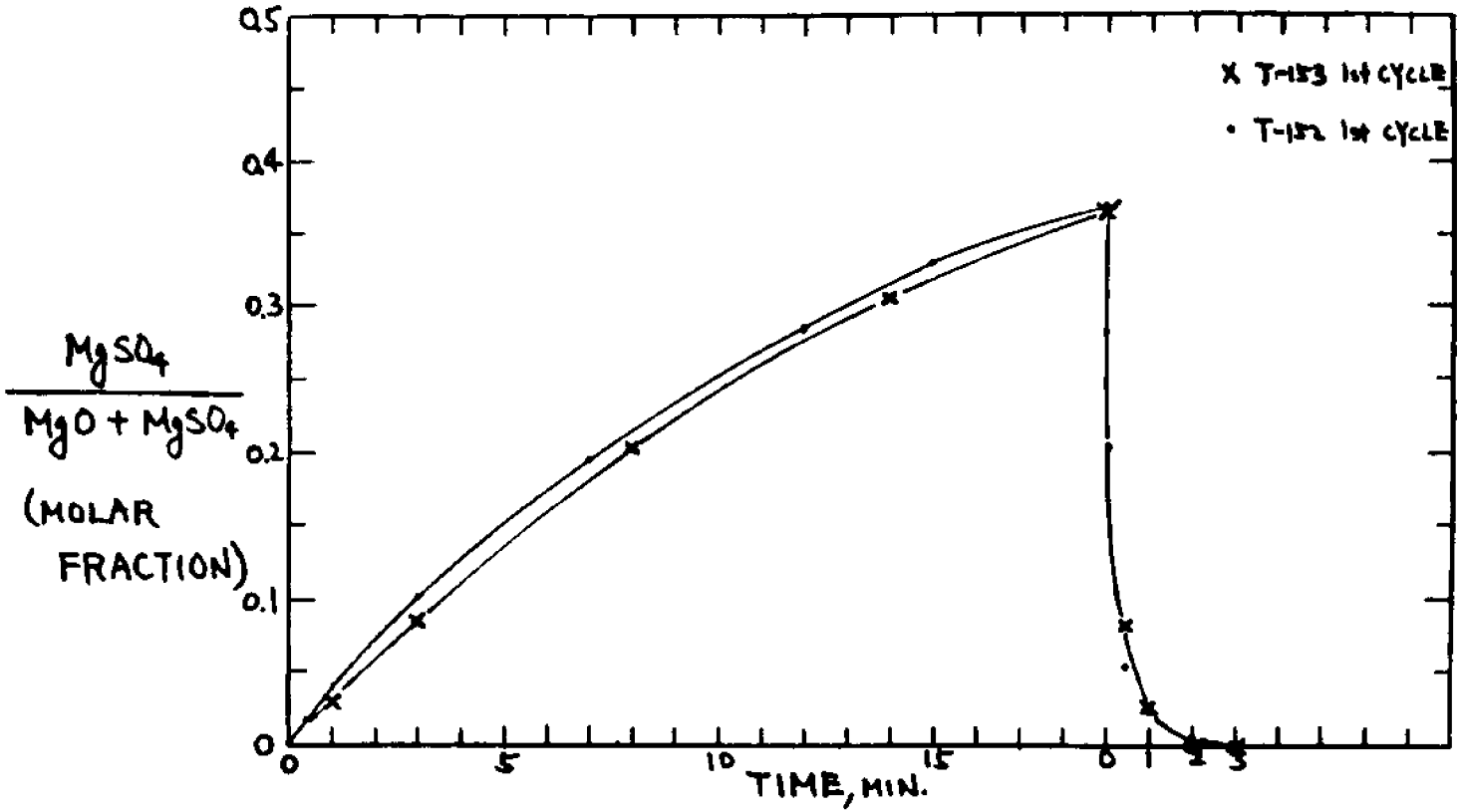

Figure 70. Reproducibility check on cyclic rates with platinum catalyzing.

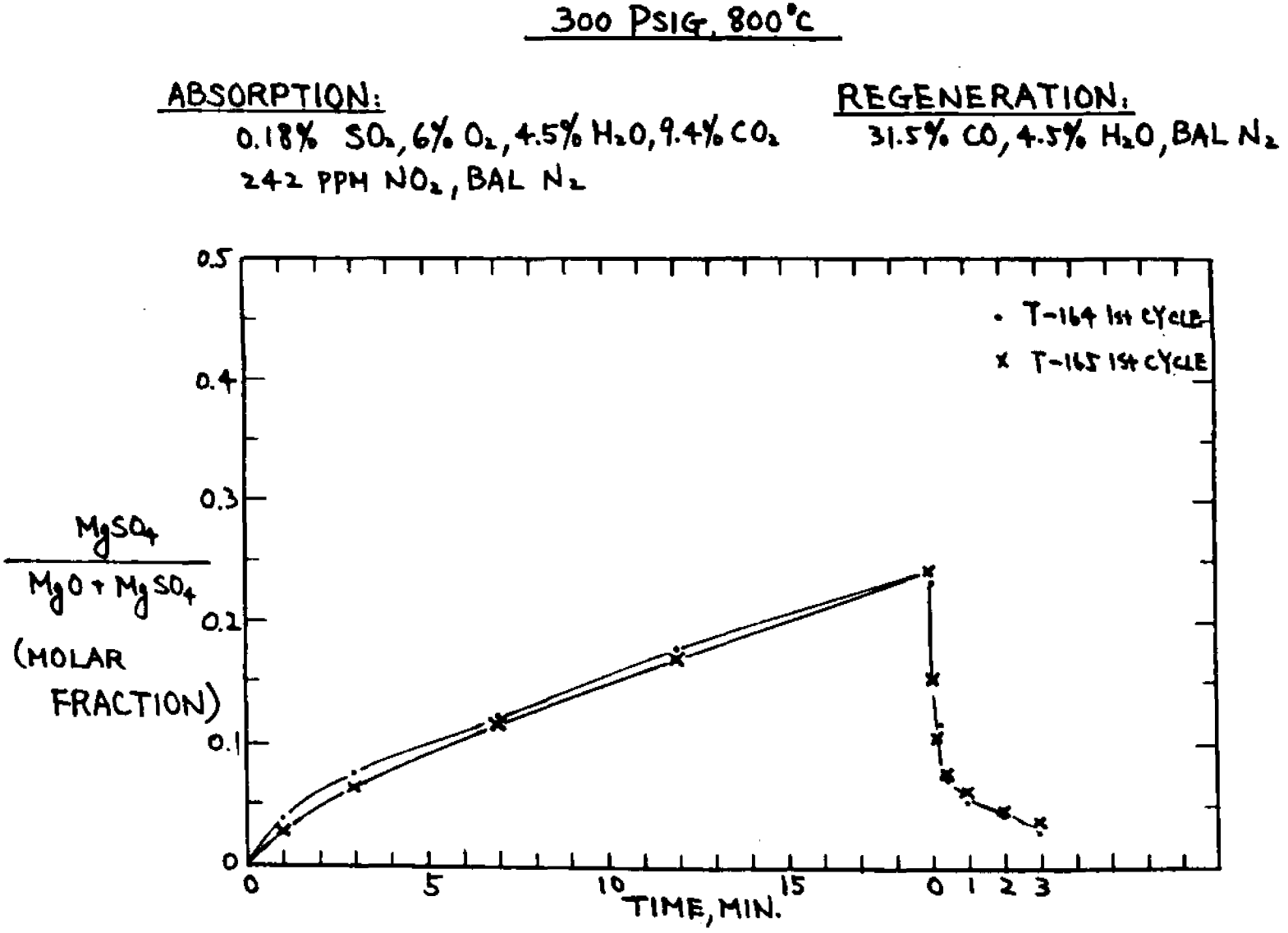

Figure 71. Reproducibility check on cyclic rates without platinum catalyzing.

300 PSIG, 800°C, Pt Pan and Gauze

ABSORPTION: 19 MINUTES
0.23% SO_2, 9.2% O_2, 13.1% CO_2, 5.7% H_2O, BAL N_2

REGENERATION: 3 MINUTES
40% H_2, 5.7% H_2O, BAL N_2

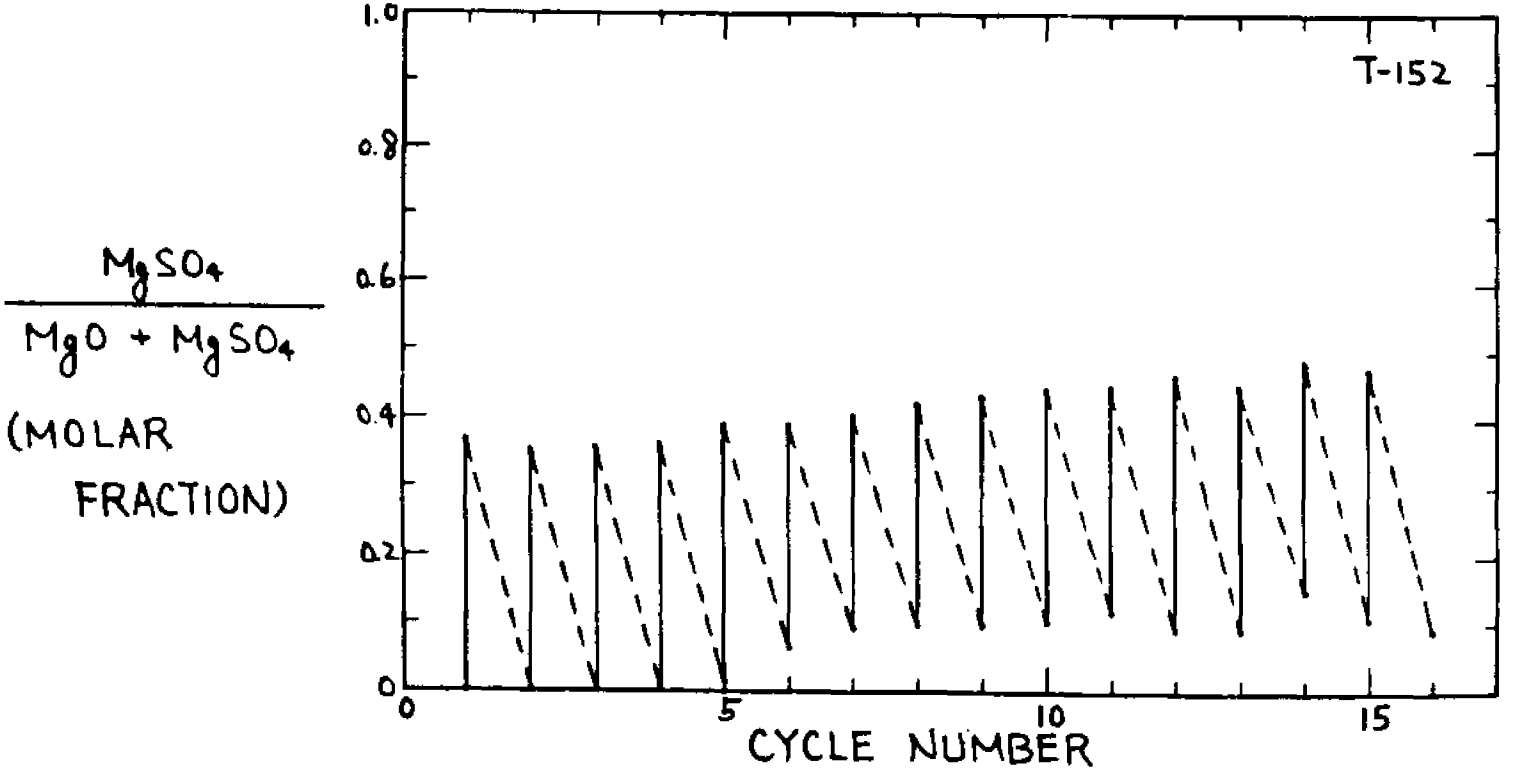

Figure 72. Zig-Zag figure of T-152.

The figures also illustrate the great speed of the regeneration reaction G in comparison with the absorption reaction F.

12.03 Effect of Catalyst on Absorption Rate

After the discovery of the catalytic effects of platinum gauze and balance pan, we wondered if even more striking catalytic effects might appear with a magnesite intimately associated with a catalytic substance. We impregnated magnesite with palladium chloride, so that we obtained upon subsequent calcination a magnesium oxide impregnated with palladium metal. Figure 73 compares absorption and regeneration at atmospheric pressure for the impregnated oxide and an oxide free of catalyst (runs T-189 and T-188 respectively). Figures 74 and 75 are zig-zag plots of the two runs. The faster rate of absorption of the catalyzed oxide is evident, and this leads of course in a nineteen-minute absorption step to a greater uptake of sulfur dioxide by the solid.

The regeneration step appeared to proceed equally fast for both catalyzed and non-catalyzed solids, and regeneration proceeded essentially to completion for both solids in a three-minute regeneration step.

Table 8 lists reaction conditions for runs T-188 and T-189, as well as for other runs discussed in this Section 12.03.

Further runs were made comparing performance with and without platinum pan and gauze, and with and without intimately associated catalyst for magnesium oxides of various origins.

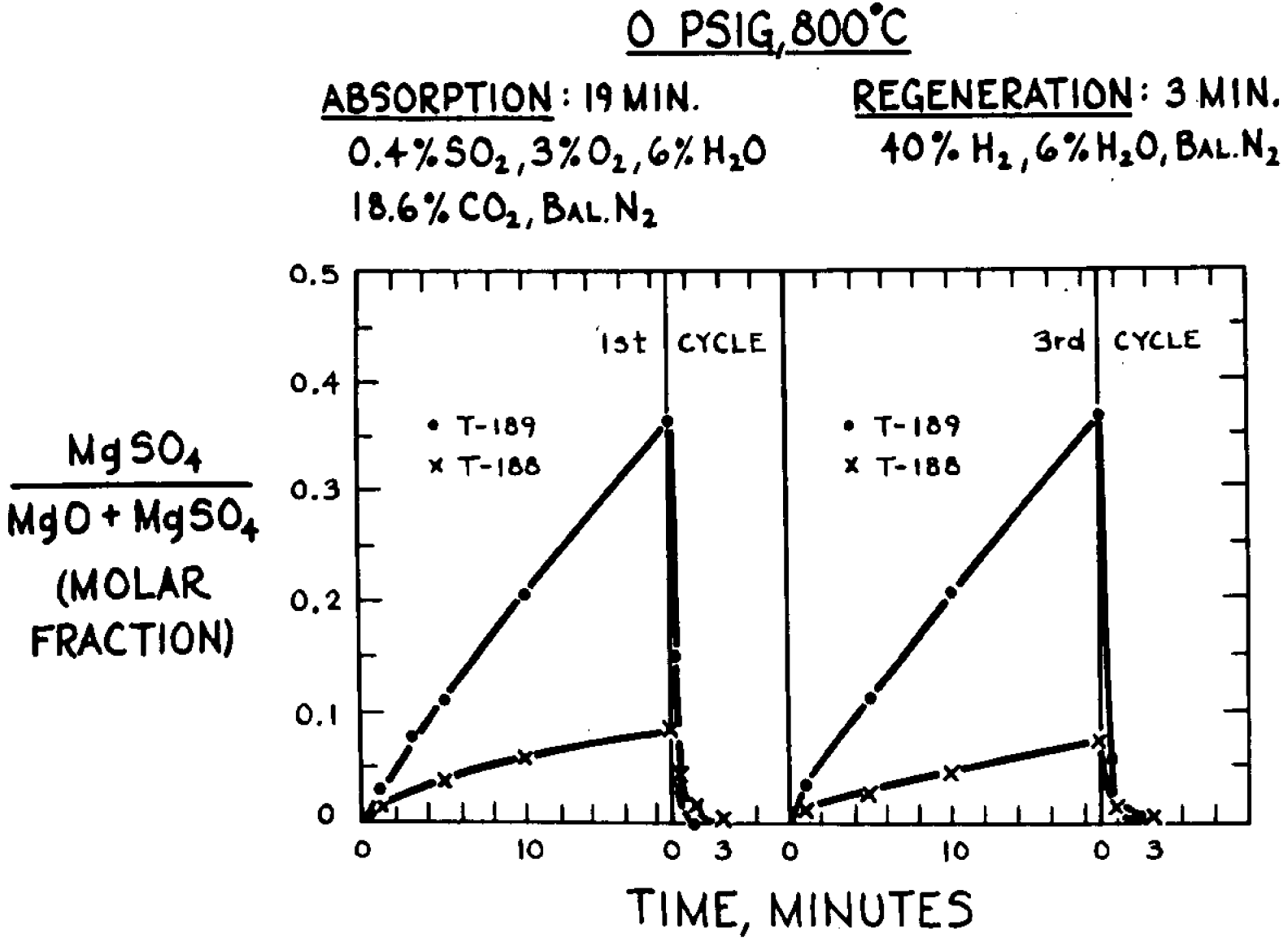

Figure 73. Effect of catalyst on rates at 1 atm. Run T-189 uses a magnesium oxide impregnated with palladium.

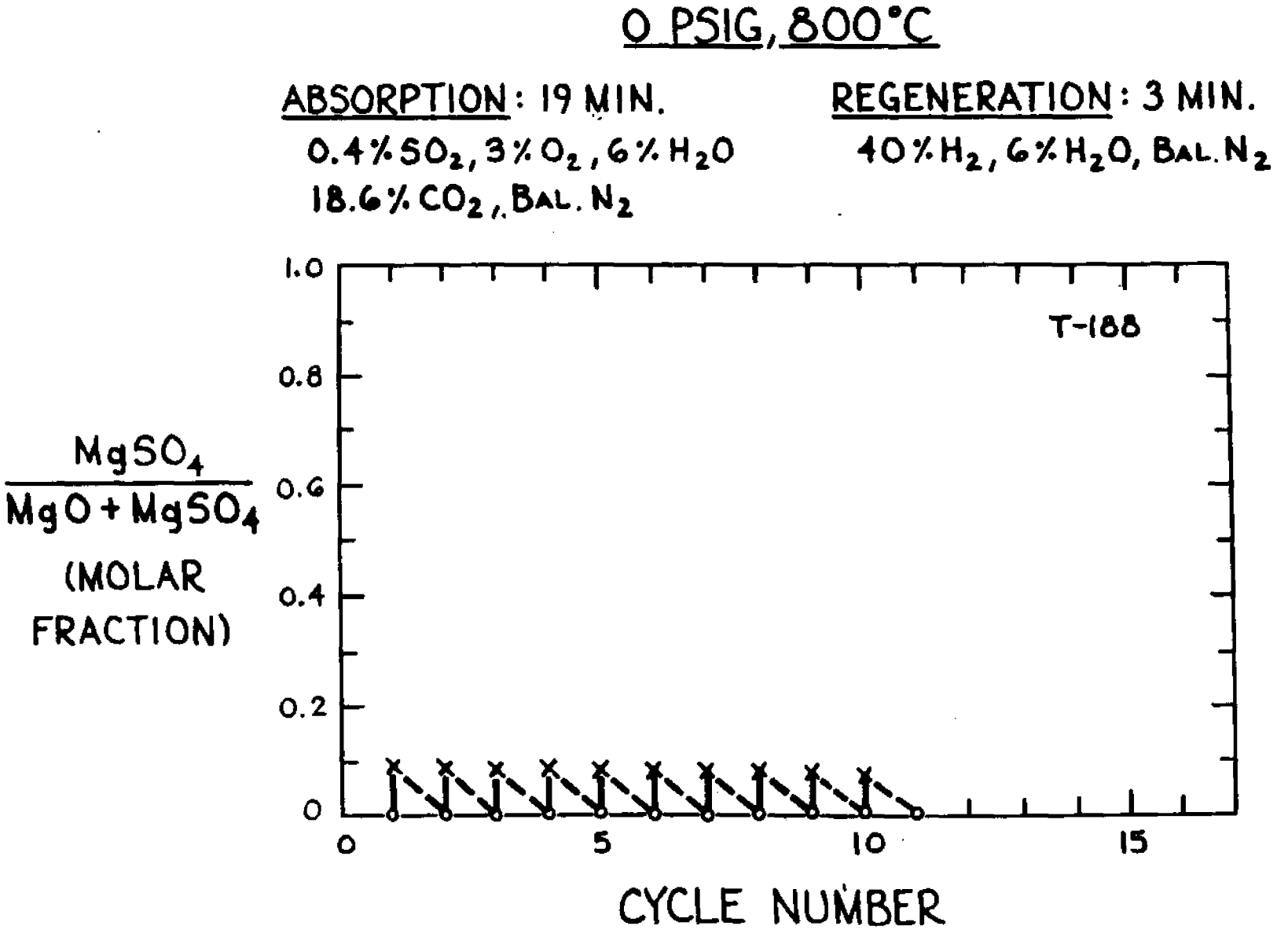

Figure 74. Zig-Zag figure of T-188.

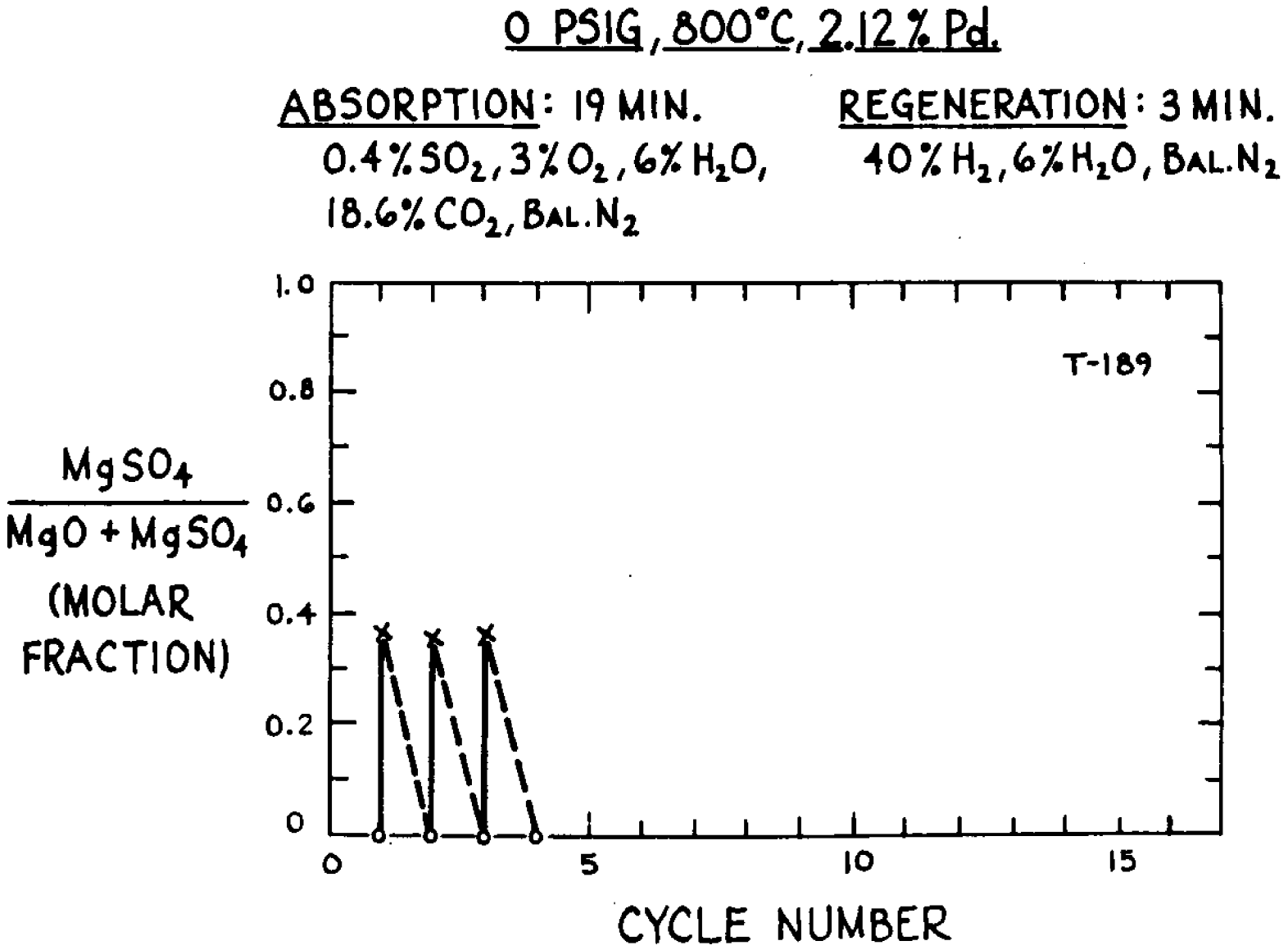

Figure 75. Zig-Zag figure of T-189.

Table 8

Runs Made to Probe Catalytic Effects Upon Calcined Magnesite as SO_2 Acceptor at 800°C [3]

Run #	Starting Solid and Catalytic Material[2]	Absorption: Last cycle Capacity %	Absorption: Gases (Bal N_2)	Regeneration: Last cycle Capacity %	Regeneration: Gases (Bal N_2)
T-188		7 (10)[1]	0.4 % SO_2 3 % O_2 6 % H_2O 19 % CO_2	7	40% H_2 6% H_2O
T-189	3.61[g] $PdCl_2$ per 100[g] $MgCO_3$	36 (3)	0.4 % SO_2 3 % O_2 6 % H_2O 19 % CO_2	36	40% H_2 6% H_2O
T-168		16 (15)	0.23% SO_2 7.7 % O_2 6 % H_2O 12 % CO_2 307ppm NO_2	13	40% H_2 6% H_2O
T-169	Pt pan only	31 (15)	0.23% SO_2 7.7 % O_2 6 % H_2O 12 % CO_2 307ppm NO_2	30	40% H_2 6% H_2O

Table 8 (continued)

Run #	Catalytic Material[2]	Absorption: Last cycle Capacity %	Absorption: Gases Bal N_2	Regeneration: Last cycle Capacity	Regeneration: Gases Bal N_2
T-170	Pt pan and Pt gauze	38 (10)	0.23% SO_2 7.7 % O_2 6 % H_2O 12 % CO_2 307ppm NO_2	36	40% H_2 6% H_2O
T-177		14 (6)	0.4 % SO_2 3 % O_2 6 % H_2O 19 % CO_2	13	40% H_2 6% H_2O
T-182	4.2g Pt per 100g $MgCO_3$	32 (8)	0.4 % SO_2 3 % O_2 6 % H_2O 19 % CO_2	28	40% H_2 6% H_2O
T-183	1.6g Pd per 100g $MgSO_4$	97 (6)	0.4 % SO_2 3 % O_2 6 % H_2O 19 % CO_2	96	40% H_2 6% H_2O
T-186	3.6g $PdCl_2$ per 100g $MgCO_3$	78 (10)	0.4 % SO_2 3 % O_2 6 % H_2O 19 % CO_2	78	40% H_2 6% H_2O

Table 8 (continued)

Run #	Catalytic Material[2]	Absorption: Last cycle Capacity %	Absorption: Gases Bal N_2	Regeneration: Last cycle Capacity	Regeneration: Gases Bal N_2
T-187	2.3[g] $PdCl_2$ per 100[g] $MgSO_4 \cdot H_2O$	84 (10)	0.4 % SO_2 3 % O_2 6 % H_2O 19 % CO_2	84	40% H_2 6% H_2O

1. Numbers in bracket indicate last cycle number.
2. Unless otherwise noted, quartz pan and quartz wool support for Vycor chips were used. T-183 solids was -270 mesh. Other runs were started with -250+270 mesh solids.
3. All absorption times were 19 minutes.
   All regeneration times were 3 minutes.
   All calcination was done with 25% H_2O, 50% CO_2, 25% N_2 up to 800°C.
   An initial regeneration is needed for $MgSO_4$ as starting material.
   All runs were made at 800°C. Runs T-188 and T-189 were made at 0 psig; other runs were made at 300 psig.

Figure 76 gives data for first and last cycles of run T-168, which used a quartz pan. Figure 77 shows the faster rates and larger capacities of run T-169 using a platinum pan. Figure 78 is for run T-170, in which a platinum gauze was present as well as platinum pan. The catalytic effect of the platinum pan upon the first absorption step is evident upon comparison of Figures 76 and 77. Addition of the platinum gauze in Figure 78 had little further effect upon the rate of the first step.

The differences in regeneration rate in Figures 76 and 77 are believed not to be due to presence or absence of catalyst, but to lack of the best possible control of temperature in the regenerations at the time of these runs. Later, as we will see in Section 12.08 below, we discovered that the temperature of the regeneration step has a marked effect upon its rate.

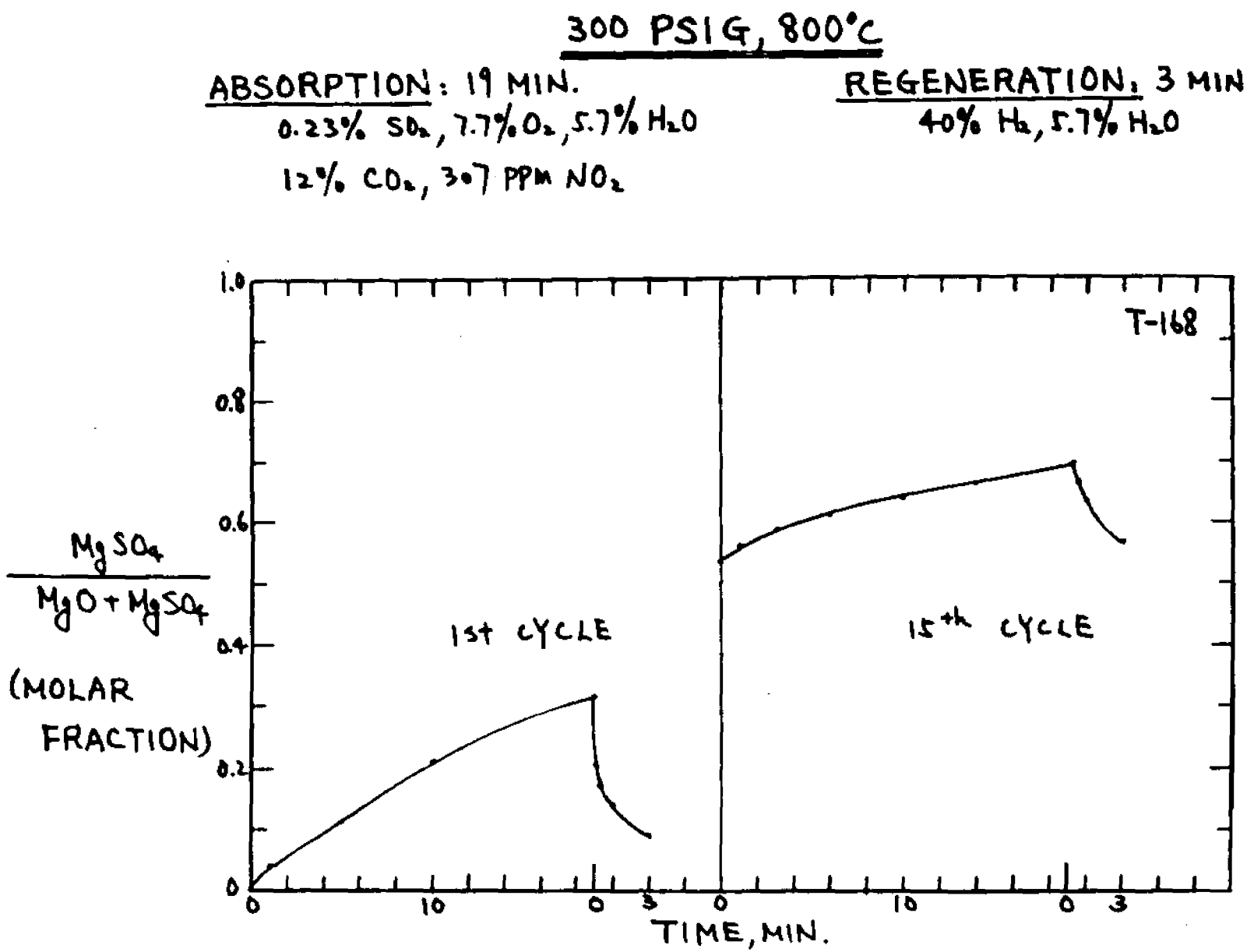

Figure 76. Cyclic rates of T-168, with quartz pan.

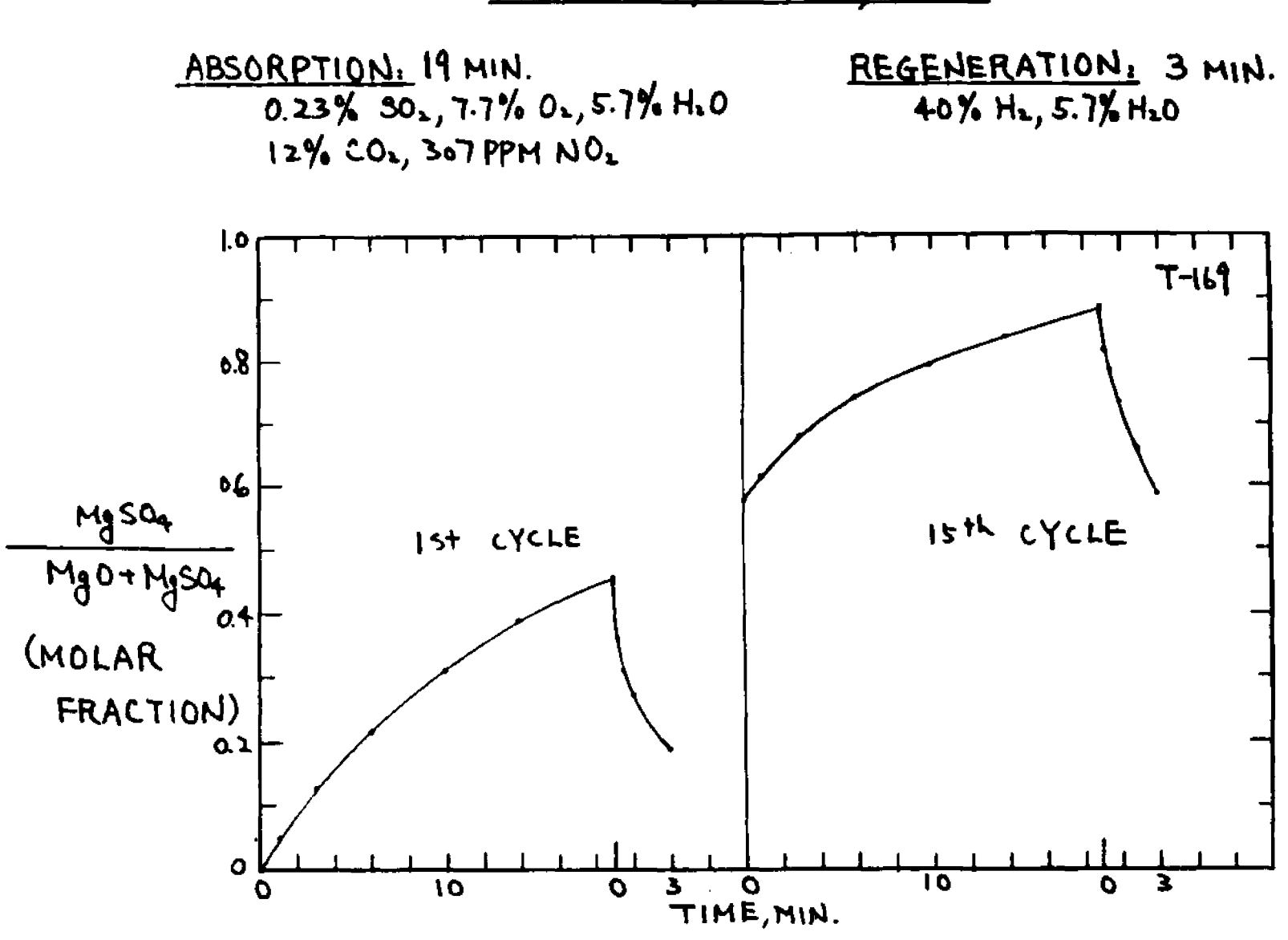

Figure 77. Cyclic rates of T-169, with platinum pan.

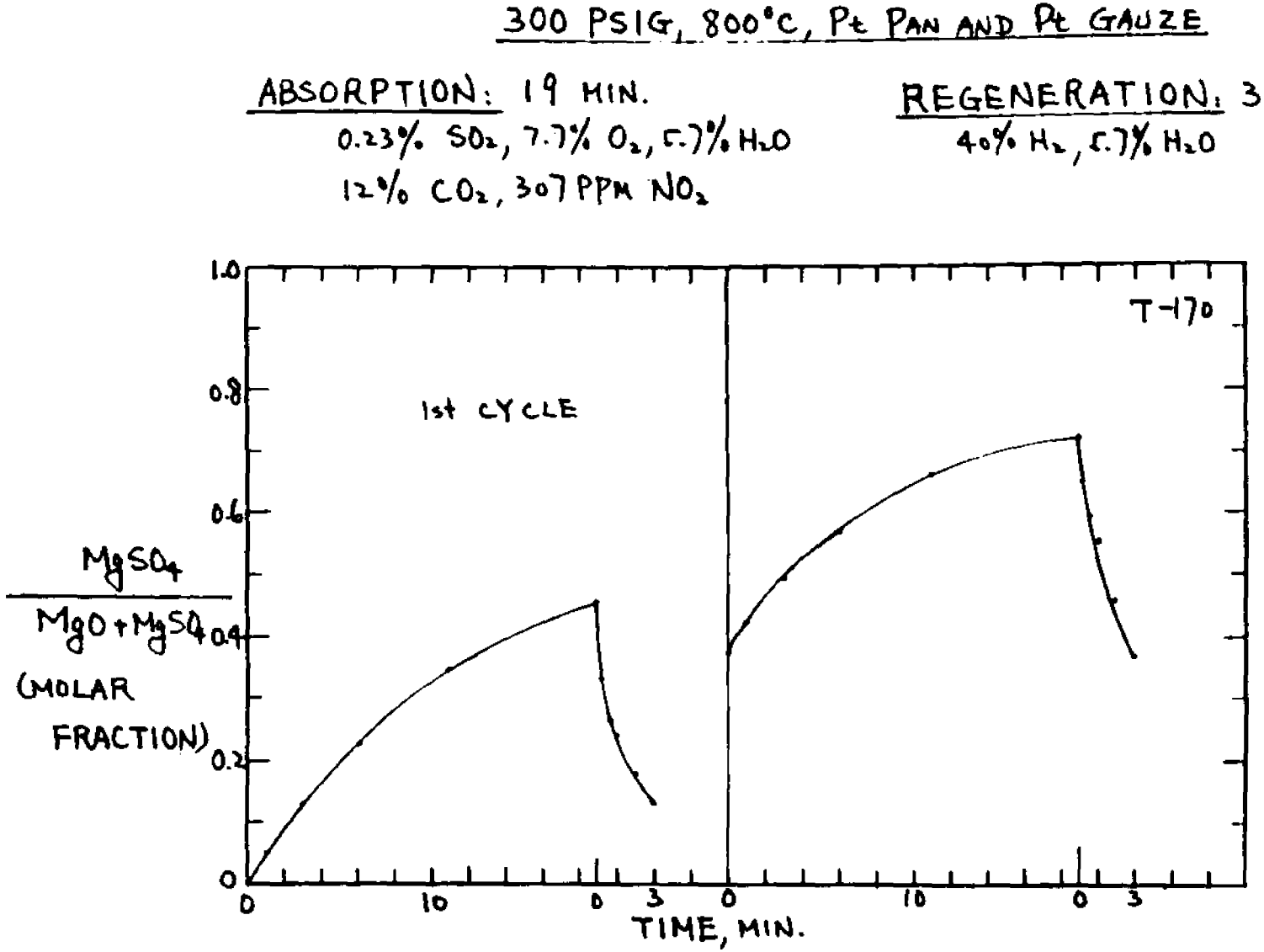

Figure 78. Cyclic rates of T-170, with platinum pan and gauze.

Runs T-177, T-182, and T-186 were made to explore effects of different catalysts in a more quantitative way. Conditions for the three runs were nominally identical and are listed in Table 8 (although the slower regeneration in run T-182 suggests, together with evidence to be given in Section 12.08, that the temperature may have been a bit lower in this run).

Run T-177 used ordinary magnesia made by calcining our Red Mountain magnesite. Run T-182 started with a magnesite upon which platinum black had been deposited. Run T-186 used palladium-impregnated magnesite, as described earlier.

Figures 79, 80, and 81 give results for first and last cycles of the three runs, and illustrate the higher absorption rates which the presence of catalyst provides. The more finely dispersed form of the palladium catalyst in run T-186 is evidently responsible for the higher rate in this run when it is compared with run T-182.

Figures 82, 83, and 84 are zig-zag plots for the three runs.

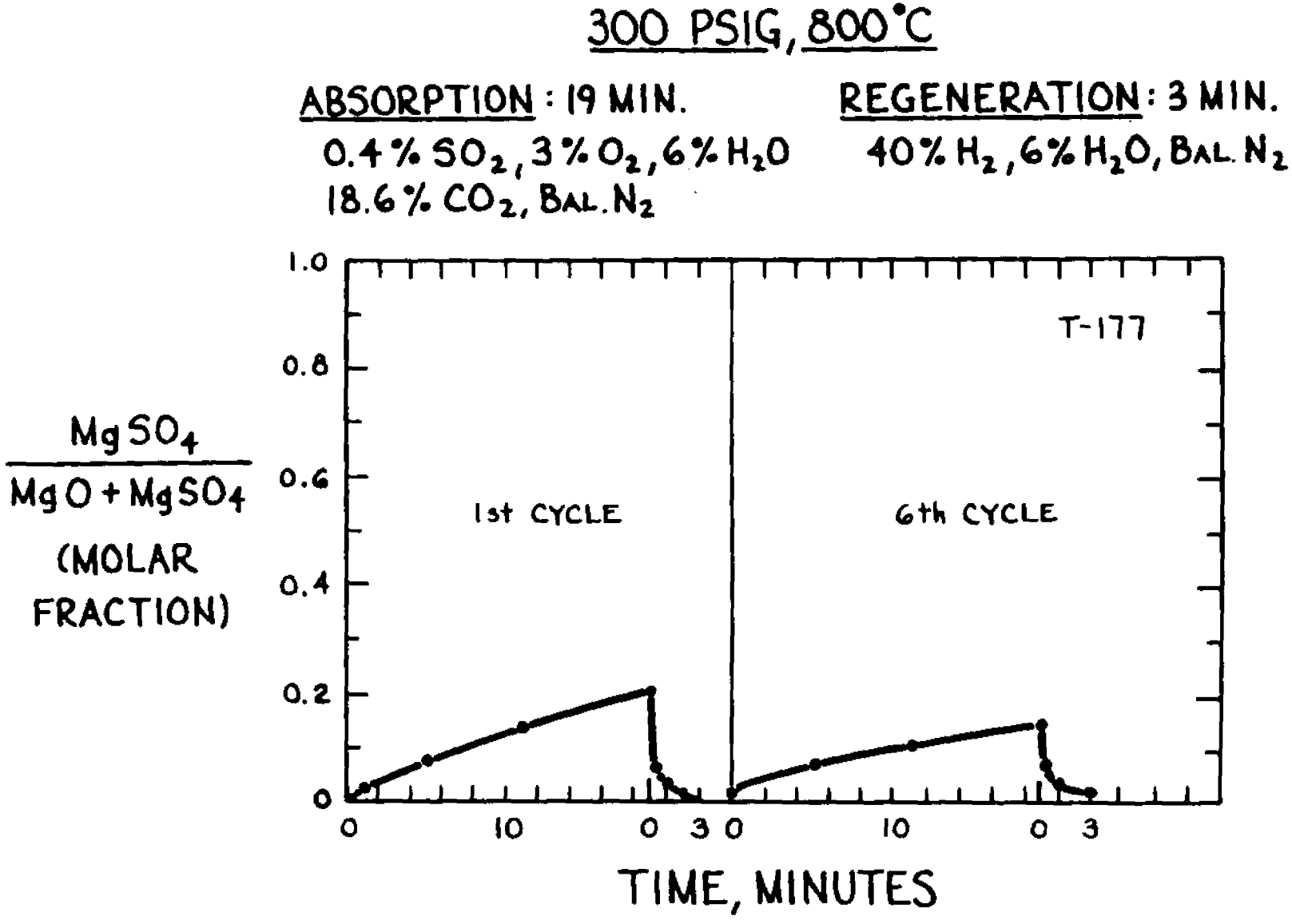

Figure 79. Cyclic rates of T-177, with quartz pan and no catalyst.

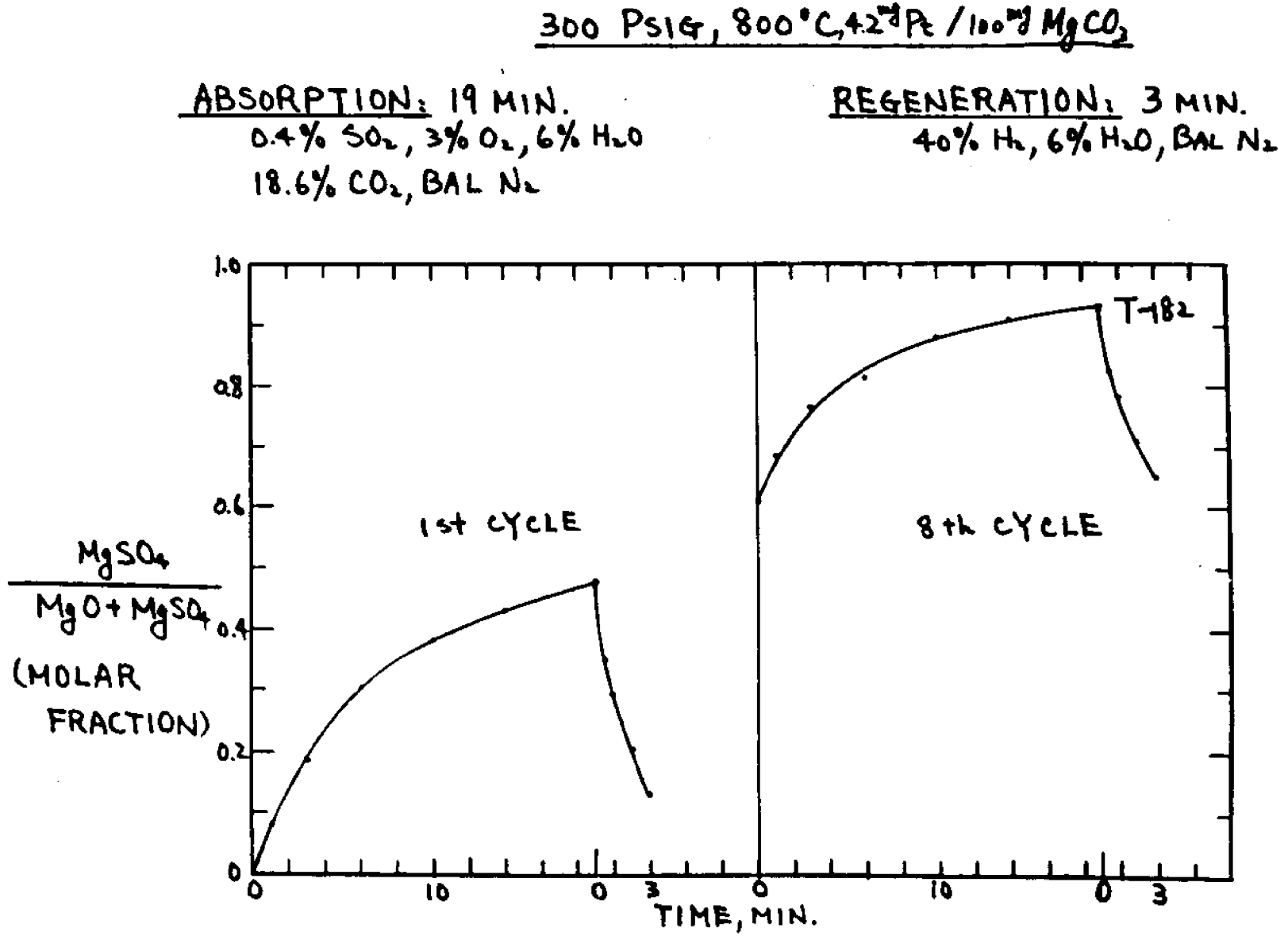

Figure 80. Cyclic rates of T-182, with platinum powder interspread in magnesia.

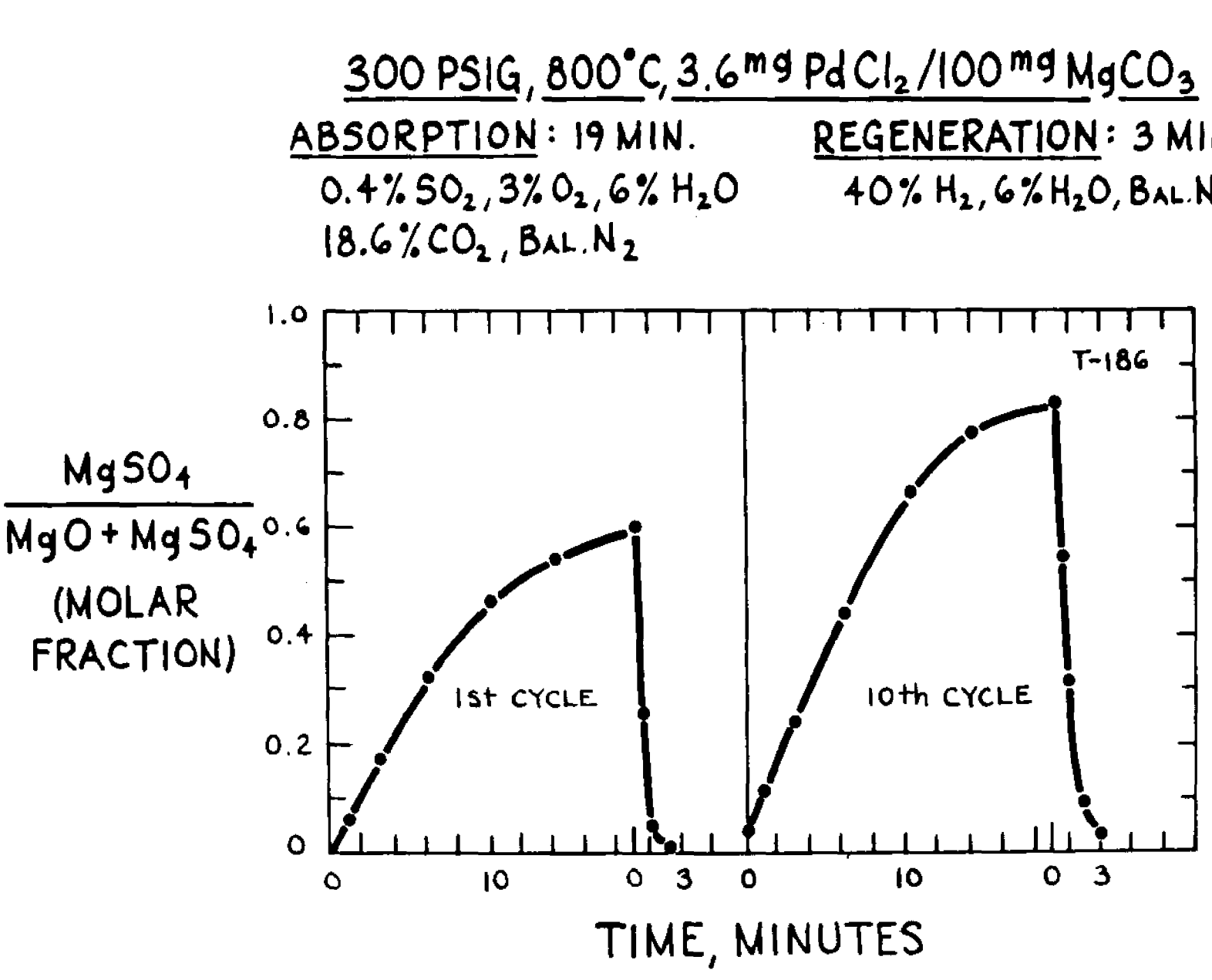

Figure 81. Cyclic rates of T-186, with magnesia impregnated with palladium.

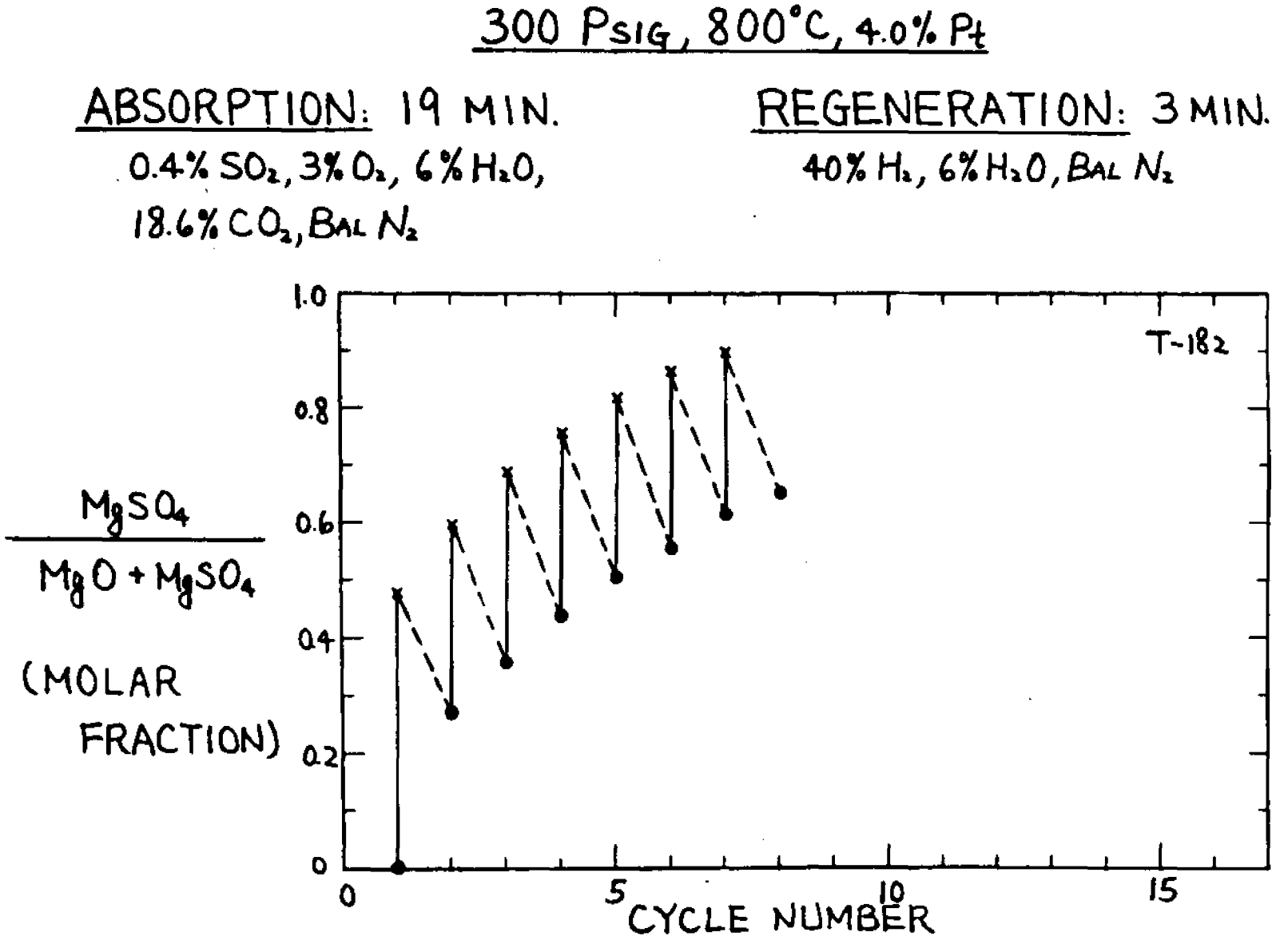

Figure 82. Zig-Zag figure of T-182.

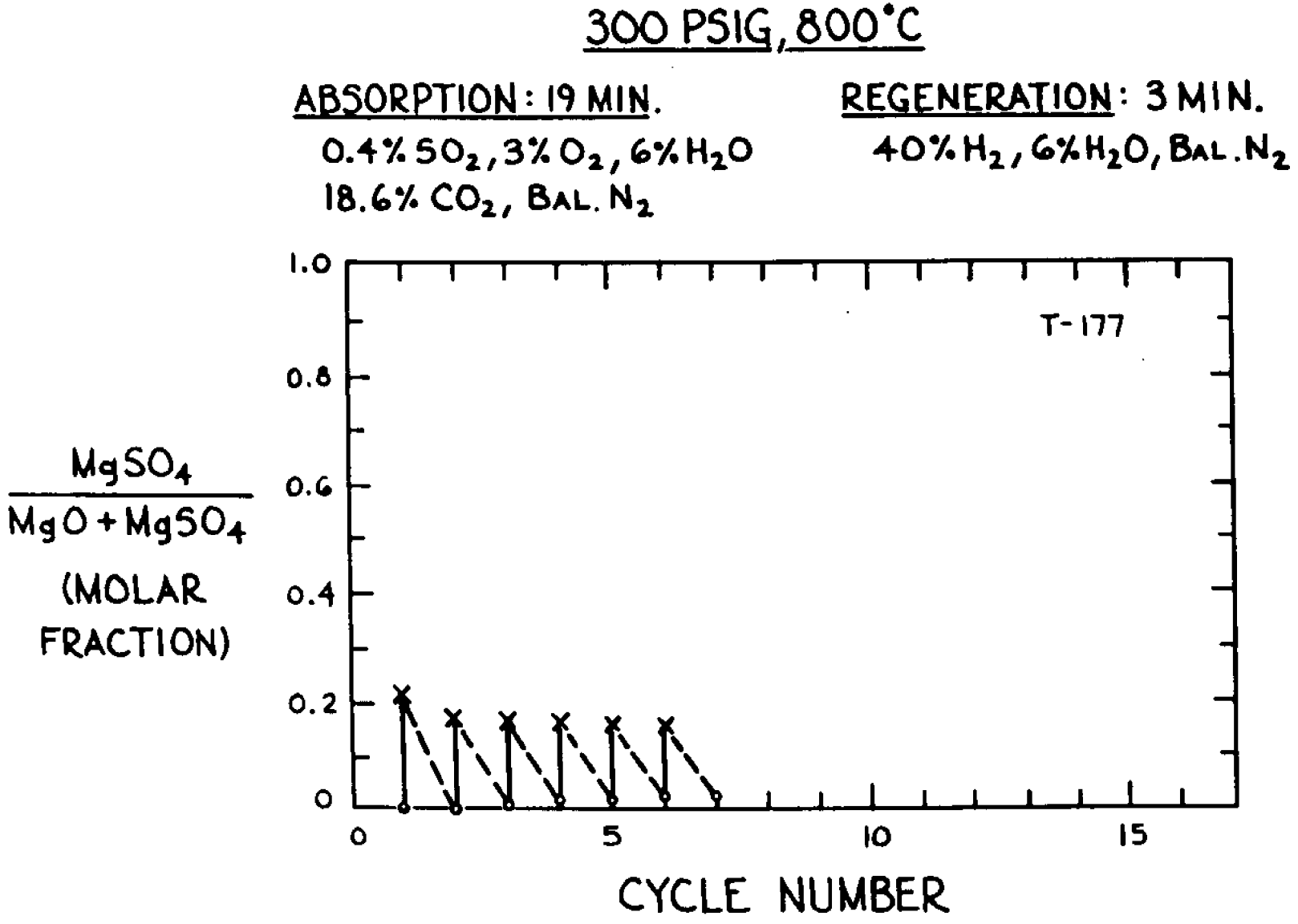

Figure 83. Zig-Zag figure of T-177.

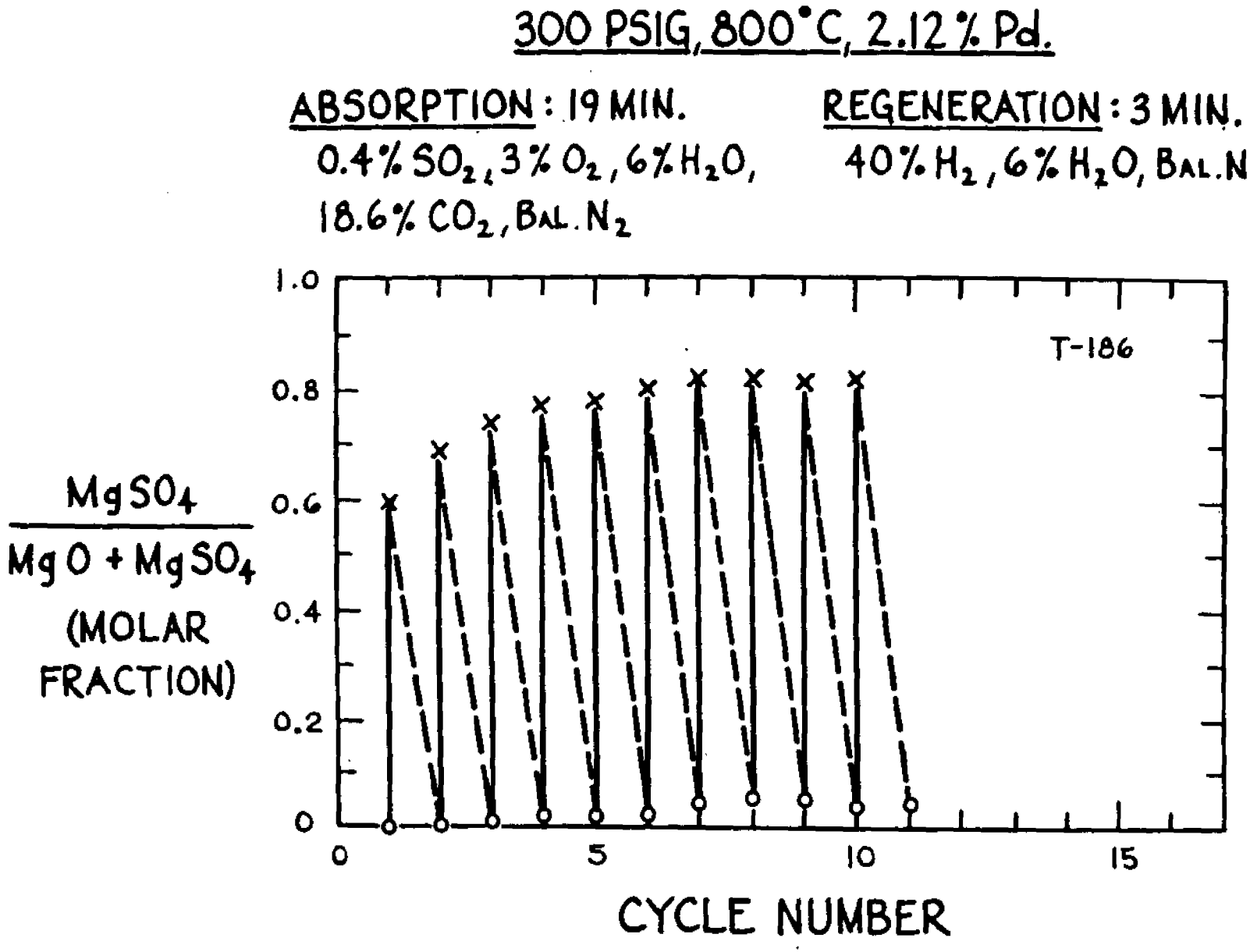

Figure 84. Zig-Zag figure of T-186.

Runs T-183 and T-187 used magnesium oxide prepared from epsom salt, $MgSO_4 \cdot 7\ H_2O$. The salt was dissolved in water together with palladium chloride to make a homogeneous solution. This was dried in an oven and the product was sized and used as a starting material. The first step of a run with this material was a "regeneration" step, using reaction G, in order to obtain magnesium oxide for a first absorption step.

Figures 85 and 86 illustrate the striking results obtained with this specially prepared oxide. The performance is little short of amazing when compared with other materials, and is probably to be credited to the intimate mixture of catalyst and magnesium oxide that resulted from the wet method of preparation.

It may reasonably assumed that catalyst was present on surfaces of inner pores of the magnesium oxide particles. The higher conversion in the last cycle of Figure 86, in comparison with the last cycle of Figure 85, is to be attributed to the finer solid used in run T-183 -- minus-270 mesh in comparison with -250+270 mesh used in run T-187.

The regeneration reaction was fast in both Figures 85 and 86.

Comparison of Figure 86 with Figure 81, where no catalyst was present, dramatically illustrates the potential for using a catalyst to promote absorption of sulfur dioxide by magnesium oxide in a cyclic operation at 300 psig.

Figures 87 and 88 are zig-zag plots for runs T-181 and T-183 respectively.

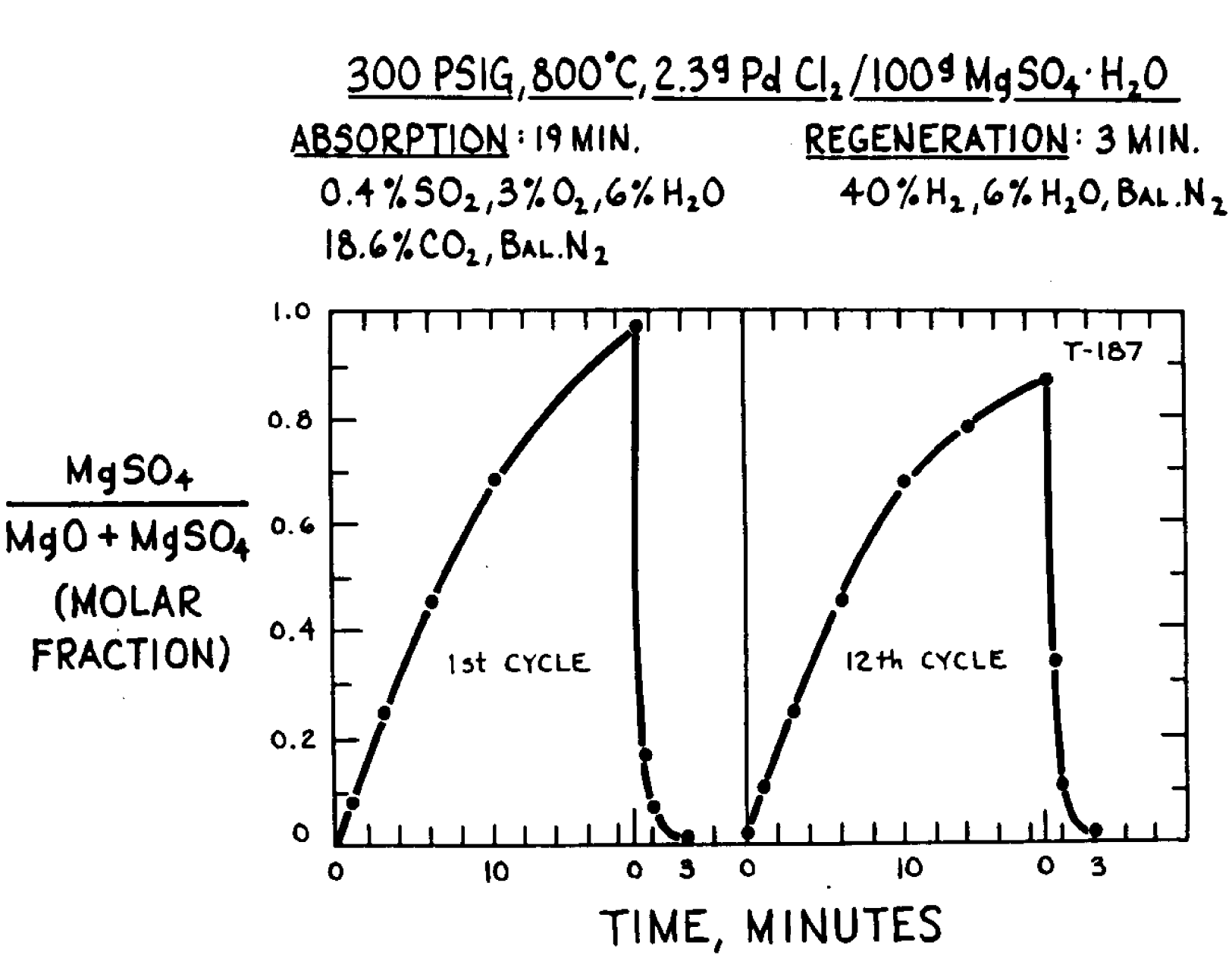

Figure 85. Cyclic rates of T-187, using magnesia from Epsom salt.

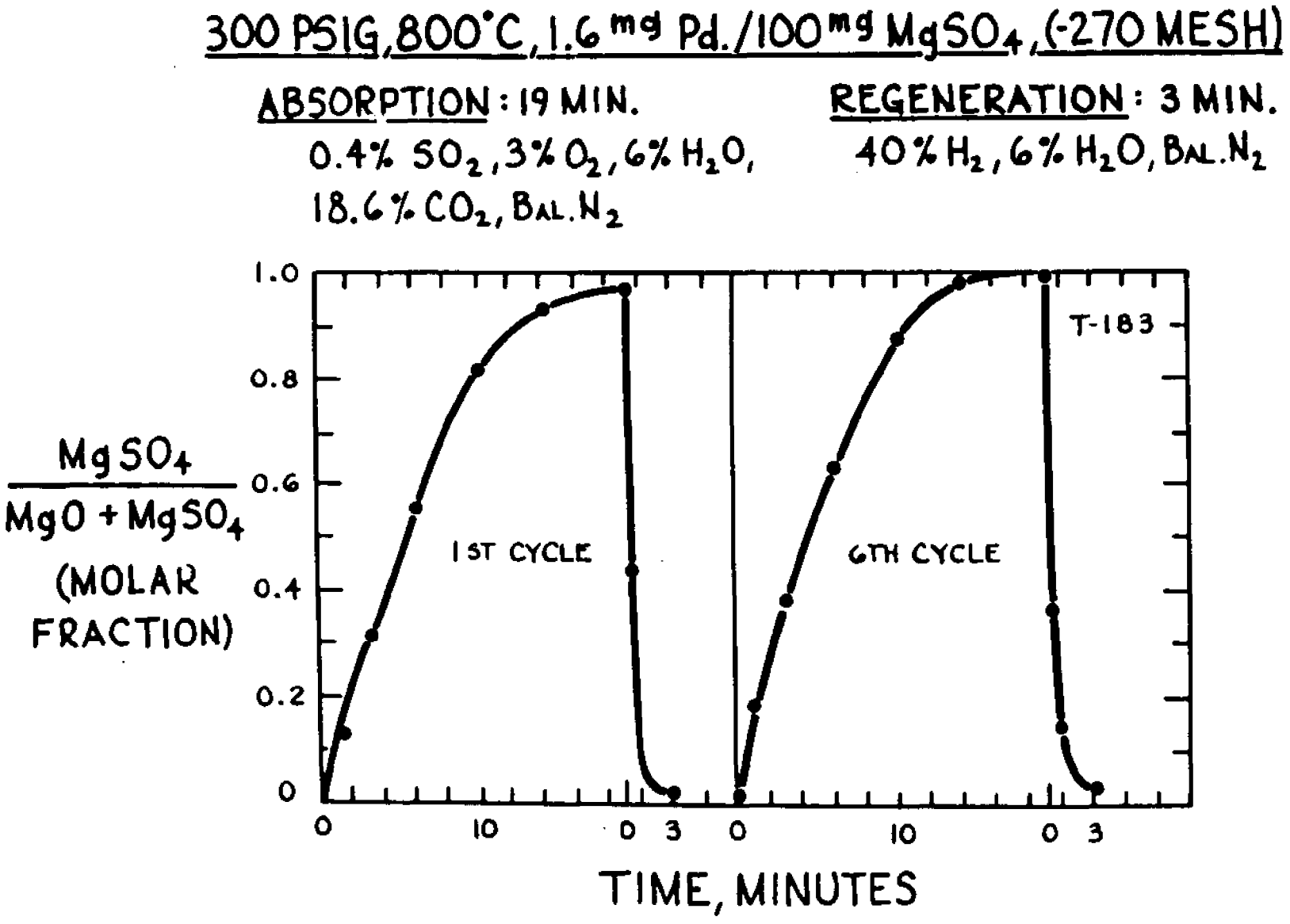

Figure 86. Cyclic rates of T-183, using magnesia from Epsom salt.

300 PSIG, 800°C, 2.317 gm $PdCl_2$ / 100 gm $MgSO_4 \cdot H_2O$

ABSORPTION: 19 MIN.

0.4% SO_2, 3% O_2, 6% H_2O,
18.6% CO_2, BAL N_2

REGENERATION: 3 MIN.

40% H_2, 6% H_2O, BAL N_2

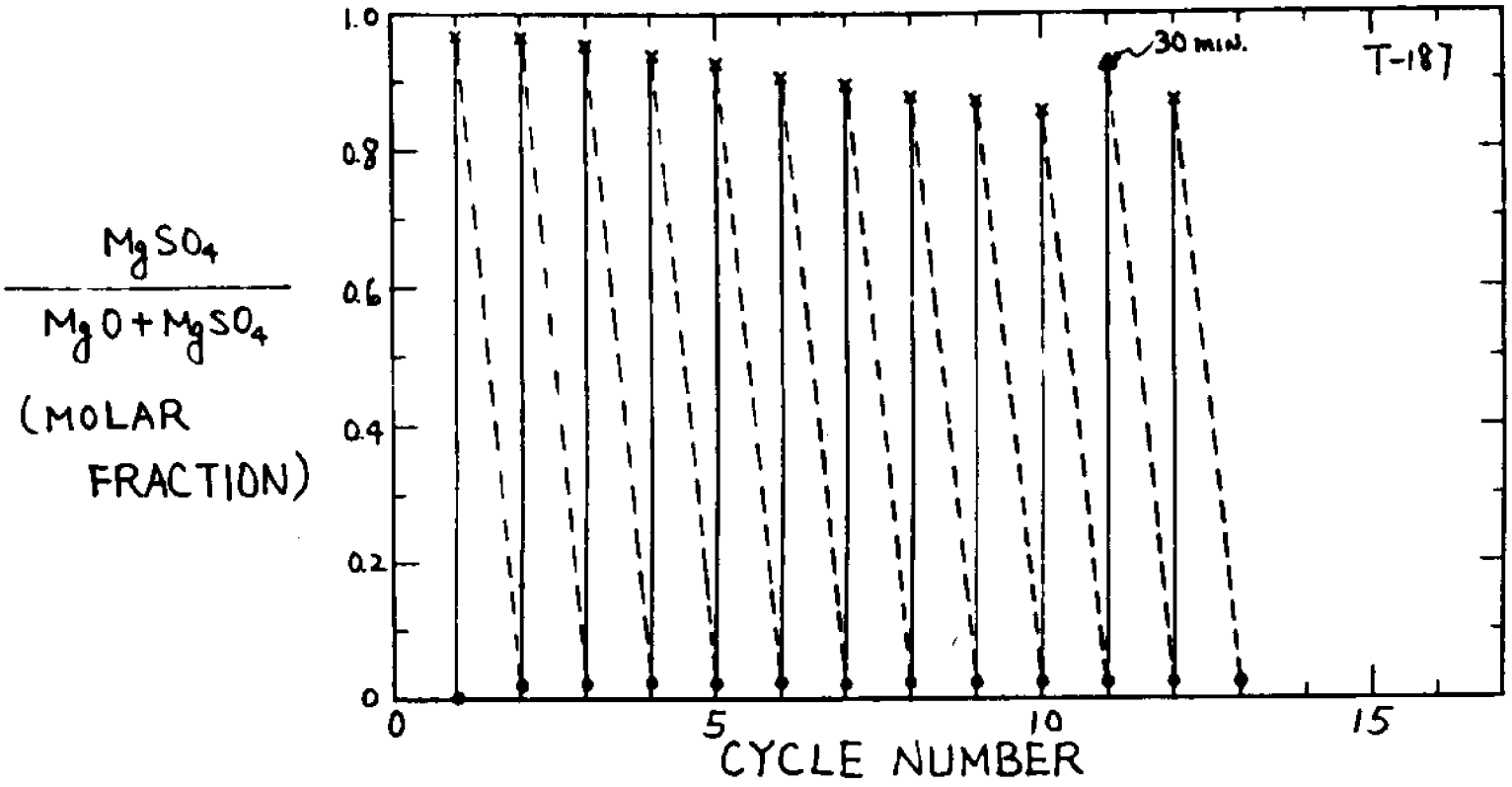

Figure 87. Zig-Zag figure of T-187.

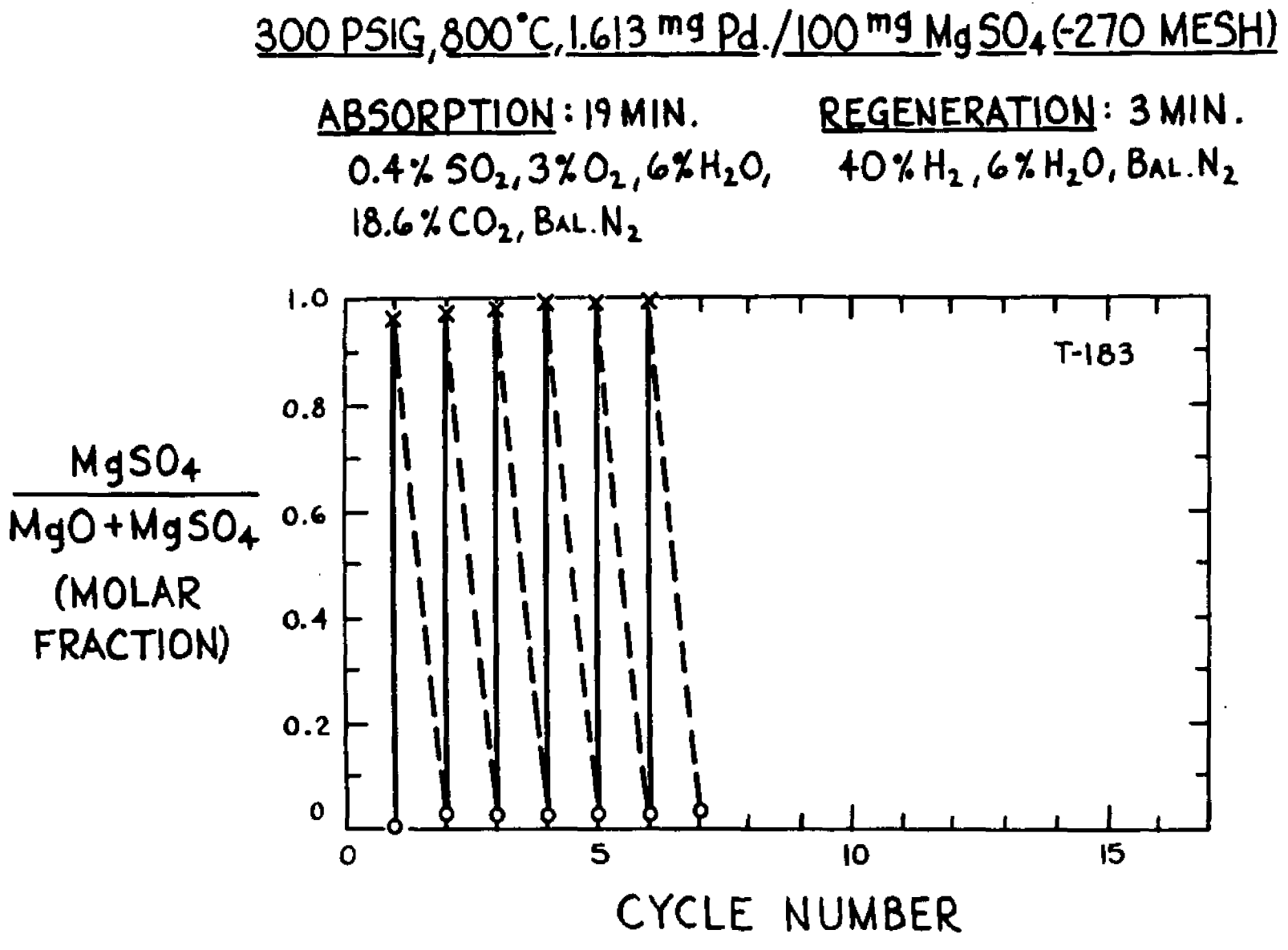

Figure 88. Zig-Zag figure of T-183.

12.04 Distinguishing between Effects of Pressure and Catalyst

Figure 69 (see Section 12.01) has shown an effect of pressure on performance of reagent grade magnesium oxide power. Since the two runs compared in Figure 69 were made with platinum pan and gauze, we felt that the rate increase might be related to a catalytic effect of platinum as well as to the change in pressure.

In order to separate these two factors, we made two runs with calcined magnesite using quartz balance pan. The first cycle rates are compared for a run at 0 psig and a run at 300 psig in Figure 89, and the effect of pressure upon rate is evident.

A further test was made using magnesite impregnated with palladium as described earlier. Figure 90 compares an atmospheric pressure and high pressure run with this solid. Again, the effect of pressure upon rate is seen.

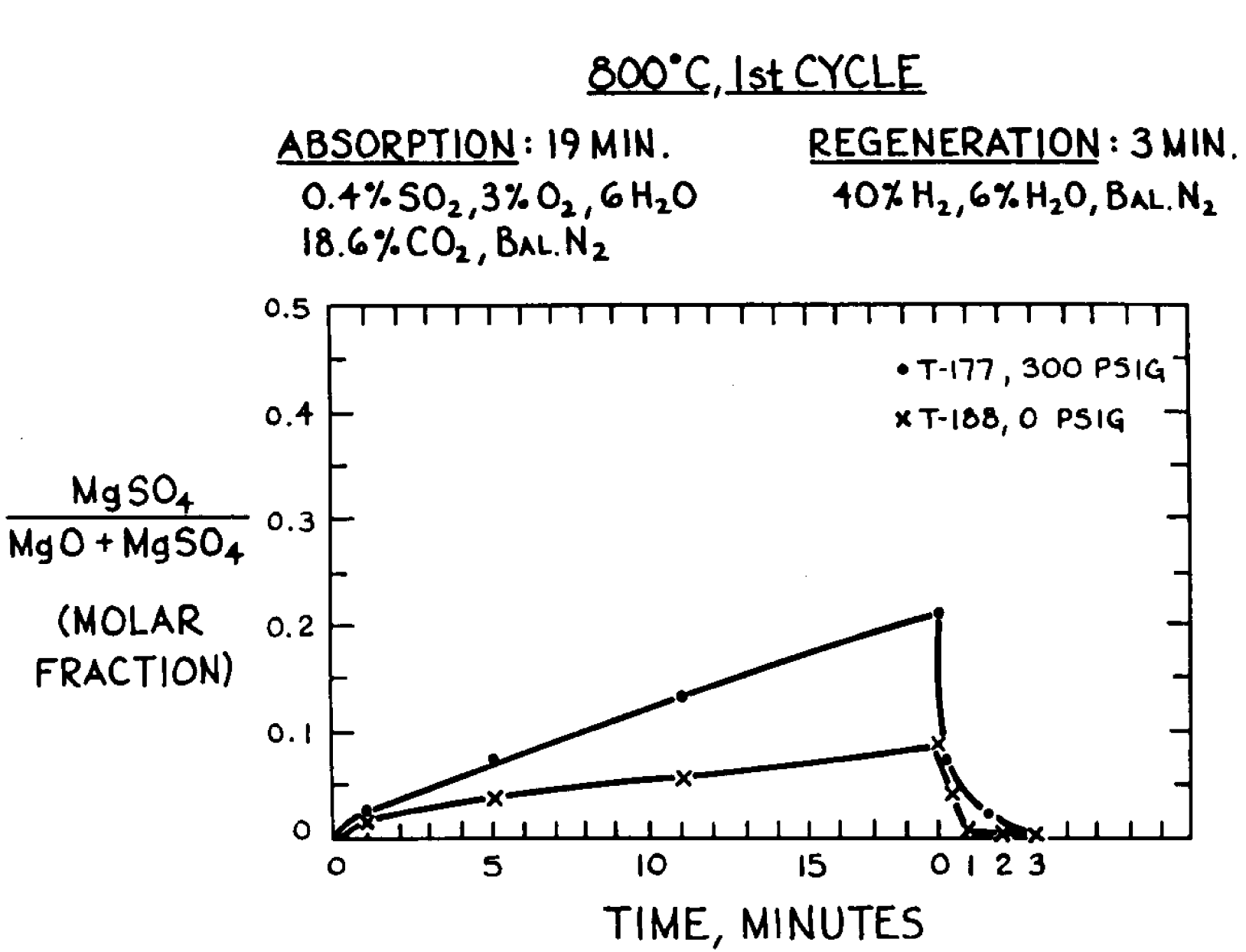

Figure 89. Effect of pressure on cyclic rates without catalyst.

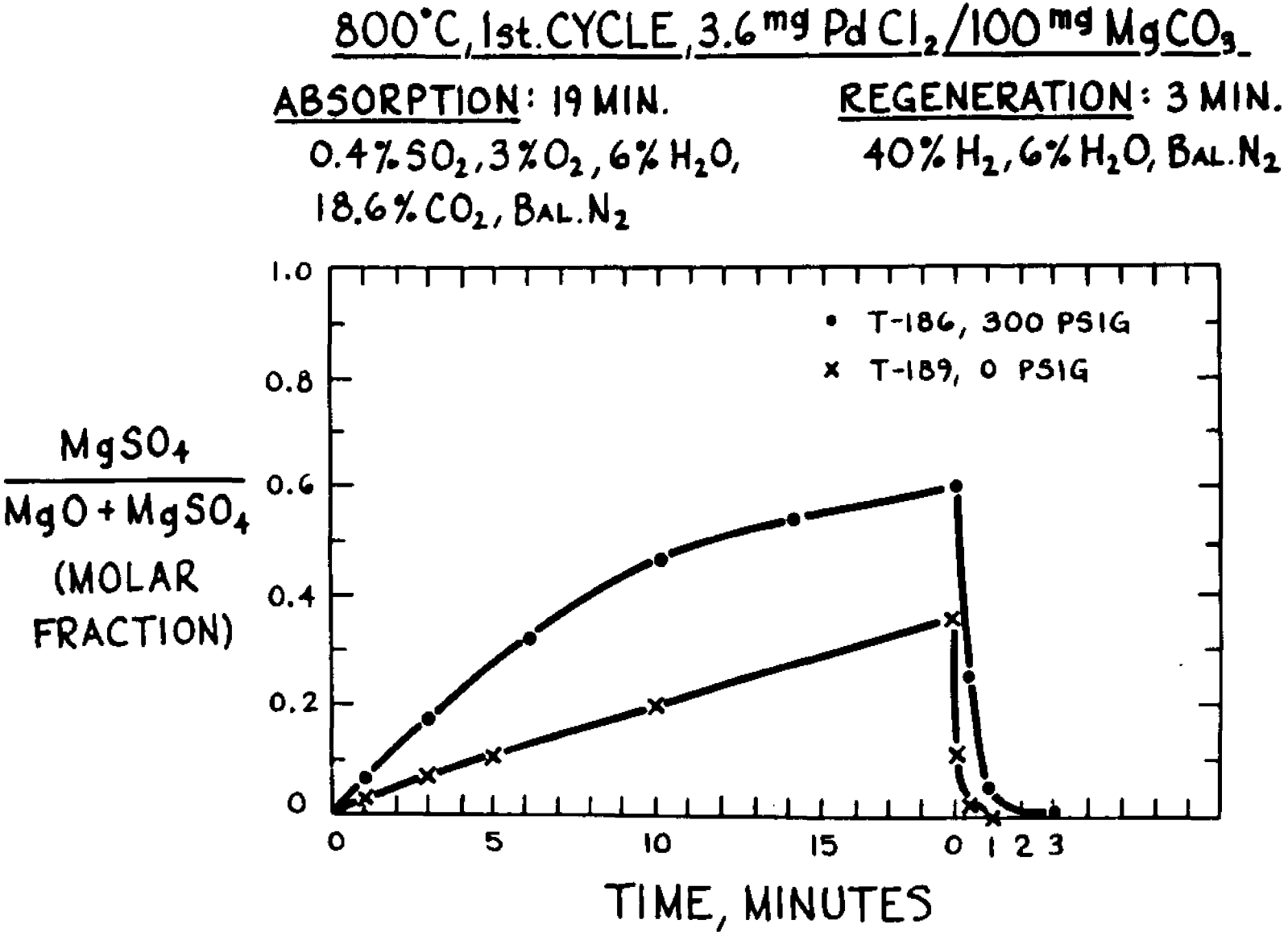

Figure 90. Effect of pressure on cyclic rates with catalyst.

12.05 Effects of Gas Composition on Absorption Step

We were not able to conduct a thorough investigation of the effect of level of each component of our gas mixture upon absorption rate. Our objective in the limited time available was to try to see if there is a "big" effect on reaction rate brought about by changing the concentration of some one gas component.

Two runs were made to study effect of nitrogen dioxide upon the rate: run T-148 was made without this constituent, and run T-162 used a gas containing nitrogen dioxide at 307 parts per million. The details of the operating conditions for these two runs, as well as for other runs discussed in this Section 12.05, are set down in Table 9. Comparison of the absorption with and without nitrogen dioxide is given in Figure 91, and it may be concluded that this constituent has no pronounced effect upon absorption rate.

Figures 92 and 93 are zig-zag plots for the runs of Figure 91.

Table 9

Runs Made to Probe Effects of Gaseous Partial Pressure on Absorption Rate - Calcined Magnesite as SO_2 Acceptor at 750°C and 300 Psig[1]

Run #	Time Min.	Capacity at Last cycle %	Gases (Bal N_2)	Time Min.	Capacity at Last cycle %	Gases (Bal N_2)
T-145	18	44 (12)[2]	.31% SO_2 9.2 % O_2 14 % CO_2 6 % H_2O	15	44	40% H_2 6% H_2O
T-148	19	10 (15)	.23% SO_2 9.2 % O_2 13 % CO_2 6 % H_2O	3	9	40% H_2 6% H_2O
T-157	19	11 (15)	.31% SO_2 1.8 % O_2 10 % CO_2 6 % H_2O	3	8	40% H_2 6% H_2O
T-159	19	10 (13)	.31% SO_2 1.8 % O_2 10 % CO_2 46 % H_2O	3	8	40% H_2 6% H_2O

Table 9 (continued)

Run #	Time Min.	Capacity at Last cycle	Gases (Bal N_2)	Time Min.	Capacity at Last cycle	Gases (Bal N_2)
T-162	19	13 (15)	.23% SO_2 7.7 % O_2 12 % CO_2 6 % H_2O 307 ppm NO_2	3	8	40% H_2 6% H_2O

1. All runs were made with platinum pan and gauze. Starting material was -250+270 mesh $MgCO_3$.
   All calcination was done with 25% H_2O, 50% CO_2 and 25% N_2 up to 750°C, except T-157 was done with 67% CO_3, 33% N_2 up to 750°C.
2. Numbers in bracket indicates last cycle number.

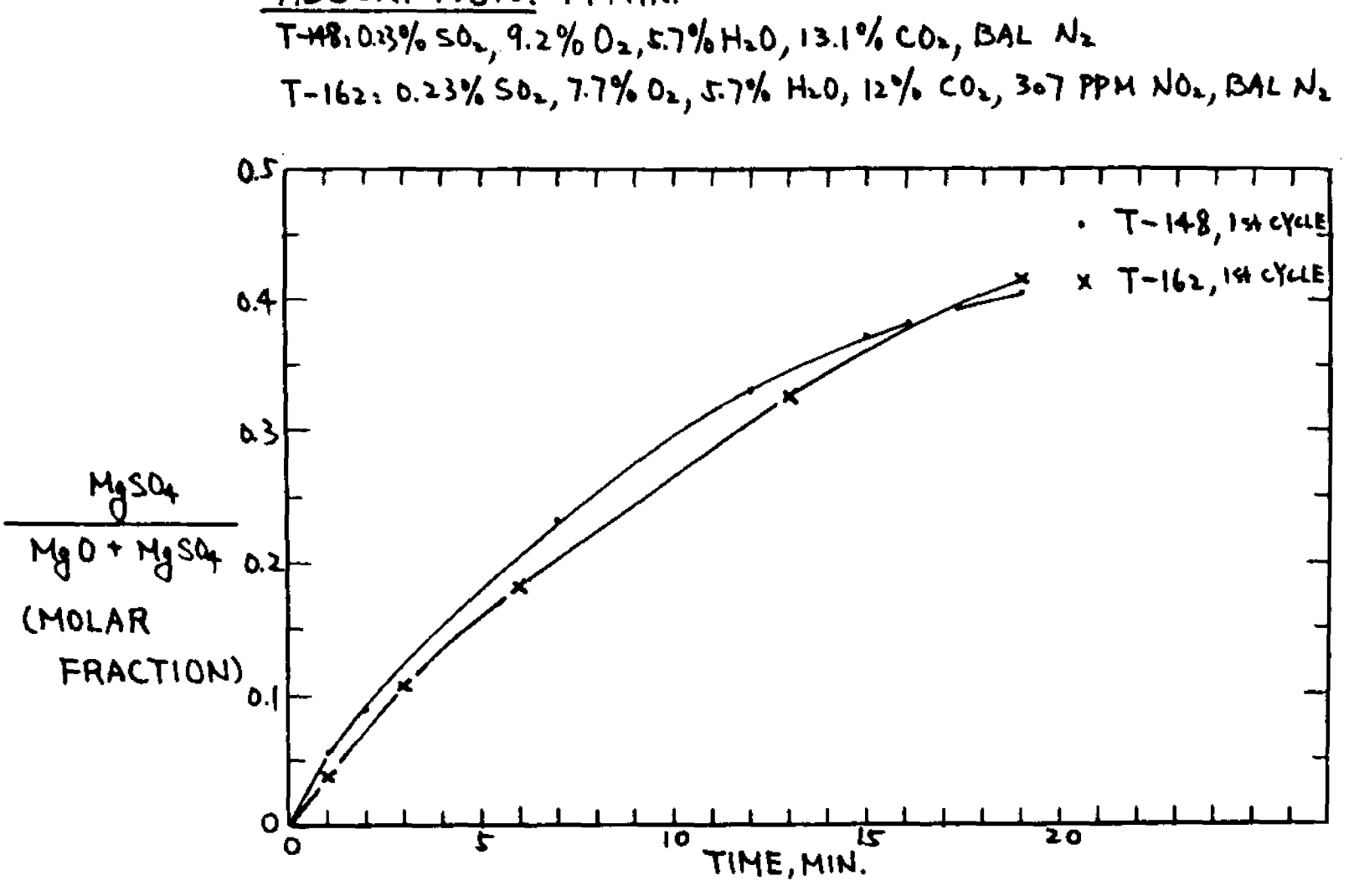

Figure 91. Effect of NO_2 on absorption rate.

300 PSIG, 750°C, Pt Pan and Gauze

ABSORPTION: 19 MINUTES — 0.23% SO_2, 9.2% O_2, 13.1% CO_2, 5.7% H_2O, Bal N_2

REGENERATION: 3 MINUTES — 40% H_2, 5.7% H_2O, Bal N_2

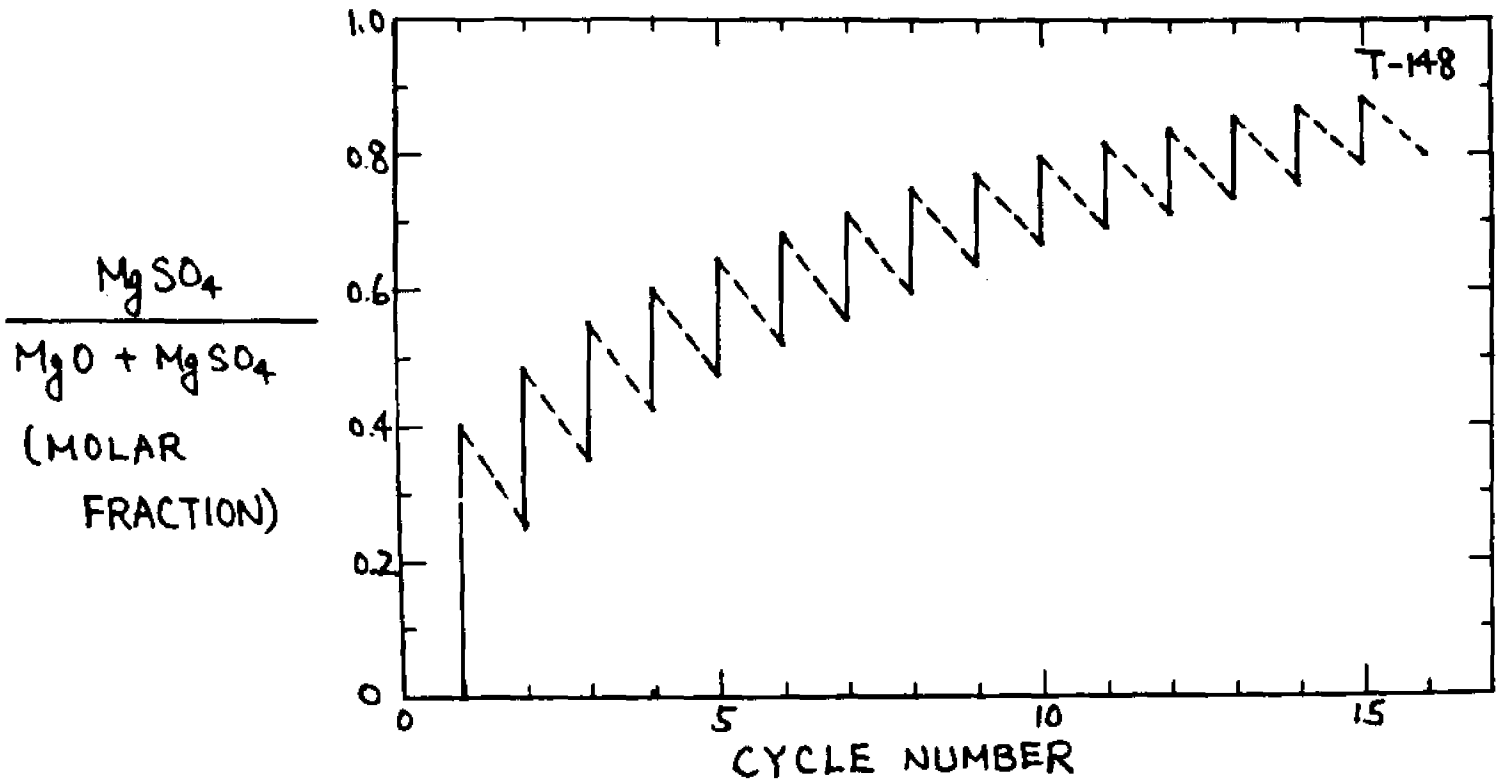

Figure 92. Zig-Zag figure of T-148.

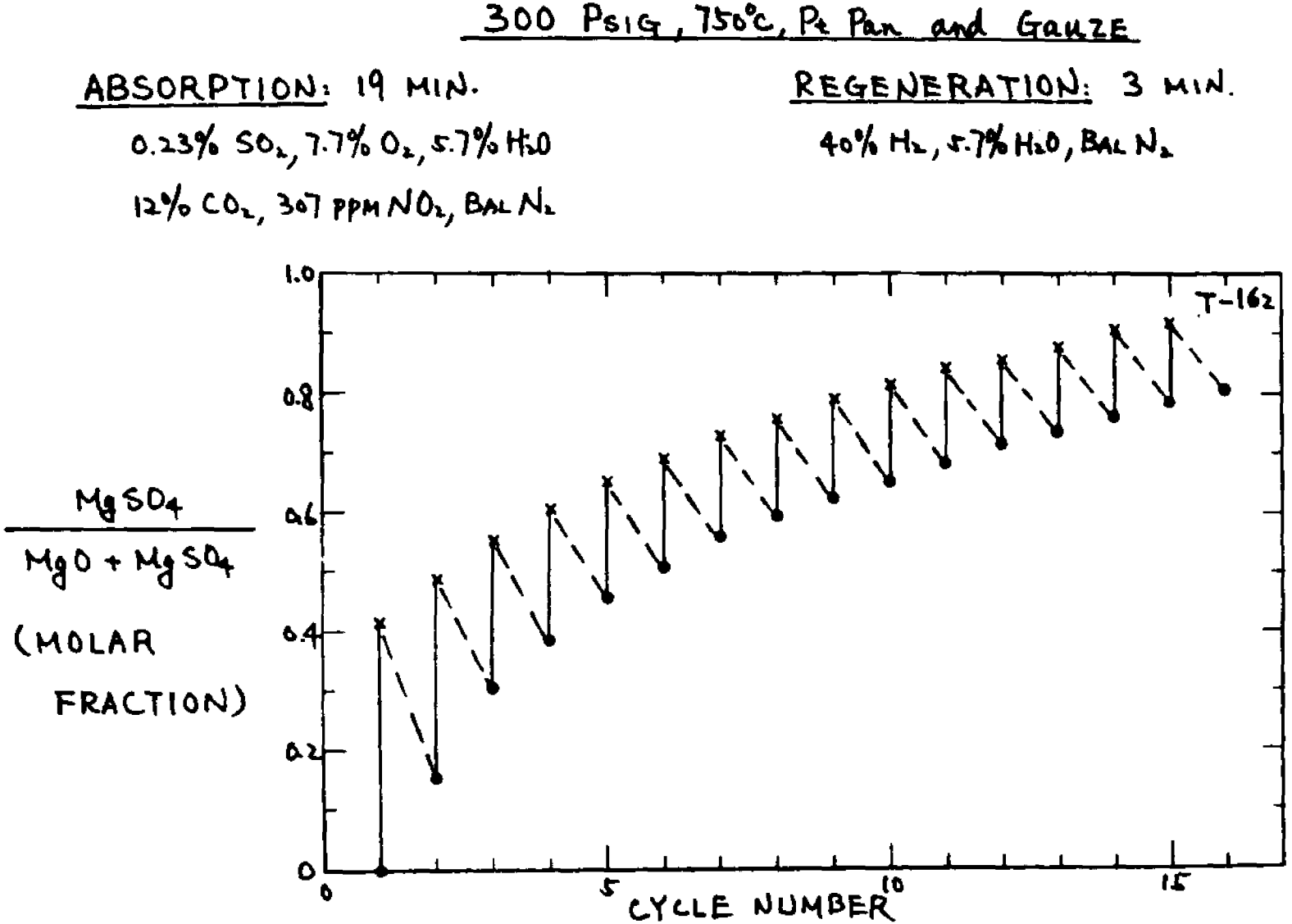

Figure 93. Zig-Zag figure of T-162.

To explore a possible effect of steam, runs T-157 and T-159 were made using 6% and 46% steam respectively. First cycle absorption rates are plotted in Figure 94. We may, cautiously, conclude that steam has a small enhancing effect upon rate, but more work would be needed to establish the effect and define it accurately. Figures 95 and 96 are zig-zag plots for the runs of Figure 94.

Runs T-145 and T-157 were made with 9.2% and 1.8% oxygen respectively. Figure 97 shows that this five-fold change in oxygen concentration seems to have only a small accelerating effect upon the absorption step. This range of oxygen level covers substantially any range that might be encountered in practicable fluidized-bed combustion. Figures 95 and 98 are zig-zag plots for the runs of Figure 97.

Runs T-148 and T-145 were made using 0.23% and 0.31% sulfur dioxide respectively. Figure 99 reveals that variation in level of sulfur dioxide over this range has, surprisingly, little effect upon absorption rate at 300 psig total pressure.

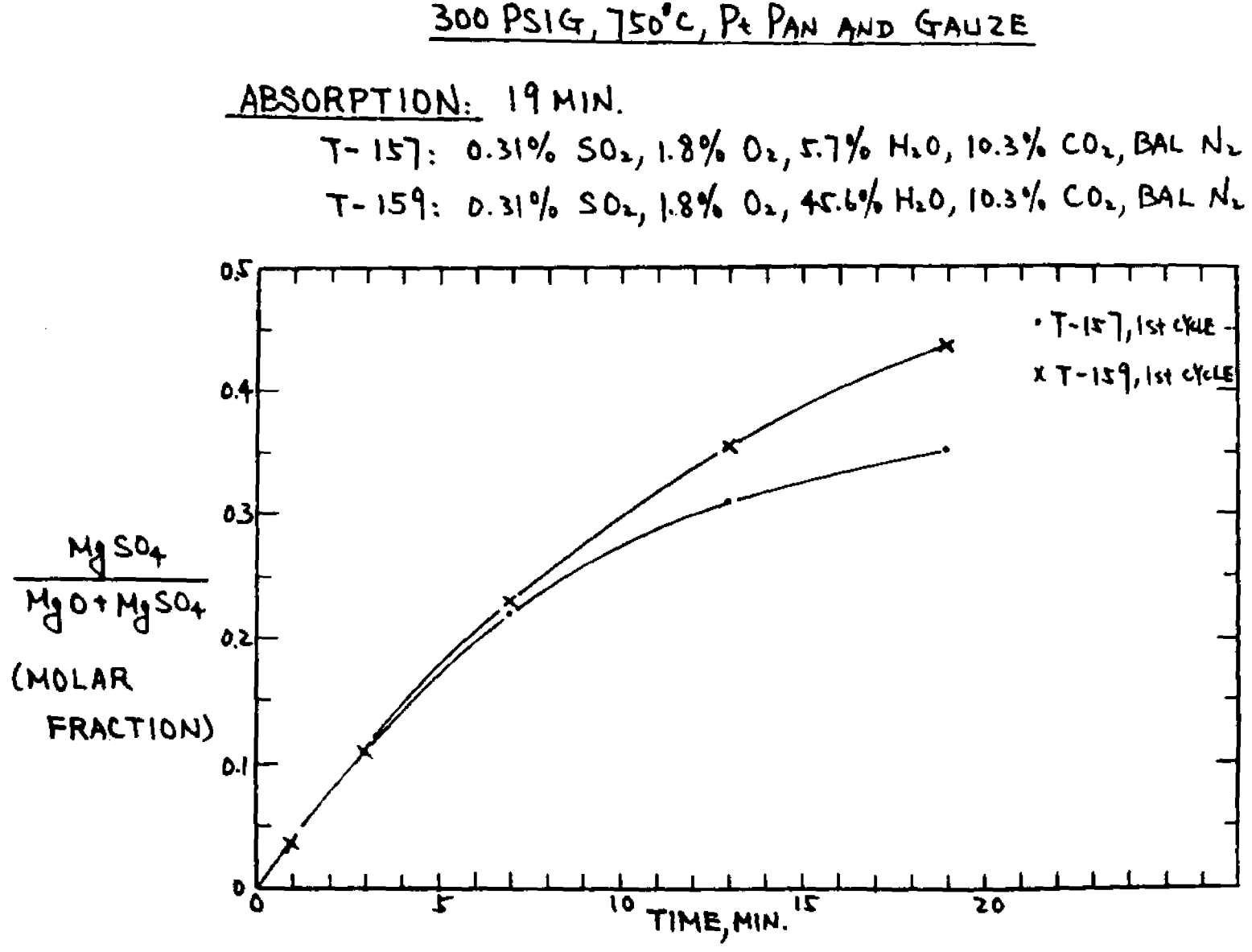

Figure 94. Effect of H_2O on absorption rate.

300 PSIG, 750°C, Pt Pan and Gauze

ABSORPTION: 19 MIN.

0.31% SO_2, 1.8% O_2, 5.7% H_2O

10.3% CO_2, BAL N_2

REGENERATION: 3 MIN.

40% H_2, 5.7% H_2O

BAL N_2

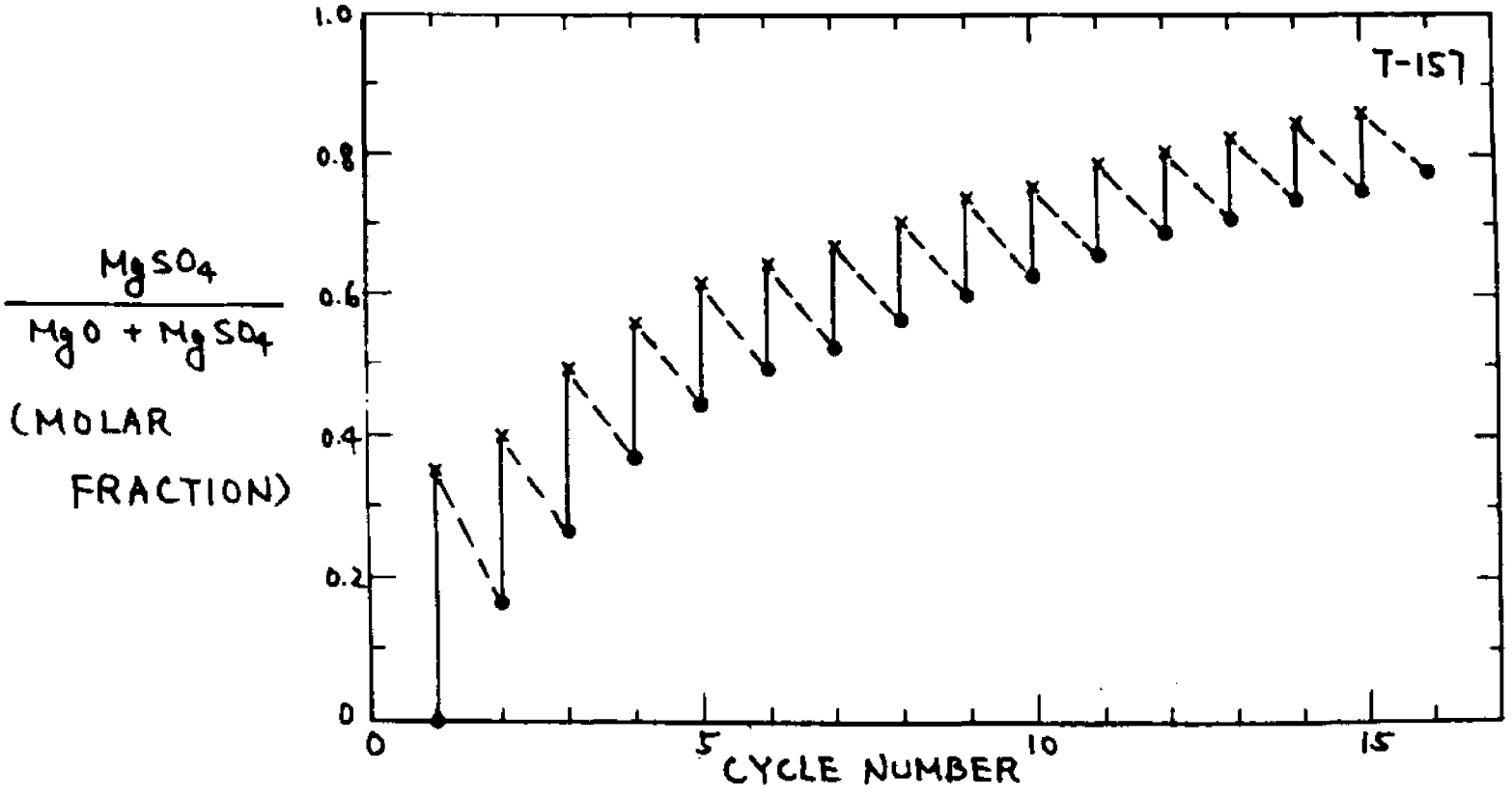

Figure 95. Zig-Zag figure of T-157.

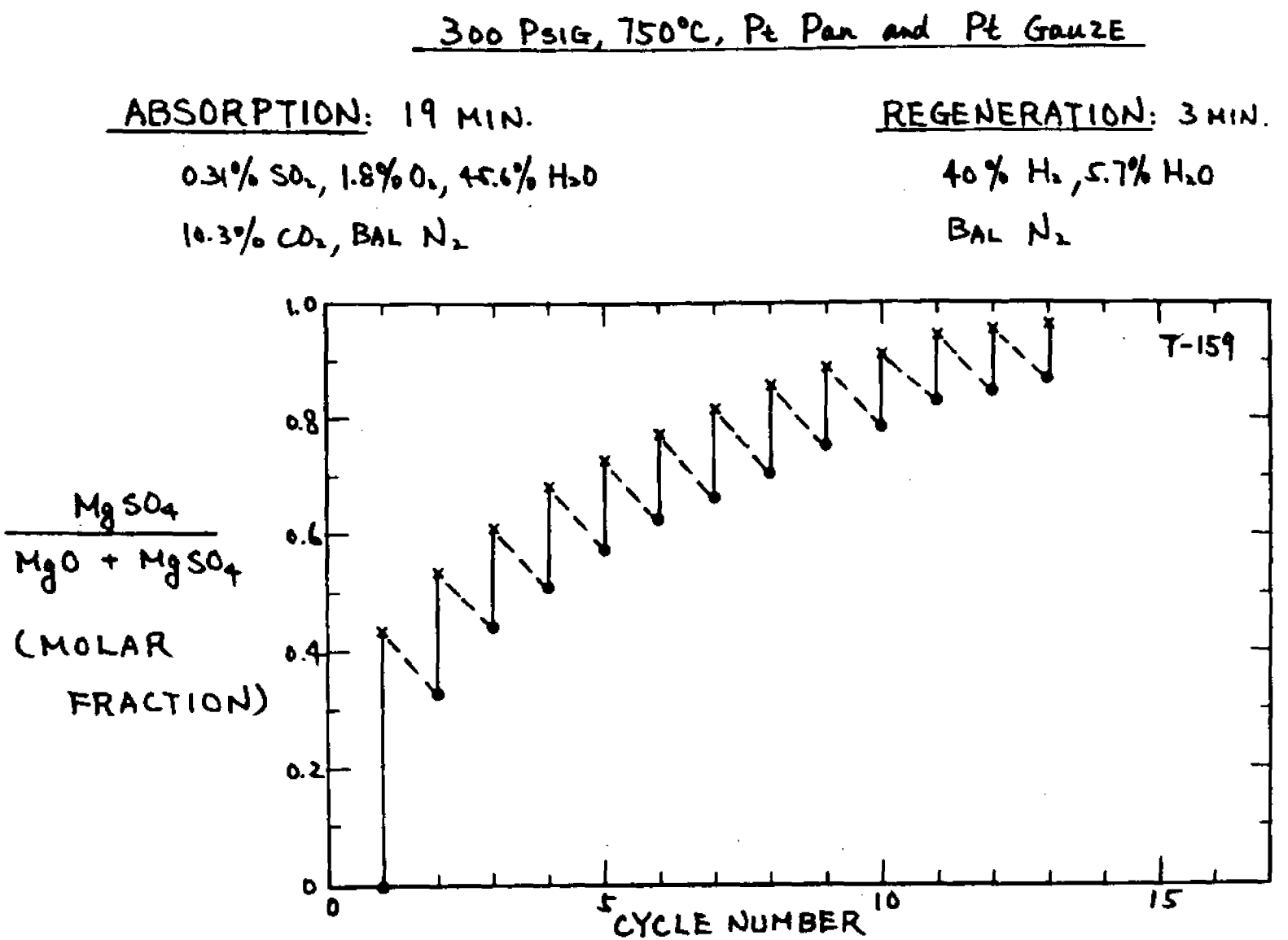

Figure 96. Zig-Zag figure of T-159.

300 PSIG, 750°C, Pt Pan and Pt Gauze

ABSORPTION: 19 MIN, 1st CYCLE

T-145: 0.31% SO_2, 9.2% O_2, 5.7% H_2O, 14.4% CO_2, BAL N_2

T-157: 0.31% SO_2, 1.8% O_2, 5.7% H_2O, 10.3% CO_2, BAL N_2

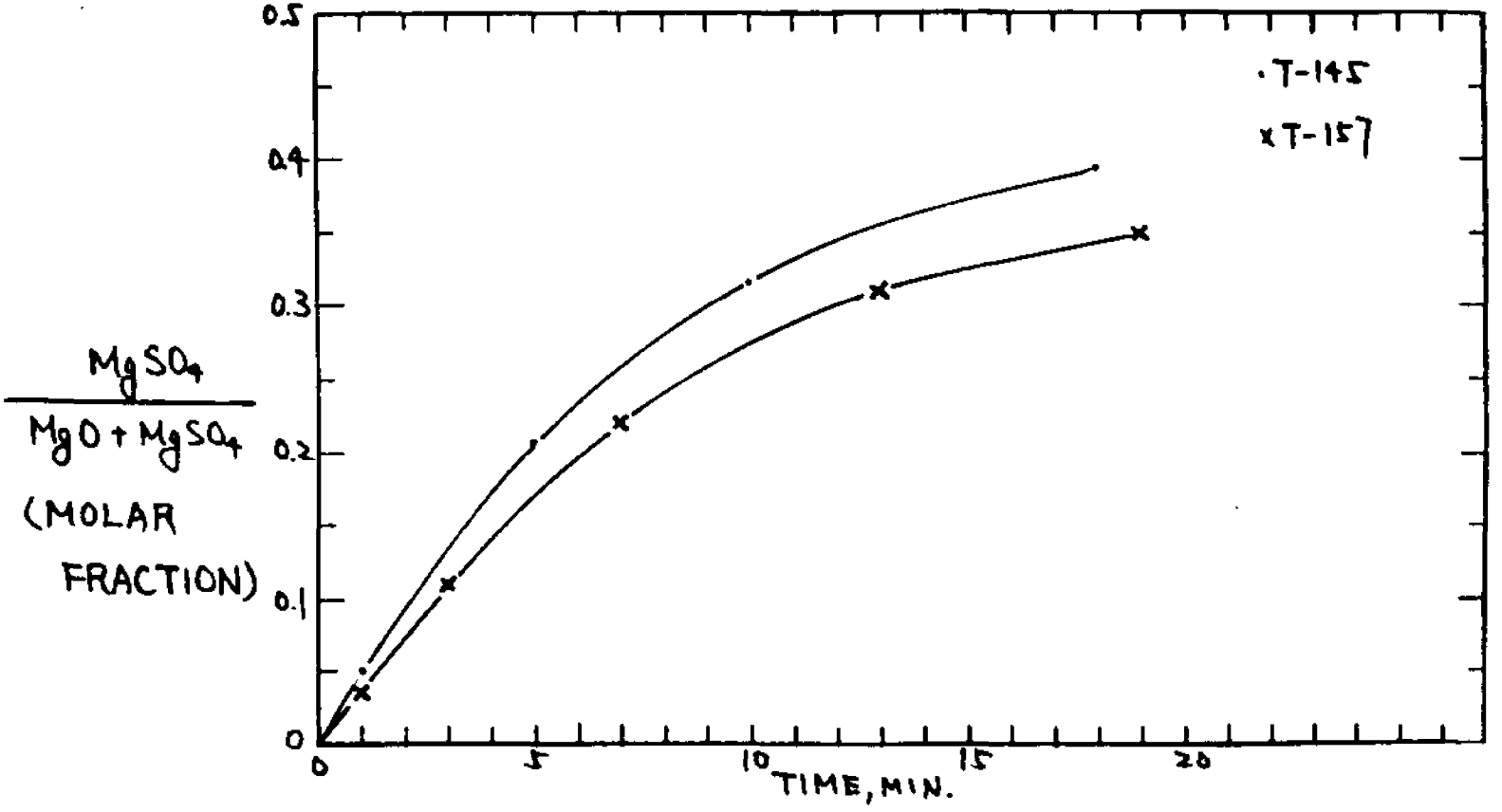

Figure 97. Effect of O_2 on absorption rate.

300 PSIG, 750°C, Pt Pan, Pt Gauze

ABSORPTION: 18 MINUTES
0.31% SO_2, 9.2% O_2, 14.4% CO_2, 5.7% H_2O, Bal N_2

REGENERATION: 15 MINUTES
4.0% H_2, 5.7% H_2O, Bal N_2

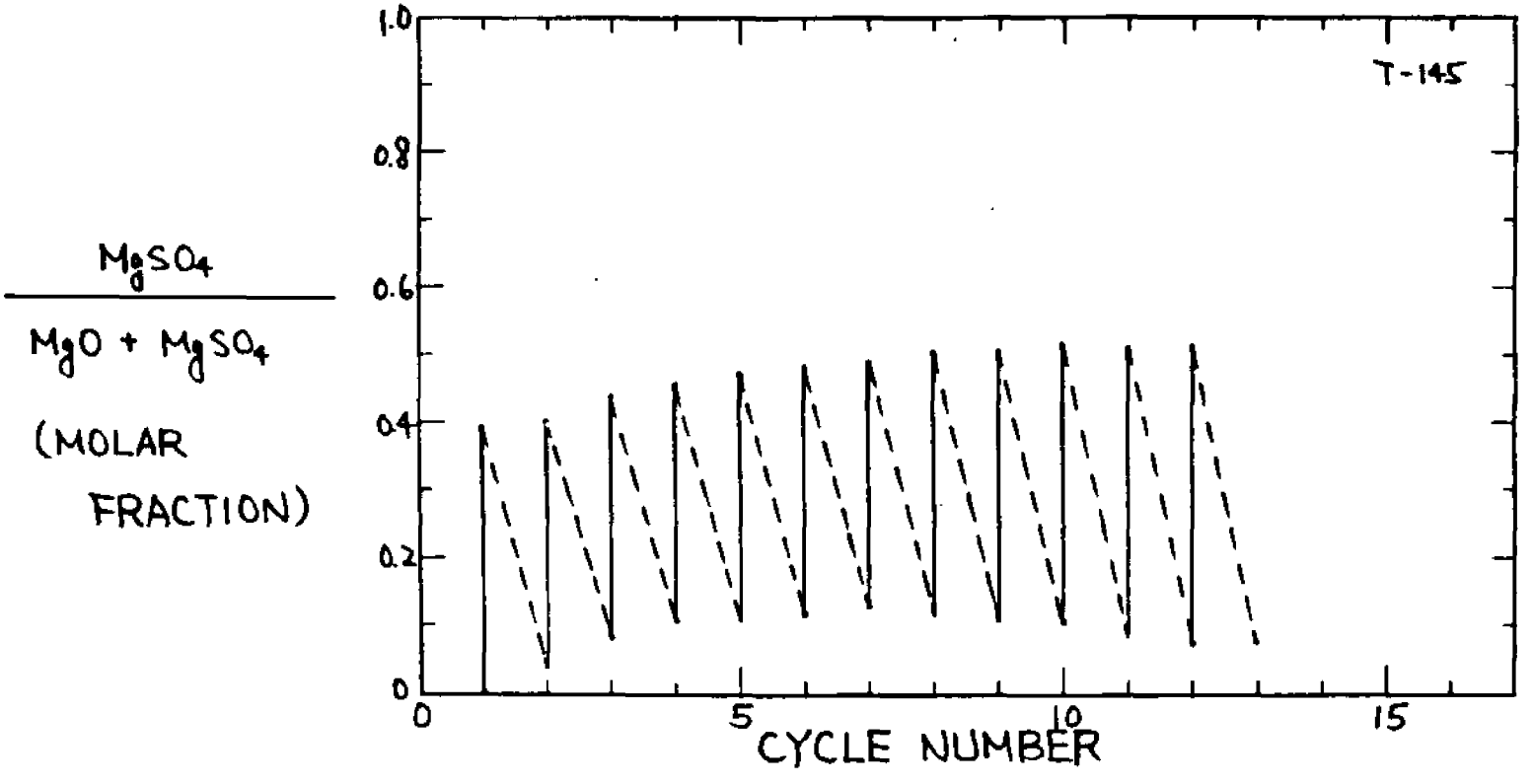

Figure 98. Zig-Zag figure of T-145.

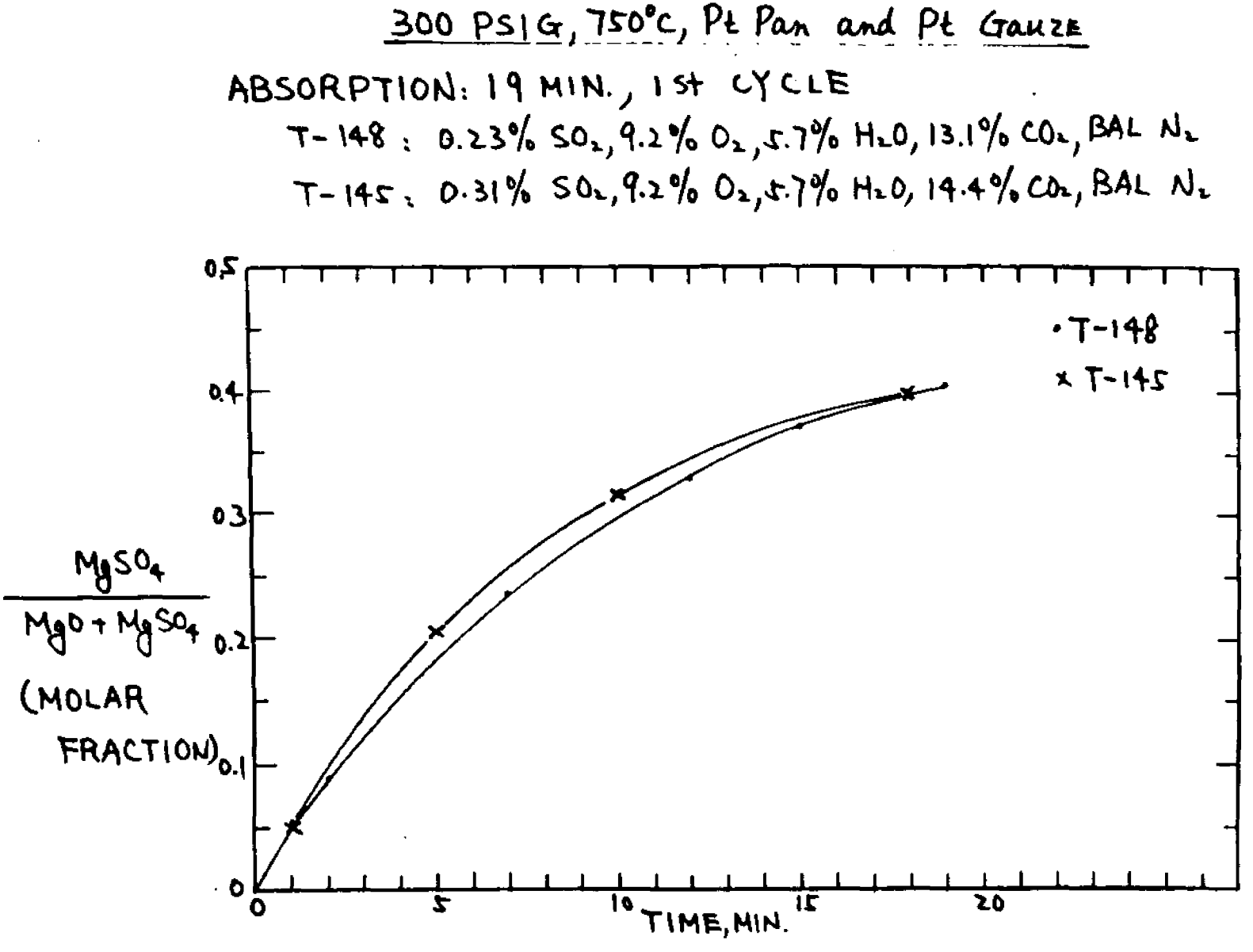

Figure 99. Effect of SO_2 on absorption rate.

12.06 Effects of Gas Composition on Regeneration Step

As in work reported in Section 12.05 above, work to look for effects of gas composition upon the regeneration step also pointed toward finding existence of "big" effects of change in one constituent.

In run T-165, the hydrogen that we ordinarily used in the regeneration gas was replaced with carbon monoxide for the eighth cycle. Table 10 gives details of the operating conditions for this run and for other runs discussed in this Section 12.06.

Figure 100 shows the course of regeneration in the 7th and 8th cycles of run T-165, with hydrogen and carbon monoxide respectively. Regeneration by the latter gas seemed to be more effective.

Figure 100 also compares the sixth cycle of run T-177, which used hydrogen, with the first cycle of run T-179, which used carbon monoxide. The purpose of selecting these particular cycles for the respective runs was to obtain a comparison starting from approximately the same level of $MgSO_4$ in the solid, about 13%. The comparison again indicates carbon monoxide to be slightly better as a regeneration gas. Indeed, what is not possible to show in the figure, carbon monoxide in run T-179 accomplished 80% of the regeneration finally achieved in just six seconds. Figure 101 is a zig-zag plot for run T-179.

Table 10

Runs Made to Probe Effects of Gaseous Partial Pressure on Regeneration Rate for Calcined Magnesite as SO_2 Acceptor at 300 Psig[1]

	Absorption		Regeneration	
Run #	Final Capacity %	Gases, %, Bal N_2 $SO_2/O_2/H_2O/CO_2$	Capacity %	Gases, %, Bal N_2 H_2/H_2O
T-145	44 (12)[2]	.31/9.2/ 5.7/14	44	40 / 5.7
T-148	10 (15)	.23/9.2/ 5.7/13	9	40 / 5.7
T-154	11 (15)	same as above	9	11.4/ 5.7
T-155	11 (9)	same as above	8	11.4/45.6
T-157	11 (15)	.31/1.8/ 5.7/10	8	40 / 5.7
T-159	10 (13)	.31/1.8/46 /10	8	40 / 5.7
T-161	11 (20)	.31/1.8/ 5.7/10	11	40 / 0
T-162	13 (15)	.23/7.7/ 5.7/12 307ppm NO_2	11	40 / 5.7
T-165	20 (5)	.18/6 / 4.5/ 9.4 242ppm NO_2	16	31.5% CO 4.5% H_2O

Table 10 (continued)

	Absorption		Regeneration	
Run #	Final Capacity %	Gases, %, Bal N_2 $SO_2/O_2/H_2O/CO_2$	Capacity %	Gases, %, Bal N_2 H_2/H_2O
T-177	14 (6)	.4 /3 / 6 /19	13	40 / 6
T-179	9 (6)	same as above	9	40% CO 6% H_2O

1. All calcinations were done with 25% H_2O, 50% CO_2, 25% N_2 up to 750°C, except T-165, T-177, T-179 up to 800°C. T-157 was done with 67% CO_2 and 33% N_2 up to 750°C.
   All runs were made with platinum pan and gauze except Runs T-165, T-177 and T-179 with quartz pan.
   T-165, T-177, T-179 were made at 800°C; other runs were made at 750°C.
   T-145 has 18 minutes absorption time and 15 minutes regeneration time; other runs have 19 minutes for absorption and 3 minutes for regeneration.
2. Numbers in bracket indicate last cycle number.

300 PSIG, 800°C

REGENERATION:

T-165 : 7th CYCLE, 32% H_2, 4.5% H_2O, BAL N_2

T-165 : 8th CYCLE, 32% CO, 4.5% H_2O, BAL N_2

T-177 : 6th CYCLE, 40% H_2, 6% H_2O, BAL N_2

T-179 : 1st CYCLE, 40% CO
6% H_2O, Bal N_2

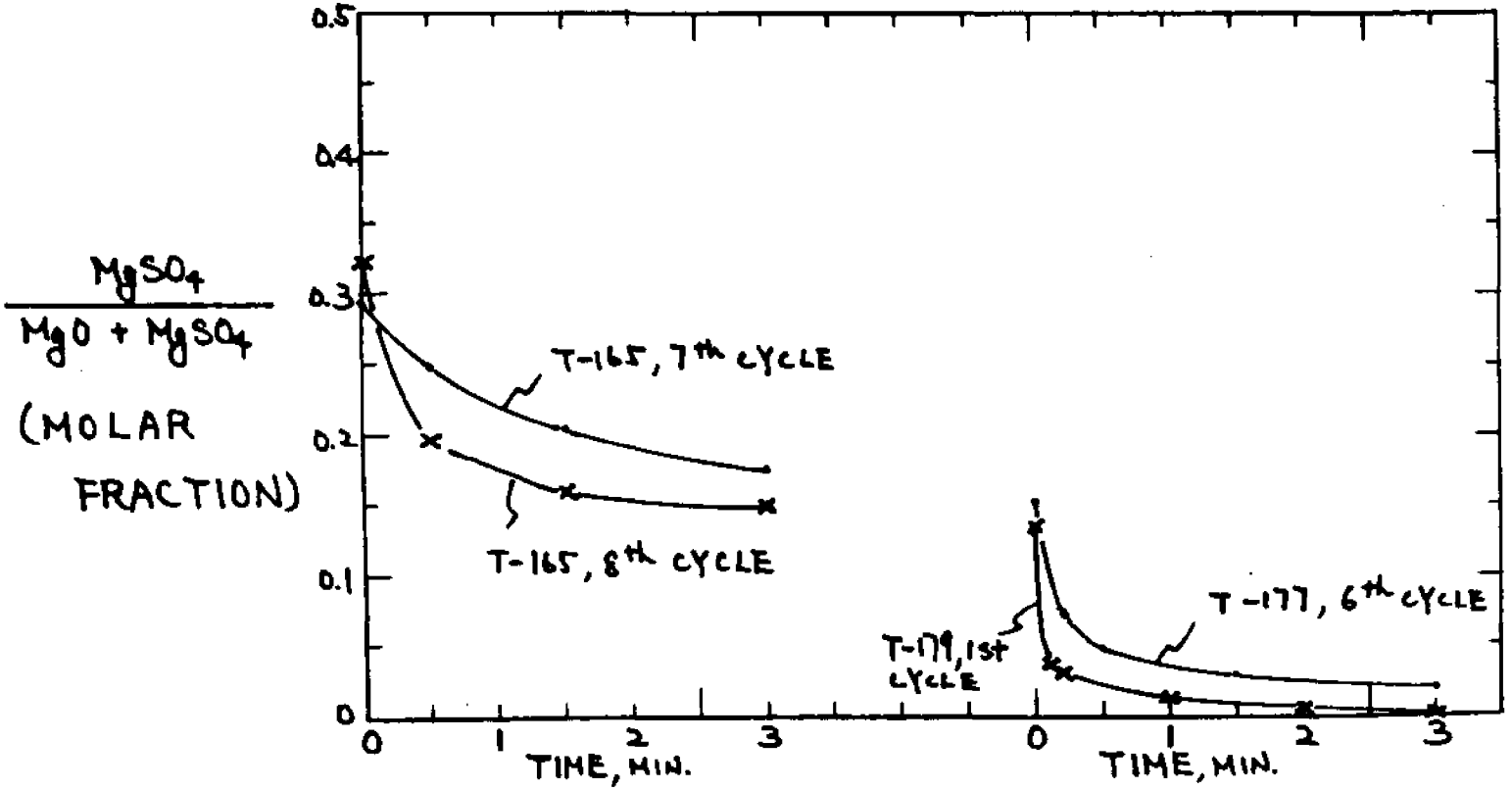

Figure 100. Effect of CO on regeneration rate.

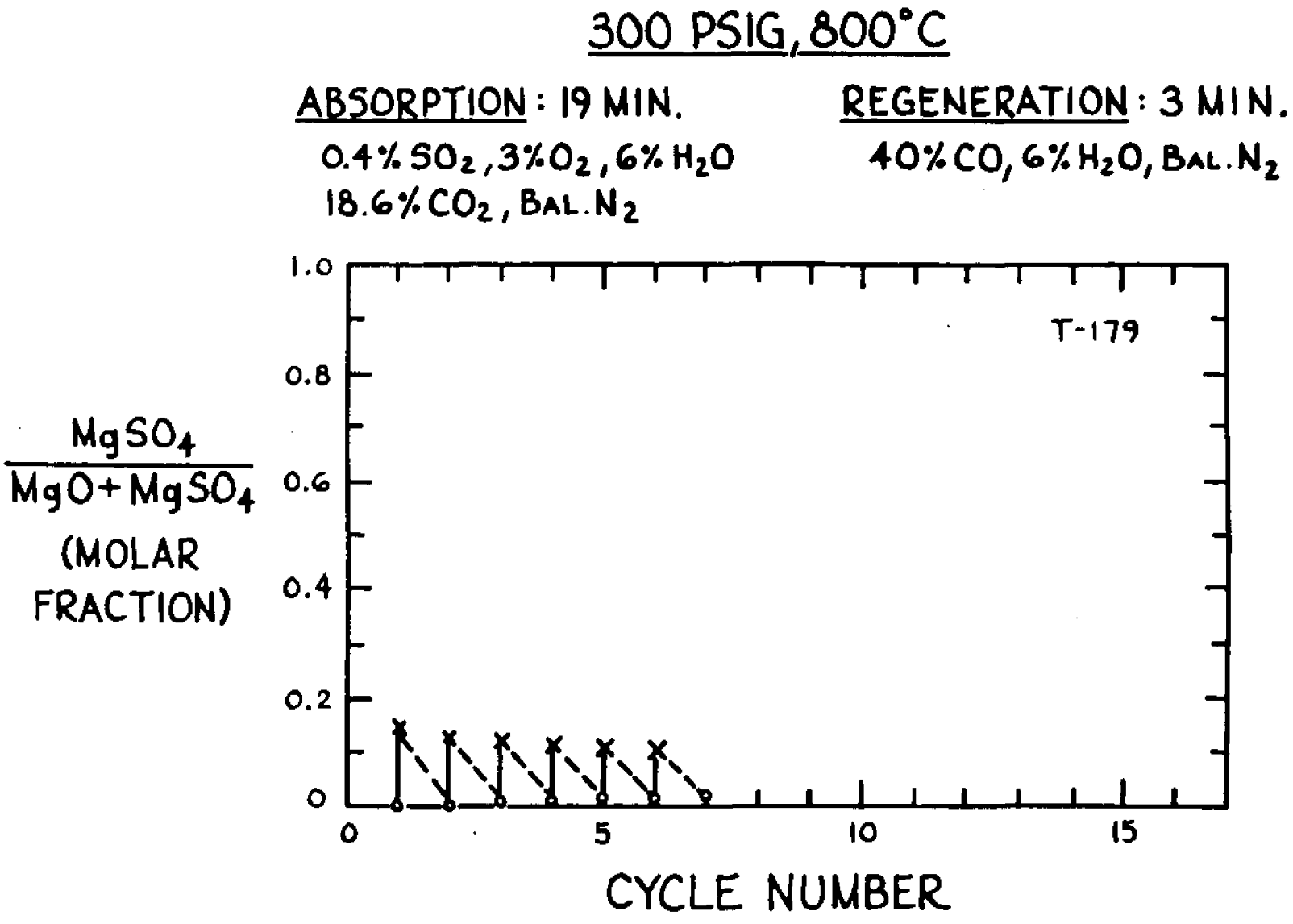

Figure 101. Zig-Zag figure of T-179.

Figure 102 gives data from two runs indicating the change in hydrogen concentration from 11% to 40% has relatively little effect upon regeneration rate. Figure 103 is a zig-zag plot for run T-154.

Figure 104 gives data from four runs in which steam was varied from nil to 46%. Although not too conclusive, it appears that steam has a somewhat inhibiting effect upon the regeneration reaction, perhaps because steam is a product of the reaction.

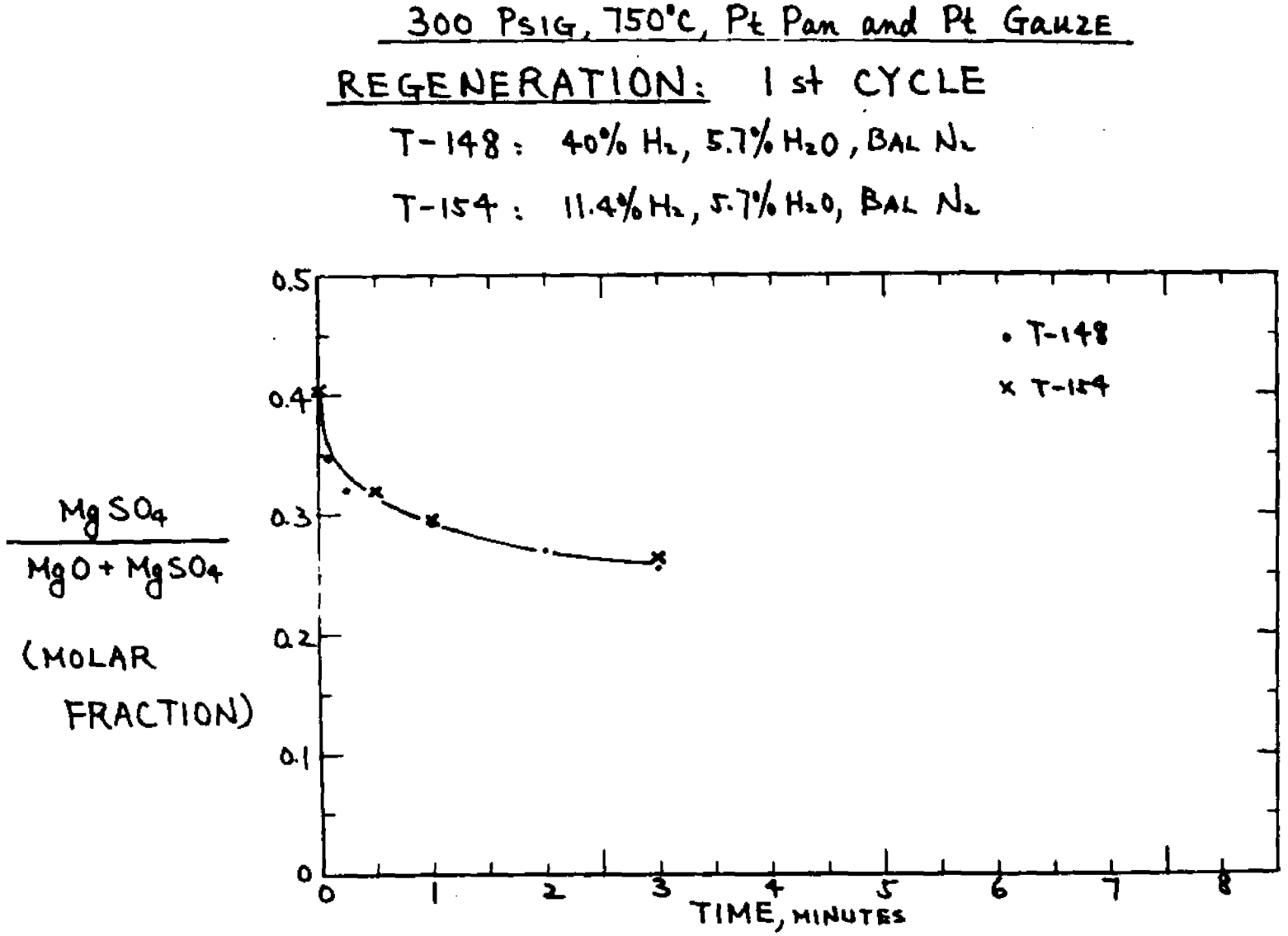

Figure 102. Effect of H_2 on regeneration rate.

300 PSIG, 750°C, Pt Pan and Pt Gauze

ABSORPTION: 19 MINUTES

0.23% SO_2, 9.2% O_2, 5.7% H_2O

13.1% CO_2, BAL N_2

REGENERATION: 3 MIN.

11.4% H_2, 5.7% H_2O, BAL N_2

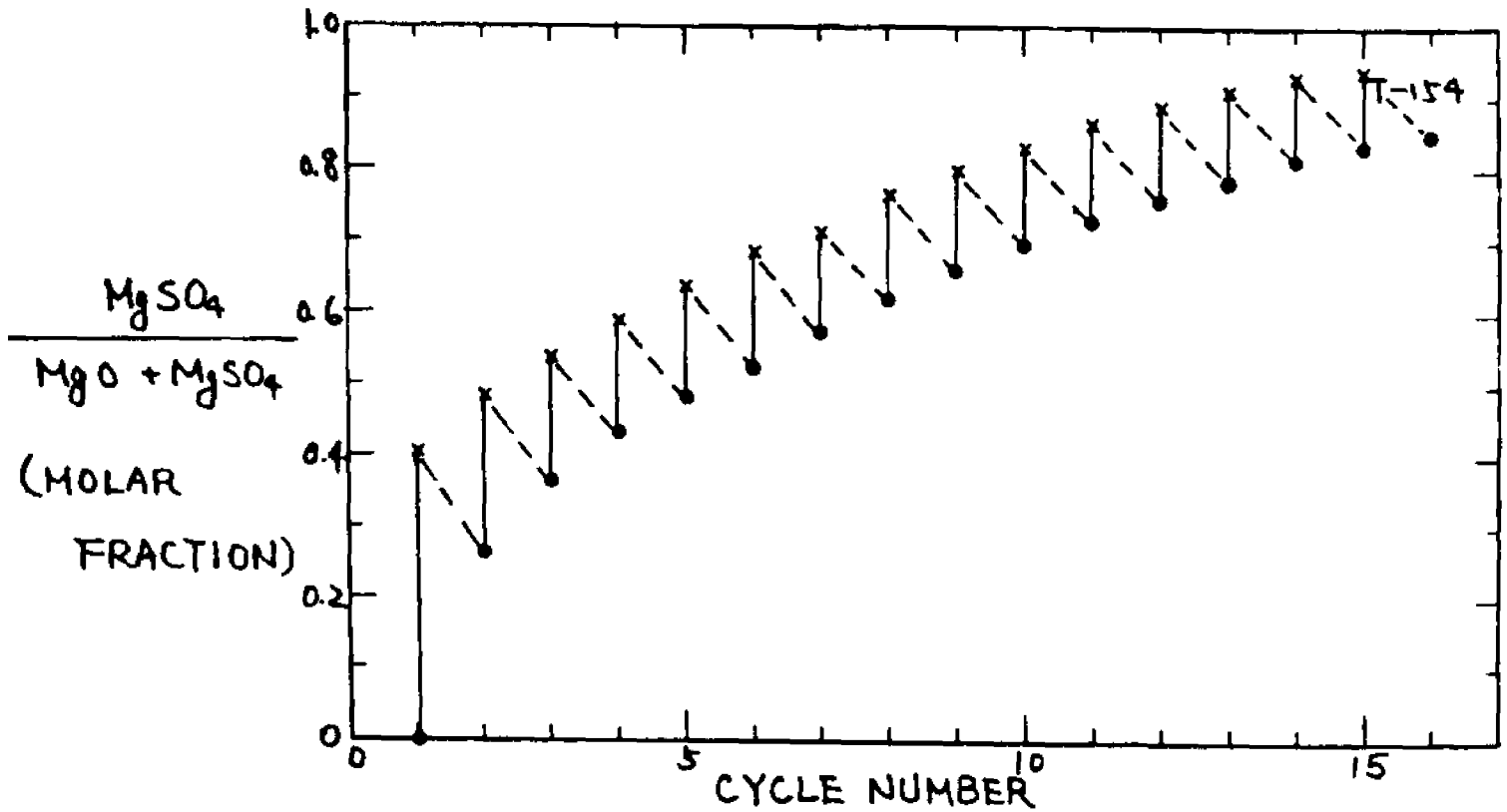

Figure 103. Zig-Zag figure of T-154.

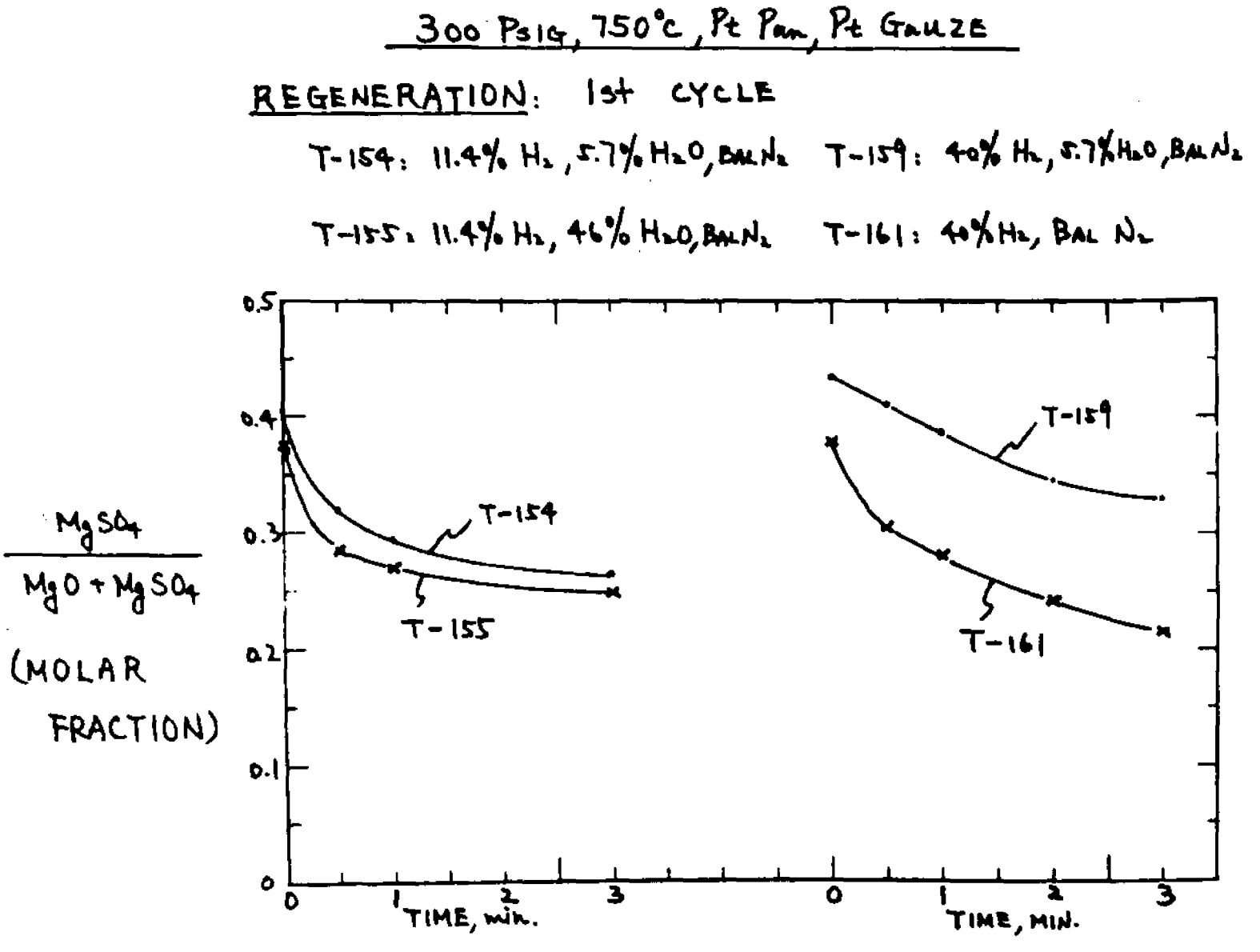

Figure 104. Effect of H_2O on regeneration rate.

12.07 Effects of Temperature on Absorption

To determine effects of temperature expeditiously, advantage was taken of the fact that regeneration at 900°C seems always essentially to go to completion. To study effect of temperature on the absorption step, therefore, it was only necessary to vary the temperature during this step in several cycles of a given run, while keeping the regeneration temperature fixed at 900°C. We appreciate that a more careful study might conduct a series of runs with constant conditions through the cycles of each individual run, but the time available recommended to us the shorter procedure, which ought to reveal at least the gross effects of temperature.

Run T-165 was conducted under constant temperature conditions (800°C absorption and 900°C regeneration) for 10 cycles in order to reach stable conditions. The run used a quartz pan and no catalyst. The effect of temperature upon absorption was explored in the eleventh through fifteenth cycles to obtain the results plotted in Figure 105. The data appear to show a slight deactivation trend from 900°C down to 650°C for the absorption. The remarkable reproducibility of the five regeneration cycles can be seen from the figure.

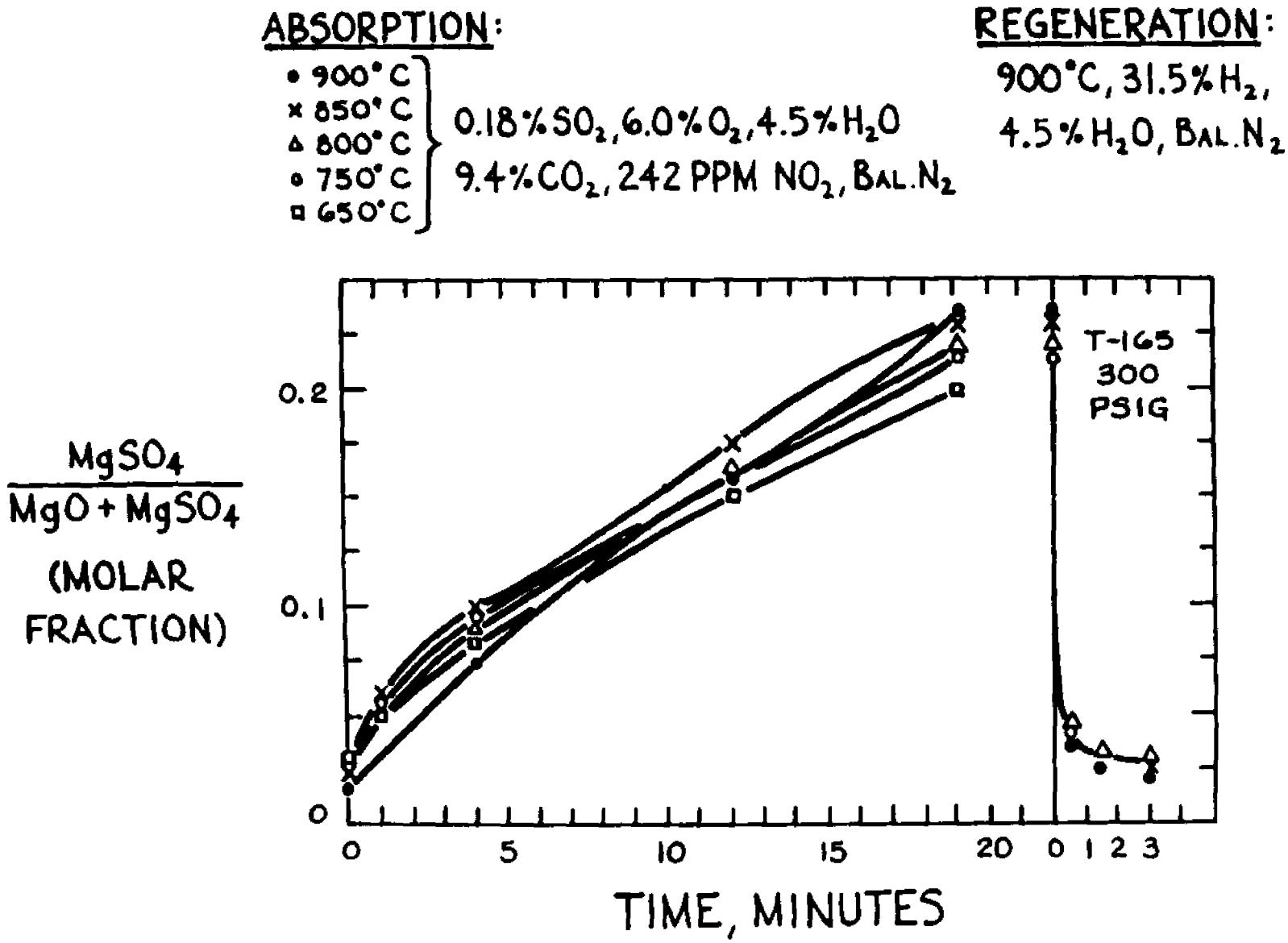

Figure 105. Effect of temperature on absorption rate, obtained from various cycles of run T-165 with quartz pan.

12.08 Effects of Temperature upon Regeneration

A short-cut was also taken to determine gross effects of temperature upon regeneration. The procedure is illustrated in Figure 106, which gives data for run T-173. Each absorption was conducted at 800°C to the same level of magnesium sulfate -- about 30% of the solid. Regeneration temperature was varied from 950°C to 650°C to show a striking effect of this temperature upon the degree of regeneration achieved in 3 minutes. After three minutes of regeneration at the selected temperature, further regeneration was practiced at 900°C in order to complete the regeneration and prepare the solid for the next absorption step.

The data of Figure 106 suggest that no amount of regeneration time would produce much regeneration of magnesium oxide at 650°C. It is unlikely, from the trend of the data at 750°C, that even a long time at this temperature would produce the degree of regeneration achieved at 900°C. One may even doubt that this degree would be achieved at 800°C. The degree of regeneration in 3 minutes at 850°C is essentially the same as that obtained at 900°C, but the rate is slower. Data at 900° and 950°C are indistinguishable.

Figure 107 is an Arrhenius plot of the initial rates of regeneration from Figure 106. Figure 107 also shows results obtained from another run (T-178) made using similar procedures. The agreement between the two runs is good. The initial rate at 650°C is not very reliable, because it is hard to distinguish the slow rate at this temperature from a baseline shift on the thermogram. The Arrhenius plot of Figure 90 suggests a high activation energy for the reaction, perhaps on the order of 90 kilocalories per gram-mole.

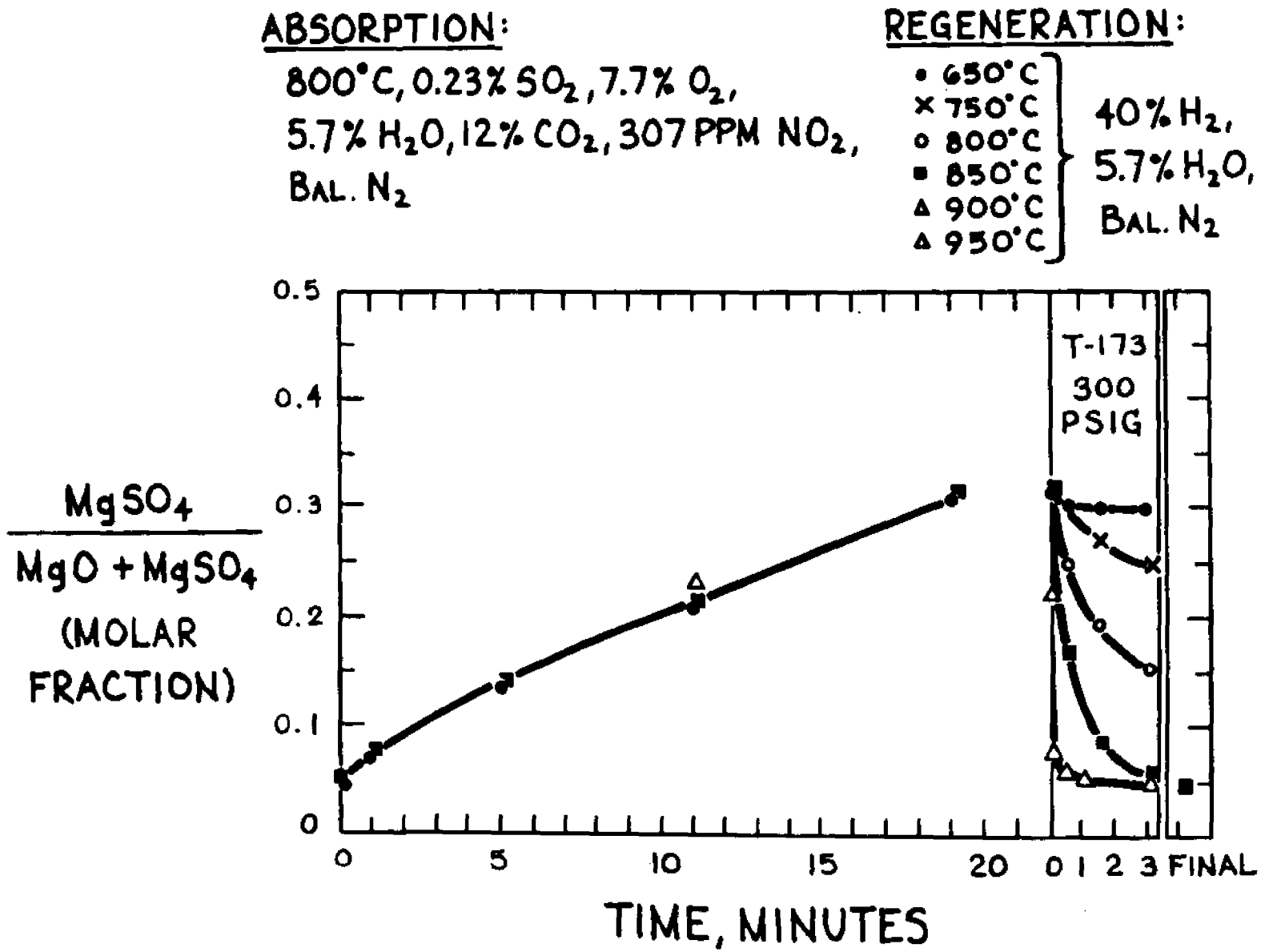

Figure 106. Effect of temperature on regeneration rate, obtained from various cycles of run T-173 with quartz pan.

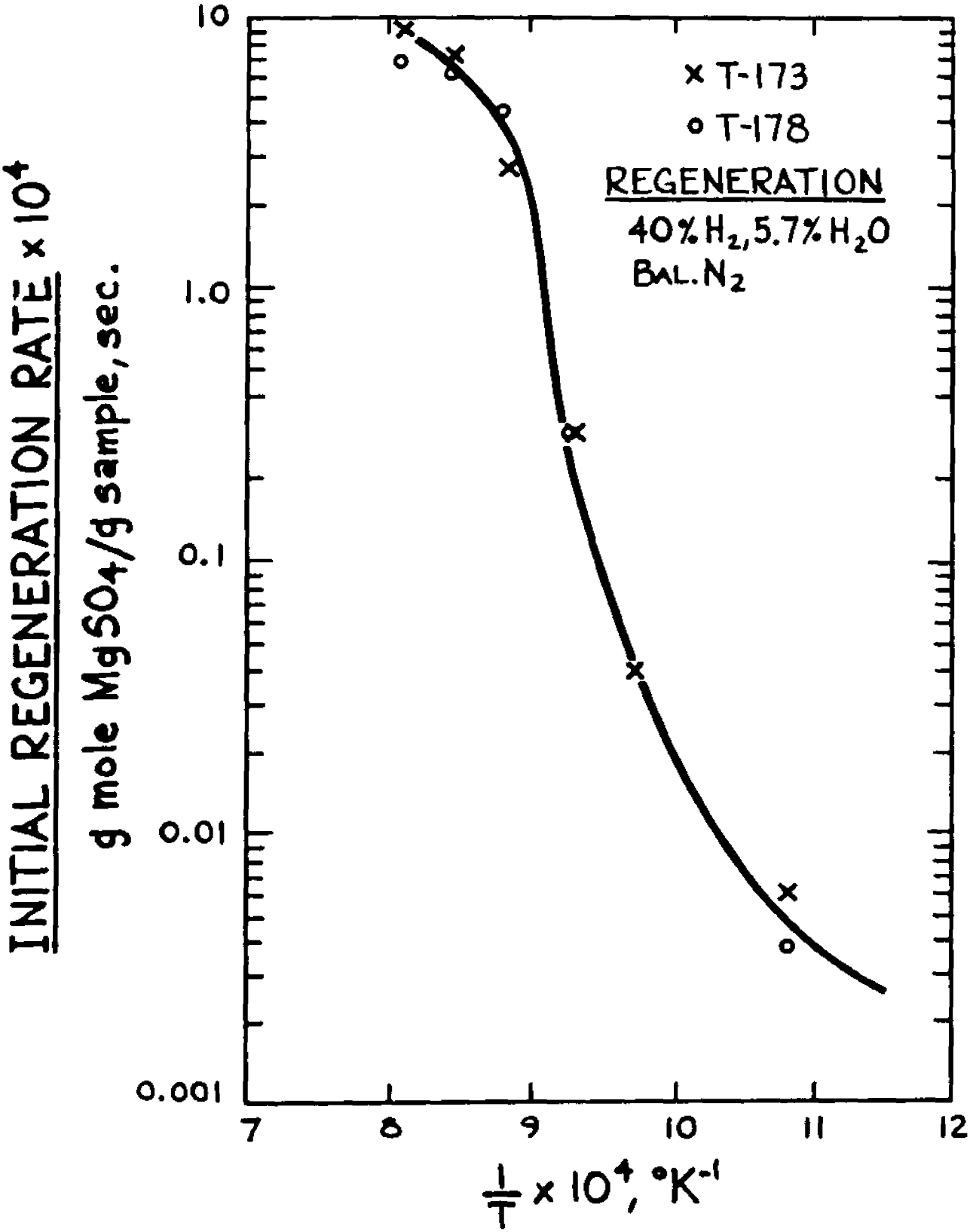

Figure 107. Arrhenius plot of initial rates of regeneration.

12.09 Effects of Calcination History

Figure 108 gives results of two runs undertaken to see if a substantial change in calcination history would have an effect upon absorption rate. Little effect was seen.

12.10 Effects of Absorption and Regeneration Times and Number of Cycles

Data for runs T-145 and T-148 illustrate the importance of choosing appropriate times for the absorption and regeneration steps. The two runs were made under otherwise almost identical conditions (shown in Table 10) except that T-145 used fifteen minutes for regeneration while T-148 used only 3 minutes.

Figure 109 shows first and last cycle absorption rates for the two runs. After twelve runs, the rate for T-145 shows no sign of flagging -- if anything, there is a slight increase in rate. This is not so for T-148, where absorption rate after 15 cycles has dropped significantly.

The reason for this is clearly seen in Figure 110, which gives the first and last cycle regeneration rates for the two runs. Regeneration rates for both runs did not flag, but in run T-418 there was too little time for regenerating the stone. The $MgSO_4$ level increased with increasing cycle number, and the absorption rate flagged with increasing $MgSO_4$ level because of diffusional difficulties.

Figures 98 and 92 are zig-zag plots for runs T-145 and T-148 respectively.

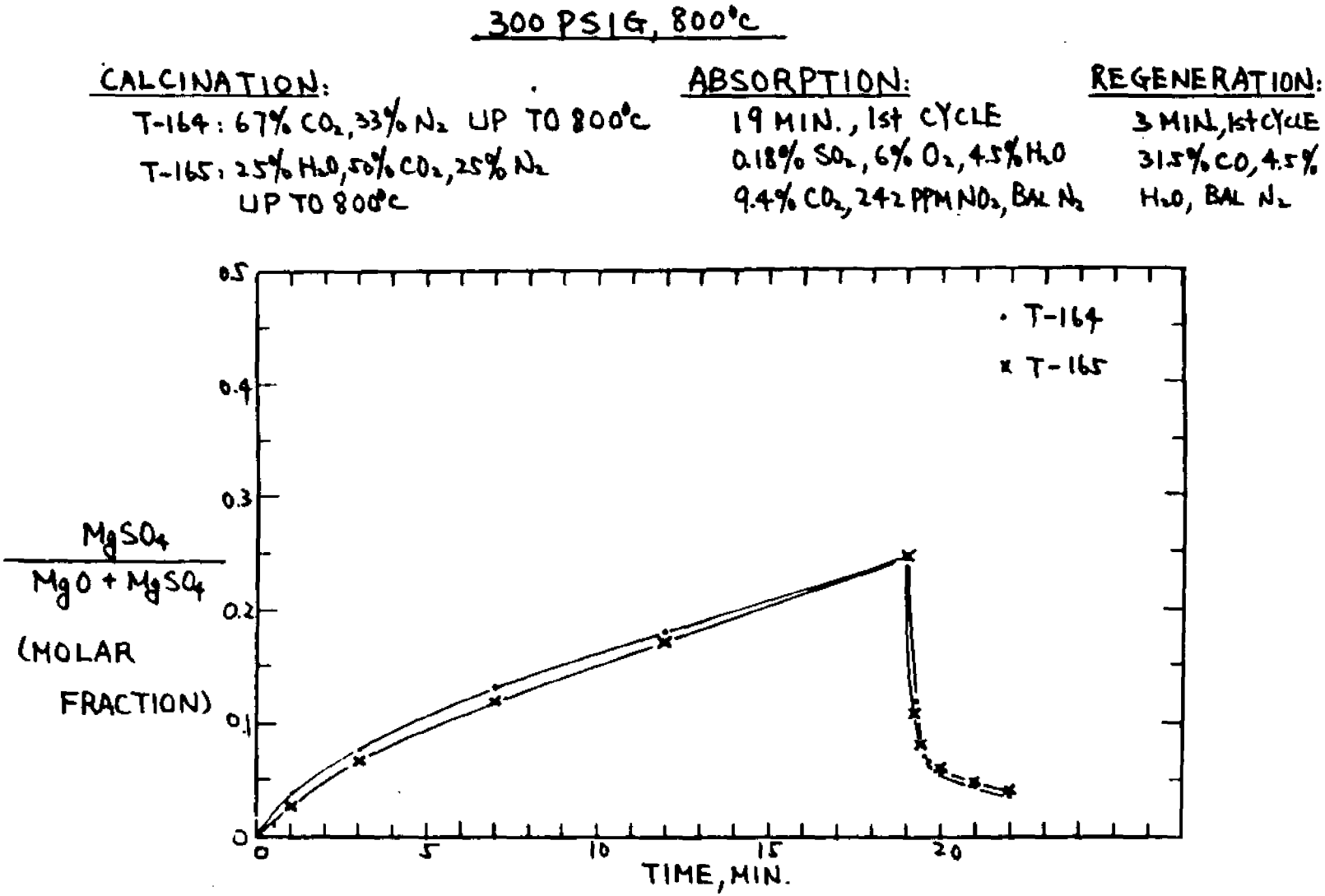

Figure 108. Effect of calcination history on rates, with quartz pan.

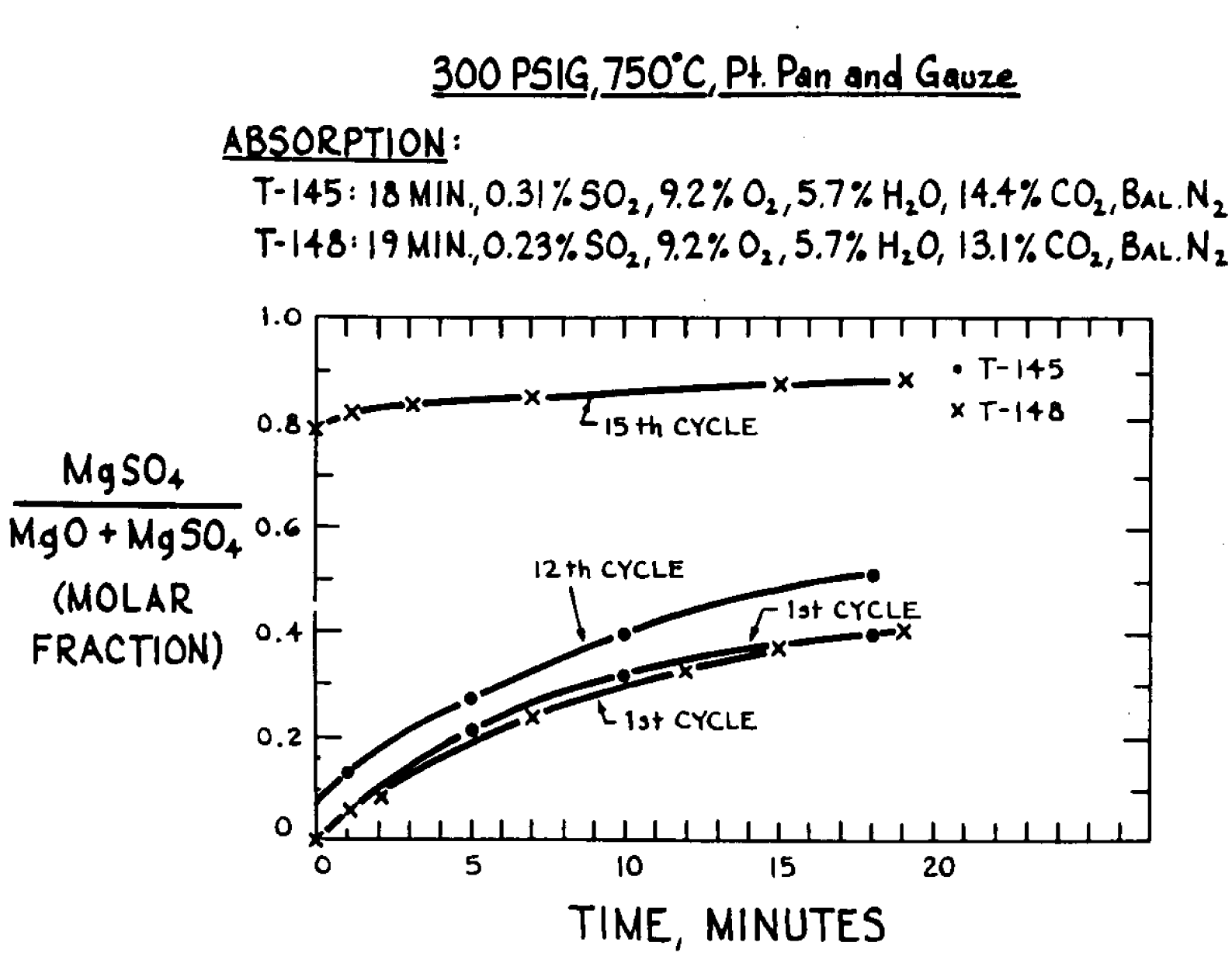

Figure 109. Effect of cycle times and cycle number on absorption rate.

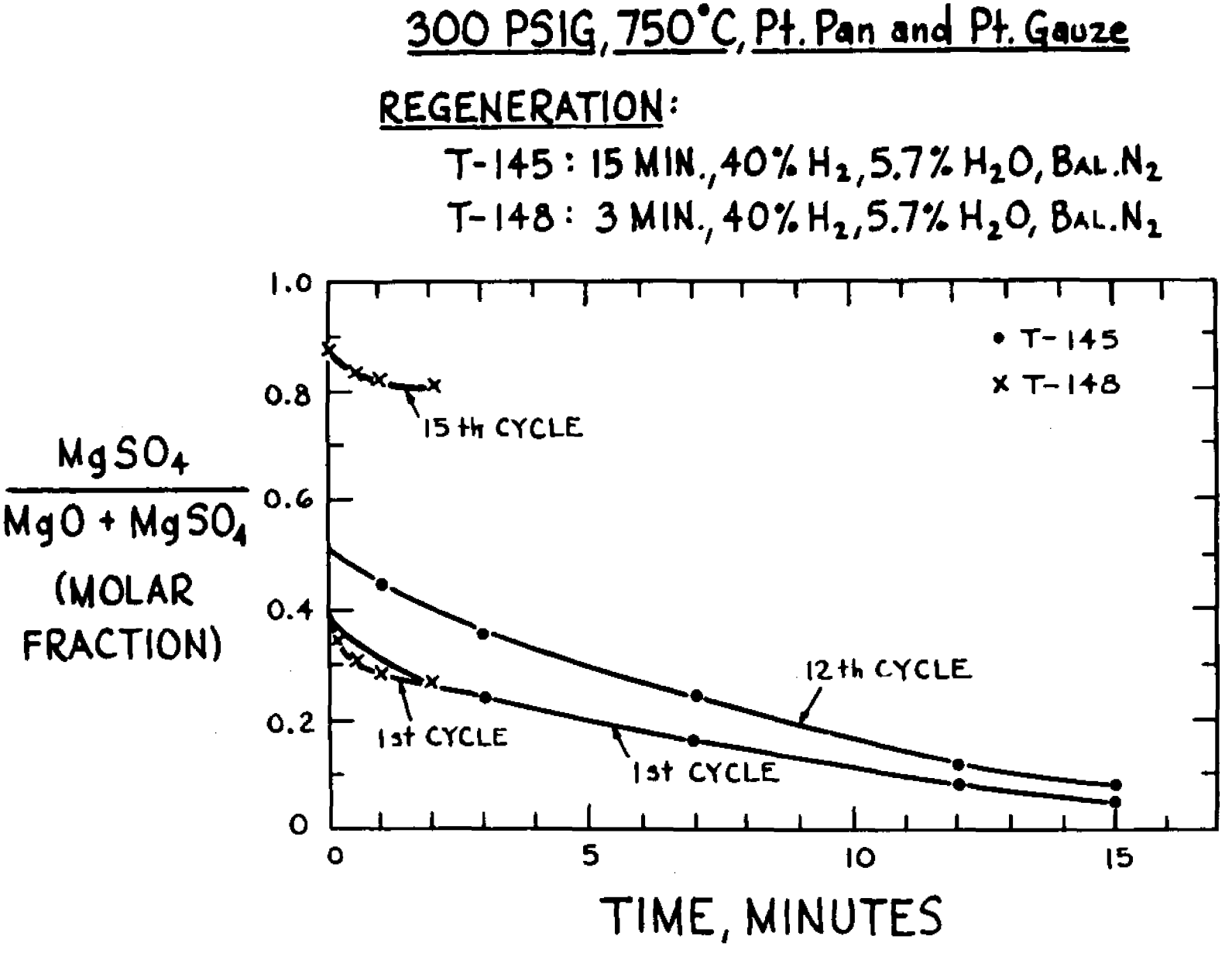

Figure 110. Effect of cycle times and cycle number on regeneration rate.

Figure 111 gives results for run T-175, which used 100 minutes for absorption and 20 minutes for regeneration. The former reaction increased in rate and extent through the sixth cycle, while the regeneration reaction is fast, generally reaching 95% of full regeneration in less than 10 minutes.

Figure 112 is a zig-zag plot for T-175.

12.11 Diffusional Effects

The effect of gas flow rate was explored by using different flow rates in two successive cycles of a run. The first three cycles of run T-173 were made using 100 cubic centimeters per minute flow of reaction gases in both absorption and regeneration steps, while the flow was reduced by one-half in the fourth and fifth cycles. Figure 113 shows that the change from 100 to 50 cm^3/min produced little change from the third to fourth cycle.

Most of our runs were made with a sample size of about 8 milligrams. A run with 40.7 milligrams was made to compare with an otherwise identical run with 8.4 milligrams (runs T-176 and T-177 respectively). The first and sixth cycles are shown in Figure 115. The figure makes it clear that bed diffusion cannot be ignored, and the smaller sample ought to give better information on rate.

Figure 115 is a zig-zag plot for run T-176.

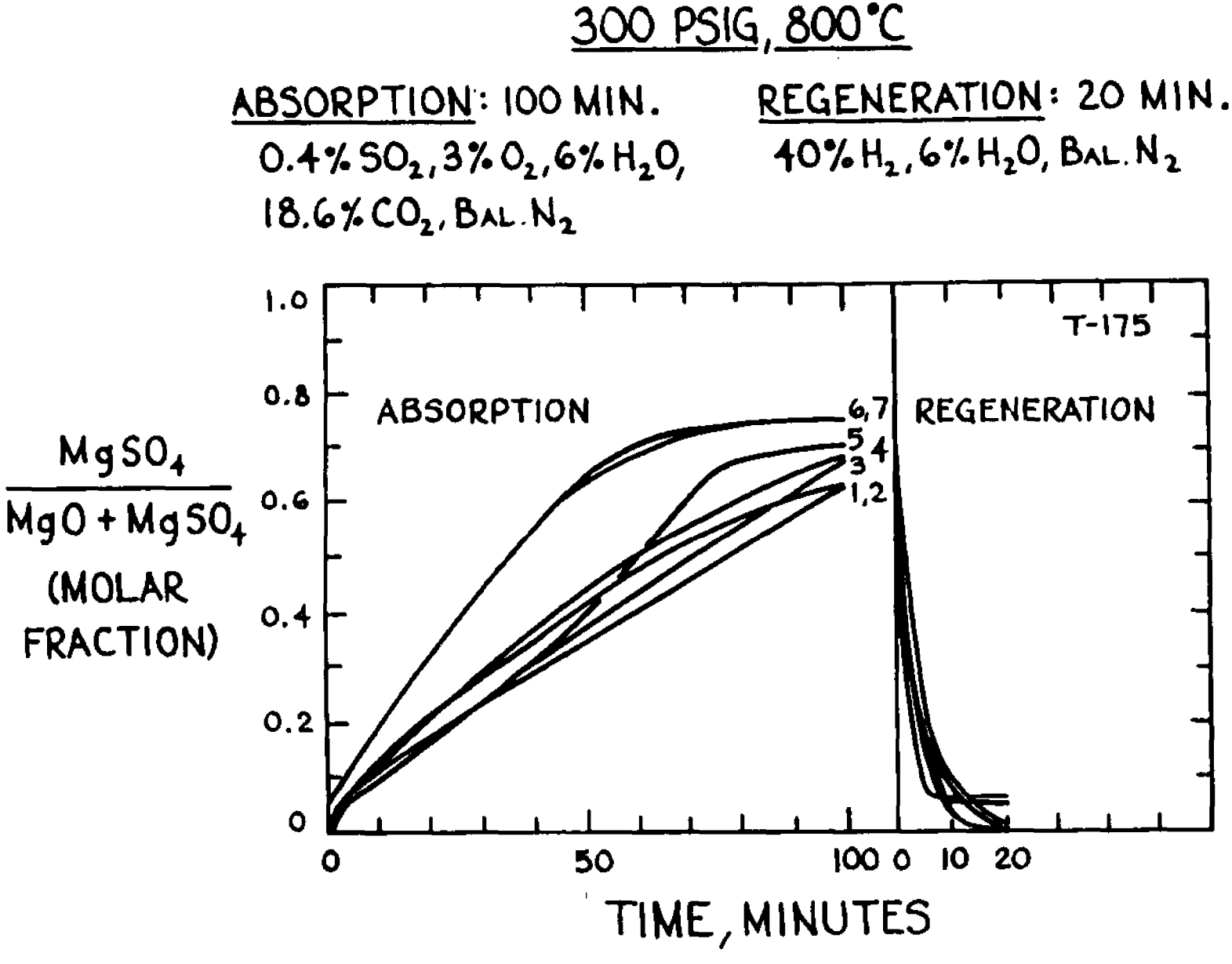

Figure 111. Effect of longer cycle time and cycle number on cyclic rates, with quartz pan.

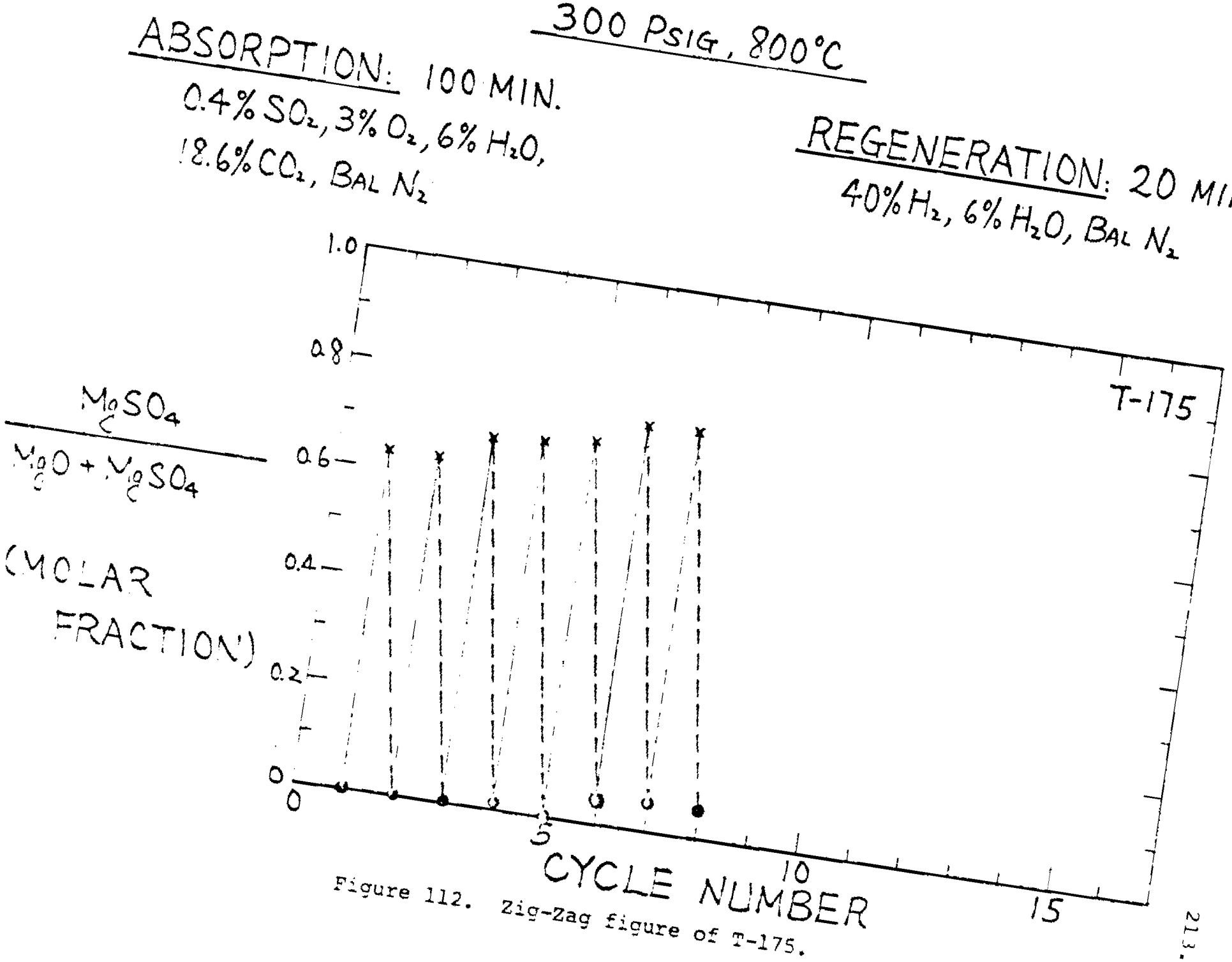

Figure 112. Zig-Zag figure of T-175.

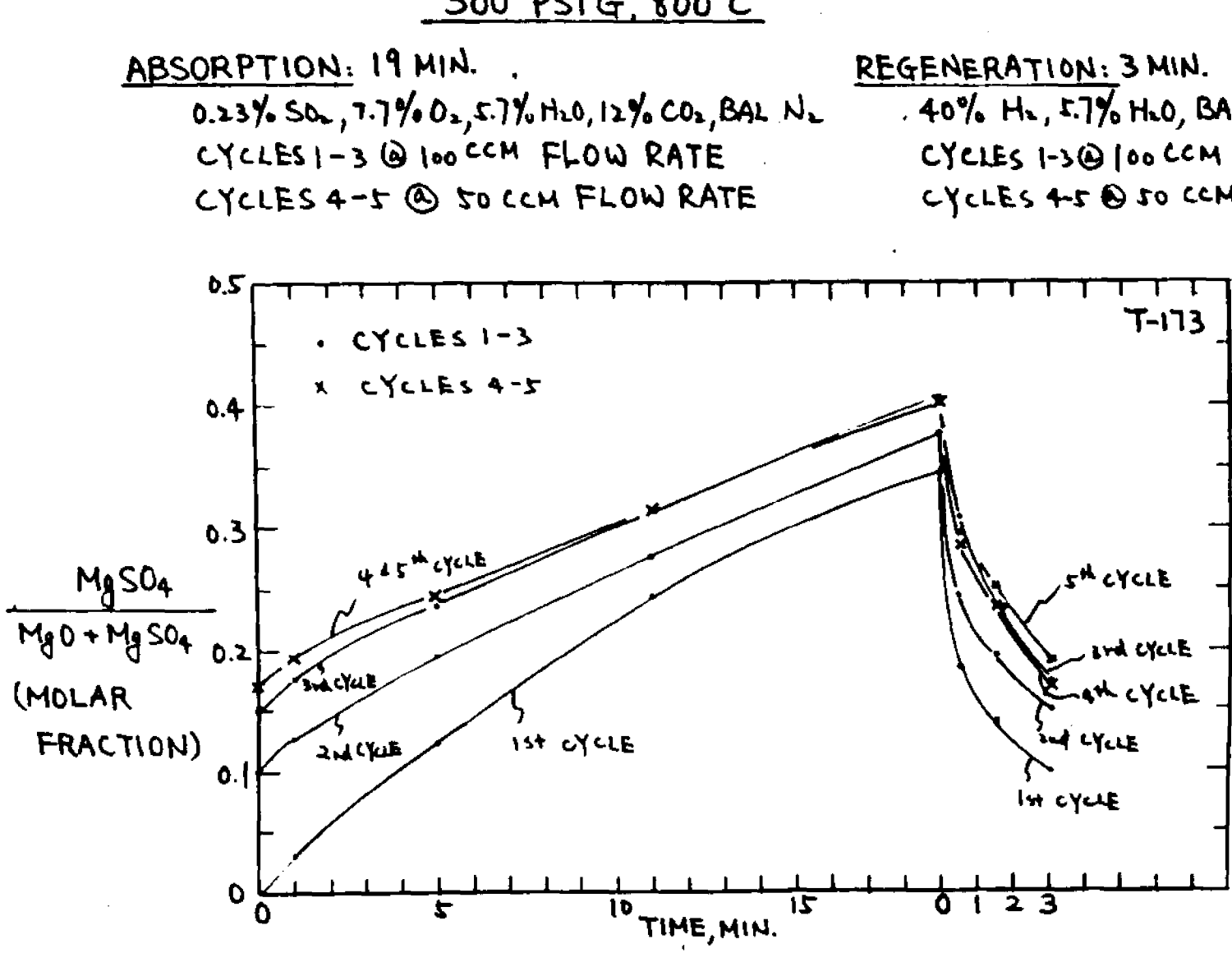

Figure 113. Effect of flow rate on cyclic rates, with quartz pan.

300 PSIG, 800°C

ABSORPTION: 19 MIN.
0.4% SO_2, 3% O_2, 6% H_2O
18.6% CO_2, BAL N_2

REGENERATION: 3 MIN.
40% H_2, 6% H_2O, BAL N_2

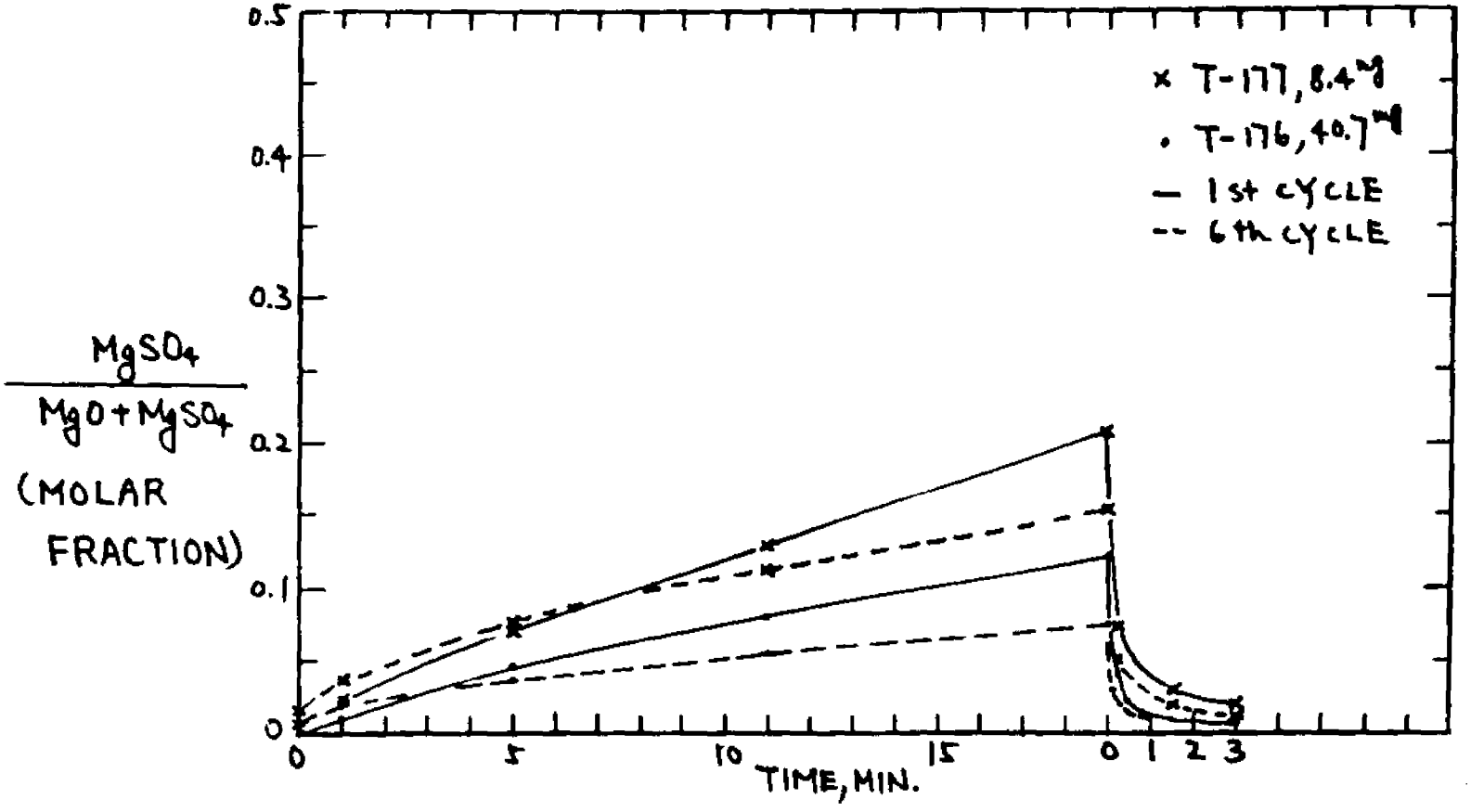

Figure 114. Effect of sample size on cyclic rates.

300 PSIG, 800°C, 40.71 mg $MgCO_3$

ABSORPTION: 19 MIN. 0.4% SO_2, 3% O_2, 6% H_2O, 18.6% CO_2, BAL N_2

REGENERATION: 3 MIN. 40% H_2, 6% H_2O, BAL N_2

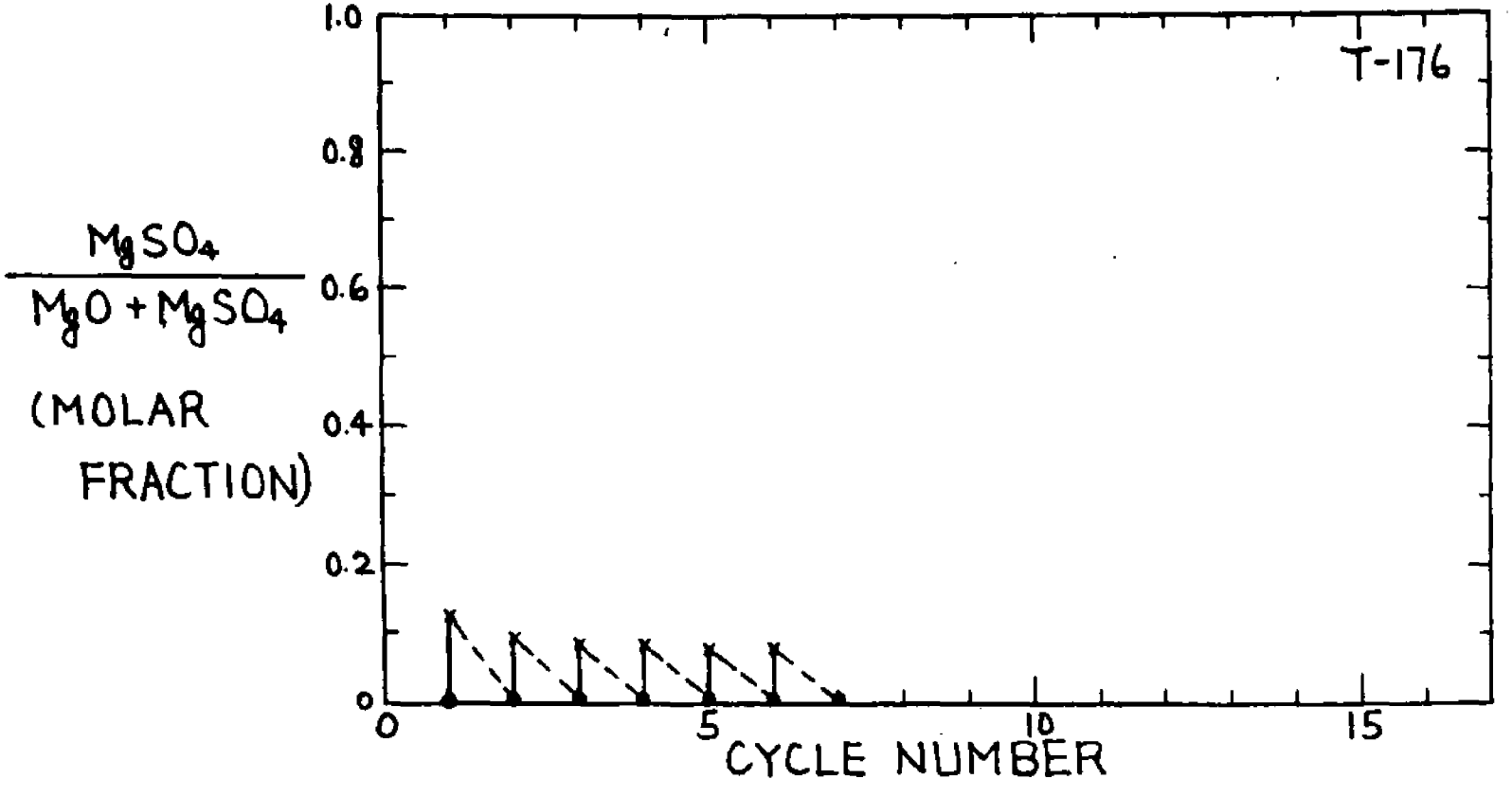

Figure 115. Zig-Zag figure of T-176.

Some idea of the importance of diffusion within magnesium oxide particles had been provided by the data shown in Figure 69 where absorption rate for magnesium oxide produced by calcining magnesite rock is compared with reagent grade magnesium oxide, probably a precipitated and less porous structure, explaining its slower reaction rate.

To get some feeling for the problem of intraparticle diffusion, a run was made using a disk of 0.44 cm diameter and 0.25 cm thickness made from a chunk of our Red Mountain magnesite rock placed in the quartz pan. The first cycle rates are given in Figure 116. The disk required 130 minutes to achieve a conversion reached in nineteen minutes by a sample of powder -250+270 mesh. The regeneration, however, seems to be very fast for the disk, reaching completion in two minutes.

A sphere of 0.325 cm diameter was made from a chunk of rock in an attempt to secure data giving an effective diffusivity for the $MgSO_4$ product layer formed in the absorption step. Figure 117 gives data for four cycles conducted with the sphere placed in the quartz pan. One striking feature of the data is that both absorption and regeneration rates appear to increase slightly with cycle number.

Data from the fourth cycle were treated to determine intraparticle diffusional resistance. Figure 118 is a plot of time versus the "diffusion statistic" (12, 14), and indicates an effective diffusivity on the order of 0.0001 cm^2/sec. When this is compared with the diffusivity in open space, we obtain a ratio of about 0.0017. This small ratio is not unexpected for a product layer of $MgSO_4$ upon MgO, in view of the far larger molecular volume of the former species.

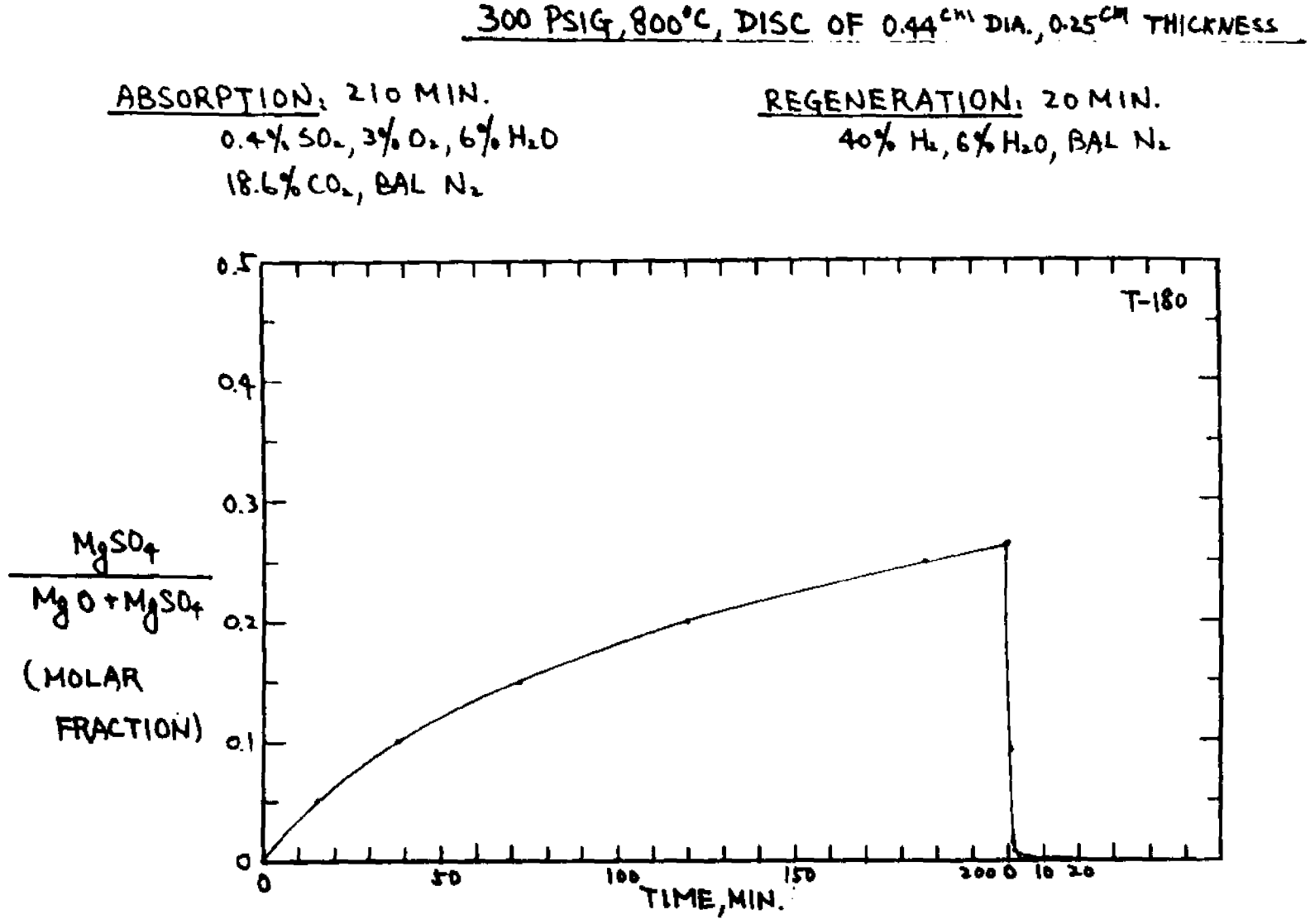

Figure 116. Cyclic rates of disk sample run.

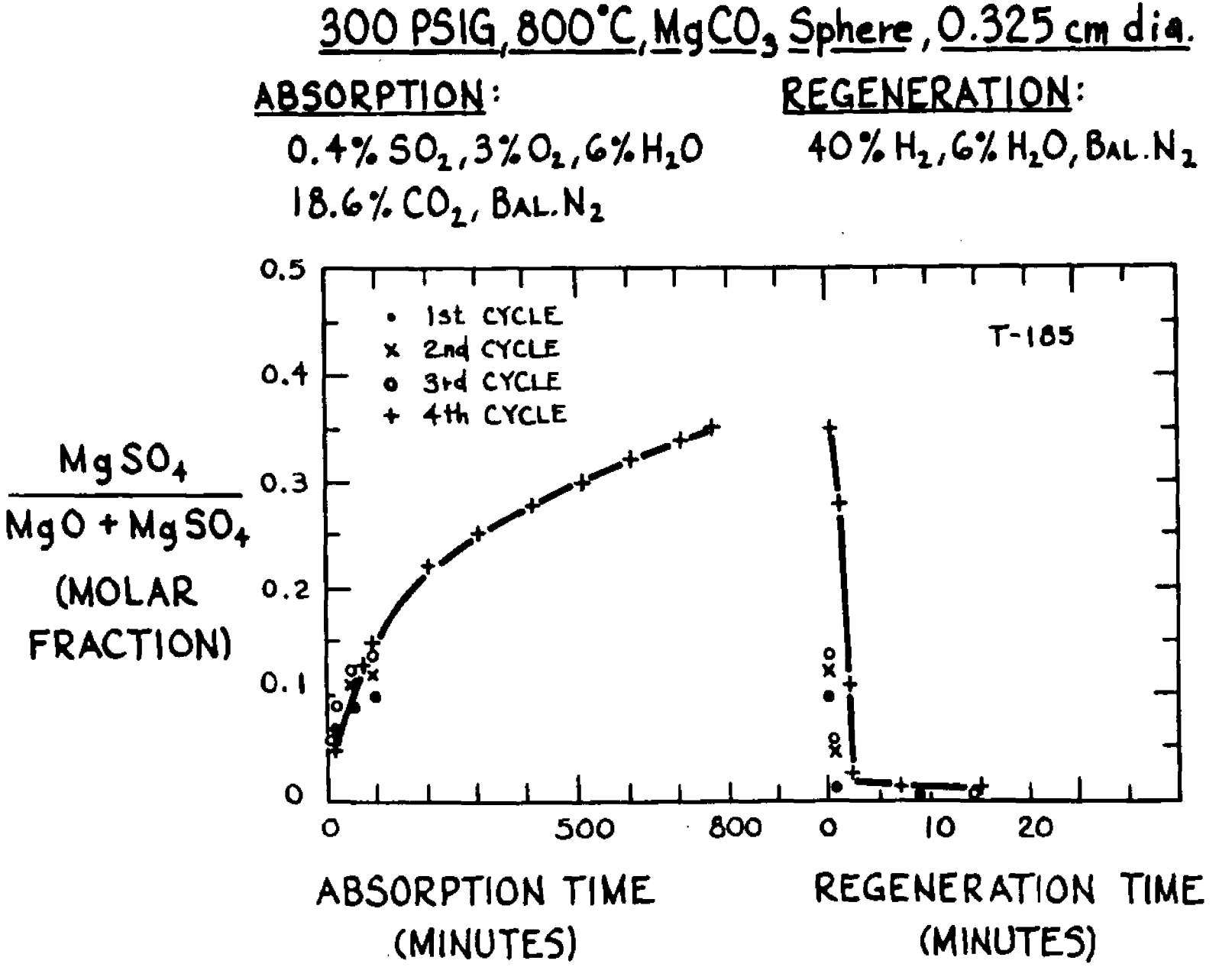

Figure 117. Cyclic rates of sphere sample run.

300 PSIG, 800°C, $MgCO_3$ Sphere, Dia. = 0.325 cm

4th ABSORPTION: 0.4% SO_2, 3% O_2, 6% H_2O, 18.6% CO_2, BAL. N_2

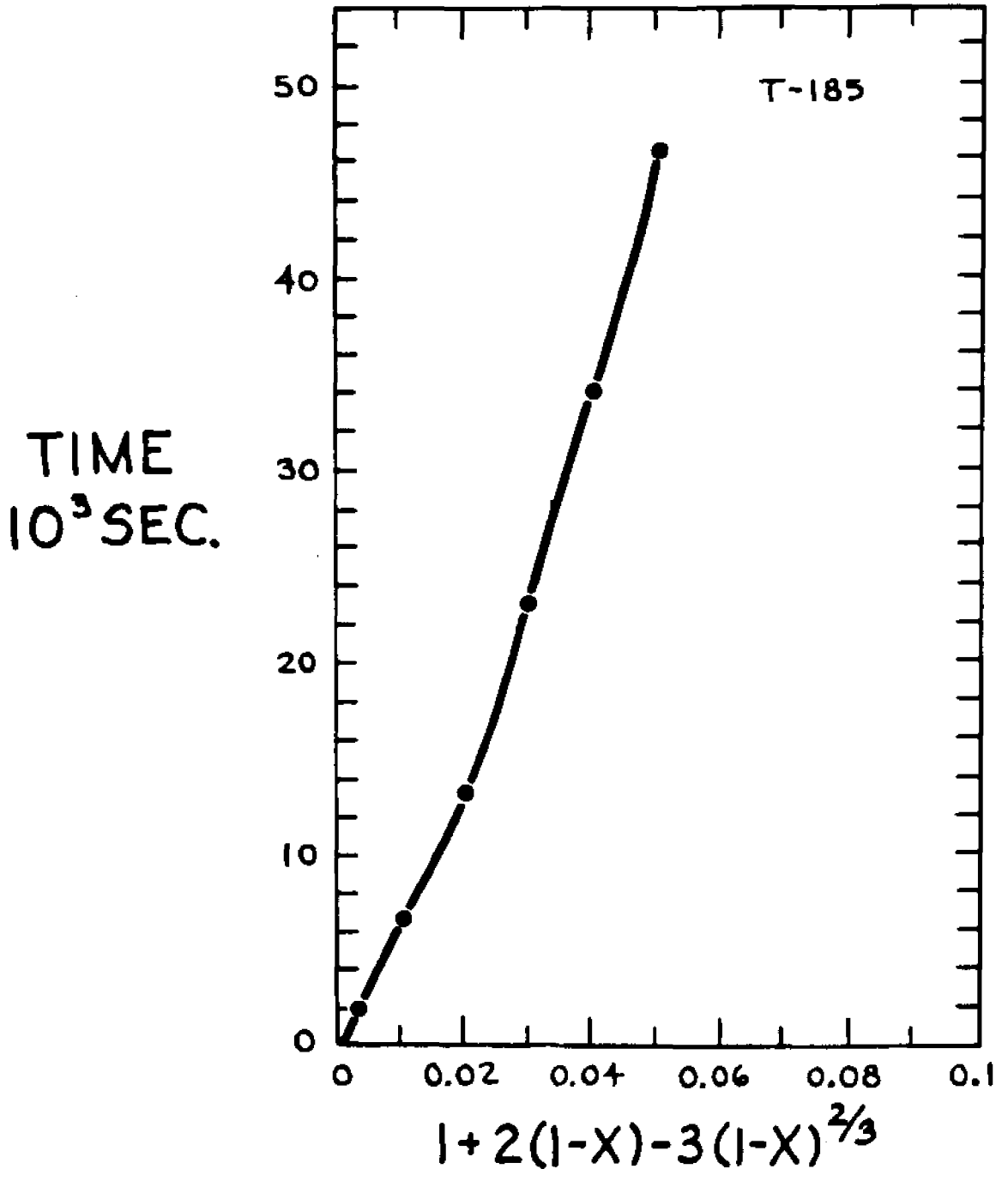

Figure 118. Time vs. diffusion statistic plot.

12.12 Discussion of Effects Relating to Absorption Capacity

A major consideration for the designer of a process to employ magnesium oxide as an absorbent for sulfur dioxide will be the capacity of the solid after it has undergone a number of reaction cycles. The information available from this research do not allow, at this time, a precise definition of capacity for a variety of possible process conditions. Valuable qualitative conclusions, however, may be drawn.

The reason our work has not given sufficient information relating to capacity in a practicable process is worth mentioning, as a guide to planning future research. At the outset of the work on magnesium oxide, we were impressed with the decline in reactivity of half-calcined dolomite in the cycle for absorption of hydrogen sulfide. Our initial plan, therefore, emphasized obtaining as many cycles as possible in a given run with magnesium oxide in order to expose such a decline in reactivity, if it exists. To this end, we usually set the respective times for the absorption and regeneration steps fairly short, so that a large number of cycles could be run off in a given day.

This plan did not always allow the solid to display as much capacity at a given set of operating conditions as it might have done if longer times had been chosen and fewer cycles settled for. For example, zig-zag plots like those seen in Figures 93, 94, 96, and 97 display poor capacity because of the low regeneration temperature, which is accompanied by a low rate of regeneration, so that the degree of regeneration was too little in the short regeneration time allowed.

The weight of the evidence from our work now points to a conclusion that the reaction cycle has little if any effect upon reactivity of the magnesium oxide in successive cycles. Further work could be planned choosing regeneration temperatures or times, for example, to obtain substantially complete regeneration. Our work suggests that a process might preferably use a high regeneration temperature, such as 900°C, in order to achieve full regeneration in a few minutes. The process could employ an absorption temperature over a relatively wide range, say from about 750° to 900°C.

The preceding Section 12.11 gave data pointing to diffusional resistance in a product layer of $MgSO_4$ as the rate-determining step in absorption. This is consistent with the weak dependence of the absorption rate upon temperature (see Figure 105). The weak dependence of absorption rate upon sulfur dioxide concentration remains a puzzle.

The effective diffusivity of reactant gas species in the product layer of $MgSO_4$ is so low, less than 0.2% of the diffusivity in open space, that the proposed cycle for magnesium oxide may well not be practicable except for particles of relatively small size. Our 0.325 cm sphere took nearly 800 minutes to achieve 35% conversion to $MgSO_4$. It would appear that the coarse particles, generally around 10- to 40-mesh, used in fluidized-bed combustion boilers of the type built by Pope, Evans and Robbins and Foster-Wheeler Corporation at Rivesville, West Virginia, may be too large for practicable application of the magnesium oxide cycle.

Accordingly, the magnesium oxide cycle appears to be limited to small particles, for example, particles on the order of 50 micrometers in size.

For such particles, good absorptive capacity may be achieved at practicable residence times in a fluidized-bed combustion step and a supporting regeneration step.

The fast fluidized bed (2) is a unit operation suitable for handling such small particles, and is also well suited for combustion. This possibility will be discussed further in Section 13.03 below.

Our work shows that higher capacities can be achieved if the particles are intermingled with a catalyst for conversion of sulfur dioxide to the trioxide, or better still, if the particles are impregnated with such a catalyst. Although our work to demonstrate this fact has used substances, platinum and palladium, that are far too expensive for use in a practicable combustion device, other catalytic agents based upon iron, vanadium, and chromium and the like might be developed for this purpose.

12.13 Decomposition of Magnesium Sulfate at High Temperatures

By chance, we discovered that magnesium sulfate decomposes at an appreciable rate at temperatures beyond about 750°C. Run T-135 used Fisher reagent grade (Lot 7366111) MgO powder as a starting material. After it had been partially converted to $MgSO_4$, it was exposed to a 50/50 mixture of steam and carbon dioxide at 750°C, and we were surprised to observe a decline in weight, as seen in Figure 119. We then conducted additional runs T-144 and T-183 exposing partially sulfated solids to nitrogen and 25/50/25 steam/CO_2/nitrogen respectively. Results of these runs are also shown in Figure 120. The solid in run T-144 was sulfated reagent grade MgO powder, and that in run T-183 was -270 mesh powder obtained by dissolving palladium chloride and epsom salt in water and evaporating, as described in Section 12.03. The data in Figure 119 illustrate an effect of temperature upon the rate of decomposition of magnesium sulfate.

This rate is far slower than the rate of regeneration of $MgSO_4$ by reaction G with hydrogen to form MgO. However, the sharp dependence of the latter rate upon temperature (see Figure 106) may well be related to the decomposition of $MgSO_4$. The decomposition may open up cracks in the product layer of $MgSO_4$, allowing hydrogen to enter and penetrate throughout the layer more easily. Another possibility is that the decomposition of $MgSO_4$ provides three-dimensional nucleating sites for the regeneration reaction G instead of two-dimensional sites restricted to crystallite surfaces.

Although the data at 650°C in Figure 107 are less reliable than data at higher temperatures, the S-shaped curve drawn in the figure is nevertheless credible, since the sharp increase in slope between 650°C and 750°C may reflect an increase in the available surface for reaction.

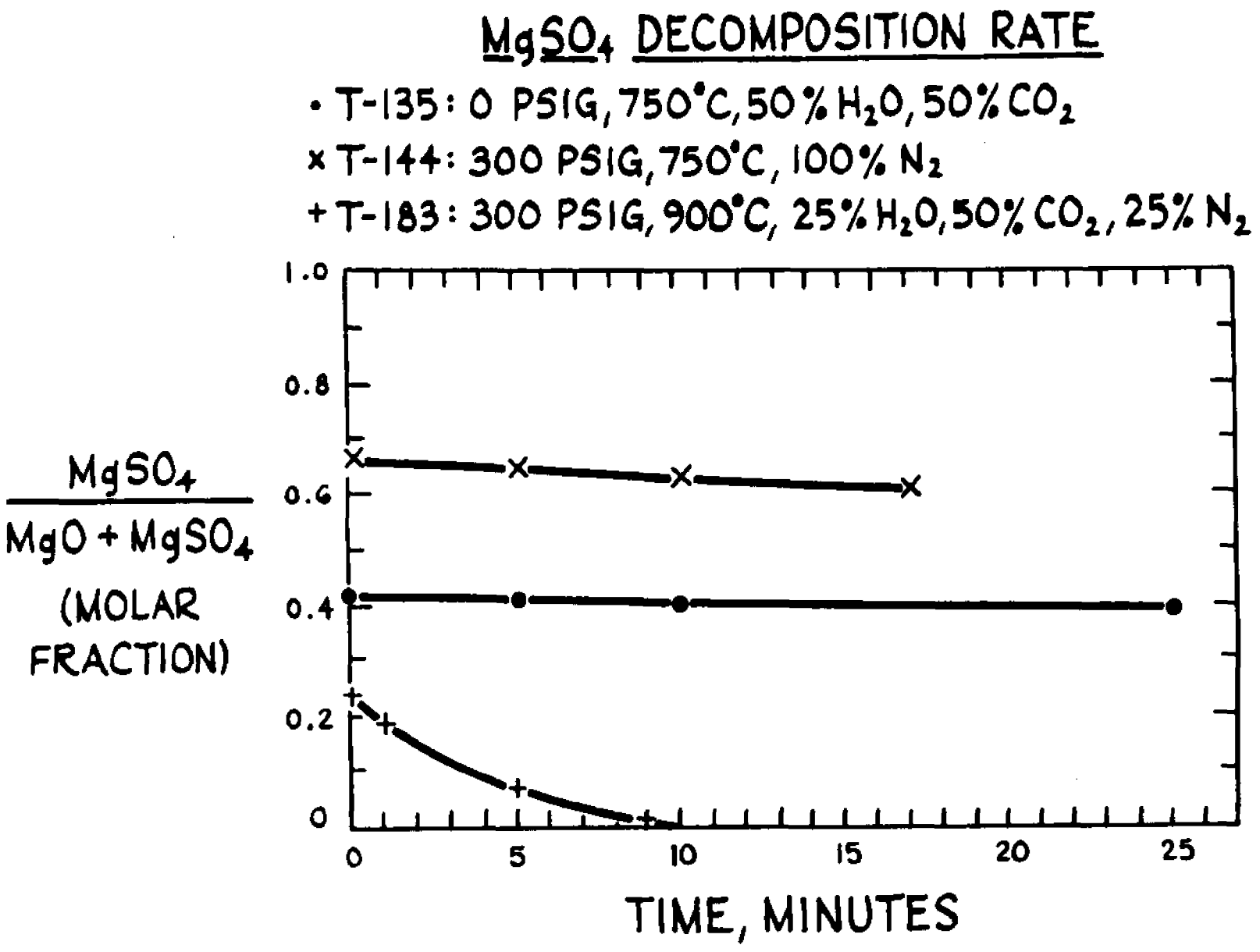

Figure 119. Runs illustrating decomposition of magnesium sulfate.

13.0 Summary of Findings

13.01 Temperatures for Application of Magnesium Oxide Cycle

We may tentatively conclude that any temperature between about 750°C and 900°C is suitable for use of magnesium oxide to absorb sulfur dioxide from combustion products in fluidized-bed combustion. The rate of absorption and final capacity do not appear to depend strongly upon temperature. This is consistent with evidence we have developed that the rate of absorption is limited by diffusion of gaseous reactants through a product layer of magnesium sulfate.

We have found the rate of regeneration of magnesium oxide by reduction of magnesium sulfate with hydrogen and release of sulfur dioxide to depend markedly upon temperature. We may tentatively conclude that a temperature of 900°C is suitable for regeneration.

We have tentative evidence that carbon monoxide may be a better reductant for magresium sulfate than hydrogen.

We attribute the marked dependence of the rate of regeneration upon temperature to the tendency for magnesium sulfate to decompose even in absence of a reducing gas such as hydrogen or carbon monoxide. Indeed, there is a possible that a process could be worked out for regeneration without use of a reducing gas, and this should be explored.

13.02 Particle Size for Application of Magnesium Oxide Cycle

The effective diffusivity of gases through the product layer of magnesium sulfate appears to be so slow -- less than about 0.2% of the diffusivity in open space -- that the magnesium oxide cycle would be restricted in practice to small particles, for example, on the order of 50 microns in size. This probably rules out its use in fluidized bed boilers of the more "conventional" type under development in recent years, for example, by Pope, Evans and Robbins in the United States and by the National Coal Board in England.

13.03 Use of Magnesium Oxide Cycle in Fast Fluidized Bed Boiler

The first application of Lurgi's modern design for a fast fluidized bed device was a combustion process for calcining aluminum hydroxide (3). This is now thoroughly accepted by the aluminum industry, and is operating in five or six large units built since 1970.

Battelle Memorial Institute has a program for development of a fast fluidized bed boiler to burn coal (50). We understand that the Electric Power Research Institute has also taken up study of such a boiler, although to our knowledge testing is not yet underway. We also understand that Lurgi itself has serious plans for development of a fast fluidized bed boiler for coal in cooperation with German boiler firms, and that Lurgi has already conducted extensive testing of a variety of fuels including several coals.

The trand of thinking is toward exploitation of the fast bed's flexibility in rate of heat removal through variation in

solid circulation rate. This rate is varied simply by varying the inventory of solid in the fast bed.

The small particle size used in the design developed by Lurgi for the fast bed -- something on the order of 50 micrometers -- allows the designer to exploit the conventional standpipe-and-riser arrangement of the catalytic cracker of the petroleum industry for moving powder into and away from the fast fluidized bed itself. Figure 120 illustrates a suitable arrangement. The storage bin at the upper middle of Figure 120 would hold solid when it is not needed in the fast bed. An increase in load would call for transfer of solid from the bin to the fast bed circulation loop, in order to increase the heat transfer coefficient. Notice that the storage bin does not need to be fluidized throughout its extent: fluidization of a trough at the bottom of the bin is sufficient to provide mobility of solid in the trough and to cause the solid to enter the standpipe that returns powder to the fast bed loop.

Only one coal feed need be provided for a relatively large bed, since the height of the unit guarantees that volatile matter will be burned out before the combustion products leave the fast bed's cyclone.

13.04 Potential Role for a Catalyst in the Magnesium Oxide Cycle

Our work has shown dramatic effects of palladium and platinum upon the capacity attained in the magnesium oxide cycle. These materials are of course too expensive for practicable use in coal combustion, but our data provide a lead for further work to identify cheaper catalytic substances, such as an iron oxide.

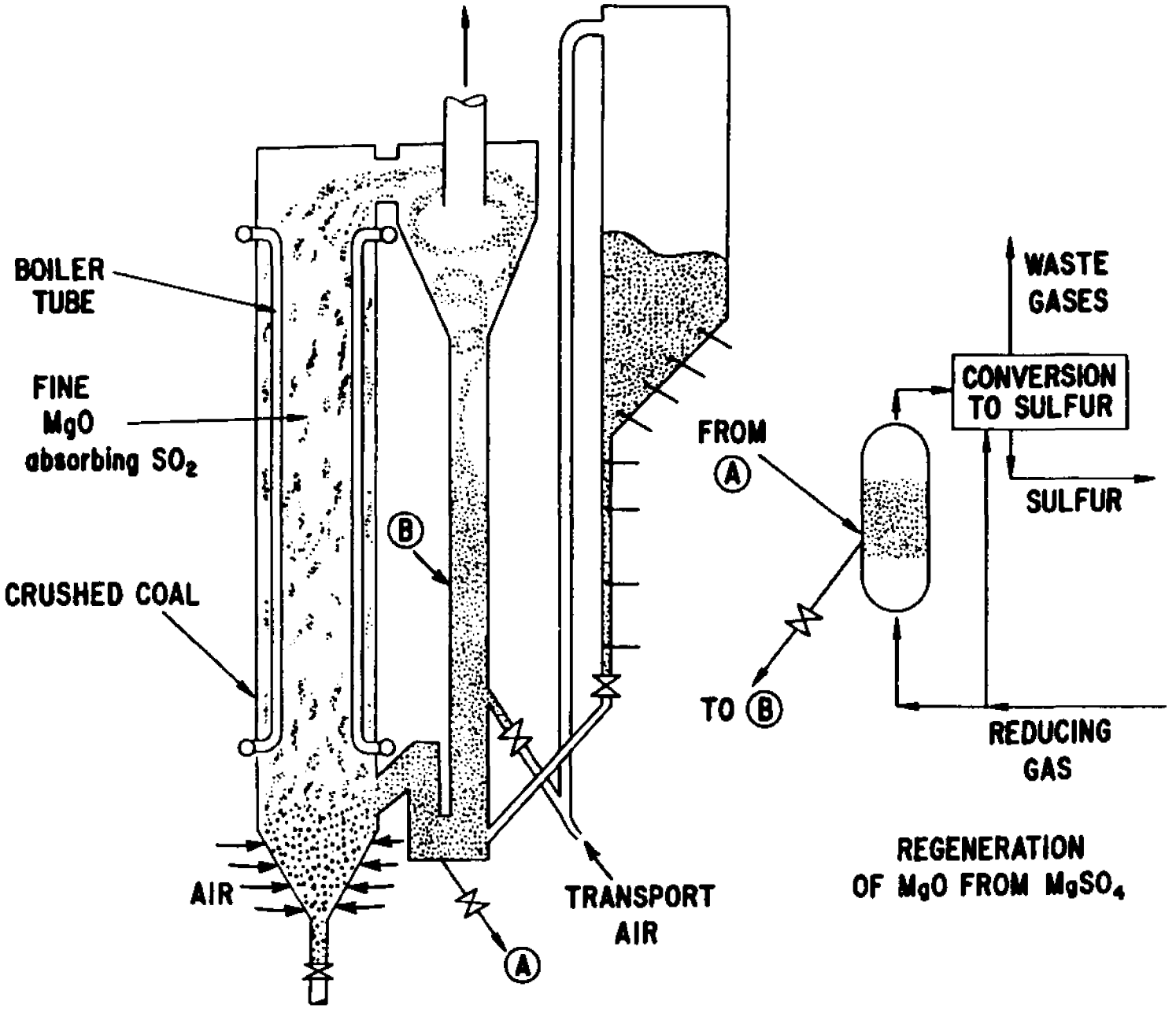

Figure 120. Conceptual fast fluidized bed coal-burning boiler.

14.0 Recommendations for Further Research

(1) Better measurements of the effective diffusivity of the product layer of magnesium sulfate should be made at several particle diameters. It would be good to relate measurements based upon rate of uptake of sulfur dioxide at high temperature to measurements made at room temperature by the technique of Weisz (51).

(2) Results from (1) will permit selection of particle sizes for practicable use over a practicable range of particle residence times in an absorption step. After such selection is made, cyclic runs should be conducted to confirm the capacities predicted for several operating conditions in light of the effective diffusivity data.

(3) Further research might establish the role of magnesium sulfate decomposition in promoting the strong temperature dependence of the regeneration reaction.

(4) Further research on the rate of magnesium sulfate decomposition might establish this reaction as a viable way to regenerate, obviating need for reducing gases. Are the products of the decomposition primarily sulfur dioxide and oxygen? Primarily sulfur trioxide? A mixture of all three, and if so, in what proportion? Answers to these questions are needed before process layouts could be attempted.

(5) A search for a cheap catalyst to promote the absorption might prove rewarding. Iron oxide is a candidate for early study.

(6) Further work to understand the dependence of the absorption reaction upon both pressure and sulfur dioxide concentration is needed. If a catalyst emerges from (5), it is possible that the magnesium oxide cycle will be attractive at atmospheric pressure as well as at elevated pressure.

15.0 References

1. P.W. Robson, Power Gas Producers: Their Design and Application, Edward Arnold, London, 1908.
2. J. Yerushalmi, D.H. Turner, A.M. Squires, I&EC Process Design & Development, 15, 47-53 (1976).
3. A.M. Squires, "Applications of Fluidized Beds in Coal Technology", chapter in Alternative Energy Sources, J.P. Hartnett, editor, Hemisphere Publishing Corporation, Washington, D.C., in press.
4. S. Dobner, M.J. Gluckman, A.M. Squires, "Production of Low-Btu Gas from Coal in Combination with Advanced Power Cycles", AICHE Symposium Series, vol. 70, no. 137, 223-229 (1974).
5. A.M. Squires, Advances in Chemistry Series, 69, 205-299 (1967); presented at New York meeting of Division of Fuel Chemistry, American Chemistry Society, September 1966.
6. L.A. Ruth, R.A. Graff, A.M. Squires, Environmental Science & Technology, 6, 1009-1014 (1972); presented at Los Angeles meeting of American Chemical Society, March 1971.
7. R.A. Graff, R. Pfeffer, A.M. Squires, "Capturing Sulfur with Calcined Dolomite", paper EN 23C presented at Second International Clean Air Congress, Washington, D.C., December 1970 (Proceedings, pp. 764-771).
8. A.M. Squires, R. Pfeffer, J. Air Pollution Control Assoc., 20, 534-538 (1970).
9. K.C. Lee, M.S. Wu, I. Rodon, R. Pfeffer, A.M. Squires, final report to Electric Power Research Institute under contract to study the panel bed filter (1974-76), in preparation.

10. G.P. Curran, B. Pasek, M. Pell, E. Gorin, "Reaction of H_2S with Half-Calcined Dolomite in a Regenerable Process", paper presented at San Francisco meeting of Division of Fuel Chemistry, American Chemical Society, August 30 - September 3, 1976.

11. D.L. Keairns, R.A. Newby, E.P. O'Neill, D.H. Archer, "High Temperature Sulfur Removal System Development for the Westinghouse Fluidized Bed Coal Gasification Process", paper presented at San Francisco meeting of Division of Fuel Chemistry, American Chemical Society, August 30 - September 3, 1976.

12. A.M. Squires, R.A. Graff, M. Pell, Chem. Eng. Progr. Symp. Series, 69, 23-34 (1971).

13. M. Pell, R.A. Graff, A.M. Squires, Chem. Eng. Progr. Technical Manual "Sulfur and SO_2 Developments", 1971, pp. 151-157.

14. M. Pell, Reaction of Fully-Calcined Dolomite with Hydrogen Sulfide, Ph.D. Thesis, The City University of New York, 1971.

15. L.A. Ruth, Reaction of Hydrogen Sulfide with Half-Calcined Dolomite, Ph.D. Thesis, The City University of New York 1972.

16. S. Dobner, A High Pressure Thermobalance for Process Studies, Ph.D. Thesis, The City University of New York, 1976.

17. E.P. O'Neill, D.L. Keairns, W.F. Kittle, "Kinetic Studies Related to the Use of Limestone and Dolomite as Sulfur Removal Agents in Fuel Processing", Proceedings of the Third International Conference on Fluidized Bed Combustion, held at Hueston Woods, Ohio, 1972, under auspices of Environmental Protection Agency.

18. D.L. Keairns, E.P. O'Neill, D.H. Archer, "Sulfur Emission Control with Limestone/Dolomite in Advanced Fossil Fuel Processing Systems", paper presented at 67th Annual Meeting of Air Pollution Control Association, June 9-13, 1974.

19. W.T. Abel, E.P. Fisher, "Limestone to Reduce Hydrogen Sulfide from Hot Producer Gas", United States Energy Research Development Administration, MERC/RI-75/3, January 1976.

20. G.P. Curran, J.T. Clancey, P. Pasek, M. Pell, G.D. Rutledge, E. Gorin, "Production of Clean Fuel Gas from Bituminous Coal", report from Conoco Coal Development Company (then Consolidation Coal Company) to Environmental Protection Agency, December 1973.

21. G.P. Curran, C.E. Fink, E. Gorin, Advances in Chemistry Series, 69, 141-165 (1967).

22. G.P. Curran, C.E. Fink, E. Gorin, Office of Coal Research and Development Report No. 16, Interim Report No. 3, "Phase III - Bench-Scale Research on CSG Process, Book 3: Operation of the Bench-Scale Continuous Gasification Unit".

23. R.A.W. Haul, Z. anor. allgem. Chem., 281, 199-211 (1955).

24. R.H. Borgwardt, R.D. Harvey, Environmental Science & Technology, 6, 350-360 (1972).

25. R.D. Harvey, "Petrographic and Mineralogical Characteristics of Carbonate Rocks Related to Sorption of Sulfur Oxides in Flue Gases", Interim Report to the National Air Pollution Control Administration, Contract Number CPA 22-69-65, Illinois State Geological Survey, Urbana, Illinois, June 22, 1970.

26. G.H. McClellan, "Physical Characterization of Calcined and Sulfated Limestones", paper presented at the Dry Limestone Injection Process Symposium, Gilbertsville, Kentucky, June 22-26, 1970.

27. W.E. Garner, Chemistry of the Solid State, Academic Press, New York, 1955.

28. A.K. Galway, Chemistry of the Solid State, Chapman & Hall, London, 1967.

29. D.A. Young, Decomposition of Solids, Pergamon Press, New York, 1966.

30. O. Levenspiel, Chemical Reaction Engineering, John Wiley & Sons, Inc., New York, 1962.

31. L. Bachmann, E. Cremer, Zeit. Electrochem., 59, 407-9, (1955); 60, 831-5, (1956).

32. H.G.F. Wilsdorf, R.A.W. Haul, Nature (London), 167, 945-946 (1951).

33. P.B. Weisz, R.D. Goodwin, Journal of Catalysis, 2, 397-403 (1963).

34. K.G. Denbigh, G.S.G. Beveridge, Trans. Inst. Chem. Engrs., 40, 23-34 (1962).

35. S.D. Norem, M.J. O'Neill, A.P. Gray, Thermochimica Acta, 1, 29-38 (1970).

36. A.M. Squires, R.A. Graff, J. Air Pollution Control Assoc., 21, 272-276 (1971).

37. S.G. Narayanan, Masters Thesis, The City College of New York, 1971.

38. G.J. Vogel, E.L. Carls, J. Ackerman, M. Haas, J. Riha, A.A. Jonke, "Bench-Scale Development of Combustion and Additive Regeneration in Fluidized Bed." Proceedings of the Third International Conference on Fluidized Bed Combustion, held at College Corners, Ohio, 1972.

39. H.R. Hoy, J.E. Stantan, American Chemical Society Division of Fuel Chemistry Preprints, 14 (2), 59 (1970).

40. K. Wickert, Mitteilungen der VGB, No. 83, 74-82 (April 1963).

41. K. Wickert, West German Patent 1,284,556, December 5, 1968.

42. V.V. Pechkovskii, Zhru. Priklad. Khim., 30, 1579-1583 (1957).

43. G. Moss, British Patent 1,183,937, March 11, 1970.

44. P. Marier, H.P. Dibbs, Thermochimica Acta, 8, 155-165 (1974).

45. M. Hartman, Collect. Czech. Chem. Commun, 39(9), 2374-9, 1974.

46. H.H. Krause, A. Levy, W.T. Reid, ASME paper No. 69-WA/CD-1, 1969.

47. H.H. Krause, A. Levy, W.T. Reid, "Sulfur Oxide Reactions: Radioactive Sulfur and Microprobe Studies of Corrosion and Deposits." ASME paper No. 67-WA/CD-1, 1967.

48. D. Flint, "A Method for the Determination of Small Concentrations of SO_2." J. Soc. Chem. Ind., 1948, 67, 2.

49. R.D. Harvey, Interim Report to NAPCA, CPA 22-69-65, June, 1970.

50. K.D. Kiang, K.T. Liu, H. Nack, J.H. Oxley, "Heat Transfer in Fast Fluidized Bed", chapter in Fluidization Technology, Vol. II, D.L. Keairns, editor, Hemisphere Publishing Corp., Washington, D.C., 1976.

51. P.B. Weisz, "Diffusivity of Porous Particles: I. Measurements and Significance for Internal Reaction Velocities," Zeitschrift fur Physikalische Chemie, Nene Folge, 11, 1-15, 1957.

Autobiographical Statement

George L. Kan was born in Ya-an, Sikang Provice, Republic of China, on August 19, 1944. He finished his high school education at High School of Taiwan Normal University and in 1966 graduated from the Department of Chemical Engineering of National Taiwan University with a Bachelor of Science degree. After a year of service in the Army, he left Taiwan and went to Montana State University. There he received the Master of Science degree from the Department of Chemical Engineering in March 1969.

He then worked as a chemical engineer in New York Testing Laboratories, Tenneco, Montrose Chemical Division of Chris and Craft. In 1971, he left Montrose to form his own company, Marzu Trading Company. In September 1972 he entered the doctoral program in the Chemical Engineering Department of The City College of New York.

He is currently employed by Stauffer Chemical Company at their Eastern Research Center in Dobbs Ferry, New York. He married Nancy Y. Tsuan in June 1974.